THE UNIVERSITY OF QUEENSLAND

AUSTRALIA

In vitro and *in vivo* RNAi screening with a West Nile virus library encoding artificial microRNAs identifies novel host restriction factors.

Faith Elizabeth Nanyonga

MEDN (MSc.), BBLT (BSc.)

A thesis submitted for the degree of Doctor of Philosophy at

The University of Queensland in 2019

School of Chemistry and Molecular Bioscience

Abstract

West Nile virus (WNV) is a mosquito-borne flavivirus, originally isolated in Uganda in 1937, and responsible for sporadic outbreaks in Africa, Europe and Asia. In 1999 WNV was introduced into the USA starting in New York City, and has since become endemic in North America leading to thousands of cases annually. In Australia, a closely related strain of West Nile virus called Kunjin virus (WNV_{KUN}) is endemic to the country. Despite the antigenic similarity between the two strains, WNV_{KUN} does not cause an overt disease and is not linked to any human outbreaks. However, in 2011 a more virulent strain of WNV initially found in New South Wales ($WNV_{NSW2011}$) caused a large equine outbreak in south-eastern Australia, illustrating the national as well as global impact of WNV disease.

This thesis investigates the role of interferon-stimulated genes (ISGs) in control of WNV *in vitro* and *in vivo* using an engineered $WNV_{NSW2011}$ library that encodes artificial microRNAs (amiRs) targeting over one hundred mouse ISGs. Three *in vitro* passages of the virus library in mouse embryonic fibroblasts resulted in selection and enrichment of $WNV_{NSW2011}$ encoding IFITM3-amiR, implying that IFITM3 was a dominant factor restricting WNV titres *in vitro*. This finding fits with the known role of IFITM3 in restricting various virus infections, including WNV. Peripheral infection of mice with the virus library led to a strong selection and enrichment in spleens and/or brains of viruses encoding amiRs targeting various ISGs, in particular ATF3-amiR. The ATF3-amiR WNV was the most enriched WNV in spleens and brains from several mice, and is a novel finding, as the transcription factor ATF3 was not previously known to have an antiviral function.

To verify the role of identified ISGs in restricting WNV infection, recombinant $WNV_{NSW2011}$ viruses encoding corresponding individual amiRs were generated and examined *in vitro* and *in vivo.* Infection with IFITM3-amiR-encoding WNV showed that depletion of IFITM3 in infected cells led to secretion of virions with increased infectivity. This implied that the most critical factor for virus replication in a cell culture environment was to increase infectivity. Furthermore, the IFITM3-amiR WNV exhibited increased replication *in vitro* and elevated virulence in mice. Moreover, the recombinant virus targeting ATF3 exhibited enhanced replication *in vitro* and virulence. Taken together, these data identify host factors that define WNV pathogenicity, and validate the artificial microRNA virus library approach as a unique tool to examine virus-host interactions in cells and in animal models.

Declaration by author

This thesis is composed of my original work, and contains no material previously published or written by another person except where due reference has been made in the text. I have clearly stated the contribution by others to jointly-authored works that I have included in my thesis.

I have clearly stated the contribution of others to my thesis as a whole, including statistical assistance, survey design, data analysis, significant technical procedures, professional editorial advice, and any other original research work used or reported in my thesis. The content of my thesis is the result of work I have carried out since the commencement of my research higher degree candidature and does not include a substantial part of work that has been submitted to qualify for the award of any other degree or diploma in any university or other tertiary institution. I have clearly stated which parts of my thesis, if any, have been submitted to qualify for another award.

I acknowledge that an electronic copy of my thesis must be lodged with the University Library and, subject to the policy and procedures of The University of Queensland, the thesis be made available for research and study in accordance with the Copyright Act 1968 unless a period of embargo has been approved by the Dean of the Graduate School.

I acknowledge that copyright of all material contained in my thesis resides with the copyright holder(s) of that material. Where appropriate I have obtained copyright permission from the copyright holder to reproduce material in this thesis.

Publications during candidature

Peer reviewed papers

1 Yin Xiang Setoh, Alberto A. Amarilla, Nias Y.G. Peng, Rebecca E. Griffiths, Julio Carrera, Morgan E. Freney, Eri Nakayama, Shinya Ogawa, Daniel Watterson, Naphak Modhiran, **Faith Elizabeth Nanyonga**, Francisco J. Torres, Andrii Slonchak, Parthiban Periasamy, Natalie A. Prow, Bing Tang, Jessica Harrison, Jody Hobson-Peters, Thom Cuddihy, Justin Cooper-White, Roy A. Hall, Paul R. Young, Jason M Mackenzie, Ernst Wolvetang, Jesse D. Bloom, Andreas Suhrbier, Alexander A. Khromykh (2019) Determinants of Zika Virus Host Tropism Uncovered by Deep Mutational Scanning, Nature Microbiology 4(5): p. 876-887.

Faith Elizabeth Nanyonga performed the Growth kinetics experiment and characterisation of mutant viruses on Aag2 mosquito cell line. The generated data were included in manuscript submitted for publication and published in Nature mirobiology.

Conference Abstracts

1. **Faith Elizabeth Nanyonga,** Yin Xiang Setoh, Alberto A. Amarilla, Morgan E. Freney, Andrii Slonchak, Andreas Suhrbier, Benjamin R tenOever, Alexander A Khromykh (2019). *In vivo* RNAi screening with West Nile virus library encoding artificial microRNAs identifies novel host restriction factors Presented at Keystone Symposia conference on positive-strand RNA viruses, Held in Kerry Ireland 9th to 13th June, 2019.

2. **Faith Elizabeth Nanyonga**, Yin Xiang Setoh, Alberto A. Amarilla, Morgan E. Freney, Andrii Slonchak, Alexander A Khromykh (2017). *In vitro* RNAi screening with a library of West Nile viruses encoding artificial miRNAs targeting host antiviral genes identifies IFITM 3 as the major antiviral factor against West Nile virus infection. Poster presentation at the 9th Australasian Virology Society Meeting held on 5th to 8th December 2017 in Adelaide, South Australia.

Publications included in this thesis

No publications included.

Submitted manuscripts included in this thesis

No manuscripts submitted for publication.

Contributions by others to the thesis

Associate Professor Alexander Khromykh, Associate Professor Katryn Stacey and Dr Yin Xiang Setoh supervised this project, assisted in experimental design and offered advice on accurate analysis and interpretation of data as well as discussion of results. Dr Alberto A Amarilla, Mr Nias Peng and Ms Moragan Freney assisted in animal work experiments included in result sections of this thesis. Dr Andrii Slonchak performed Northern blot analysis included in the results section.

Statement of parts of the thesis sub mitted to qualify for the award of another degree

None

Research Involving Human or Animal Subjects

All procedures and experiments that involved use of animal subjects were prior approved by the University of Queensland Animal Ethics Committee in accordance with the Australian National Health and Medical Research Council guidelines before commencement. Ethics approval numbers since commencement of candidature are listed below. Copies of the ethics approval letters are included in the appendix 6 of the thesis.

1. AEC 327/15

2. SCMB/008/17

Acknowledgement

I wish to extend my sincere gratitude to Associate Prof. Alexander Khromykh for taking me on to pursue my PhD under your mentorship and supervision. Thank you for believing in my capabilities and entrusting me this huge task of handling the amiR project. I am forever grateful for your advice, guidance and mentorship. Your guidance has been so instrumental in modelling me to becoming a better scientist.

Secondly, I wish to extend my heartfelt gratitude to Dr Yin Xiang Setoh for being the best mentor I could ever ask for. You have taught me everything I know about flaviviruses. Your keenness to listen, friendliness, pro-active and problem-solving approach has enabled me complete this PhD. Thank you for all the help and guidance you have rendered to me during my candidature. I have learnt a lot from you.

I would like to thank Associate Prof. Katryn Stacey for voluntarily taking me on as your student and joining my advisory committee at the last instance of my PhD. Thank you for accepting to be my principal advisor, your invaluable help, advice and mentorship have enabled me reach this milestone of my career.

I wish to extend my sincere gratitude to my PhD committee for helping solve all the problems and hurdles I have encountered during my studentship. My chair, Professor Roy Hall, examiners: Dr Philip Stevenson and Dr David Warrillow, thank you for making this journey a success. Without your keen ear, mediation skills and constructive criticism, I doubt I would have made this far.

To the Khromykh Laboratory members the past and present, Dr Alberto A. Amarilla, Dr Andrii Slonchak, Ms Morgan Freney, Mr Nias YongGao Peng, and Mr Francisco J. Torres, thank you for creating such a conducive environment to work in. Dr Amarilla, thank you for being so approachable, for all the experimental troubleshooting you helped me with, the animal handling techniques that you have taught me and always making delicious Brazilian barbeques among others. Mr Peng, thank you for always reminding me not to be stressed.

Special thanks to School of Chemistry and Molecular Bioscience staff especially members from Level 5 laboratories for all the help rendered to me during my PhD journey. Thank you Dr Naphak Modhiran for your input in my PhD, Dr Daniel Watterson and Dr Jody Hobson-Peters for generously

providing antibodies used in my PhD experiments, if it was not for your generosity, my PhD research wouldn't have been smoothly conducted.

I am forever indebted to the Australian taxpayer, The Australian Government, Australian Infectious Diseases Research Centre, and The University of Queensland who generously provided financial and infrastructural support for my PhD candidature. This research was supported by the Australian Government Research Training Program Scholarship.

Special thanks to my long-term mentors, Dr Chris M Parry, Dr Bernard Kikaire, Dr Tom Blanchard and Dr Kato Drago, who have continually and diligently supported my career prospects, inspired and endorsed me for various positions throughout my career. Without your confidence in me, I wouldn't be who I am today.

I am grateful to my husband Mr Mukwana Anthony Daniel for the love, support and friendship during the course of my PhD, thank you for sacrificing everything for me. Thank you for believing in me and understanding this PhD journey. You have continually supported my career plans and encouraged me throughout my higher education. Your love and confidence in me have been a constant reminder that when you put your heart to anything, you can achieve anything.

I wish to thank my friends in Australia, Uganda and all around the world for always checking on me, providing invaluable advice and support during my education. A huge thanks to Ms Diana Ms Kiwanuka, Ms Racheal Mubeezi, Mr Samuel Wasike, Ms Freedom Samantha Kukunda, Ms Anne Kapaata, Dr Aloysious Ssemaganda, Ms Natukunda Sheila, Ms Gloria Akobye, Dr Khamis Tomusange, Ms Stacey Cheung, Mr Nathan Otim, Mr Patrick Junior, Ms Christine Nsamba, Dr Ismail and Mrs Paula Sebina, Ms Maureen Namusayi among others for all your love and care.

I wish to express my sincere gratitude to my loving and supportive family. I would love to thank my parents, Mr and Mrs Katumwa for instilling in me attributes of hard work, passion and tenacity. Throughout my time in school, you have been my anchor, sacrificed all you had to ensure that I went to the best schools and excelled in my studies. Even though I have not been home in three years, you have always made me feel like am at home, you have made phone calls, prayed for me, given me all the love and moral support I needed on this PhD journey. I am forever indebted to you. In a special way, I thank my lovely sister Irene Sanyu, for always lending an ear, thank you for supporting me financially, morally and physically throughout my education. You travelled miles and miles to come

check on me, when I made it to Australia, and have continually made sure that I am fine. Your love and kind heart have given me the best mental state as I pursued this career, I am forever grateful. My nieces Nicole and Natalie Karani, thank you for all the love and kindness shown to me. To my brothers, Kenneth, Victor, and Ian. Thank you for believing in me and supporting in me. I am grateful for all the support I have received from my extended family, my father and mother in law Mr and Mrs Mukwana.

I would love to thank the Almighty GOD for bringing me this far, thank you Jesus for guiding me with your might hand and for making everything possible. If I weren't for your will, I would not have reached this part of my career.

Keywords

West Nile virus, innate immunity, interferon stimulated genes, virus-host interactions, artificial micro RNA

Australian and New Zealand Standard Research Classifications (ANZSRC)

ANZSRC code: 060506 Medical Virology, 80%

ANZSRC code: 110704 Cellular Immunology, 20%

ANZSRC code: 1108 Medical Microbiology

Fields of Research (FoR) Classification

FoR code: 0605, Microbiology, 80%

FoR code: 0699, Other Biological Sciences, 20%

Table of contents

List of figures

List of tables

Chapter 1: Literature review

1.1 Flaviviridae

Flaviviridae is a family of small-enveloped viruses with positive sense RNA genomes, which consists of four genera: Flavivirus, Pestivirus, Hepacivirus and Pegivirus [1]. The family is named after yellow fever virus, as flavus refers to yellow in Latin. Although phylogenetic analysis has shown that members in within flaviviridae family have similar genomic organization, replication strategy and physicochemical properties, they are genetically and biologically different [2]. All members within the family encode at least two to four structural proteins together with seven to eight non-structural protein genes flanked by 5′ and 3′ untranslated regions (UTRs). In addition, the genera Hepacivirus, Pegivirus and Pestivirus share a closer degree of similarity [3]. A Phylogenetic tree based on conserved amino acid sequences in RNA-dependent RNA polymerase (RdRP) region of members in the Flaviviridae family was generated. To generate the phylogenetic tree, partial gene sequences from representative isolates of each species and related unclassified viruses were aligned using MUltiple Sequence Comparison by Log-Expectation (MUSCLE) software and confirmed by the presence of aligned motifs [4].

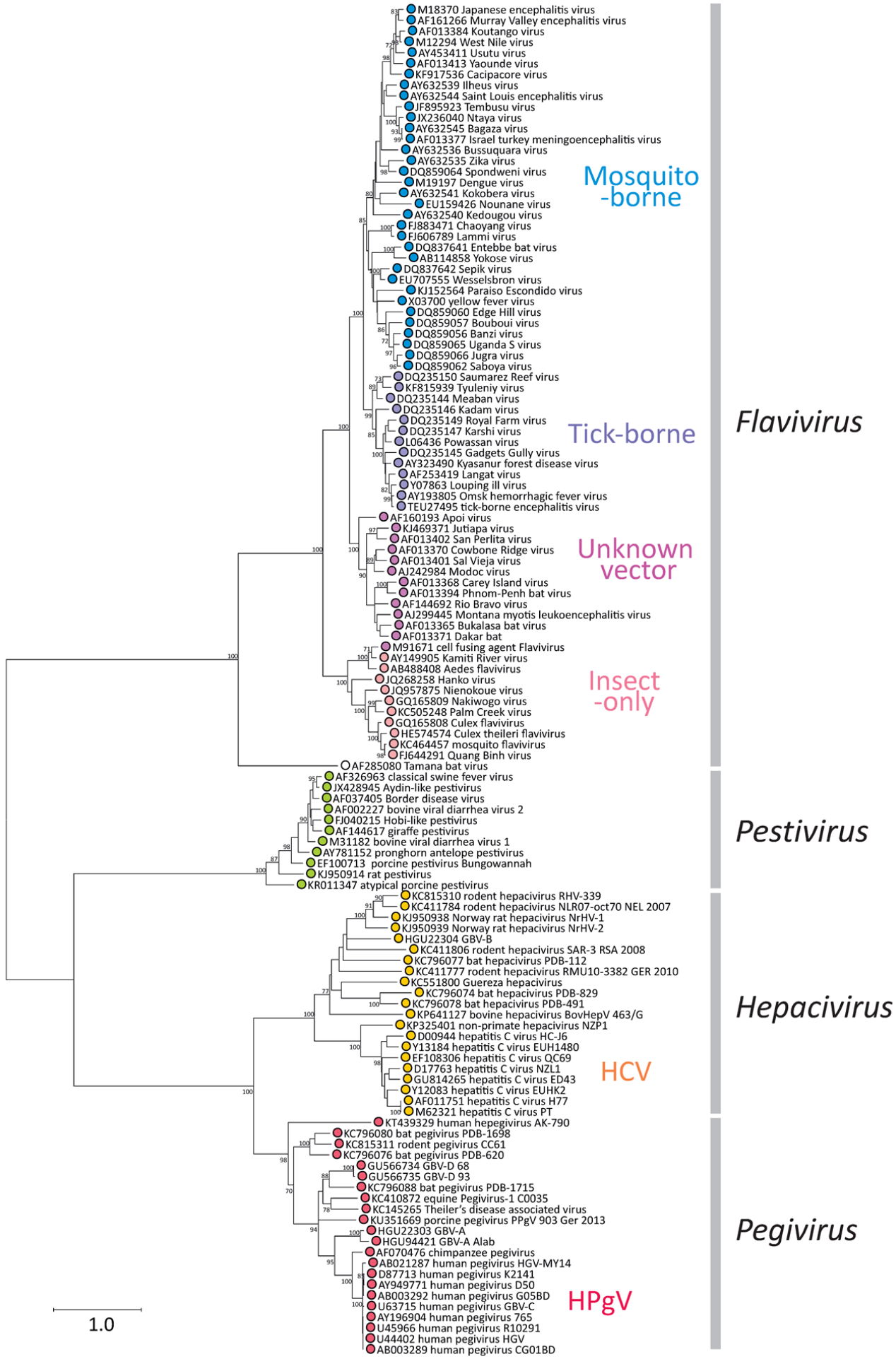
M18370 Japanese encephalitis virus
AF161266 Murray Valley encephalitis virus
AF013384 Koutango virus
M12294 West Nile virus
AY453411 Usutu virus
AF013413 Yaounde virus
KF917536 Cacipacore virus
AY632539 Ilheus virus
AY632544 Saint Louis encephalitis virus
JF895923 Tembusu virus
JX236040 Ntaya virus
AY632545 Bagaza virus
AF013377 Israel turkey meningoencephalitis virus
AY632536 Bussuquara virus
AY632535 Zika virus
DQ859064 Spondweni virus
M19197 Dengue virus
AY632541 Kokobera virus
EU159426 Nounane virus
AY632540 Kedougou virus
FJ883471 Chaoyang virus
FJ606789 Lammi virus
DQ837641 Entebbe bat virus
AB114858 Yokose virus
DQ837642 Sepik virus
EU707555 Wesselsbron virus
KJ152564 Paraiso Escondido virus
X03700 yellow fever virus
DQ859060 Edge Hill virus
DQ859057 Bouboui virus
DQ859056 Banzi virus
DQ859065 Uganda S virus
DQ859066 Jugra virus
DQ859062 Saboya virus
DQ235150 Saumarez Reef virus
KF815939 Tyuleniy virus
DQ235144 Meaban virus
DQ235146 Kadam virus
DQ235149 Royal Farm virus
DQ235147 Karshi virus
L06436 Powassan virus
DQ235145 Gadgets Gully virus
AY323490 Kyasanur forest disease virus
AF253419 Langat virus
Y07863 Louping ill virus
AY193805 Omsk hemorrhagic fever virus
TEU27495 tick-borne encephalitis virus
AF160193 Apoi virus
KJ469371 Jutiapa virus
AF013402 San Perlita virus
AF013370 Cowbone Ridge virus
AF013401 Sal Vieja virus
AJ242984 Modoc virus
AF013368 Carey Island virus
AF013394 Phnom-Penh bat virus
AF144692 Rio Bravo virus
AJ299445 Montana myotis leukoencephalitis virus
AF013365 Bukalasa bat virus
AF013371 Dakar bat
M91671 cell fusing agent Flavivirus
AY149905 Kamiti River virus
AB488408 Aedes flavivirus
JQ268258 Hanko virus
JQ957875 Nienokoue virus
GQ165809 Nakiwogo virus
KC505248 Palm Creek virus
GQ165808 Culex flavivirus
HE574574 Culex theileri flavivirus
KC464457 mosquito flavivirus
FJ644291 Quang Binh virus
AF285080 Tamana bat virus
AF326963 classical swine fever virus
JX428945 Aydin-like pestivirus
AF037405 Border disease virus
AF002227 bovine viral diarrhea virus 2
FJ040215 Hobi-like pestivirus
AF144617 giraffe pestivirus
M31182 bovine viral diarrhea virus 1
AY781152 pronghorn antelope pestivirus
EF100713 porcine pestivirus Bungowannah
KJ950914 rat pestivirus
KR011347 atypical porcine pestivirus
KC815310 rodent hepacivirus RHV-339
KC411784 rodent hepacivirus NLR07-oct70 NEL 2007
KJ950938 Norway rat hepacivirus NrHV-1
KJ950939 Norway rat hepacivirus NrHV-2
HGU22304 GBV-B
KC411806 rodent hepacivirus SAR-3 RSA 2008
KC796077 bat hepacivirus PDB-112
KC411777 rodent hepacivirus RMU10-3382 GER 2010
KC551800 Guereza hepacivirus
KC796074 bat hepacivirus PDB-829
KC796078 bat hepacivirus PDB-491
KP641127 bovine hepacivirus BovHepV 463/G
KP325401 non-primate hepacivirus NZP1
D00944 hepatitis C virus HC-J6
Y13184 hepatitis C virus EUH1480
EF108306 hepatitis C virus QC69
D17763 hepatitis C virus NZL1
GU814265 hepatitis C virus ED43
Y12083 hepatitis C virus EUHK2
AF011751 hepatitis C virus H77
M62321 hepatitis C virus PT
KT439329 human hepegivirus AK-790
KC796080 bat pegivirus PDB-1698
KC815311 rodent pegivirus CC61
KC796076 bat pegivirus PDB-620
GU566734 GBV-D 68
GU566735 GBV-D 93
KC796088 bat pegivirus PDB-1715
KC410872 equine Pegivirus-1 C0035
KC145265 Theiler's disease associated virus
KU351669 porcine pegivirus PPgV 903 Ger 2013
HGU22303 GBV-A
HGU94421 GBV-A Alab
AF070476 chimpanzee pegivirus
AB021287 human pegivirus HGV-MY14
D87713 human pegivirus K2141
AY949771 human pegivirus D50
AB003292 human pegivirus G05BD
U63715 human pegivirus GBV-C
AY196904 human pegivirus 765
U45966 human pegivirus R10291
U44402 human pegivirus HGV
AB003289 human pegivirus CG01BD
Mosquito -borne
Tick-borne
Unknown vector
Insect -only
HCV
HPgV
Flavivirus
Pestivirus
Hepacivirus
Pegivirus
1.0

Figure 1.1 Phylogenetic tree of conserved amino acids of the RdRP in the Flaviviridae family. The scale bar depicts the evolutionary distance in numbers of substitutions per amino acid site. (Adapted from Ictvonline)

1.2 Flaviviruses

The flavivirus genus consists of over 73 unique arthropod-borne viruses, some of which cause high morbidity and mortality. Flaviviruses are generally mosquito-borne or tick-borne and insect-specific flaviviruses, although some can be maintained in a vertebrate only transmission, without a known vector [5-7]. Mosquito-borne and tick-borne flaviviruses present the most public health concern. Mosquito-borne flaviviruses include Murray valley encephalitis virus (MVEV), St. Louis encephalitis virus (SLEV), yellow fever virus (YFV), dengue virus (DENV) serotypes 1–4, Japanese encephalitis virus (JEV), Zika virus (ZIKV) and West Nile virus (WNV) whereas tick-borne encephalitis virus is the most prominent flavivirus spread by ticks [1]. Most flavivirus infections are reported in tropical and temperate regions where climatic conditions allow arthropods to thrive and favour flavivirus replicative lifecycles in arthropods [8, 9]. Emergence of new flaviviruses in areas where they were not known as endemic has been attributed to urbanisation, tourism, travel and improved surveillance programs [10, 11]. Furthermore, there is an increasing threat of emergence of highly virulent strains from previously less virulent strains [12].

Flaviviruses are classified based on nucleotide sequence, antigenicity, pathogenicity, geographical distribution and ecological association [13]. Members of the flavivirus genus are positive-sense RNA viruses, which belong to nine serological complexes, with the JEV serological clade as the largest. Flaviviruses within JEV clade are maintained in a *Culex* mosquito-bird cycle and cause neurological infections. These include JEV, WNV, MVEV and (SLEV), Kunjin (WNV_{KUN}), Alfuy, Koutango (KOU), Cacipacore (CPC), and Yaounde (YAO) viruses [14, 15]. MVEV and WNV_{KUN} are the most endemic flaviviruses within Australia [16, 17]. JEV is closely related to MVEV and is a common human pathogen in Torres Strait Islands and Cape York with increasing threat of JEV infection on the Australian mainland [18-21]. Although other flaviviruses such as Kokobera (KOKV), Alfuy (ALFV), Stratford (STRV) and Edge Hill (EHV) have been identified in Australia; only KOKV is known to cause virus infection in humans [22-25]. Flaviviruses related to Yellow fever virus are spread by *Aedes* mosquitoes and cause systemic infections by feeding on humans, simians and other mammalian species. These include YFV, ZIKV and DENV [26].

1.3 West Nile Virus as a health concern

West Nile virus was first isolated from a febrile female patient in 1937 in Uganda [27]. Since then, this particular strain has been linked to mild outbreaks in Africa and some parts of Europe [28]. In addition, a more virulent strain was reported in the United States of America (USA) in 1999. This WNV strain was named West Nile virus New York 99 (WNV_{NY99}) strain and has since become endemic in America leading to thousands of cases annually [29]. By 2011, close to 1.8 million people had been infected, with up to 360,000 illnesses and close to 1,300 deaths reported [30]. According to the Centres for Disease Control and Prevention (CDC), 2387 cases and 243 deaths were reported in 2012, 2374 cases and 114 deaths in 2013 and 1935 cases and 71 deaths in 2014 [31]. Furthermore, since 2010, WNV_{NY99} has caused outbreaks of febrile and neurological disease in Europe with close to 500 cases per year. This strain poses a huge threat to Australia because Australian birds and mosquitoes are capable of facilitating WNV_{NY99} replication and transmission [32].

Although WNV_{NY99} is antigenically closely related to Australia's endemic WNV_{KUN}, WNV_{KUN} is avirulent [33]. WNV_{KUN} is named after an Australian aboriginal clan that inhabited areas around the Mitchell River in far north Queensland [34]. Until 2011, WNV_{KUN} was a known non-threatening endemic strain in the Northern Territory and Kimberly region of Western Australia, with a few isolations in North Queensland and patients presenting with mild illness and no encephalitic signs [35]. However in 2011, an unprecedented WNV outbreak was reported in New South Wales, Australia, causing equine neurological disease, with no reported human cases [36]. This strain was named $WNV_{NSW2011}$ and was shown to have emerged from benign WNV_{KUN} strain [12, 37]. In addition, surveillance of recent deadly WNV outbreaks in United States of America and Europe suggest that virulent WNV strains could have emerged from known benign strains [12, 38]. Collectively, these incidents highlight the vulnerability of Australia and world at large to future deadly WNV outbreaks.

Despite major past outbreaks, future threats and increased resurgence of WNV that pose a huge public health concern, there are neither vaccines nor antivirals available to combat flavivirus infection. This reinforces the need for comprehensive research in understanding how WNV causes infection and how the host immune system antagonises WNV lifecycle to limit virus spread. Understanding WNV-host interaction will eventually identify and elucidate WNV therapeutic targets for generating vaccine and antivirals. In this thesis, the aim was to identify and understand host factors that control $WNV_{NSW2011}$ replication both *in vivo* and *in vitro*. Identified host factors were further characterised by mechanistic studies to understand their role in WNV replication. Findings described herein further elucidate the role of host factors in WNV infection as well as how

West Nile virus causes infections in the host.

1.4 West Nile virus strains and lineages

According to phylogenetic analyses, WNV is divided into five distinctive genetically related lineages, namely lineages 1, 2, 3, 4 and 5. Lineage 1 is subdivided into 1a, 1b and 1c clades, lineage 1a consists of viruses causing encephalitis and meningitis, including strains isolated from north-eastern USA, Europe, Israel, Africa, India, Russia, and Australia. [39-41]. The WNV strains in clade 1b and Clade 1c are mainly isolated from Australia and India respectively [42]. Recent WNV surveillance studies in birds, mosquitoes and human populations have attributed huge human outbreaks in southern Europe to lineage 2 WNV. Lineage 2 WNV strains are considered as less virulent than lineage 1 WNV strains and are commonly isolated only in sub-Saharan Africa and Madagascar [40-44]. Therefore, the recent isolation of lineage 2 WNV strains in Europe suggests migration of WNV reservoir birds from sub-Saharan Africa and Madagascar to Europe [45, 46]. Lineage 3, 4 and 5 WNV strains are associated with symptomatic human cases in Austria, Russia and India respectively [39, 47-50].

1.5 West Nile virus Life cycle and Pathogenesis

WNV life cycle is primarily maintained in a *Culex* mosquito-bird transmission cycle but often infects and causes disease in humans and horses [51, 52]. Humans and horses are considered dead-end hosts, as they do not develop sufficient viraemia to transmit the virus [53, 54]. During a blood meal, WNV-infected mosquitoes transfer the virus to the dermis and to some extent directly into the blood stream of a vertebrate host [55]. The incubation period of WNV infection in human is 2-14 days and infections in immunocompetent humans are either asymptomatic or self-limited febrile illness with general body weakness, muscle and joint pains, headache, gastrointestinal complaints, skin rash and lymphadenopathy. However in immunocompromised individuals, infants, elderly and rare situations, a small proportion of WNV cases develop neurological infections characterised by flaccid paralysis, meningitis and encephalitis, which can often lead to death [56]. Following WNV neuroinvasive infection, 10% of infected individuals die while greater than 50% of patients are left with long-term neurological sequelae [57, 58]. Most of the neural damage is seen in the brain stem and anterior horn of the spinal cord while in immunocompromised individuals the damage could spread to entire CNS [59]. Although viraemia seen in various mouse model organs is not comparable with that observed in humans and horses, mouse models are used to hypothesise how WNV infection occurs *in vivo*. As a result, viral and host genetic factors that influence WNV replication and pathogenesis have been identified and mechanisms of action of elucidated [54, 59-62]**.**

Following several WNV epidemics globally, several research studies have attempted to explain how both innate and adaptive immune systems protect hosts against WNV infection. Consequently pathogenesis of WNV has been described in three phases, namely: early, peripheral virus amplification and neuroinvasion phases [63, 64]. In the initial phase after subcutaneous infection of mice, WNV is infects and spreads to dermal dendritic cells and Langerhans cells to cause increased viraemia and stimulation of innate cytokines responses controlled by toll like receptor 7 [65-67]. Increased viraemia the represents amplification phase in which WNV spreads to organs, primarily the spleen and kidney [68]. Although specific viral target cells in the spleen are poorly understood, dendritic cells, macrophages and neutrophils are believed to be WNV targets [69-71]. By seven days post-infection viraemia is cleared and WNV is undetectable in sera but can be detected in spinal cords and brains of infected mice, thus marking the last phase of neuroinvasion. Increased viraemia enables WNV to enter, infect and spread within central nervous system (CNS) cells by breaking the integrity of blood brain barriers (BBB) to cause encephalitis.

1.6 Neuroinvasiveness and Neuropathogenesis

WNV enters the CNS and proficiently proliferates within neurons and myeloid cells [60]. WNV neuroinvasiveness is attributed to the glycosylation motif on envelope (E) protein although the precise mechanism of how WNV invades CNS is not fully understood [72]. The N-linked glycan domain of WNV-E protein is thought to increase virus attachment, entry into endothelial cells and eventual CNS invasion [73, 74]. Furthermore, changes in endothelial monolayer permeability are believed to trigger breakdown of blood brain barrier (BBB) thereby permitting WNV to invade the CNS [75]. In addition, activation of matrix metalloproteinase and release of tumor necrosis factor-α (TNF-α) impairs BBB tight junctions allowing WNV to penetrate and infect the nervous system [76, 77]. Dissemination of WNV in the mouse CNS causes into extensive neural damage, high WNV titres and increased leukocyte levels in the brain [78, 79]. Neuronal damage is attributed to increased apoptotic response following virus infection, release of toxic cytokines by dying neuronal cells, reduction of cytotoxic T lymphocytes and accumulation of ubiquitinated proteins in neuronal cells [80, 81].

1.7 Replication cycle of West Nile Virus

WNV replication cycle is complex and involves well-coordinated steps (Figure 1.2). The cycle is initiated when the WNV virion binds to unknown cell surface receptor via its Envelope (E) protein, and enters the cell through clathrin-mediated endocytosis [82]. Subsequently WNV resides in an early endosome before maturation, causing a drop in endosomal pH. The drop in pH initiates virion-endosomal membrane fusion, subsequent un-coating and release of the positive single-stranded

RNA (+ssRNA) genome into the cytoplasm [64, 83]. Consequently, +ssRNA migrates to the cytosolic face of the endoplasmic reticulum (ER) where the genome is translated into a single highly membrane-associated polyprotein polyprotein [84]. The single polyprotein is processed into mature proteins by cellular proteases and viral serine protease non-structural proteins (NS2B–NS3) [85]. Increase in non-structural proteins in the cytoplasm causes morphological changes that result in formation of vesicle pockets in the ER and viral +ssRNA is translocated into vesicle pockets with the ER membrane to form the viral envelope membrane [86, 87]. Non-structural proteins combine to form a replication complex that is utilised in forming complete negative-sense ssRNA (-ssRNA) intermediates [88]. The -ssRNA is used as template to synthesize positive single stranded RNA. Structural proteins capsid, envelope and pre-membrane are utilised in early stages of WNV replication. Pre-membrane protein (prM) ensures proper folding of the envelope (E) protein and inhibits early fusion during virus release [89]. The capsid protein then encapsidates the viral genome RNA at the ER, and the vesicle pocket buds as a virion into the ER. Immature virus particles are transported through secretory pathway and processed to form mature virions. Mature virions are released by exocytosis and the process is repeated [89, 90].

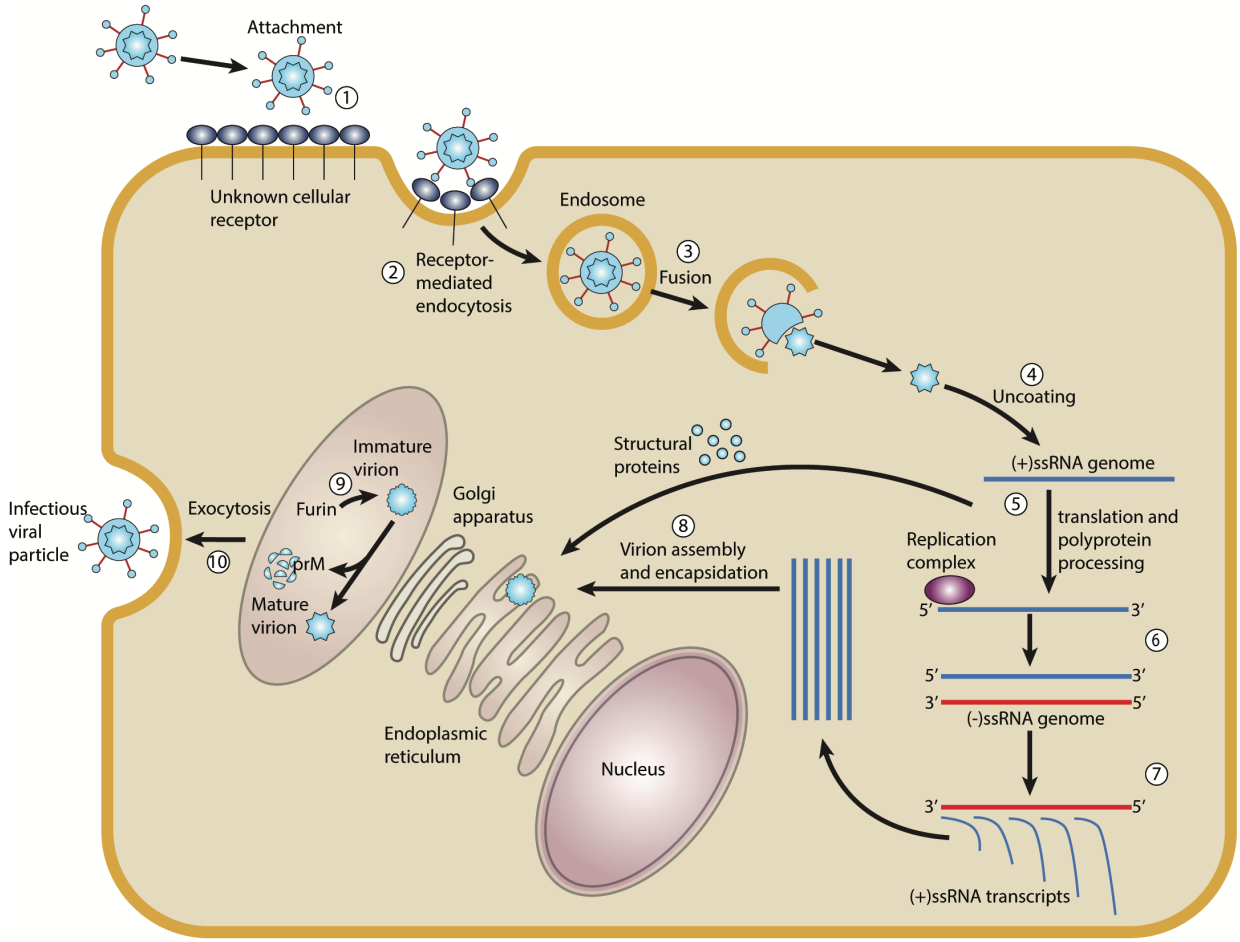

Figure 1.2 Diagram of WNV replication cycle. 1. WNV infects a wide range of target cells and attaches to host cells through unknown receptors. 2. WNV-E protein facilitates virion entry into

target cells via receptor-mediated endocytosis. 3. A drop in pH within the endosomal vesicles allows virion-membrane fusion. 4. This leads to un-coating and release of viral genome into the cytosol where +ssRNA genome is translated and processed into a single poly protein at the endoplasmic reticulum (5 and 6). The polyprotein is cleaved into mature proteins by NS2B-NS3 serine protease and cellular proteases. The non-structural proteins form the replication complex utilised in formation of −ssRNA intermediates and synthesis of full-length +ssRNA (7). The capsid protein encapsulates viral genome (8) at the ER membrane and virus buds into the ER. RNA replication stages (5, 6, 7 and 8) occur in the vesicle packets formed in the endoplasmic reticulum membrane. Immature virions are shuttled through host secretory pathway causing WNV-E glycosylation and cleavage of prM into mature M by furin (9). Consequently, mature virions are shuttled and released from the plasma membrane by exocytosis (10). (Adapted from Suthar et al., 2013 ^ [64]).

1.8 West Nile Virus genome

West Nile virion is an icosahedral-enveloped virus about 40-60nm in diameter with a single stranded positive sense RNA genome. It is translated into a polyprotein that is cleaved co- and post-translationally into three structural, and seven non-structural proteins [69, 84, 91].

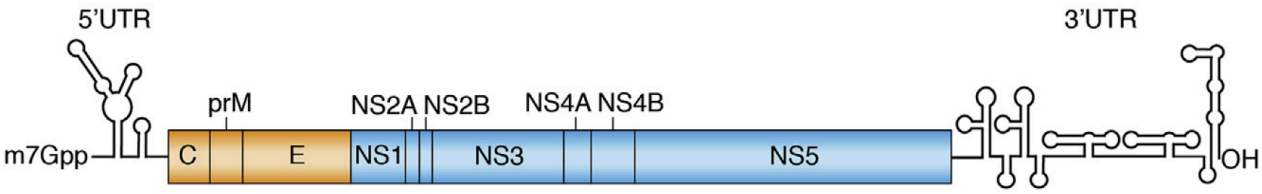

Figure 1.3 Diagram showing WNV genome organisation. WNV encodes a single open reading frame of about 11,000 nucleotides that is flanked with two non-coding regions, 5' UTR and 3' UTR. It encodes three structural proteins (C, PrM and E, brown colour) and 7 non-structural proteins (NS1-NS5, blue colour).

1.8.1 Structural proteins

Structural proteins capsid (C), pre-membrane (PrM) and envelope (E) are vital in viral attachment, entry, encapsidation and formation of virions. Specifically E protein facilitates viral entry and assembly and is the most immunogenic virus protein [92]. Envelope protein is often glycosylated at position 154 to facilitate infection in different hosts. Furthermore, E glycosylation has been linked to increased virulence and dissemination of WNV into brains [72]. Capsid binds viral RNA to form the nucleocapsid and contains α helices, believed to aid in viral RNA binding [93-95]. Structural analysis of capsid N- and C-terminal suggests that both termini could aid RNA folding and control the role of capsid during viral replication [96]. PrM inhibits premature fusion and has been linked to virulence [89].

1.8.2 Non-structural proteins

Non-structural proteins (NS1 to NS5) facilitate viral RNA synthesis, WNV transcription, replication, maturation and immune evasion [97]. NS1 is a glycoprotein with three highly conserved N-linked glycosylation sites and several cysteines, which form disulphide bonds. The disulphide bonds are potentially involved in dimerisation and influence hydrophobic nature of NS1 [98]. Members of the JEV sero-comp lex including WNV can encode both NS1 and an alternative form of NS1 with a 52 amino acid N-terminal or C-terminal extension termed NS1′. Removal of NS1′ reduces the neurovirulence of both WNV and JEV [99]. Although the actual function of NS1′ is unknown, NS1′ can function as NS1 during virus replication [100]. Intracellular and secreted NS1 forms serve as co-factor for viral replication and control complement activation as well as Toll-like receptor signalling respectively [101]. NS2A protein is a 25 kDa hydrophobic trans-membrane protein utilised during viral RNA replication, virion assembly, control of host immune responses and virus dissemination [102-104]. NS2B is a small hydrophobic protein that serves as a co-factor for NS3 protease that cuts the viral protein into structural and non-structural viral proteins [105, 106]. NS3 is both a helicase and a viral serine protease in the C and N-termini respectively and NS3 is only active when coupled with its co-factor NS2B [107, 108]. In addition, the helicase domain of NS3 hinders type I interferon (IFN-I) signalling by blocking Signal transducer and activator of transcription 1 (STAT1) phosphorylation [109]. NS4A and NS4B are hydrophobic proteins that possess several trans-membrane domains and are bound to the viral replication complex in virus-induced ER membrane compartments. NS4A acts as co-factor that controls ATPase activity of NS3 helicase while NS4B inhibits interferon signalling [110, 111]. Flavivirus NS5 constitutes the largest WNV protein that co-localises with genomic RNA at viral replication complex sites [112]. NS5 encodes N-terminal methyltransferase (MTase) and C-terminal RNA-dependent RNA polymerase (RdRp) domains, which facilitate flavivirus replication [113, 114]. The RdRp is utilised during viral genome replication to synthesise negative and positive RNA strands [115, 116]. The MTase has guanylyltransferase and methyltransferase enzymatic actions and facilitates 5'-RNA capping and methylation of the viral genome [117, 118]. In addition, studies have shown that NS5 protein antagonises interferon production by blocking alpha/beta interferon–mediated JAK-STAT signalling pathway as discussed in detail in section 1.10.4. Particularly, NS5 protein impedes interferon-dependent STAT1 phosphorylation by reducing accumulation of phosphorylated STAT1 and subsequent IFN-dependent gene expression [119, 120].

1.8.3 The 5′ UTR

The WNV RNA genome is devoid of a polyadenylate (poly-A) tail and is monocistronic in that there is a single translation start for the polyprotein [14, 121, 122]. The Open reading frame (ORF) is flanked by highly conserved 5′ UTR and 3′ UTR involved in initiation of RNA replication, translation and immunomodulation and likely determines genome packaging [123-126].

1.8.4 The 3′ UTR

The 3′ UTR of WNV is about 380–600 nucleotides long with highly structured RNA including 4 stem-loop (SL) structures and two dumbbell (DB) structures [14]. In between these structures are spacer sequences with unrevealed functions although evidence suggests that these sequences may induce correct folding of viral protein and protect neighbouring structural domains from interference [127].

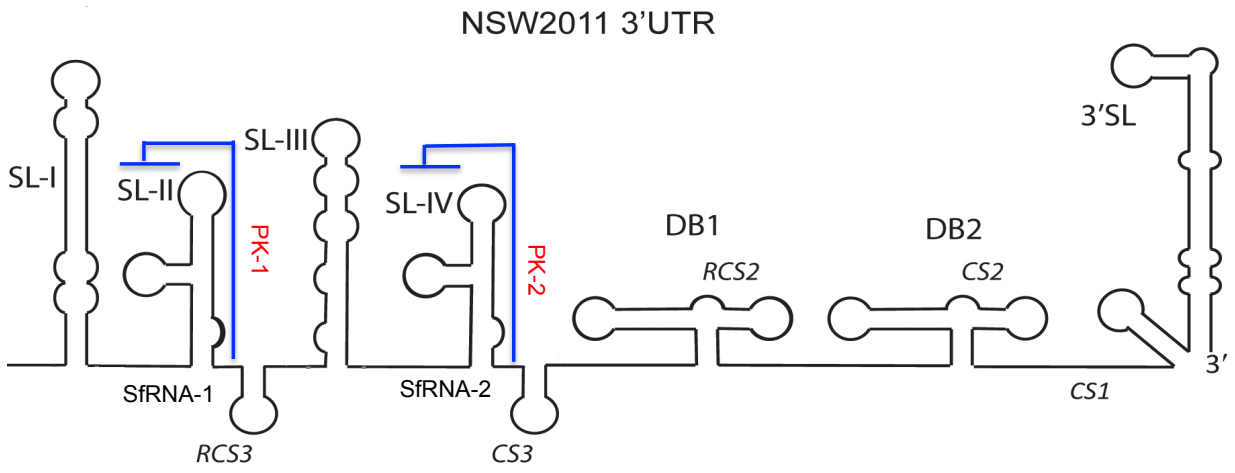

Figure 1.4 Structural components within the 3'UTR of WNV: Diagram showing the parts of the 3' UTR of WNV. The 3' UTR of WNV encodes stem-loops (SL), Dumb bell structures (DB) and pseudo knots (PK). SL-II and SL-1V constitute two pseudo knots that provide steric hindrance to 5'-3' exoribonuclease enzyme and block complete degradation of WNV genome resulting in sfRNA accumulation. Adopted from Pijlman *et al.,* 2008 ^ [122] and Roby *et al.,* 2014^ [14].

The 3' UTR of WNV is not only vital in viral RNA replication, translation, genome packing but also generates a sub-genomic flavivirus RNA (sfRNA) fragment. The WNV sfRNA is about 525-nt long noncoding RNA structure produced due to stalling of cellular 5'-3' exoribonuclease XRN-1 on a rigid RNA structure about 100 nucleotides from the start of the 3' UTR [122, 128, 129]. Crystallographic study of sfRNA structures has shown intertwined pseudoknots that directly interact with XRN-1 enzyme [130]. Consequently, SfRNA controls numerous functions in virus-host interactions and pathogenesis. Specifically, sfRNA production subverts the interferon response

by inactivating cellular RNA sensors such as Toll-like receptor 3, RIG-I, and MDA5 (discussed in details in section 1.10), regulates host mRNA decay and RNAi pathways [14, 131-133]. Furthermore, previous studies have shown that mutations leading to loss of normal sfRNA structure attenuate flaviviruses, reducing cytopathic effect and virulence in both *in vitro* and *in vivo* studies [131, 132].

1.9 RNA interference

RNA interference (RNAi*)* is a post-transcriptional response, which controls sequence-specific degradation or down-regulation of the target messenger RNA [134]. RNAi is a concise nucleic acid-based gene silencing strategy in which small noncoding RNAs are used to control gene expression. During flavivirus replication in vectors such as mosquitoes and ticks, flaviviruses are subjected to the vectors' innate immune response known as antiviral RNAi to produce small interfering (siRNA) that degrade viral RNA and ultimately inhibit flavivirus replication (reviewed in [135]), In mosquito cells, micro RNA (miRNA)-mediated response to WNV Aae-miR-2940-5p, which is a mosquito microRNA is down-regulated during WNV infection to inhibit WNV replication. This is achieved by blocking metalloprotease m41 FtsH gene expression that is vital for WNV replication [136]. In addition, WNV has been shown to encode microRNA-like small RNA known as KUN-miR-1 with in its 3' UTR, which facilitates WNV replication in mosquito cells by up regulating GATA4 mRNA expression [137]. A number of studies have utilized RNAi to directly inhibit virus replication in cells and organisms such as siRNAs targeting WNV Capsid and NS5 genes resulted into close to 80% inhibition of WNV replication [138]. Furthermore, in another study RNAi was used to inhibit NS5 expression and subsequent viral replication *in vitro* [139]. Since its discovery, the RNAi concept has been used as valuable research tool in generation of therapeutics, study of virus-host interactions among others.

1.9.1 Canonical Biogenesis of miRNA

Micro RNAs (miRNAs) are small noncoding RNAs expressed by all eukaryotic multicellular organisms. They regulate cellular processes and are promising therapeutic targets and disease biomarkers [140]. MiRNAs are about 22 nucleotides single stranded genome-encoded noncoding RNA molecules produced from precursor miRNA (pre-miRNA) hairpins [141, 142]. Genes encoding miRNAs are transcribed by RNA polymerase II into long primary transcripts (pri-miRNAs). RNase III enzyme, Drosha coupled with Di-George critical Region factor (Drosha-DGCR8) cleaves the pri-miRNA transcript to produce a pre-miRNA [143]. Exportin 5 transports the pre-miRNA from the nucleus into the cytoplasm [144, 145]. In the cytoplasm pre-miRNA

undergoes further processing by dicer-TAR binding Protein complex (dicer-TRBP), eliminating the loop sequence on the hairpin to form a double stranded RNA (dsRNA) [146]. This RNA duplex is passed onto an argonaute (AGo2) protein in the RNA-induced silencing complex (RISC) for further processing [147]. Consequently, a 22-nucleotide long strand is retained in the argonaute complex as the guide strand while the other, passenger strand, is discarded [141, 142]. Nucleotide 2-7 of the miRNA referred to as the seed region, is presented to target mRNA and when complementary, post-transcriptional repression and subsequent mRNA degradation occurs [148]. MicroRNA bind the target mRNA forming an imperfect duplex. While mismatches are tolerated in the duplex, the seed region of the miRNA should be perfectly complementary to target mRNA if target recognition is to occur [149].

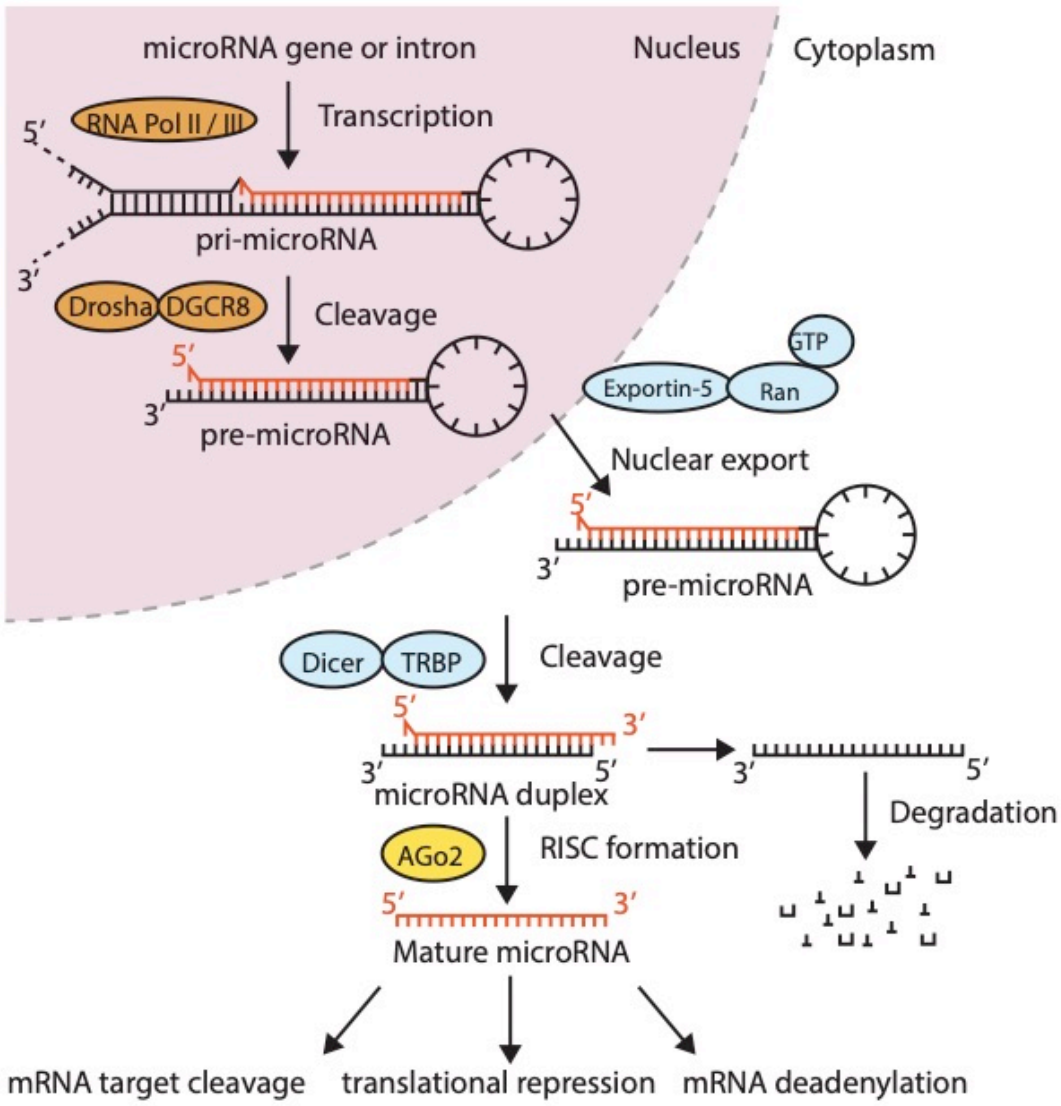

Figure 1.5 Canonical Micro RNA biogenesis Genes encoding miRNAs are transcribed by RNA polymerase II into long primary transcripts (pri-miRNAs). RNase III enzyme, Drosha coupled with Di-George critical region factor (Drosha-DGCR8) cleaves the Pri-microRNA transcript to produce a precursor microRNA. Exportin 5 transports the pre-miRNA from the nucleus into the cytoplasm in a GTP dependent manner. In the cytoplasm pre-microRNA undergoes further processing by

Dicer-TAR binding Protein complex (Dicer-TRBP) to eliminate the loop sequence on the hairpin and a double stranded RNA micro RNA duplex is formed that is loaded onto Argonaute 2 (AGo2) to form the RNA-induced silencing complex (RISC). The leading strand (red) is retained while the passenger strand (black) is degraded. The leading strand constitutes the mature miRNA that binds the 3′ UTR of mRNA to cleave, repress translation or deadenylate mRNA and subsequent regulation of gene expression.

1.9.2 The use of artificial miRNA

Artificial microRNAs (amiRs) are chemically synthesised small RNAs in which the miRNA guide strand and corresponding passenger strand are modified to silence a target gene. AmiRs can encode sequences in the stem region, which when processed by host cell microprocessor produce siRNAs that precisely target mRNA transcripts with 100% complementarity. Introducing artificial miRNA (amiRs) into human cells could be used to induce degradation of homologous mRNA molecules. Although canonical miRNA biogenesis starts from the nucleus, previous studies have that shown cytoplasmic RNA viruses can be modified to produce functional amiRs. Regardless of the site of replication and genomic structure, a virus can encode miRNA, which restrict specific host gene activity [150-154]. Since miRNAs are cell/species-specific in nature, viruses can be modified to efficiently control viral tropism [154, 155]. AmiRs can be designed to maintain the general structure and loop sequence of precursors of amiR (pre-amiR) hairpin but with various specific miRNA sequences inserted in the stem. The pre-amiRs are processed and loaded into the RISC similarly to native host pre-miRNAs. Artificial microRNAs (amiRNA) are essentially a hybrid of the two miRNA and siRNAs. They encode vital structures recognised and processed by the host's cellular miRNA bioprocessor *i.e.*, Drosha and Dicer to produce pre-amiRs. The amiRs also encode artificially engineered sequence within the stem region which when processed, produce siRNA that specifically targets a single mRNA transcript with 100% complementarity (Figure 1.6). Different pre-amiR encoding viruses can be generated with each virus targeting different host genes, to study virus-host interactions. This approach has been used to analyse effect of knocking down various interferon stimulated genes (ISGs) on WNV virulence [154]. Insertions such as hairpin precursors of amiR (pre-amiR) targeting specific host genes are easily tolerated in particular sites of flavivirus genome [153, 156]. When multiple brain-specific miRNAs were inserted in the 3' UTR of a flavivirus genome, there was increased viral suppression in the CNS of mice versus when a single brain-specific miRNA was used [157, 158]. Conversely, studies have shown that insertion of miRNA target sequences at two distant positions of the 3' UTR could result in effective viral repression in cell cultures [159]. With advancement in technology and rising need for safe flavivirus vaccines and therapeutics, microRNA-based approaches are being employed to study virus-host interactions [153, 160]. This is proven an efficient method capable of inhibiting replication and pathogenesis of DNA and RNA viruses in a cell, tissue or species-specific manner [154, 155, 161].

1.9.3 Small interfering RNAs compared to microRNAs

Small interfering RNAs (siRNAs) and microRNAs (miRNAs) affect gene regulation and have been utilised in drug discovery and development against various cancers [162-164] and viral infections [165-167]. Small interfering RNAs are chemically synthesised dsRNA molecules processed in the cytoplasm by Dicer into a smaller dsRNA molecule of approximately 20-23 nucleotides long. This dsRNA is then loaded into RISC, where AGo2 cleaves the passenger strand of the siRNA, leaving the guide strand associated with RISC. The guide strands are designed with 100% complementarity to mRNA. Consequently, RISC binds to mRNA with full complementarity causing specific mRNA target cleavage [168] (Figure 1.6). The unique feature for siRNA is that 100% complementarity is prerequisite to induce mRNA target cleavage and subsequent gene silencing. In contrast, miRNAs do not generally have 100% complementarity to targets, and they tend to block translation rather than mRNA cleavage. Artificial microRNAs (amiRs) are able to serve as siRNAs or miRNA depending on the degree of complementarity to targets with a common outcome of target cleavage.

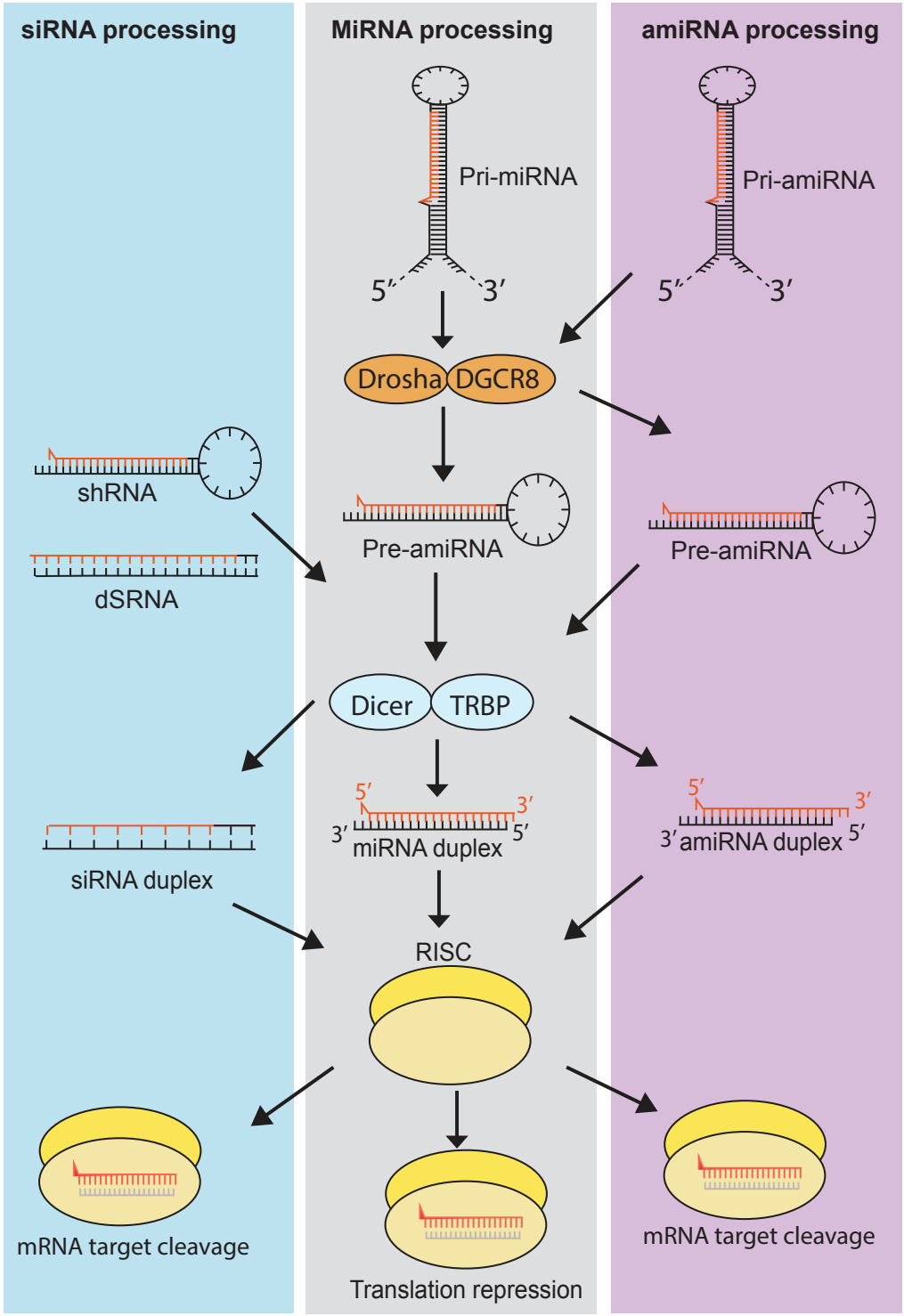

Figure 1.6 Processing of amiR and siRNA in cells compared to miRNA processing. The processing of amiR and siRNA is essentially similar. However, when amiR has 100% complementarity to the corresponding mRNA, it can act as siRNA to cause mRNA target cleavage. Both siRNA and amiR processing require host cell machinery to control gene expression.

1.10 Host anti-viral response against RNA viruses

Following several years of research in how the host immune system fights WNV infection, the antiviral response has been described in three steps namely: (i) detection of invading viruses, (ii)

induction of interferon (IFN) response and (iii) expression of interferon stimulated genes. The early detection of invading viruses is very crucial in controlling virus infections and host cells are adept at detecting virus invasion to establish antiviral responses. Pattern recognition receptors detect unique features on invading pathogens known as pathogen associated molecular patterns (PAMPs), and distinguish between self and non-self. There are at least three classes of pattern recognition receptors relevant to WNV responses, namely retinoic acid-inducible gene I protein (RIG-I)-like receptors (RLRs), toll-like receptors (TLRs), and nucleotide-binding oligomerisation domain (NOD)-like receptors (NLRs). The detection of viral double-stranded RNA (dsRNA), and single-stranded RNA is of particular importance during antiviral signalling against WNV infection [169, 170].

1.10.1 Toll-like Receptors

Toll-like Receptors (TLRs) are type 1 trans-membrane proteins, which possess leucine-rich repeat (LRR) ligand-binding domains and conserved Toll/IL-1 receptor (TIR) signalling domains in the cytoplasmic tail [171, 172]. The TLR family contains ten members named TLR1 to TLR10 in humans and twelve TLR1 to TLR9, TLR11 to TLR13, in mice, shown facilitate innate immune response to viral infections [169, 173]. TLRs are found on cell surfaces, intracellular compartments such as ER, endosomes and lysosomes [174]. TLRs are generally categorized into cell surface TLRs and intracellular TLRs. Cell surface TLRs include TLR1, TLR2, TLR4, TLR5, TLR6, and TLR10 while intracellular TLRs are found in endosomes include TLR3, TLR7, TLR8, TLR9, TLR11 and TLR12 [175, 176]. TLRs identify PAMPs, structures or molecules from damaged cells that are termed as danger associated molecular patterns (DAMPs) to initiate immune responses [177, 178]. TLRs sense various PAMPs such as bacterial lipopolysaccharides, bacterial proteins and viral nucleic acids, bacterial lipoproteins, and flagella among others [179].

Activation of TLRs initiates a cascade of events that lead to activation of transcription factors mainly activator protein 1 (AP-1), interferon regulatory factor (IRF) and Nuclear factor kappa B (NF-κB) [180]. NF-κB drives the expression of many pro-inflammatory cytokines including TNF-α, pro-interleukin-18 (pro-IL-18) and pro-interleukin-1b (pro-IL-1b). Pro-IL-18 and pro-IL-1b are inactive forms that are activated by cytoplasmic caspase-1 protease. Caspase-1 activation is the outcome of activation of the inflammasomes, which can be initiated by a number of NLR proteins. The release of IL-1b and IL-18 enhances the immune response by activating lymphocytes. TNF-α enhances immune response and induces apoptosis by binding onto receptors of infected cells causing cell death [181].

TLR3 found in endosomes is important in activating host immune responses to viral infections.

TLR3 senses viral double-stranded RNA (dsRNA), siRNAs, and self RNAs derived from damaged cells [174]. During WNV infections in a mammalian cell, TLR3 recognizes dsRNAs produced as RNA replication intermediates [182]. Consequently TLR3 TIR domains dimerise and bind to Toll/IL-1R domain-containing adaptor-inducing IFN-β (TRIF) to stimulate IRF-3, NF-κB and IFN-I production [178, 183]. TLR3-deficient (*Tlr3*$^{-/-}$) mice showed susceptibility to lethal WNV as compared to wild type. Additionally, infected mice showed increased viraemia in the periphery and less viraemia and neuropathology in the brain as compared to wild-type mice [184]. Consequently WNV infection in the periphery was thought to damage the blood-brain barrier and facilitate CNS infection in wild-type mice but not in *Tlr3*$^{-/-}$ mice [185].

TLR7 and TLR8 located in endosome recognise ssRNAs to activate IRF-7 and NF-κB and initiate IFN-I response through myeloid differentiation factor 88 (MyD88) signalling [186]. TLR7 is expressed in plasmacytoid dendritic cells (pDCs), and senses viral single stranded ssRNA [174]**.** TLR7 is shown to foster movement of Langerhans cells from the skin when WNV is inoculated into mice through the skin, leading to WNV clearance in mice [187]. MyD88 is a signalling protein utilised by most of the toll-like receptors except TLR3 to stimulate NF-κB activity. MyD88 is an innate immune adaptor molecule shown to control WNV dissemination and replication in the CNS. WNV Infection of MyD88-deficient (*MyD88*$^{-/-}$*)* micewith WNV increased neurological burden compared to WNV infection in wild type mice [188]. Furthermore TRIF and MyD88 double-deficient (*MyD88/Trif*$^{/-}$) mice showed severe WNV infection characterized by increased encephalitis signs and mortality compared to the same infection in wild type mice. Therefore these studies highlighted the role of TLR signalling during early WNV infection [189].

1.10.2 RIG-like receptors

RIG-I-like receptors (RLR) comprise a cytosolic PRR protein family that sense intracellular viral RNA produced by actively replicating viruses [190]. The family consists of retinoic acid-inducible gene I protein, (RIG-I), melanoma differentiation antigen 5 (MDA5) and LGP2 [64, 191]. RLRs contain a DExD/H helicase domain and signal via two caspase activation and recruitment domains (CARDs) at their N termini, leading to subsequent type I interferon (IFN-I) gene expression [192, 193]. Studies have shown that RIG-I signalling occurs is during early stages of WNV infections while MDA5 signalling occurs at later stages of infection [191, 194]. RLRs are ubiquitous in almost all cell types. Following virus infection and stimulation by interferon, levels of RIG-like receptors increase [195].

Cytosolic RIG-I senses short dsRNA sequences, short dsRNAs and adenosine/uridine rich RNAs PAMPs through its repressor domain as non-self (reviewed in [196, 197]). RIG-I binds to RNA structures in a ubiquitination ligase Tripartite motif 25 (TRIM-25) dependent manner to activate

RIG-I signalling [198]. TRIM25 activates RIG-I by adding ubiquitin, stimulating RIG-I signalling pathway in a process controlled by Caspase-12 and 14-3-3-ε proteins [198-201]. Furthermore one study showed that caspase-12 deficient mice exhibited increased WNV disease depicted by CNS dissemination and death, and impaired interferon β (IFN- β) production as compared wild-type mice [199]. Protein 14-3-3-ε stabilizes RIG-I and TRIM25 interaction enabling RIG-I activation [200]. Consequently active RIG-I binds mitochondrial antiviral signalling (MAVS) protein through CARD interactions to form MAVS signalosome, which initiates IRF-3 and NF-κB activation and later IFN-β production [200, 202].

MDA5 is activated by long double-stranded RNA (dsRNA) during virus acute infection and through CARD interactions initiates downstream signalling to induce IFN-I [193]. *In vitro* studies have shown that during acute WNV infection RIG-I and MDA5 sense unique viral RNA features normally absent in mature host RNA species [192, 203]. MDA5 enhances CD8 T cell activation and clears WNV from CNS. When MDA5-deficient (*Mda5*$^{-/-}$) mice were infected with WNV, mice showed increased encephalitis and higher virus burden in CNS than wild type mice [204, 205]. The absence or RIG-I or MDA5 alone reduced innate immune signalling in cells and increased mortality in mice. Furthermore, knock-down of both RLRs caused severe CNS dissemination of WNV and absolute inactivation of innate immune signalling in mice and mammalian cells respectively [191]. Therefore RLR signalling is crucial in initiating IFN-I signalling, innate antiviral responses and control of dissemination of WNV to the CNS [191]. Current research has focused on understanding host PRRs and mechanisms by which these receptors activate antiviral immunity.

1.10.3 Interferon system

Interferons (IFNs) are secreted cytokines that control host processes and possess antiviral and anti-proliferative properties. Interferons directly or indirectly control host immune system by inducing expression of interferon-stimulated genes or inducing major histocompatibility complex expression to subsequently activate immune cells respectively [206]. They are categorised into three classes based on amino acid sequence and recognition by specific receptors, including IFN-I, Type II interferon and Type III interferon [207, 208]. Although IFN-I include Interferon - alpha (α), -beta (β), omega (ω), -epsilon (ε), -kappa (κ), - delta (Δ), -tau (τ) and – zeta (ζ), IFN-α and IFN-β are the most studied members of IFN-I. In addition, numerous cells such as macrophages, lymphocytes, fibroblasts, endothelial cells, osteoblasts and plasmacytoid dendritic cells secrete IFN-α and IFN-β in large quantities during infection. Type I interferons mediate host innate antiviral immune responses by inducing transcription of ISGs, which ultimately control virus replication [209]. When mice deficient in interferon-alpha/beta receptor (*Ifnar1*$^{-/-}$) were infected with sub-lethal WNV, they presented with severe WNV infection as depicted by rapid progression of clinical signs, weight

loss, encephalitis and death compared to wild type mice [210, 211]. These studies highlighted the role of IFN-I in controlling WNV infection. This review will exclusively focus on IFN-α and IFN-β as numerous research studies have shown that IFN-α and IFN-β influence secretion and transcription of ISGs that were studied in the subsequent chapters of this thesis (reviewed in [212]) . In addition, IFN-α and IFN-β are shown to regulate innate immune response to flaviviruses particularly WNV infection [211, 213].

The type II IFN class has only one member, IFN-γ that has been shown to play a critical antiviral role by limiting WNV spread to the CNS. The IFN-γ deficient (*Ifn-γ*$^{-/-}$) mice infected with WNV showed increased viraemia and elevated virus replication in lymphoid tissues [214]. IFN-γ can be secreted by macrophages, natural killer cells (NK), CD4 T helper cells and CD8 cytotoxic T cells. Lastly Type III IFNs includes IFN-lambda λ members such as IFN- λ1, IFN- λ2 and IFN- λ3, which are closely related to type I IFNs and have been shown to restrict WNV infection by maintaining integrity of blood brain barriers [215].

1.10.4 Type I Interferon signalling pathway

Following entry into a host cell, WNV replicates and accumulates dsRNA and ssRNA intermediates that can be recognised via RIG-I, MDA5 in the cytosol and cytosolic DNA sensor known as cyclic GMP-AMP synthase (cGAS), or otherwise by TLR3 and TLR7 in the endosome. Interferons are produced after sensing PAMPs, secreted IFN-α and IFN-β bind to interferon-α/β receptor 1/2 (IFNAR1/2) heterodimer (Figure 1.6) to activate tyrosine kinases of the Janus kinase (JAK) family of proteins. Subsequently the activated JAK proteins phosphorylate STAT proteins to form a complex with IRF9 known as interferon stimulated gene factor 3 (ISGF3) complex. The phosphorylated ISGF3 complex that consists activated forms of STAT1 and STAT2 and IRF9 then translocates to the nucleus where it preferentially binds to interferon stimulated response element (ISRE) to initiate transcription of ISGs (reviewed in [208, 212, 216, 217]. The role of ISGs in virus replication is well studied in mice and humans [218]. Infection of *Ifnar1*$^{-/-}$ and *Stat*$^{-/-}$ mice with sub-lethal WNV strains showed high susceptibility to WNV compared to wild type mice. Host genes such as *RigI, Mda5, cGas, tlr3, Mavs, Irf1, Irf3 and Irf7* have been shown to possess antiviral effects during WNV infection as further discussed in section 1.12. In addition, knockout of *RigI*, *Mda5*, *cGas*, *tlr3*, *Mavs*, *Irf1, Irf3* and *Irf7* mice showed increased viral burden, dissemination of virus to mouse brains, increased weight loss and elevated progression of clinical symptoms on infection with sub-lethal WNV strains (reviewed in [216]).

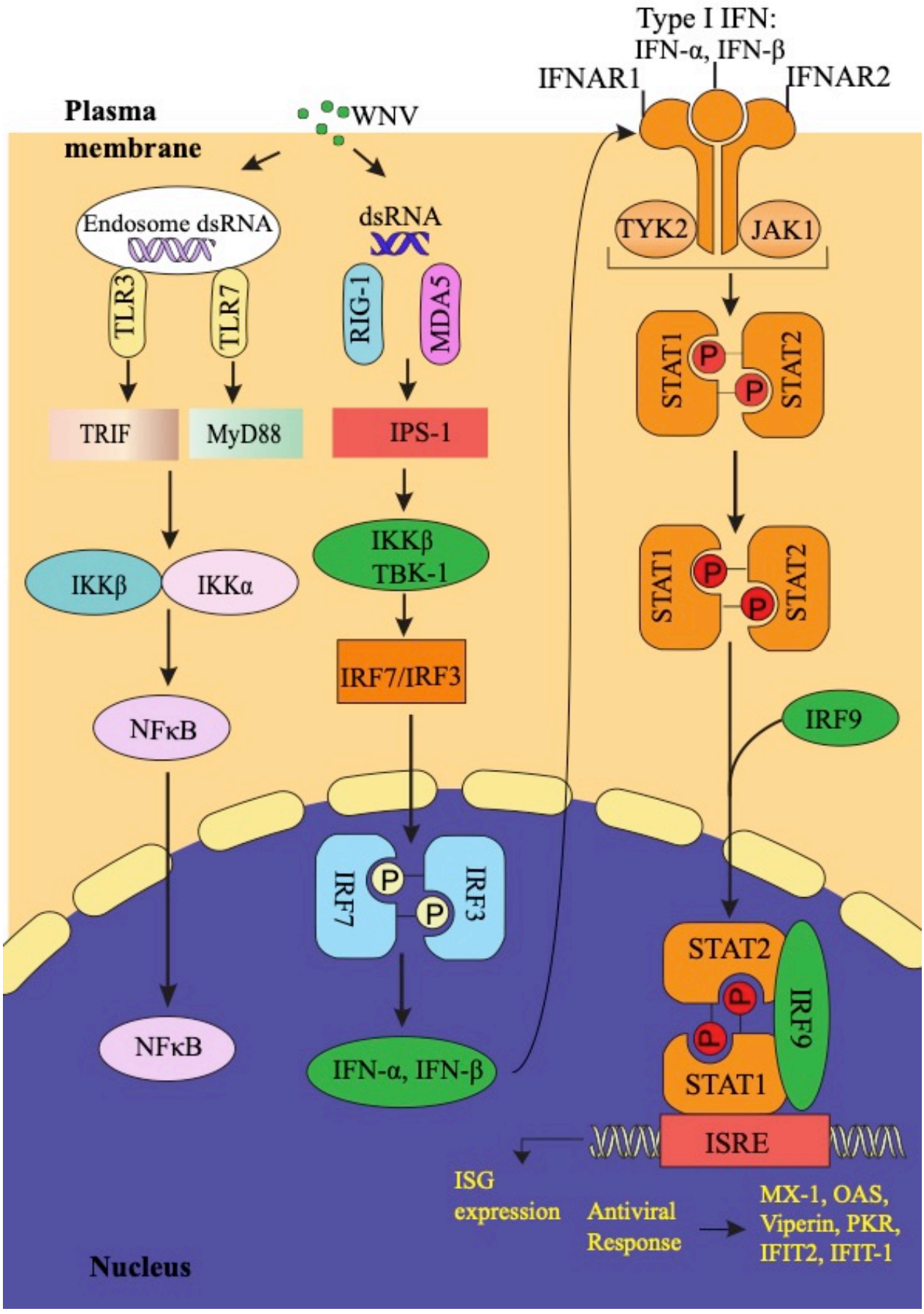
Type I IFN:
IFN-α, IFN-β
IFNAR1
IFNAR2
Plasma membrane
WNV
Endosome dsRNA
dsRNA
TLR3
TLR7
RIG-1
MDA5
TYK2
JAK1
STAT1
STAT2
TRIF
MyD88
IPS-1
IKKβ
IKKα
IKKβ
TBK-1
IRF7/IRF3
IRF9
NFκB
IRF7
IRF3
STAT2
IRF9
STAT1
NFκB
IFN-α, IFN-β
ISRE
ISG expression
Antiviral Response
MX-1, OAS, Viperin, PKR, IFIT2, IFIT-1
Nucleus

Figure 1.7 Induction of type I interferon signaling during WNV infection: During WNV infection, endosomal RNA sensors TLR3 and TLR7, together with cytoplasmic RNA helicases RIG-I and MDA5 detect viral dsRNA and ssRNA. As a result, these PRR are activated and subsequent adaptor molecules recruited. In case of TLRs, TRIF and MyD88 interact with TLR3 and TLR7 respectively. Consequently, two kinase complexes TAK1 (transforming growth factor-β-activated kinase 1), TBK1 (TANK-binding kinase 1) and IKKε (inhibitor of κB kinase epsilon) are activated together with IKKα and IKKβ. On the other hand, RIG-I and MDA5 interact with the adaptor molecule mitochondrial anti-viral signaling (MAVS), which is localized to mitochondria to activate TBK1 and IKKβ and eventual activation of IRF3, IRF7 and nuclear factor-κB (NF-κB) respectively. The activated transcriptional factors translocate into the nucleus and induce the expression of IFNs as well as pro-inflammatory cytokines. Secreted IFN-α and IFN-β bind to IFNAR1/2 receptor complex. This in turn leads to activation of tyrosine and Janus kinases (TYK2 and JAK1) that recruit and activate STAT1 and STAT2 by phosphorylation. Phosphorylated STAT1 and STAT2 then form a trimeric complex with IRF9 known as ISGF-3 that is translocated to the nucleus. In the nucleus ISGF-3 binds to ISRE promoter element to initiate expression of more than 300 interferon-stimulated genes, which possess antiviral activities. (Adapted and modified from Ivashkiv *et al*., 2014 [212])

1.11 West Nile virus evasion of the host immune response

West Nile virus is an obligate intracellular parasite that requires access to host cellular compartments and as such this requires evasion, inhibition and subversion of host innate immune response to permit productive infection. WNV NS4B inhibits the IFN-I signalling by blocking phosphorylation of JAK and STAT transcription factors to inhibit expression of interferon stimulated genes [219]. Furthermore, WNV overcomes IFN signalling by reducing IFNAR1 production and blocking IFN-β transcription [220, 221]. WNV-E protein has been shown to block RIG-1 and TLR3 signalling through receptor-interacting protein 1to inhibit prompt production of antiviral cytokines and activation of immune cells against WNV infection [222]. In addition, WNV NS1 protein antagonises the TLR3 pathway by inhibiting IRF3 and NF-κB translocation to the nucleus [223]. Furthermore, WNV NS5 inhibits IFN-I signalling by blocking STAT1 and STAT2 phosphorylation [102, 119]. WNV also limits the effects of the expressed ISGs such as OAS1b, IFIT, MxA proteins [224-227]. Just as WNV is equipped to evade the host immune response, the host immune system has a well-established defence mechanisms that recognise WNV evasion and eventually limit its spread and CNS dissemination, such as use of PAMPS, induction of interferon response and activation of ISGs (reviewed in [228]).

1.12 Host determinants controlling WNV infection

In the past twelve years an immense amount of work has been done to understand host factors that influence WNV infection through *in vitro* and small interfering RNA (siRNA) screens. As a result, the role of various host factors that influence viral infection in mice, and human cells has been highlighted. Host factors such as known PRRs (RIG-I, MDA5, cGAS), TLRs (TLR3 and TLR7),

NLRs (NLRP3, ASC, AIM2), transcription factors (IRF 1, 3, 5 and 7 and ATF3), and ISGs (Mavs, Stat2, IFITM2, IFITM3, IFIT2, IFIT3, PKR, Viperin, ASCC3) have been identified [15, 218]. Although the precise mechanisms of action of the identified novel host genes against WNV are still undefined, novel anti-viral proteins such as HPSE, NAMPT, PBEF1, SAAI, PHF15, DDX24, IFI44L, IFI6, TRIM21, TRIM6 among others have been identified [209, 229-231]. The use of *Rig-I*$^{-/-}$, *Mda5*$^{-/-}$, *Mavs*$^{-/-}$, *Irf3*$^{-/-}$, *Irf5*$^{-/-}$, *Irf7*$^{-/-}$, *Viperin*$^{-/-}$ and *Pkr*$^{-/-}$ mice has revealed their antiviral mechanisms [191, 232, 233]. Furthermore, novel host antiviral factors that influence WNV infections have been identified [234, 235]. However more extensive research is still required to understand how these host factors suppress WNV infection, and use of $WNV_{NSW2011}$ provides a convenient tool to allow studies under PC2 containment conditions.

1.13 Overall aim of the project

The overall aim of this thesis was to provide a better understanding of WNV-host interactions in context of natural disease and identify host genes that control West Nile Virus infection *in vitro* and *in vivo*. In order to achieve this, $WNV_{NSW2011}$ was modified to encode artificial micro RNA (refered to as amiR) in the 3' UTR. Each inserted precursor of amiR hairpin (pre-amiR) encodes a unique amiR sequence that targets a specific region of cognate mouse gene. Consequently amiR-encoding $WNV_{NSW2011}$ virus libraries were generated and used as a tool to study WNV-host interactions.

1.14 Hypothesis

In vivo and *in vitro* RNAi screening with libraries of WNV producing siRNAs that target specific mouse interferon stimulated genes will allow identification of host genes that influence west Nile virus replication.

1.15 Specific aims to test the hypotheses

To identify host factors controlling WNV infection under *in vitro* and *in vivo* conditions by RNAi screening with WNV libraries three aims were stipulated.

- Firstly, an amiR-encoding plasmid library was to be generated as a tool for generating subsequent amiR encoding virus libraries.
- Next we aimed at performing *in vitro* and *in vivo* RNAi screening to identify host factors that control virus replication both *in vitro* and *in vivo* using the generated virus libraries.
- The last aim of this thesis was to characterise the identified host factors to determine how these host factors influence West Nile virus replication

Chapter 2: General Materials and methods

This chapter describes the general materials and methods used across all the three results chapters. Specific materials and methods are included in each respective chapter.

2.1 Materials and Reagents

Table 2.1: Table showing list of reagents and materials used to perform the different experiments performed to test hypothesis and achieve set project aims.

Reagents	Manufacturer
Amicon Ultra-15 centrifugal filter units (100K)	Merck (USA)
RNA Nucleospin Extraction kit	Machery-Nagel (GmbH & Co. KG, Germany)
TRI LS	Sigma Aldrich Pty Ltd (St Louis Missouri, USA)
TRI reagent	Sigma Aldrich Pty Ltd (St Louis Missouri, USA)
DNA gel extraction Kit	New England BioLabs (Ipswich, MA USA)
10 × Blocking Buffer	Thermo Scientific (Waltham MA, USA)
Lipofectamine LTX	Thermo Scientific (Waltham MA, USA)
Optimem	Thermo Scientific (Waltham MA, USA)
GXL polymerase Kit	Taraka Bio (USA, Mountain view, California)
One Step RT-PCR	Thermo Scientific (Waltham MA, USA)
Agarose	Sigma Aldrich Pty Ltd (St Louis Missouri, USA)
RedSafe	Montreal Biotech Inc (Canada)
Protein Ladder Kaleidoscope	BioRad (California, USA)
IFITM3 Polyclonal Rabbit IgG	ProteinTech, Rosemont, Illinois, USA
CLEC4E Monoclonal mouse	Abcam, Cambridge, UK
PARP11 Rabbit Polyclonal	Proteintech, Rosemont, Illinois, USA
ATF3 (D2Y5W) Rabbit monoclonal Ab	Cell signalling Technology, (Massachusetts, USA)
IRF7 (H-246) Rabbit Polyclonal IgG	Santa Cruz Biotechnology, Inc (Dallas, U.S.A)
Mouse WNV-E 4G2	In house

Human WNV-E E-16	In house
Dulbecco's Modified Eagle Media	Sigma Aldrich Pty Ltd (St Louis Missouri, USA)
Phosphate Buffered Saline	ChemStore, Australia
Tween 20	Sigma Aldrich Pty Ltd (St Louis Missouri, USA)
NuPage 4-12 bis-tris 15 well Protein gels	Thermo Scientific (Waltham MA, USA)
NuPage 4-12 bis-tris 10 well Protein gels	Thermo Scientific (Waltham MA, USA)
RPMI	Sigma Aldrich Pty Ltd (St Louis Missouri, USA)
Glutamax	Thermo Scientific (Waltham MA, USA)
Penicillin-Streptomycin	Thermo Scientific (Waltham MA, USA)
Carboxymethyl cellulose	Sigma Aldrich Pty Ltd (St Louis Missouri, USA)
M199 Media	Sigma Aldrich Pty Ltd (St Louis Missouri, USA)
Q5 high-fidelity DNA Polymerase	New England BioLabs, (Ipswich, MA USA)
Wizard Plus SV miniPreps DNA purification system	Promega (Madison, Wisconsin, USA)
Fetal Bovine Serum	Sigma Aldrich Pty Ltd (St Louis Missouri, USA)
1× PBS-T	In house
1X PBS	In house

2.2 DNA manipulations

The exact primer sets, DNA and RNA templates as well as plasmids used to perform experiments included in this table below

Table 2.2: List of primers, PCR templates sequences and corresponding PCR amplicon generated

Primer Name	**Amplicon Name**	**Sequence 5 ′- 3 ′**
Amplicon_adaptor_F	Δ15-89 cDNA	TCGTCGGCAGCGTCAGATGTGTATAAGAGACAGGAAGACACGACATTTGTTGAGGATACAGTATTGTAAATAGTTTG
Amplicon_adaptor_R		GTCTCGTGGGCTCGGAGATGTGTATAAGAGACAG CAT TCA AGT GCA GCC GTA GGC TCC GC
Flavi UTRlinker_F	UTR-linker	GTGGTGCGAGAACACAGGA

Flavi UTRlinker_r		CAGCTCACACAGGCGAACTACT
5′UTR_F	5′UTR+ C-prM-E	AGTAGTTCGCCTGTGTGAGCTG
C-prM-E_R		GGAAAGAAAGAGCAGAACTCCTCCAAC
NS1_F	NS1-2A-2B	GTTGGAGGAGTTCTGCTCTTTCTTTCC
NS2B_R		CTCCTCTCTTTGTGTATTGGAGAGTTATC
NS3_F	NS3	GATAACTCTCCAATACACAAAGAGAGGAG
NS3_R		CCTGAGGCGAAGTCTTTGAA
NS4_F	NS4A-4B	TTCAAAGACTTCGCCTCAGG
NS4B-R		CGTCCTTTTGCCCCACCTC
NS5_F	NS5	GAGGTGGGGCAAAAGGACG
NS5_R		GTGTATCCTCAACAAATGTCGTGTCTTC
3'UTR_F	3'UTR	GAAGACACGACATTTGTTGAGGATACAG
3'UTR_R		TCCTGTGTTCTCGCACCAC
Bef AmiR_R	NS5-Before AmiR	AGAGCAGAGTCTCTGATCTTGAT
AmiR_F	AmiR	ATCAAGATCAGAGACTCTGCT
AmiR_R		TTCAAGTGCAGCCGTAGGCTCCGCTCT

2.2.1 Polymerase chain Reaction (PCR)

Before performing any PCR, laboratory bench tops were thoroughly cleaned and disinfected using 70% ethanol. PCR mixes were prepared as per manufacturer's instructions using nuclease free water. The Q5 high fidelity DNA polymerase (New England Biolabs, USA) or PrimeSTAR GXL DNA Polymerase (Clontech, USA) PCRs were performed to generate high fidelity amplifications. Taq Polymerase kit (Thermo Scientific, USA) for PCR was used to generate low fidelity reactions such as DNA contamination tests. Primers used for PCR reactions were designed according to Integrated DNA Technologies (IDT, USA) primer design instructions and PCR thermal cycles were performed using SimpliAmp™ Thermal Cycler (Thermo Scientific USA).

2.2.2 Agarose gel Electrophoresis

Depending on the expected DNA bands size, agarose gels were cast by disolving 1% or 2% (w/v) agarose in 1 × TAE buffer containing 0.2 μg/mL RedSafe and left to set. A mixture of 1× loading dye and DNA samples were loaded into gel along with an appropriate DNA Ladder loaded and

electrophoresis performed in 1 × TAE buffer at 110V for 40 minutes. The gel was visualized under Gel Logic 212 PRO UV/white light trans-illuminator (Carestream, USA) and gel image captured using a camera for documentation. DNA band sizes were compared to appropriate DNA Ladder in order to determine their sizes. The UV trans-illuminator was only used to determine the band sizes and capture the gel picture since UV distorts DNA. In cases where the DNA bands were required for subsequent experiments, Safe Imager Blue light trans-illuminator (Invitrogen, USA) was used to view gel images. Thereafter, bands were excised, purified and quantified as described below.

2.2.3 DNA extraction from gels and quantification

Basing on the DNA ladder, the correct DNA fragments were excised from the agarose gel using a sterile scalpel blade and placed in a DNase free-labelled microfuge tube. The DNA fragments were purified using Monarch DNA Gel Extraction Kit (New England BioLabs, USA) according to manufacturer's instructions. DNA concentrations were determined by either using Nanodrop 1000 spectrophotometry (Thermo Scientific, USA) or Qubit fluorometer and Qubit dsDNA BR Assay Kit (Thermo Scientific, USA) following manufacturers' instructions.

2.2.4 DNA Sequencing

Purified plasmid DNA was prepared for sequencing following Australian Genome Research Facility's (AGRF) recommendations. 0.2-1µg of DNA was prepared into 12 µL reaction by adding 1uL of 10µM sequencing primer and topping up with ultra pure nuclease free water. The resultant DNA mix was sent to AGRF for Sanger DNA sequencing. For Deep sequencing the correct DNA purified amplicon PCR fragment was diluted to at least 20 ng/ µL and sent Australian Centre of Ecogenomics (ACE) for amplicon deep sequencing.

2.3 RNA manipulations

2.3.1 Viral RNA isolation from culture fluid

Viral RNA was isolated from virus culture fluid using Nucleospin RNA virus kit and protocol (Macherey-Nagel, Germany). Extracted purified RNA was treated with RQ1 RNase-Free DNase I kit (Promega USA) according to manufacturer's protocol to remove of any DNA contamination from transfection.

2.3.2 Viral RNA isolation from cells

Total RNA was extracted from Vero cells at 3 days post infection (dpi) using TRI Reagent (Sigma-Aldrich, USA), according to manufacturer's instructions. Extracted RNA was re-suspended into 50 µL of ultra pure nuclease free water and RNA concentration determined by using Nanodrop spectrophotometry (Thermo Scientific, USA).

2.3.3 Generation of $WNV_{NSW2011}$ cDNA fragments

RNA was extracted from wild-type $WNV_{NSW2011}$ (WT-WNV) stocks previously generated by infecting Vero cells using TRI Reagent Sigma-Aldrich (St Louis Missouri, USA) according to manufacturer's instructions. Complementary DNA (cDNA) was synthesised from purified RNA using Superscript IV reverse transcriptase (Thermo Scientific, USA) kit and protocol. Subsequently generated cDNA was used as DNA template for, Q5 high-fidelity DNA polymerase PCR (New England Biolabs, USA) PCR along with precise sets of oligonucleotide primers (Table 2.1). As aresult , overlapping cDNA fragments of $WNV_{NSW2011}$ genome were generated. Thereafter, 1% (w/v) agarose TAE gel electrophoresis was performed and generated $WNV_{NSW2011}$ cDNA fragments were excised from gel and later purified using Monarch DNA Gel Extraction Kit (New England BioLabs, USA) as per manufacturer's instruction. Purified fragments were eluted in ultra nuclease-free water and DNA concentrations determined using Nanodrop spectrophotometry (Thermo Scientific, USA). The fragments were stored at −20°C until required for Circular polymerase Extension Reaction (CPER) reaction to make infectious $WNV_{NSW2011}$ cDNA.

2.4 Culturing of cells

Mammalian cells such as green monkey kidney epithelial Vero cells, 293T human embryonic kidney (HEK), wild type (WT MEF) and IFNAR knock out mouse embryonic fibroblasts (*Ifnar1*$^{-/-}$ MEF) were cultured in Dulbecco's modified Eagle medium (DMEM) while A549 cells were cultured in F-12K media. Cells were supplemented with 10% foetal calf serum (FCS), 50 units/mL of penicillin and 50 μg/mL of streptomycin. Mammalian cells were cultured at 37°C in a 5% Carbon dioxide (CO_2) humidified incubator. *Aedes albopictus* clone C6/36 mosquito cells were propagated in Roswell Park Memorial Institute (RPMI) 1640 medium supplemented with 10% foetal bovine serum 50 units/mL of penicillin and 50 μg/mL of streptomycin and incubated at 28°C in a 5% CO_2 humidified incubator.

2.5 Circular Polymerase Extension Reaction

Circular Polymerase extension Reaction (CPER) is an accurate rapid and cheap method used to generate infectious cDNA [236, 237]. It assembles multiple overlapping cDNA fragments along with UTR flavi-linker and a CMV promoter upstream of the WNV cDNA to produce full-length infectious $WNV_{NSW2011}$ cDNA. The UTR linker consists of a CMV promoter for constitutive expression in mammalian cells while Hepatitis Delta Virus ribozyme (HDVr) region for cleavage of poly adenylation tail added to WNV genome during transfection. Lastly, the poly Adenylation signal (pA-signal) allows effective termination of WNV transcription by RNA polymerase II as a poly-A tail is added to WNV genome and cleaved to form an authentic 3' UTR [237]. To generate

individual viruses, a total of 0.5 ρmol concentration of each viral reverse transcriptase (RT) amplicon was assembled using Q5 high fidelity DNA polymerase (New England Biolabs, USA), Deoxynucleotides (dNTPs) and under low cycle PCR conditions to form infectious cDNA product. Reverse transcriptase amplicons were designed to have over-lapping ends and the last RT-PCR amplicon end overlapped with the UTR linker fragment for correct circularization of cDNA. During CPER, RT-amplicons are denatured and overlapping ends anneal to each other. Thereafter, Q5 high-fidelity DNA polymerase then extends neighbouring fragment as a primer to form circular infectious cDNA product [237]. The generated CPER products were stored at −20°C until required for transfection into human embryonic kidney (HEK) 293 cells

2.6 Transfection of HEK 293T cells to passage zero (p0) to recover virus stocks

Human embryonic kidney fibroblast cells were seeded at 5×10^5 cells per well in a six well plate and incubated in a 5% CO_2 humidified incubator at 37 °C for 12 hour until 95% confluent. The next day, HEK 293 cells were transfected with CPER products using Lipofectamine LTX following manufacturer's protocol and plates returned to a 5% CO_2 humidified incubator. At 5 hours post transfection, CPER-transfection mix was removed and replaced with DMEM supplemented with 10% FCS, 50 units/mL of penicillin and 50 µg/mL of streptomycin. The plates were incubated at 37°C in a 5% CO_2 humidified incubator for 3 days or until cytopathic effect (CPE) was observed when cells were viewed under microscope. Thereafter, virus culture fluid was collected as p0-293T virus stock and virus stock titres determined by immunoplaque assay on Vero cells monolayer.

2.7 Immuno-plaque assay

Vero and C6/36 cells were seeded at 2×10^4 cells and 1×10^5 cells per well in 96-well plates respectively and incubated at 37 °C and 28°C for 12 hour in 5% CO_2 incubator until 95% confluent respectively. The next day, virus samples were diluted in ten fold serial dilutions in DMEM supplemented with 50 units/mL of penicillin and 50 µg/mL of streptomycin and 5% FCS. Thereafter, 25 µL from each dilution was added to each well of cells and incubated at 37 °C for two hours. At two hours post-infection, 175 µL of overlay media, made by mixing ×2 M199 medium (2 M199 medium supplemented with 5% FCS, 50 units/mL of penicillin and 50 µg/mL of streptomycin) with 2% carboxymethyl cellulose in a ratio of 1:1 was added to each well and plates incubated for 36 hours and 96 hours for Vero and C6/36 cells respectively. At 36 hpi and 96 hpi, the overlay was removed and 100 µL of ice-cold 80% acetone in phosphate buffered saline (PBS) was added and incubated at –20°C for 1 hour to fix the cells before completely air-drying the plates. To detect WNV-E protein, plates were first blocked by adding 50 µL of Pierce Clear Milk Blocking Buffer (Thermo Scientific, USA) to each well and incubating the plates at 37 °C for 1 hour.

Thereafter, 50 µL of mAb 4G2 (mouse anti-E) was added to each well and plates incubated at 37°C. Plates were then washed six times using 1× PBS containing 0.05% Tween 20 (PBS-T) to remove any traces of unbound primary antibody before adding 25 µl of IRDye 800 cw Goat anti-Mouse, (LI-COR, USA) as secondary antibody to each well. Plates were then incubated at 37 °C for 1 hour and thereafter washed six times, air-dried and then kept in the dark at room temperature until ready for imaging. Plates were scanned using the LI-COR Biosciences Odyssey Infrared Imaging System with the following specifications: channel =800, intensity = auto, focal length = 3 mm, resolution = 42 µm. Viral titres from iPA are expressed as pfu/mL

2.8 Generation of passage one (p1) of virus on Vero cells

To generate p1-vero virus stocks, Vero cells were seeded at 2×10^6 cells in a T175 flask and flask incubated at 37 °C for 12 hour until 95% confluent. The next day, cells were infected with p0-293T virus stock at MOI =1 in 3 mL of DMEM media supplemented with 50 units/mL of penicillin and 50 µg/mL of streptomycin and flasks incubated at 37 °C for 2 hours, with rocking the flask every 15 minutes. At 2 hours post infection, virus-DMEM mix was removed and replaced with fresh DMEM supplemented with 5% FCS, 50 units/mL of penicillin and 50 µg/mL of streptomycin. The flasks were incubated at 37°C in a 5% CO_2 humidified incubator for 3 days or until cytopathic effect (CPE) was evident. Thereafter, virus culture fluid was harvested as p1-Vero virus stock and virus titres determined by immunoplaque assay on Vero cells monolayer. Each generated virus stock was Sanger sequenced to confirm that the correct intended virus was generated as described above.

2.9 Deep sequencing and analysis of deep sequence

On generation of amplicons for deep sequencing, DNA gel extraction was performed; samples eluted in nuclease free water and submitted to Australian Centre for Ecogenetics (ACE) for deep sequencing. On deep sequencing, data were downloaded from ACE website and analysed using a Salmon transcription tool and protocol as described in appendix 2. Deep sequence reads produced pre-miRNA encoding the following sequence, ATCAAGATCAGAGACTCTGCTCT-XXXXXXXXXXXXXXXXXXXXX-ATTTAATGTCATACAAT-XXXXXXXXXXXXXXXXXXXXX-AGAGCGGAGCCTACGGCTGCACTTGAA. All reads possessed the known sequence shown and Xs (two stretches of 21 nucleotides on either side) were the region of interest containing unique corresponding siRNA sequences.

Chapter 3: Generation of amiR-encoding libraries

3.1 Introduction

This chapter describes how amiR-encoding plasmid library was generated as a tool for generation of subsequent p0-293T and p1-Vero amiR-encoding virus libraries. It highlights the advantages of using CPER to generate virus libraries and some of the bottlenecks encountered during generation of libraries.

3.1.1 Use of Artificial micro RNA to study flavivirus-host interactions

Conventional approaches have facilitated study of host responses to flavivirus infections and subsequently enabled identification of host genes that influence flavivirus infection. Some well-studied approaches include use of knockout mouse models and reverse genetics using both cell culture infections and *ex-vivo* analysis (reviewed in [63]). Knockout mice with defects in type I IFN production or sensing pathways, such as *Rig-I*$^{-/-}$, *Ifih1*$^{-/-}$, *Mavs*$^{-/-}$ *and Ifnar1*$^{-/-}$ infected with sub-lethal WNV strains showed significant increase in mortality and morbidity compared to wild type controls [191, 202, 211]. Further mechanistic studies corroborated the role of these genes in controlling WNV [223, 238-240]. Therefore, knockout mice studies have been used to elucidate role of RLR signaling pathways in controlling WNV infection *in vivo*.

Numerous known and novel ISGs have been confirmed to hinder flavivirus infection, by *in vitro* ISG over-expression and RNAi screens [150, 229, 230, 235, 241-249]. The gain-of-function approach involves over-expression of specific host gene and studying the effects on virus infection. A decline in virus replication following ISG over-expression indicates that the over-expressed gene inhibits virus replication and *vice versa*. *In vitro* over-expression of 36 ISGs in HEK 293 cells revealed viperin and ISG-20 as novel antiviral host genes against West Nile and dengue viruses and confirmed the role of IFITM2 and IFITM3 in antagonising the initial steps of WNV and dengue virus lifecycle [209]. Mechanistic studies revealed that both viperin and ISG-20 genes hindered RNA virus replication. This study not only identified novel ISGs that antagonise WNV infection but also revealed that the flavivirus antiviral system is mediated by numerous ISGs that work together to hinder different stages of flavivirus life cycle. Additionally, a Lentivirus-based screening approach with 380 human ISGs identified MDA5, cGAS, IRF1, ATF3, IRF7 as well as NAMPT, PBEFI, SAAI and PHFIS to restrict West Nile virus infection [218, 245].

Conversely, use of loss-of-function approach can utilise RNAi to understand host-virus interactions.

RNAi studies predominantly use an artificial microRNA (amiR) platform such as siRNA or small hairpin RNA (shRNA) to knockdown gene expression and evaluate the impact of gene knockdown on virus replication. These act similarly to microRNAs (miRNAs), that are genome-encoded small non-coding RNAs usually 21-23 nucleotides long that regulate post-transcriptional gene expression in eukaryotic organisms [250]. RNA interference screening methods involve introduction of amiRs particularly siRNA into cells to induce degradation of homologous mRNA molecules. Artificial miRNAs can be designed to maintain the general structure of pre-amiR hairpin with specific miR sequence in the stem that targets a cognate mRNA sequence to inhibit gene expression. Most RNAi screening methods result into sequence-specific cleavage, suppression of translation and de-adenylation of cognate mRNA targets causing post-transcriptional gene silencing (reviewed in [251, 252]). Following gene knockdown, an increase in virus replication implies that the gene that is knocked down inhibits virus replication and is an antiviral gene. Consequently loss-of-function studies are used to identify and define the roles of novel or known virus-host factors that influence virus replication.

Numerous RNAi screening approaches have been employed to study virus-host interactions. For instance, a genome-wide RNAi screen containing 21,000 human genes identified host genes associated with virus infection in cells. Consequently 305 human host genes that affected West Nile virus infection were identified. Of these, 283 genes were host susceptibility factors required for optimal virus infection, and 22 were host factors restricting viral output [229]. Furthermore, another RNAi screen used an shRNA flow cytometry approach to screen for host genes that influence West Nile virus infection in human cells. Subsequently, 46 antiviral genes including MAVS, STAT2, IRF1, IFITM2, PKR, known ISGs DDX24, IFI44L, IFI6, TRIM2, TRIM6 and novel genes such as activating signal co-integrator complex 3 (ASCC3) were identified as antiviral genes against West Nile virus infection. Mechanistic studies and RNA sequencing revealed that ASCC3 utilises IRF-3 and IRF-7 transcription factors to regulate ISG activity [230]. Furthermore, Clustered Regularly Interspaced Short Palindromic Repeats (CRISPR) based study with library containing 77,406 single genome RNAs targeting 20,121 genes identified seven genes such as EMC2, EMC3, SEL1L, DERL2, UBE2G2, UBE2J1, and HRD1. Further mechanistic knockout studies showed that the identified genes were linked to WNV-induced cell death [253].

Collectively large-scale over-expression and RNAi screens have facilitated understanding of host-virus interactions *in vitro* [209, 218, 229, 230]. Both approaches have not only identified previously known ISGs and uncovered novel ISGs that control West Nile virus infection but revealed novel cellular pathways and possible drug targets for development of antivirals (Reviewed in [232, 254]).

Although conventional methods have greatly facilitated the understanding of West Nile virus immunobiology, these strategies have several drawbacks. Conventional approaches exclusively rely on studying a single immune component or pre-selected collections of knockdown gene targets. However, virus infections induce an arsenal of antiviral host pathways that work in concert to limit severity of infection. Therefore, conventional approaches often portray a non-comprehensive representation of host response to virus infection (reviewed in [63, 242, 249]). Eliminating one antiviral gene could be counteracted by alternative antiviral pathway [209]. Individually over-expressed ISGs often do not interact with other regulatory ISGs present during antiviral response and virus infection. Furthermore most previous screens have been performed in cell lines such as HeLa and Huh-7 cell lines, that could portray different antiviral effects than the host cells normally infected in an *in vivo* infection model. Lastly, all genome-wide studies are limited to *in vitro* experiments due to it being unfeasible to study large panels of knockout mice.

Recently, a novel *in vivo* RNA interference screening method that allows direct measure of virus infection and study of host-virus interactions in a biological setting was developed [151]. This RNAi screening approach bypassed some of these hurdles as it allowed identification of host genes closely linked with virus pathogenesis. In order to identify novel host genes controlling Sindbis virus replication, this RNA virus was designed to encode unique amiRs that target specific host genes. Under normal infection, Sindbis amiR-encoding virus libraries were subjected to selective pressure to identify host factors that control virus replication *in vitro* and *in vivo*. Consequently known ISGs and two new mouse host genes related to transcription; zinc finger protein x (*Zfx*) and MAX gene-associated protein (*Mga*), restricted Sindbis virus replication *in vitro* and in mice respectively. Notably, further conventional siRNA-depletion studies in cells followed by RNA-seq analysis showed that loss of *Zfx* and *Mga* resulted in an intense re-modeling of the cellular transcriptome and an extensive loss of activation of many anti-viral genes, implicating the broader role of *Zfx* and *Mga* in induction of antiviral responses [255, 256]. Thus this *in vivo* RNAi screening approach represented a unique strategy for studying virus-host interactions in the context of viral infection as it relied on the power of virus competition and selection. Based on this approach, we aimed to identify novel host genes that influence West Nile virus replication both *in vitro* and *in vivo* by utilising ISG-targeting amiR-encoding West Nile virus libraries.

3.1.2 Prior optimisation of pre-amiR hairpin insertion site in 3′ UTR of $WNV_{NSW2011}$

In order to generate virus libraries that encode ISG-targeting pre-amiR hairpins, it was first necessary to find a suitable site in the WNV genome for insertion of the pre-amiR sequence, that would minimally disrupt viral replication. Furthermore the chosen site would have to stably retain the inserted pre-miRNA hairpin and also allow proper processing of pre-miRNA into a functional

amiR. A prior preliminary study (Setoh *et al*., unpublished data) screened different sites in 3′ UTR of $WNV_{NSW2011}$ to identify an optimal site for insertion of a hairpin encoding artificial microRNA targeting GFP (GFP amiR).

A 109-nucleotide pre-miR-124 hairpin in which miR-124 3p sequence was replaced with an siRNA targeting the coding region of green fluorescent protein (GFP) was designed (Figure 3.1 A) (Setoh *et al.,* unpublished). To enable efficient processing of GFP-siRNA by host miRNA-processing machinery, the sequence complementary to GFP-siRNA (5p region) was also modified to maintain the pre-miR-124 RNA structure (Figure 3.1 A) [151].

Four sites within domain I of $WNV_{NSW2011}$ 3′ UTR, which contains SL-I to CS3, were selected for insertion because this region contains the least conserved sequences in flaviviruses (Figure 3.1 B) [14, 257]. Mutants 44 (top of SL-I loop), 177 (between RCS3 and SL-III), 214 (top of SL-III loop) and 331 (after CS3) consisted of GFP pre-amiR inserted at respective nucleotide positions in the 3′ UTR. The Δ15-89 and Δ187-244 mutants had the native SL-I and SL-III structures deleted and replaced with GFP pre-amiRs respectively (Figure 3.1 B). The CPER approach, as described in methods [109, 237, 258], was then used to recover all 6 viruses (44, 177, 214, 313, Δ15-89 and Δ187-244). Further *in vitro* and *in vivo* characterisation of mutant viruses revealed that both Δ15-89 and 44 mutants stably retained GFP pre-amiR insertion. However, the Δ15-89 mutant displayed the least attenuation in mice compared to WT-WNV (Setoh *et al.,* unpublished). Therefore Δ15-89 insertion site was chosen for this project.

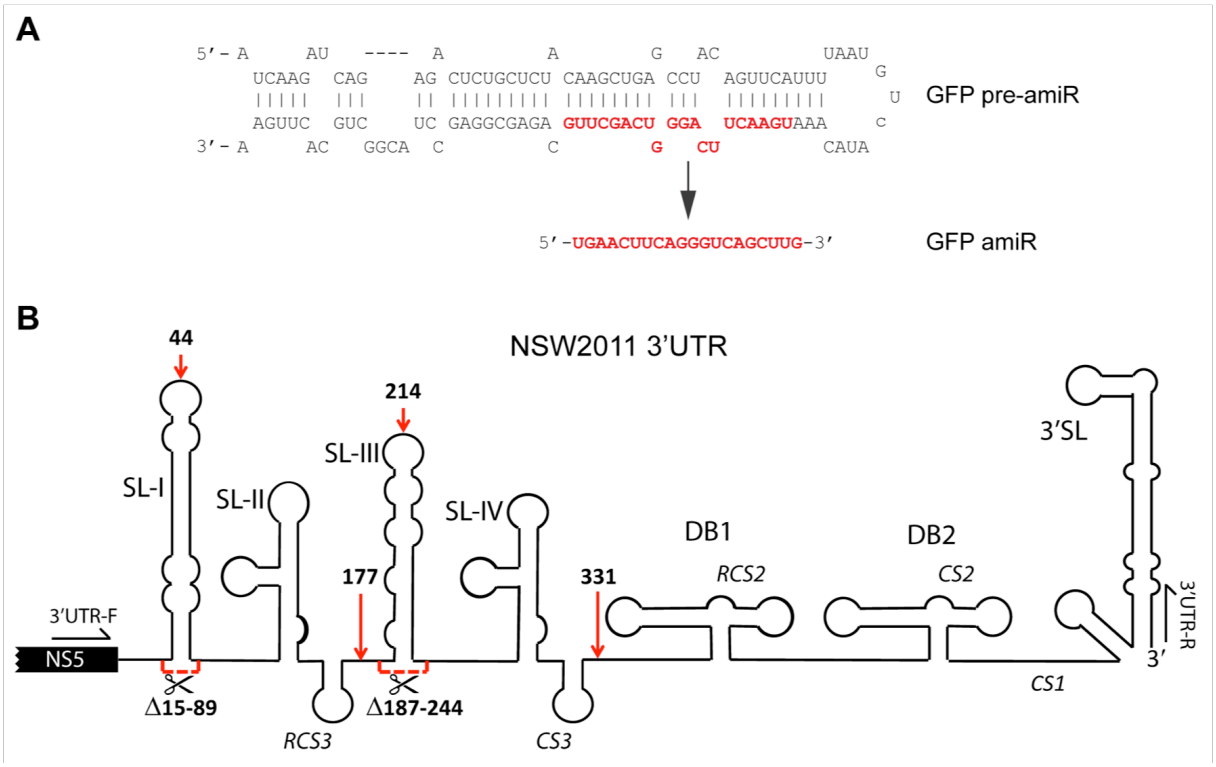

Figure 3.1 Generation of recombinant WNVNSW2011 expressing GFP amiR. A) Sequence of miR-124-based GFP pre-amiR hairpin and processed mature GFP amiR. B) Diagram representation of sites in $WNV_{NSW2011}$ 3′ UTR where the GFP pre-amiR was inserted. The Δ15-89 and Δ187-244 mutants have the specified nucleotides deleted and GFP pre-amiR inserted in place of deleted nucleotides at positions 15 nt and 187 nt respectively. The 44, 177, 214 and 331 mutants have the GFP pre-amiR inserted at the indicated nucleotide positions (Setoh et al., unpublished).

3.1.3 Aims

The aim of this chapter was to prepare a library of viruses containing amiRs targetting ISGs. A total of 204 ISG targeting pre-amiR hairpins were cloned into Δ15-89 site of WNV 3′ UTR to generate an amiR-encoding plasmid library. With the generated plasmid library, two virus libraries, named p0-293T and subsequently p1-Vero were generated as tools for *in vitro* and *in vivo* RNAi screening to study West Nile virus-host interaction. Using the same approach, a miR-124 scrambled sequences virus library was generated as an internal control for *in vitro* and *in vivo* RNAi screening studies.

3.2 Materials and methods

For ease of reading, materials and methods specific to this chapter are included below.

3.2.1 Preparation of chemical competent cells

To perform bacterial transformation, chemically competent DH5α E.coli cells were first prepared using the Inoue method for preparation of ultra competent *E. coli* cells and tested for transformation efficiency prior to transformation. The generated DH5α *E.coli* stocks were stored at −80°C until

required for transformation.

3.2.2 Mutagenesis PCR

Mutagenesis PCR was performed using GFP-amiR encoding plasmid as template, Q5 high-fidelity DNA polymerase kit (New England Biolabs, USA) and specific mutagenesis forward and reverse set of primers. *DpnI* digestion was performed to eliminate methylated DNA template. Thereafter, 1% (w/v) TAE agarose gel electrophoresis was performed on *DpnI* digested product. DNA bands were excised from gels, purified using Monarch DNA Gel Extraction Kit, (New England Biolabs, USA) and DNA concentration determined by Nanodrop spectrophotometry.

3.2.3 Chemical transformation

A total of 1.5 µL of *DpnI* digested gel purified DNA was mixed with 50µL of chemically competent DH5α *E. coli* cells and incubated on ice for 30 minutes. The tube containing the mixture was heat shocked at 42°C for 45 seconds before returning it on ice for 2 minutes. Pre-warmed additive free Luria-Bertani (LB) broth (1% tryptone, 0.5% yeast extract, 1% NaCl) was added to transformed cells and incubated in at 37°C at maximum speed in a heat block for one hour to revive the cells. Thereafter 100 µL of revived cells were inoculated onto on LB agar plates containing 100 µg/mL of ampicillin (AMP) by surface spreading. The plates were then incubated overnight at 37°C in an incubator to allow formation of ampicillin resistant colonies. The following day, formed single colonies were randomly picked and each colony grown overnight in 5 mL of LB broth containing with 100 µL/L of ampicillin at 37°C in an aerobic shaker.

3.2.4 Purification and plasmid Sequencing

A total 2 mL of overnight bacteria culture broth was purified to obtain plasmid DNA using the Wizard Plus SV Plasmid Miniprep System (Promega, USA) kit and protocol. Purified plasmid DNA was quantified using Nanodrop spectrophotometry (Thermo Scientific, USA). Each plasmid was later Sanger sequenced to confirm that it contained a correct amiR sequence.

3.3 Results

3.3.1 Generation of an amiR-encoding plasmid library

In this study an *in vitro* and *in vivo* RNA interference (RNAi) screening technique was employed with the aim of identifying antiviral host genes that could potentially affect West Nile virus replication. In order to do that, a library of recombinant WNV, each virus capable of producing a unique artificial microRNA (amiR) hairpin that silences a corresponding host gene was generated. To generate subsequent amiR-encoding virus libraries, an amiR-encoding plasmid library was first

constructed. A total of 204 amiR sequences targeting 102 ISGs obtained from Professor Benjamin tenOever of Icahn School of Medicine at Mount Sinai, USA. The library was selected based on the Influenza A virus screen performed by our collaborator Professor Benjamin tenOever [151]. Several of these ISGs previously shown to limit West Nile virus infection in conventional RNAi screens were included in plasmid library [151]. To increase possibility of gene knockdown, two pre-amiR hairpins were utilised with each targeting a unique site on the same host gene open reading frame (Table 3.1).

Table 3.1 List of murine ISGs and corresponding siRNA sequences and Gene IDs that were included in the plasmid library.

Clone #	Gene Name	Gene ID	siRNA (3p region)
1	Adar	56417	TTTCTGAGAGTCACACTCCTG
2			TCTTGTAGGGTGAACACCGTG
3	Atf2	11909	AAAGACACTTTGTAGCTGGTG
4			TGACACTGTCATTACGTGCTG
5	Atf3	11910	TTGAGTGGGATTAAACACTGA
6			TCAAGGTAGACACTTCTGCCT
7	B2m	12010	TTGGATTTCAATGTGAGGCGG
8			TTATTGCTCAGCTATCTAGGA
9	Birc6	12211	TAACAGTCTTTCTAACTGCGG
10			TCTATGATGACACTGCACCGG
11	Brd4	57261	TAATCTTATAGTAATCAGGGA
12			TTAAGCTATAGCTCGCTGGGA
13	Cdkl4	381113	TATAGCTTTCTTAAACATCTT
14			TTTAGAACACTTCTGCTTCTA
15	Clec4d	17474	TACATCTGTCTTATTCTGGTA

16			TTAACAGTGGTCTATGACCCA
17	Clec4e	56619	AATAATTTCACTTTGAACCTA
18			TTTGTTAGAGAATTGATCTGT
19	Cmpk2	22169	TACAATAACAGGAAAGTTGGT
20			AACTAGGTCAAGTACTGCCCG
21	Cpeb3	208922	TATAACATTAAGAACTTGGGG
22			TCCATCTGCATCTTGTCGGGG
23	Cxcl10	15945	ATAGCTTACAGTACAGAGCTA
24			TTGATGACACAAGTTCTTCCA
25	Cytip	227929	TTGTCTTCCATCGTGAGCTGG
26			TCCACAGTAACAACCTTCCTT
27	Daxx	13163	TTAATGTACACATAGATCTTA
28			TACAATGATGCTGTCATCGGT
29	Ddx58	230073	TTAGTGTCTCGGATCTGTCTG
30			TAGCTGTCAACTATAGTCTTT
31	Ddx60	234311	TAAGCTGGAGTAGTCAGCCTT
32			TAATGAAATGTCGTATCGGGA
33	Dhx9	13211	TTGTACTTCTTGTTCTTCCTT
34			TCACACATGAATTTCTGTCTG
35	Dtx3l	209200	TACTCTATGAACTCTAGTCTA
36			TAAACAACTAATGTATTGCTA
37	Eif2ak2	19106	TTTGAGGACTTCTCTAACCTG
38			TTGTACTTCGTGCTCCGCCTT

39	Fa2h	338521	TTGAATACTCTCTTGTGAGTG
40			TAGTACAGCTGGTATCTGGGG
41	Fbxo39	628100	TTATTGTTGAACTCGAACGTT
42			TTGTTCTCGCTCAAGGTCTCG
43	Gbp2	14469	TTGTAGATGAAGGTGCTGCTG
44			TGTTTCAACAACATCTGCCTT
45	Gbp3	55932	TTGGTTTGTATCTTTAACCTT
46			TTTATCTGTAGTGTACAACTG
47	Gbp6	100702	TTTCTGTCTTAGTAGCTCCTG
48			TTCTGTGACATAGTGCAGCTG
49	Gcc	14917	TTAAAGAACAGAATTAACCAA
50			TATACTTGTCCTTCAGCTCTG
51	Gvin	74558	TTCTCTTCTAGGTTTGATCTG
52			TTAATTACATCACTGAAGCGG
53	Ifi35	70110	TTAGAAACTACAAACTTGGGC
54			TATACAGAGAAATCTAGTCTC
55	Ifi44	99899	TATTGATCCAACACAGTTCTA
56			TAATATAGCACTCTAAAGGGA
57	Ifih1	71586	TTATACATCATCTTCTCTCGG
58			TAAGATTTGACAACTTCTGGA
59	Ifit1	15957	TATATTAACGTCACAGAGGTG
60			TTCTCCTAAATCCTGAAGCTT
61	Ifit3	15959	TTCTGCATGAACTCCATCGTT

62			TTGTCTCACCTTGTCAACGTA
63	Ifitm3	66141	TTGATTCTTTCGTAGTTTGGG
64			TAAATGAGTGTTACACCTGCG
65	Ifna1	15962	TTCTCTCTCAGGTACACAGTG
66			TTTGATGTGAAGATGTTCAGG
67	Ifna4	15967	TTGTGGGTCTTGTAGATGCTG
68			TTATCCACCTTCTCCAAGGGG
69	Ifnb1	15977	TACAACAATAGTCTCATTCCA
70			TTCCTGAAGATCTCTGCTCGG
71	Ikbka	12675	TAACACTCTCTCAACAGTGTT
72			TTTGTGACATCTTCTTCCCTG
73	Ikbkb	16150	TATACTATGGAAATACACCTT
74			TTGGACTAGCTGAAGTTCCTG
75	Ikbke	56489	TAGATGACTGAAATTTACCTT
76			TAGACAGAAACAAACTTCTCA
77	Il15	16168	TATCTTACATCTATCCAGTTG
78			TATCCATACAACTTTATTCCA
79	Il6	16193	TAGAGTTTCTGTATCTCTCTG
80			TACATTCCAAGAAACCATCTG
81	Irf1	16362	TTATTGATCCAGATCAGCCCT
82			TTGTCTCCTAGTACAGAGCCA
83	Irf2	16363	TTTCTTTATGCTTCTGTCCTT
84			TACAACTATGATGTTCACCGT

85	Irf3	54131	TAGTTCTGAGACTCGCAGCCA
86			TTGTTCCTCAGCTAGCAGCTG
87	Irf5	27056	TAGAACAGCTGGAAGTCACGG
88			TTGAAGATGGTGTTGTCCCCA
89	Irf7	54123	TTCCTCGTAAACACGGTCTTG
90			TCTTCGTAGAGACTGTTGGTG
91	Irf9	16391	TATGTAAGTATACTGTAGCTG
92			TAAGTTTCAATTCTCCTCCGG
93	Irgm	15944	TATGTAAGTACACTGTAGCTG
94			TTCTCTTAAAGCTCTTTCGGT
95	Lgals3bp	19039	TTGTCCTTGAAGAGGAAGCTG
96			TTAACCAAGCGCATGTCTCCA
97	Lgals8	56048	TTTGCTTTGATAGTGCTTGTT
98			TTCCATACTCTGTAAATCCGA
99	Lrp4	228357	TTTCAGAGCATCTTCCTCCTG
100			TTGTTGATTAGCACTTTGCGA
101	Ly6e	17069	TTAGACATCCTTGTCAGTGTG
102			TAACATAGCGAGACCGTCTTA
103	Map3K8	26410	TTAAACTTACACTAGAGTCGA
104			TTGACTAGTCACATTGGACTA
105	Map4k2	293694	TTAACAATTCTCACACAGCGT
106			TTTGGTGTCAGGAATCTTGGT
107	Mapk8	26419	TTCTTGATTGCAACATTTCTT

108			TTGTTGTCACGTTTGCTTCTG
109	Mbnl1	56758	TTAGTACCAACCTCTCACGTG
110			TCTTCTAAACTAAAGCAGCCT
111	Mitd1	69028	ATCACTGTGACAACTCCTGGG
112			AACTTCTGTAACTGTCTCGTG
113	Mlkl	74568	TATTCCAACACTTTCGGCCTG
114			TTGAACTGGATCTCTCTGCTT
115	Mov10	17454	TAGATGTGGAGTTCATAGCTT
116			TCGTGGTTGTAAATCGTCCGC
117	Myd88	17874	TTTGTTTGTGGGACACTGCTT
118			TAAGCCGATAGTCTGTCTGTT
119	Nfkbia	18035	TAAATATACATCTTAGAAGTA
120			TTGTACAAATATACAAGTCCA
121	Nmi	64685	TAGAACTGAACTCTACCTCGA
122			TTATTTATGTGCATTATGCGG
123	Oas1a	246730	TAAGTCTGGAGCTTCCTGGGT
124			TTTGACATCAGCACCAAAGGT
125	Oas2	246728	TTCTCTGTTAGGTTTGAGGTT
126			TATAATGTCAACAGCTTCCTT
127	Oasl1	231655	TCTTCTTTCCACTCTCTGGTT
128			TTGTCTCTCACATACTGCTGG
129	Oasl2	23962	TTGAAAGTGAAACTGCAGGGA
130			TATTTCATTCTTAATCACGCA

131	p50 (RelB)	19698	AATCTCTGAGAATCTGTCCTG
132			TTTCGCTTCTTGTCCACACCG
133	p65 (RelA)	19697	TTGAAGGTCTCATAGGTCCTT
134			TTGTTGGTCTGGATTCGCTGG
135	Parp14	547253	TTGTTTCACAGCATCTTCTTT
136		547253	TTGTTGATCAAGTTCTTTGGG
137	Parp11	101187	TTGAATGTTGGTATCCGGCTG
138			TAACGGTGCGAAATCGAGCGG
139	Parp12	243771	TTGGAAGCTACAACTCTTCCG
140			TTGTGATCAGTCTTCAAGTTG
141	Parp9	80285	TAGCTGACTCTCATTGCTCTT
142			TTGTCTTGGAAATAAAGCCGG
143	Plec	18810	TACAGGTCACTGATGTGCCTC
144			TAGCTTGCTCACAATGCGCTG
145	Ppm1k	243382	TAAACTAGACTGACTTCTCTG
146			TAGAGCAATAATAGTATTCCG
147	Ppp3cb	19056	TTCTTCAGAACATCAACCCTG
148			TTAAATCTATCTAATCTCCTA
149	Rnasel	24014	TAATCTTGGTCCATCTGACTT
150			TTTCTGTTCGTTCTCTCCGTC
151	Rsad	237926	TTAACCTGCTCATCGAAGCTG
152			TATTCTAATAACAACAGTCCG
153	Rtp4	67775	TTCTTGAAATGTCTGCTCCCA

154			TTTATTTAATCAACATAGCTT
155	Samd9l	209086	TTGGTGGTCTTAACCAGTCTG
156			TTCTCTGGAATCTTGATTGTG
157	Sfxn2	94279	TTGTTCACAAACTACAGACTG
158			TAGAACTGGAGCATGAAGCCC
159	Sh3bgrl	56726	TATACACGGATCACCATCCTG
160			TAACATATGAACATAACCTGT
161	Stat1	20846	TTTACTGTCCAGCTCCTTCTG
162			TTTAAAGTCATATTCATCTTG
163	Stat2	20847	TTCTGGTCTTCAATCCAGGTA
164			TTCTGCAACATCTCCCACTGC
165	Stat3	20848	TTAAGTTTCTGAACAGCTCCA
166			TTGAAATCAAAGTCGTCCTGG
167	Tap1	21354	TTTAGAGGAAGAAGAAACCGA
168			TTCTCCATGAATCTCATTCTC
169	Tapbp	21356	TAGCTTTGGGTCAAGATCTGG
170			ATAGTGAACTCCATGCTGCTT
171	Tbk1	56480	TCTCATTTGAACATCCACTGG
172			TTGATTTGAGGAAACAATCTT
173	Ticam1	106759	TTGAGCTGGTAGATCTCCCGG
174			TTGATATCTGAACTGCACCGA
175	Tlr3	142980	TTAGATAAGAGGAACACCCTT
176			TAAAGTCGAACTTAATCTCTT

177	Tlr7	51284	TTTACTTTAACTTCACAAGGT
178			TAGAGTGGTTCTATAGATGGA
179	Tlr9	81897	TATAGCTCAAGTTCAGCTCCT
180			TTAGCATCTAGAACCAGGATG
181	Tmem140	68487	TATCTTCTGCTGTTGCAGGGA
182			TTCTAGTTTGACACTTTGCCA
183	Tor3a	30935	TACGTGTCCACATACTTGGGG
184			TAAGCCTGTCAAGTTGTTGGA
185	Trex1	22040	TATGTGAGTCTGTCGGTGCTT
186			TAGGTTGGTTGTTCCAGTGGT
187	Trim21	20821	TAGAGGGTGATATCTGCCGTG
188			TTAGTTATGTGCTCCCAGCTT
189	Trim25	217069	TTTAACTTGCGCAAGGAGCTG
190			TTCATTTCCATATACTCCTGT
191	Wwoxv	80707	ATCTCTAAAGAATTGCTTGTG
192			TATCAGGTTATTCTAAGGTTG
193	Zc3hav1	78781	TTAGTGAACTTCATCTCTCCA
194			TATTCGTCTGAATCATCCCTT
195	Zfp182	319535	TTGTTTATCTTGATGTTGCCT
196			TTGTCTACCATAGTATTTCCA
197	Isg15	100038882	TGCTTGATCACTGTGCACTGG
198			TTAAGCGTGTCTACAGTCTGC
199	Ifi27	52668	TTGAGCTGATAGAAGTGTCAT

200			TTGATGTGGAGAGTCCAAGGA
201	Usp18	24110	TATTTCAGACTGTTCCTTGGT
202			ATGTTCATCATGAACACTTGA
203	Parp10	671535	TTAAGGACTTTGTAGAGCAGG
204			TTGGAGACTCACTGTCTCCTC
205	EGFP		TGAACTTCAGGGTCAGCTTGC
206	MiR-24		TAAGGCACGCGGTGAATGCCA

A pIDTSmart (AmpR) plasmid vector was designed to encode the last 32 nucleotides of WNV NS5, the first 14 nucleotides of 3′ UTR, a 109 nucleotide GFP pre-amiR hairpin at Δ15-89 position at the start of $WNV_{NSW2011}$ 3′ UTR and 44 nucelotides of the 3′ UTR from 90^{th} nucelotide (Setoh *et al.*, unpublished) (Figure 3.2). Based on the pre-miR-124 hairpin structure, miR-124 sequence was replaced with a GFP siRNA sequence that targets GFP coding region, shown in Figure 3.1 A. The GFP pre-amiR hairpin encodes: 5′ arm, 5p, loop, 3p and 3′ arm sequences. For proper miRNA processing by the host cell, the 3p (GFP siRNA) sequence is partially complementary with 5p and includes non-complementary residues and maintains bulges to mimic the original pre-miR-124 structure (Figure 3.1). The loop comprises non-hybridising miR-124 sequences vital for proper processing of the GFP pre-amiR [259]

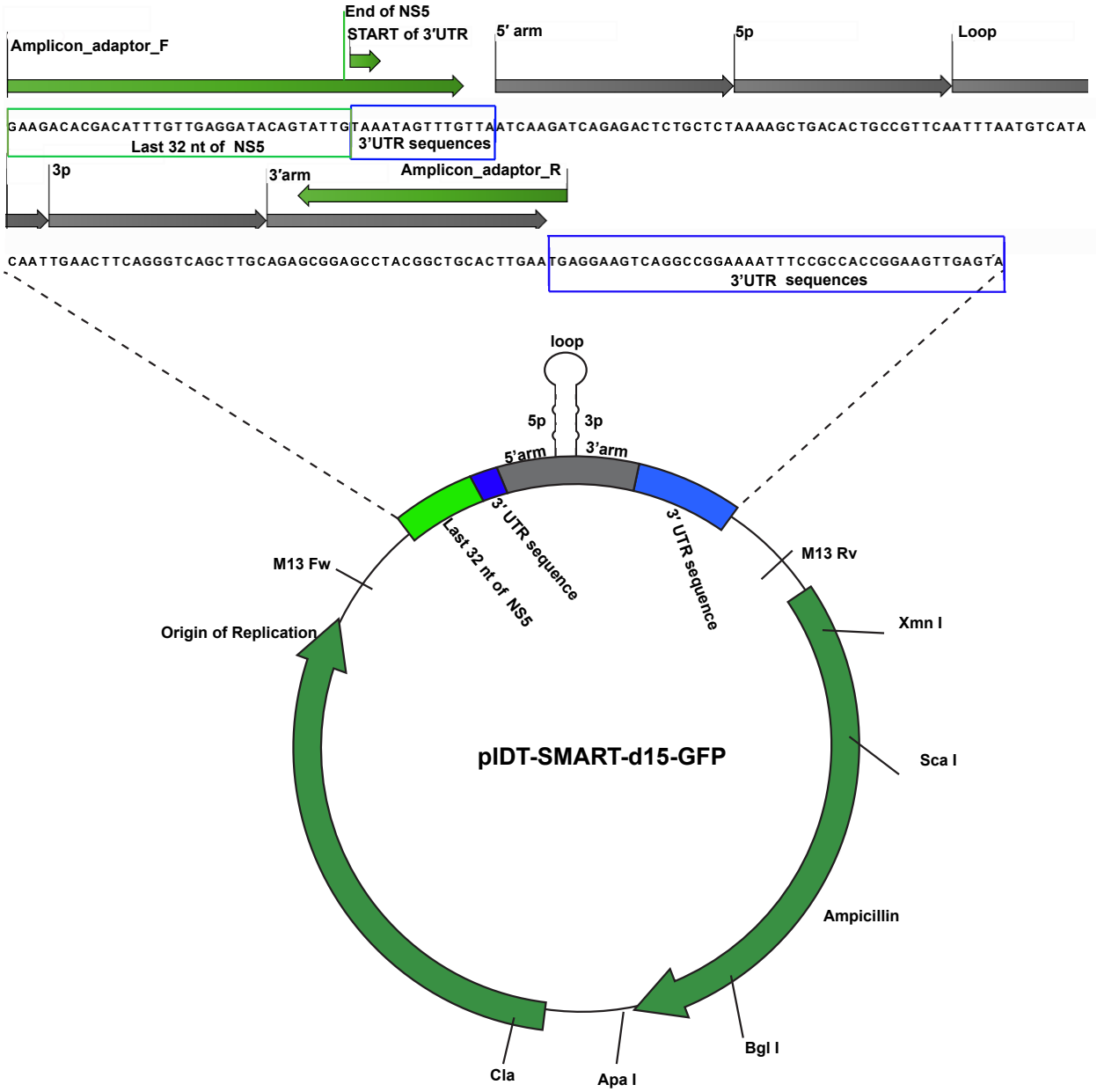

Figure 3.2 Diagram of pIDTSMART-d15GFP plasmid vector. A 109-nucleotide miR-124 based GFP pre-amiR hairpin was inserted at Δ15-89 nucleotide position at the start of the $WNV_{NSW2011}$ 3′ UTR (3′ UTR sequences highlighted blue box). The last 32 nucleotides at the end of $WNV_{NSW2011}$ NS5 are also included in the construct (highlighted light green box). The GFP pre-amiR hairpin includes 5p and 3p stem regions, which are partially complementary, and 5′ arm 3′ arm and loop sequences, which are miR-124 sequence and d15 stands for (Δ15-89). Adaptor sequence primers (amplicon adaptor_F and amplicon adaptor_R with flanking illumina sequences bind to either ends of 3′ UTR are used for generating illumina deep sequence amplicons.

The pIDTSMART-d15GFP plasmid was mutagenised into 204 different plasmid clones with each plasmid encoding a unique pre-amiR hairpin (Table 3.1). For instance, to generate Adar clone #2 amiR-encoding plasmid, PCR was performed using pIDTSMART-d15GFP as DNA template, a Q5 high fidelity DNA polymerase (New England Biolabs, USA) kit and Adar clone #2 forward and

reverse mutagenesis primers as shown in Figure 3.3 (all mutagenesis primer sequences are listed in Appendix 1). As a result, the 3p sequence i.e., Adar clone #2 siRNA and corresponding 5p sequence were introduced in the stem whilst retaining pre-amiR hairpin structure. Thereafter, *DpnI* digestion was performed to eliminate methylated pIDTSMASRT-d1515GFP DNA template since *DpnI* restriction enzyme recognises methylated sequences that will not be present in the amplified product.

Following *DpnI* digestion, pIDTSMART-d15-Adar clone #2 plasmid DNA was purified by DNA gel extraction to completely remove *DpnI* reagents and cleaved template DNA as well as maximise the chances of obtaining the new mutagenised plasmid. Thereafter, products were transformed into chemically-competent DH5α *E.coli* to allow re-circularisation of pIDTSMASRT-d15-Adar plasmid by homologous recombination (Figure 3.3). The resultant plasmid sequence was Sanger sequenced to confirm that the correct pre-amiR hairpin was introduced. Therefore, to generate a complete amiR-encoding plasmid library, these steps were repeated until 204 amiR-encoding plasmids were successfully cloned and confirmed by Sanger sequencing (Figure 3.4).

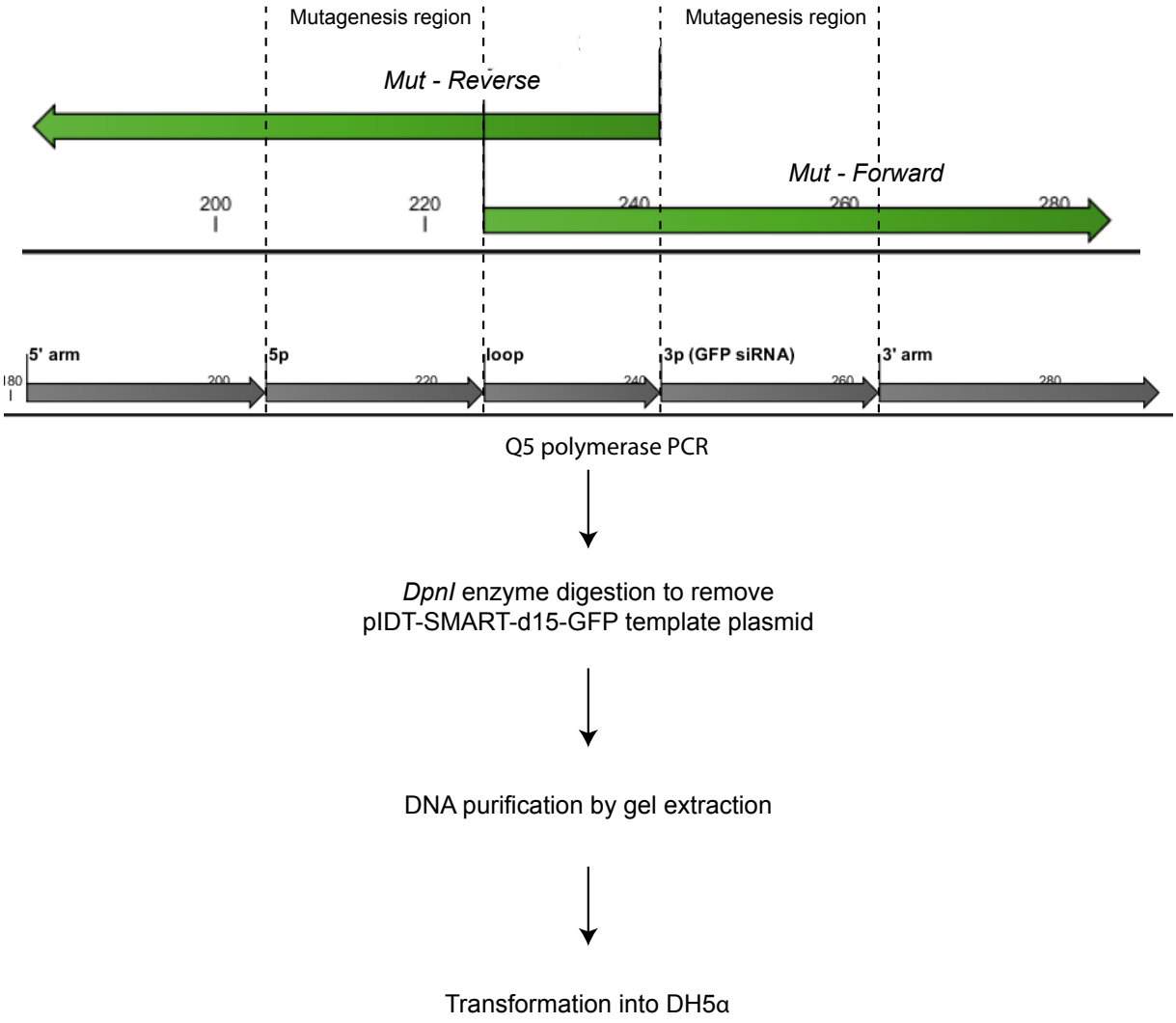

Figure 3.3: The strategy for mutagenesis to introduce 204 different siRNA-encoding sequences into the stem region of miR-124 in the pIDTSMART-d15. Mut-Forward and Mut-Reverse (green) maintained the miR-124 3' and 5' arms, respectively, and the loop region. Mut-Forward mutagenesis region encodes Adar clone #2 siRNA sequence that replaces GFP-siRNA (3p) during mutagenesis PCR. Mut-R mutagenesis region encodes a unique sequence partially complementary to Adar clone #2 siRNA that replaces the GFP miRNA 5p sequence. The 5p and 3p sequences are partially complementary with bulges to mimic miR-124 structure for proper processing by the host cell microRNA processor. Mutagenised plasmids were DpnI digested to remove methylated parental plasmid DNA by slicing it into small pieces, gel purified and transformed into DH5α *E.coli* to recover the Adar clone #2 plasmid. This strategy was used to generate a complete set of 204 amiR-encoding plasmids (Appendix 1).

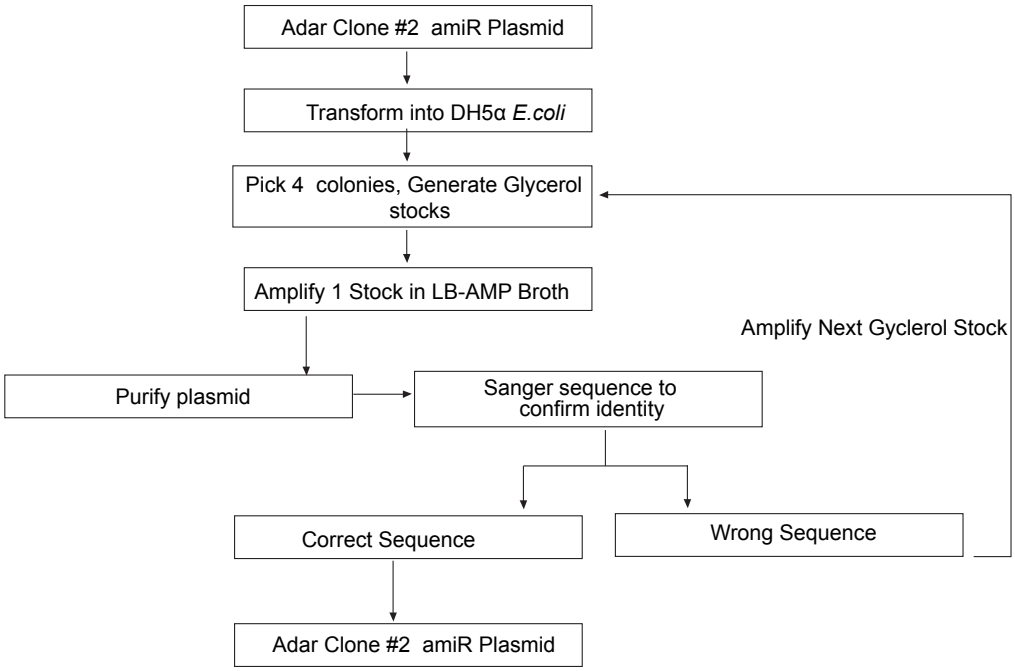

Figure 3.4 Flowchart showing logical steps taken to generate the Adar clone #2 amiR encoding plasmid. These steps were repeated until a plasmid library containing 204 ISG amiR-encoding plasmids was generated.

3.3.2 Characterisation of amiR encoding plasmid library by deep sequencing

Each plasmid concentration was determined by Qubit fluorometer using Qubit dsDNA BR Assay kit and protocol (Thermo Scientific, USA). A total of 204 individual amiR-encoding plasmids were combined in equimolar amounts (100 ng of each plasmid) to generate a complete ISG-targeting amiR-encoding plasmid library. Thereafter 10-cycle PCR was performed using Q5 high-fidelity DNA Polymerase PCR kit (New England Biolabs, USA), plasmid library as DNA template and amplicon_adaptor_F and amplicon_adaptor_R set of primers to generate a single amiR-encoding plasmid library amplicon for Illumina deep sequencing (Figure 3.5). Deep sequence reads produced pre-miRNA encoding the following sequence: ATCAAGATCAGAGACTCTGCTCT-XXXXXXXXXXXXXXXXXXXXX-ATTTAATGTCATACAAT-XXXXXXXXXXXXXXXXXXXXX-AGAGCGGAGCCTACGGCTGCACTTGAA. All reads possessed the known sequence shown and Xs (two stretches of 21 nt on either side) were the region of interest containing unique corresponding siRNA sequences.

Deep sequencing data were uploaded onto Galaxy Australia (UQ Research Computing Center) and analysed using Salmon transcript quantification data script tool to ascertain number of each amiR-encoding transcript variant in the plasmid library. Library diversity was determined by quantifying the proportion of each amiR-encoding transcript variant in relation to the total number of amiR-

encoding transcript variants within the library. The mean frequency of reads for individual amiRs will be 1/204 (0.49%) of the total reads. Results showed that 196/204 of the amiR-encoding plasmids were ($0.1\% \leq x \leq 1\%$) whereas 8/204 and 4/204 of the amiR-encoding plasmids were over-represented ($x > 1\%$) and under-represented ($x < 0.05\%$) respectively, where x is the percentage number of reads for each amiR encoding plasmid. (Figure 3.5) Clones Atf3 #2 (1.96%), Atf2 #2 (1.19%), Cmpk2 #1 (1.54%), II5 #2 (1.25%), p50-(Rel B) (0.95%), Stat3 #2 (0.99%), Stat1 #2 (1.142%) and Sh3bgrl #1(1.22%) amiR-encoding plasmids were over-represented as highlighted on Figure 3.5 . Clones Adar #1, Gbp6 #1, Irf7 #1 and Gfp amiR-encoding plasmids were not detected in the plasmid library.

The majority of amiR-encoding plasmids clustered close to the mean (Figure 3.5), but it is notable that there was a distinct drop in frequencies of reads from plasmids #140 and above. This could be because the equimolar mixing of all plasmids was done on three different days; that is, each day 70 plasmids were mixed, and the drop from #140 suggests a systematic pipetting error, perhaps due to poor pipette calibration. In addition, descriptive statistical analysis of plasmid library revealed that mean, median as well as standard deviation of the mean (SEM) were 0.49%, 0.47% and 0.24% respectively. The closeness of the mean to median implied that amiR-encoding plasmids in the plasmid library were not greatly skewed.

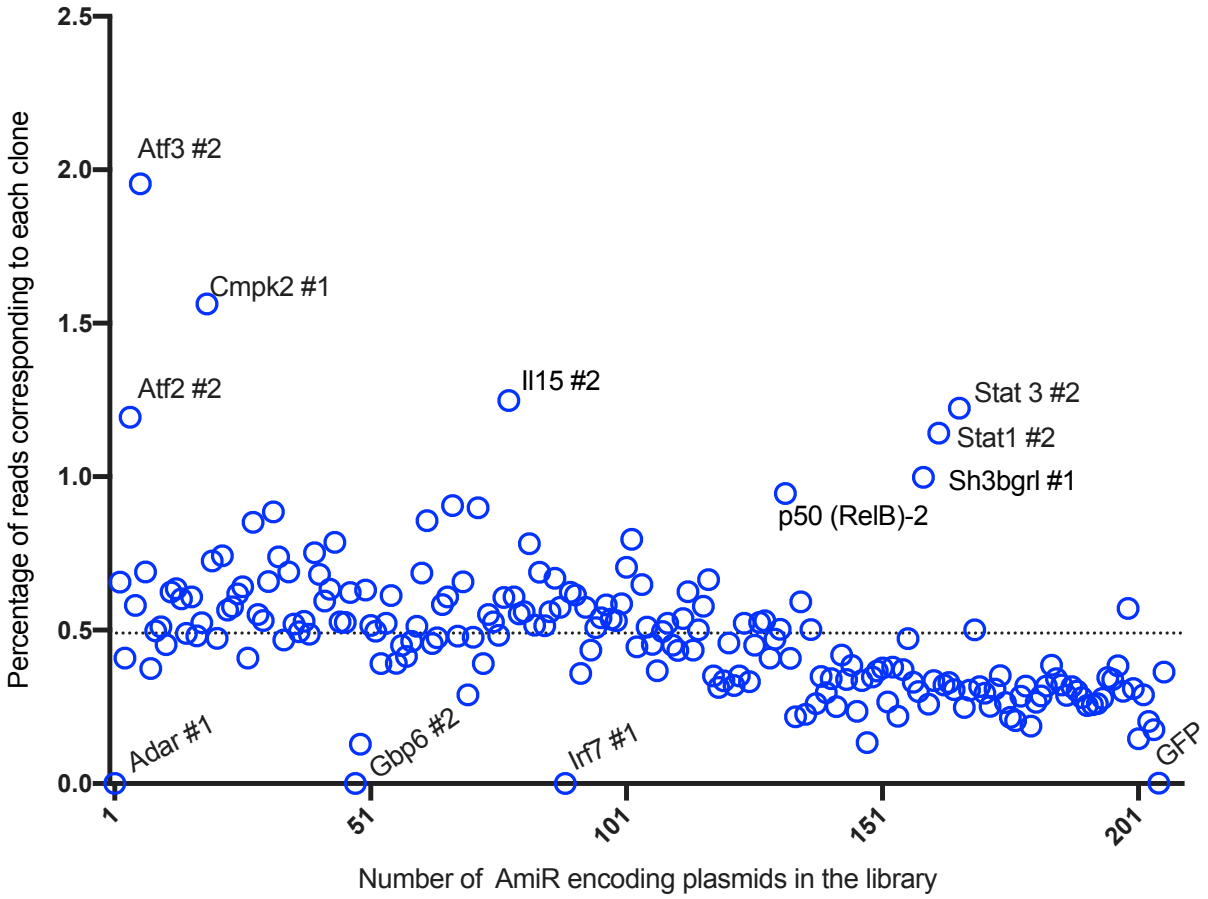

Figure 3.5: Generation of an amiR-encoding plasmid library. Results from deep sequencing confirmed a largely uniform distribution of amiR-encoding plasmids within the plasmid library as shown by percentage number of reads per amiR-encoding plasmid within the plasmid library. Highlighted clones represent clones with percentage reads ≥ 1% or < 0.05% of the entire library. The dotted line depicts the mean frequency of reads for each plasmid, i.e., 100%/204=~0.49%.

3.3.3 Generation of amiR-encoding virus library

Having constructed an amiR-encoding plasmid library, the next step was to generate an amiR-encoding virus library. To facilitate this, $WNV_{NSW2011}$ CPER fragments (fragments 1 to 5) were amplified from $WNV_{NSW2011}$ cDNA using specific primers (see chapter two, Table 2.2) that generate amplicons with overlapping regions for CPER assembly (Figure 3.6 B) [237]. To generate the 3' UTR containing the amiR library, the 3' UTR was divided into two CPER fragments, fragment 6 (containing the amiR library) and fragment 7 (remainder of 3' UTR). The library fragment was generated by a 15-cycle PCR using Q5 high-fidelity DNA Polymerase PCR kit (New England Biolabs, USA), amiR-encoding plasmid library as DNA template and 3' UTR_Forward and amiR_Reverse set of primers. The 3' UTR _Forward binds to flanking NS5 sequences and the start of 3' UTR while the amiR_Reverse primer that binds to end of the amiR hairpin (Figure 3.6A). The after amiR fragment was generated from d15GFP-amiR WNV cDNA using after amiR_Forward and 3' UTR _Reverse set of primers that bind to the end of amiR hairpin and the end of 3' UTR

respectively (Figure 3.6A). A UTR-linker that encodes first 22 and last 22 nucleotides of the 5' UTR and 3' UTR of flaviviruses was used as fragment 8. The UTR-linker was amplified from a previously constructed pUC19-flavi-UTR-linker plasmid, using UTR_Forward and UTR_Reverse primers [237]. The UTR linker encodes a CMV promoter, hepatitis delta virus ribozyme and a polyadenylation signal for effective expression in mammalian cells, authentic formation of 3' UTR and efficient termination of transcription by RNA polymerase II respectively [237].

Thereafter, using 0.45 pmol of each fragment, equivalent to 2.7 X 10^{11} DNA copies of generated amiR library fragment, RT-PCR-amplified fragments encompassing the rest of the $WNV_{NSW2011}$ genome, and CMV UTR-linker, were assembled by CPER. In this procedure denaturation and annealing of all CPER fragments followed by polymerase-mediated fragment extension generates a complete circular infectious cDNA product for transfection into HEK 293 cells [109, 237, 258] (Figure 3.6B)

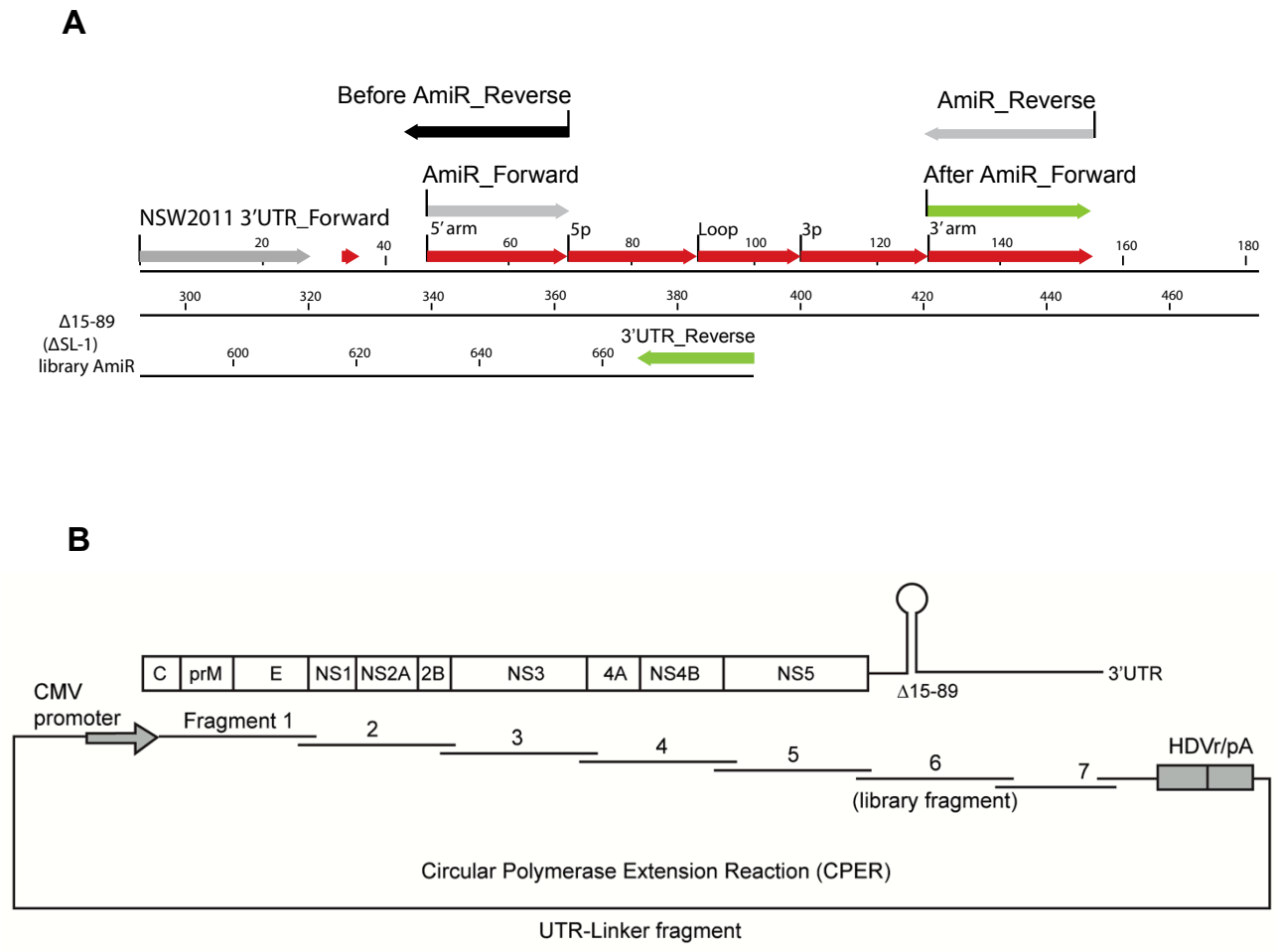

Figure 3.6: Generation of p0-293T amiR encoding virus library. A) Diagram showing the 3' UTR of $WNV_{NSW2011}$ and primer binding sites of respective primers used to generate the 3' UTR fragments. The 3' UTR was divided into two fragments, the amiR library fragment and after amiR fragment. To generate library fragment the plasmid library was used as PCR template with 3' UTR_Forward and AmiR_Reverse set of primers. To generate the after amiR fragment, the

d15GFP-amiR WNV cDNA was used as PCR template along with the after amiR_Forward and 3' UTR_Reverse set of primers. B) Diagram showing CPER strategy used to generate infectious amiR-encoding cDNA library. Fragments are generated in separate PCR amplifications, assembled by CPER through denaturation and annealing of overlapping sequences, followed by polymerase extension of fragments. Fragment 6 represents the amiR library fragment containing 204 amiR-encoding fragments generated by low-cycle PCR and represents the first fragment of the 3' UTR while fragment 7 represents the rest of the 3' UTR of $WNV_{NSW2011}$ (after amiR fragment). Fragments 1-5 were amplified from $WNV_{NSW2011}$ cDNA and the UTR-linker was amplified from a previously constructed pUC19-flavi-UTR-linker plasmid.

The resultant CPER product was transfected into HEK 293 cells to recover amiR-encoding virus library (we named it passage zero; p0-293T). At three days post transfection, 2 mL of p0-293T virus culture supernatant was collected as p0-293T virus stock, immunoplaque assay on Vero cell was performed and virus titre determined as 2.8×10^6 pfu/mL (Figure 3.7 A).

Using Nucleospin RNA kit and protocol (Macherey Nagel, Germany), viral RNA was purified from virus culture supernatant. To generate p0-293T virus library amplicon for deep sequencing, RT-PCR was performed using superscript III one-step RT-PCR system with platinum Taq high fidelity DNA polymerase kit (Thermo Scientific, USA), purified RNA and Amplicon_adaptor_F and Amplicon_adaptor_R set of primers (Figure 3.7 B).

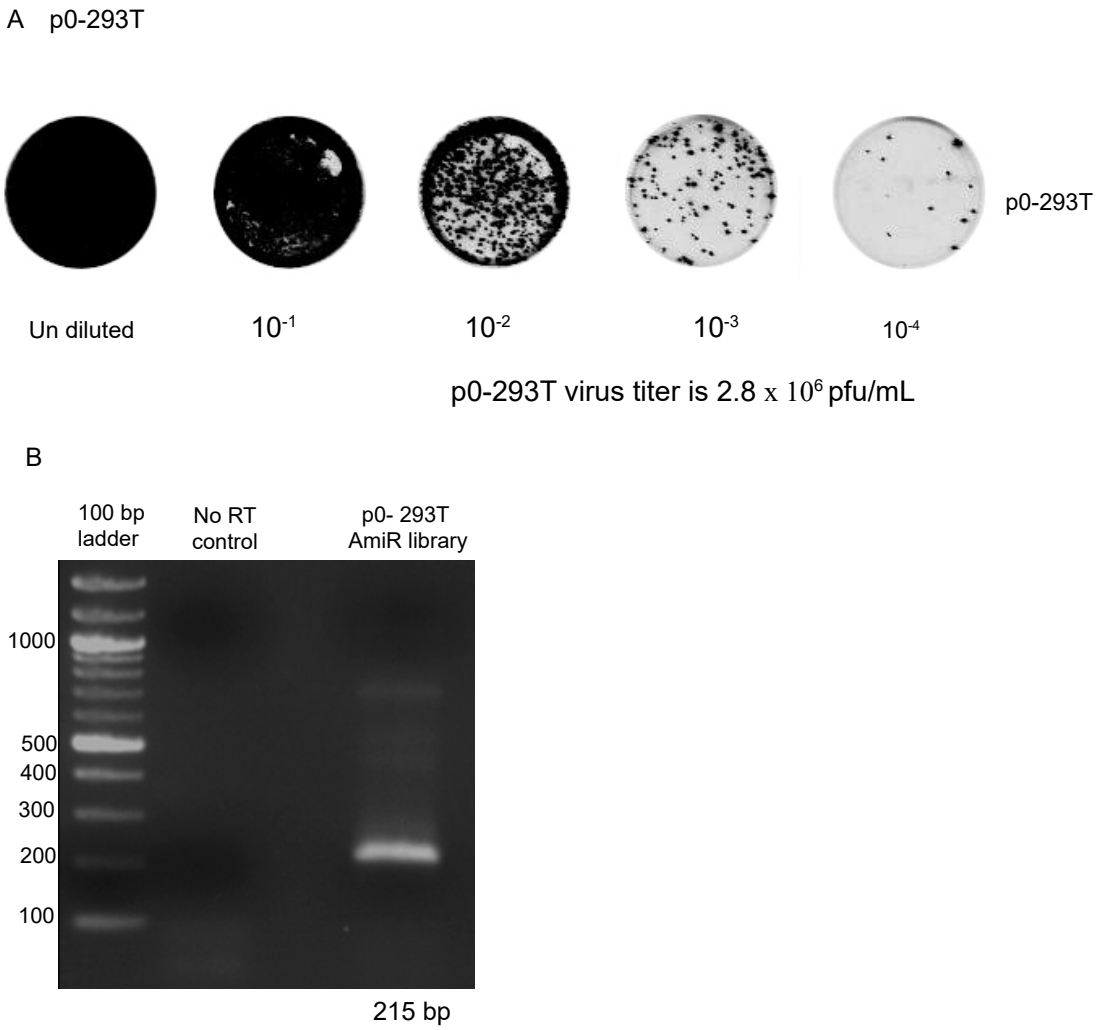

Figure 3.7 Generation of p0-293T amiR-encoding virus library. CPER product was transfected in HEK 293 cells, 3 days post transfection (dpt) virus culture supernatant was harvested. A) Virus titre was determined on Vero cells by immunoplaque assay. B) Viral RNA was purified from culture supernatant and treated with DNAse I enzyme to remove traces of CPER DNA products. Using purified RNA, RT-PCR was performed and an amplicon for deep sequencing generated. A no RT control PCR was added to determine the purity of purified RNA. A 100bp DNA ladder was loaded in to Left lane as a marker. Expected DNA band size of 215 bp was obtained, purified by DNA gel extraction and deep sequenced.

Deep sequencing data were uploaded onto Galaxy Australia (UQ Research Computing Center) and analysed using Salmon transcript quantification data script tool to determine percentage number of each amiR-encoding virus variant in p0-293T amiR-encoding virus library (Appendix 2). Analysis of p0-293T deep sequence data revealed that most of the amiR-encoding viruses clustered between 0.2 and 0.8% representation (Figure 3.8). Descriptive statistical analysis of p0-293T deep sequencing results showed that a median frequency and standard deviation of the mean of amiR encoding viruses in the virus library as 0.39% and 0.39% respectivlely, indicating increased spread of frequencies compared to the data from obtained from amiR encodong plasmid library (Figure 3.8) and (Figure 3.5).

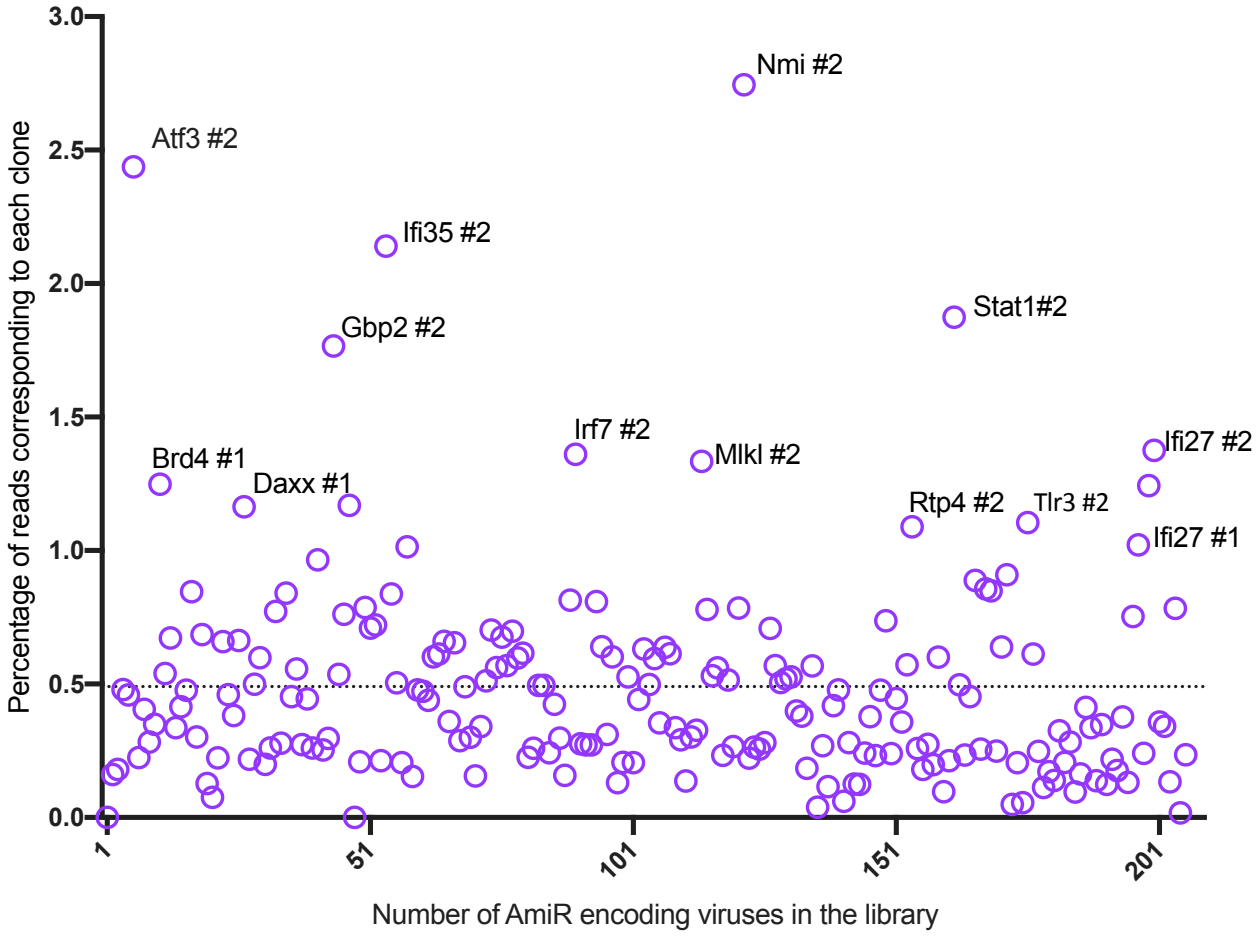

Figure 3.8 The distribution of amiR-encoding West Nile viruses in p0-293T virus library. Deep sequencing of p0-293T virus library depicted by a scatter plot showing the percentage reads for each amiR-encoding virus within the entire virus library. Highlighted clones present clones with percentage reads ≥ 1%**.** The dotted line depicts the mean frequency of reads for each plasmid, i.e. 100%/204 = ~0.49%.

To generate p1-Vero virus stocks for subsequent experiments, p0-293T amiR-encoding virus library was passaged on Vero cells. Vero cells were infected with p0-293T amiR-encoding virus library stock at multiplicity of infection (MOI) =1. At 3 days post infection (dpi) culture supernatant was harvested as p1-Vero virus stock. Virus stock titre was determined by immunoplaque assay on Vero cells (Figure 3.9 A) as previously described [260]. Titration of p1-Vero virus library showed a titre of 4.27 X 10^7 pfu/mL. Next, viral RNA was purified from harvested culture supernatant using Nucleospin RNA kit and protocol (Macherey Nagel, Germany). Purified RNA was eluted in 30 µL of nuclease free water and treated with RQ1 RNase-free DNase enzyme (Promega, USA) to remove any traces of DNA. To generate p1-Vero virus library amplicon for deep sequencing, RT-PCR was performed using superscript III one-step RT-PCR system with platinum Taq high fidelity DNA polymerase kit (Thermo Scientific, USA), RNA and amplicon_adaptor_F and amplicon_adaptor_R set of primers (Figure 3.9 B).

The resultant RT-PCR amplicon was deep sequenced (Figure 3.9 B). Statistical analysis of p1-Vero deep sequencing results revealed that percentage mean, median and standard deviation from the mean of amiR-encoding virus variants as 0.49%, 0.32% and 0.56% respectively. Ninety six percent of the amiR-encoding virus variants clustered between 0.05% and 1% representation in the library. This range of 0.05 to 1% was chosen because the expected mean of the library would be 0.49% (100/204) if equally distributed (Figure 3.10).

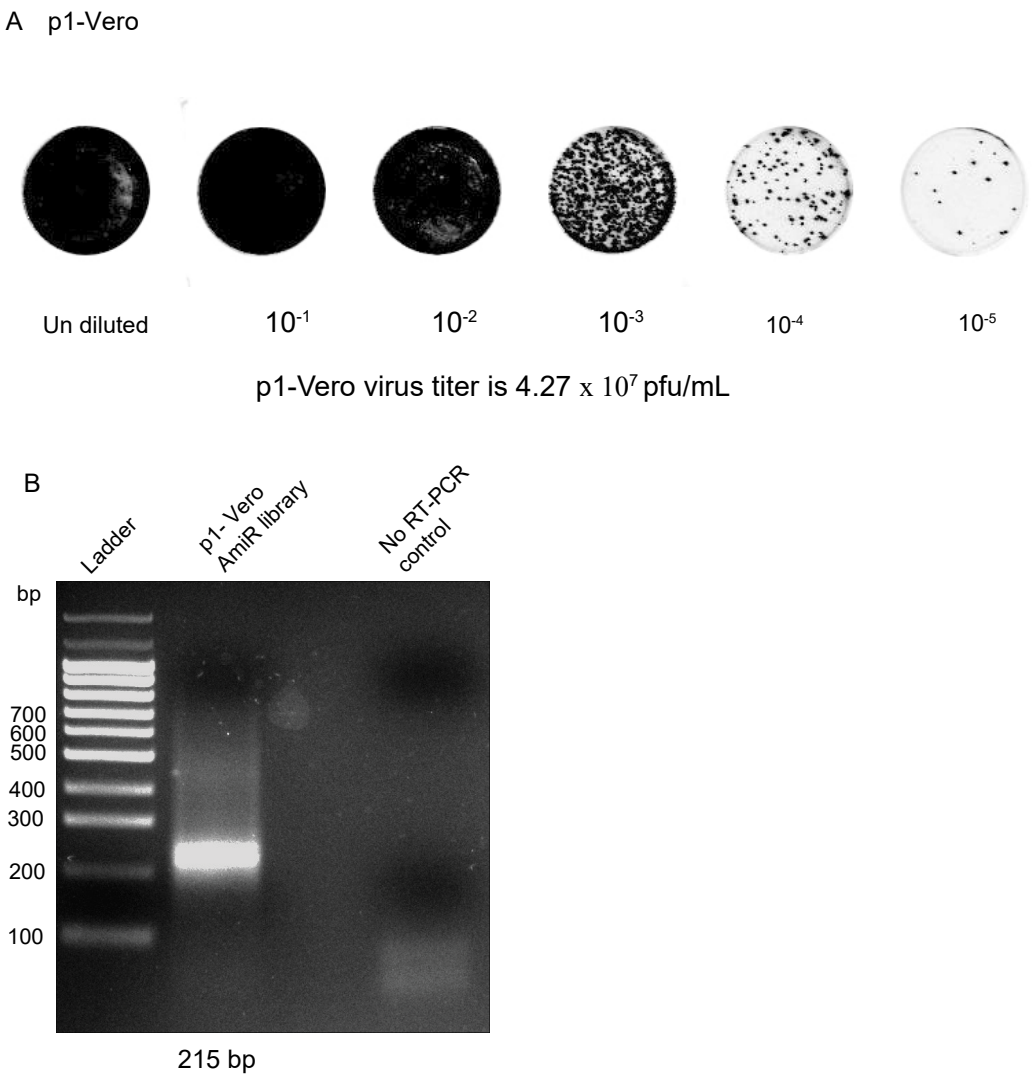

Figure 3.9 Generation of p1-Vero amiR-encoding virus library. A) Virus titre was determined on Vero cells by immunoplaque assay. B) Viral RNA was purified from culture supernatant, DNase treated and RT-PCR performed to generate amplicon for deep sequencing. A no RT PCR was performed using RNA as template for Taq DNA polymerase PCR as a control to determine the purity of purified RNA. A 100bp DNA ladder was loaded in to the left lane as a marker. Expected DNA band size of 215 bp was obtained, purified by DNA gel extraction and deep sequenced.

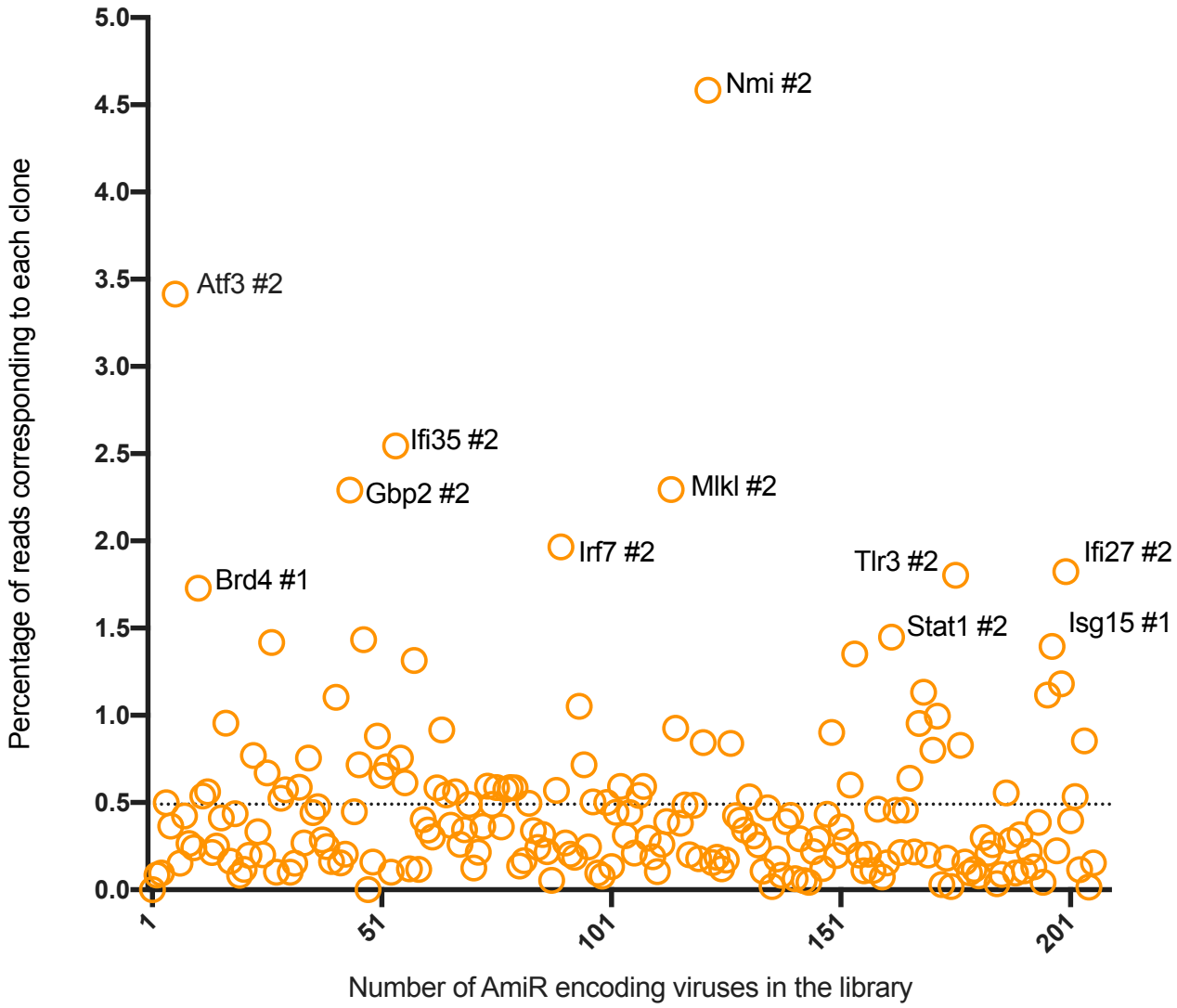

Figure 3.10 Deep sequencing of p1-Vero amiR-encoding virus library. A) A scatter plot showing percentage number of each amiR-encoding virus in the entire p1-Vero amiR-encoding virus library Highlighted variants represent viruses with percentage reads ≥ 1.3%**.** Dotted line depicts expected percentage for an even distribution of plasmids within the plasmid library i.e., (100% /204 = ~0.49 %).

3.3.4 Evaluation of generated plasmid and virus libraries

Scatter plots were generated based on percentage reads of each amiR-encoding plasmid or virus in the plasmid or virus libraries respectively. The expected mean percentage representation of each amiR-encoding plasmid or virus in respective library was determined as 1/204 × 100 = ~0.49%. Descriptive statistical analysis of the three amiR-encoding libraries revealed an increasing lowering of the percentage median in comparison to the constant mean of 0.49%. The median reduced from 0.474%, to 0.39% and 0.32% for plasmid library, p0-293T and p1-Vero amiR encoding libraries respectively. This highlighted the increased skewing of the libraries at each stage of generation (plasmid library to p0-293T and p1-Vero library). Furthermore, the correspondingly increasing standard deviation of each amiR-encoding library at each the stage in library generation highlighted

an increased variance in each subsequently generated library. The standard deviation for the plasmid library was 0.24%, but increased to 0.39% for p0-293T and 0.56% for p1-Vero libraries (Figure 3.11 A). A total of four amiRs that were not represented in plasmid amiR encoding library was maintained through p0-293T and p1-Vero amiR-encoding virus libraries. Despite the increasing variance and skewing as the virus library was amplified, a stacked bar plot for each amiR-encoding library emphasised that the libraries still encoded mixed poputions of either plasmid or viruses (Figure 3.11 B).

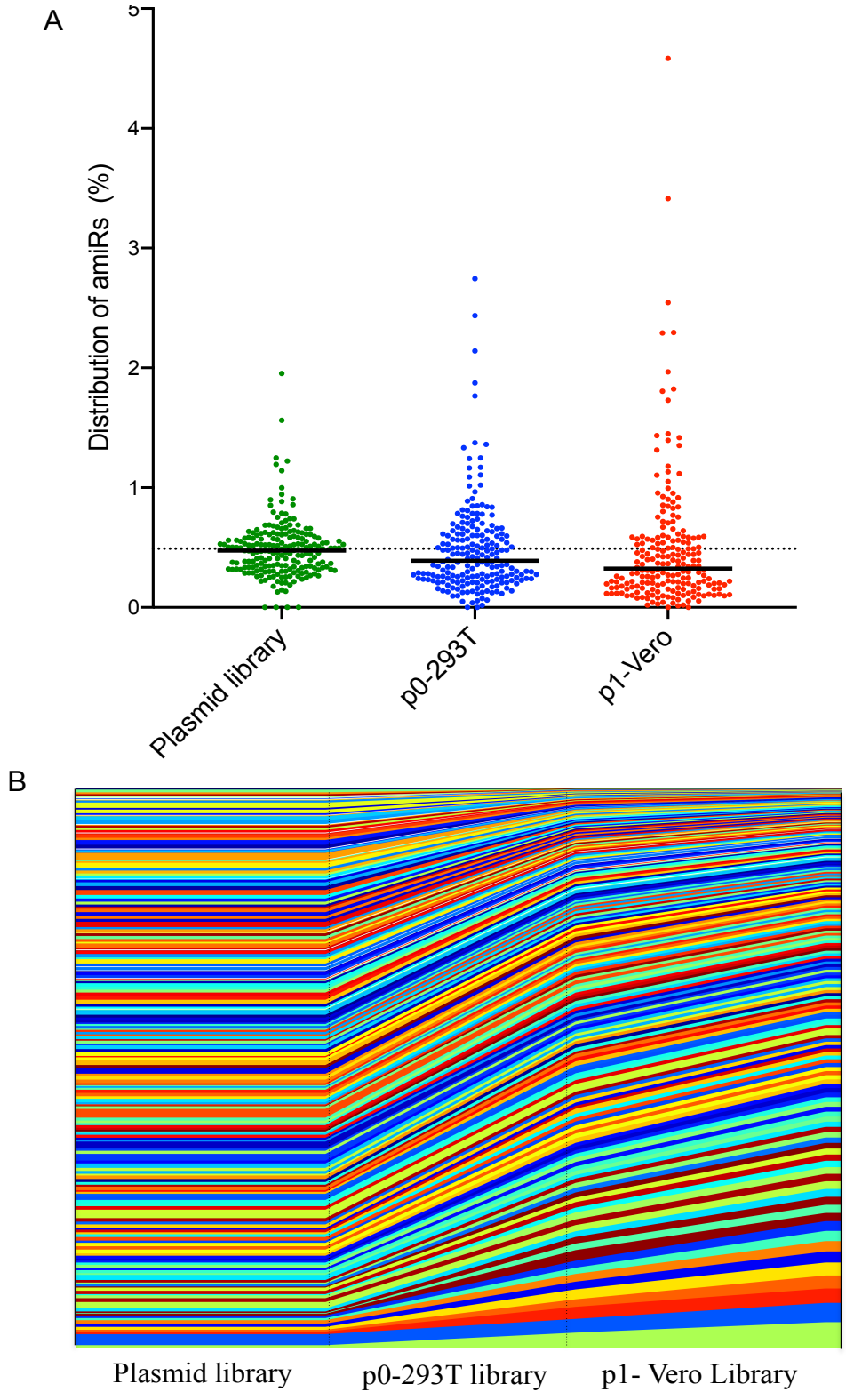

Figure 3.11 Distribution of amiR-encoding variants within the respective libraries. A) Scatterplot showing distribution of amiR-encoding variants within the respective libraries. The mean percentage representation was determined as 100/204 ~0.49%, shown by the dotted line. The median value for each library is indicated by a black horizontal line. B) Stacked interpolated bar plot showing distribution of amiR-encoding variants within the respective libraries. Each colour represents a single amiR whose relative proportion corresponds to its composition in the respective library.

3.3.5 Generation of scrambled amiR virus library as a control library

In order to ensure that selection is not occurring stochastically during *in vitro* and *in vivo* RNAi screening, a scrambled-amiR virus library was generated as control for studies performed in the subsequent chapters. A scrambled-amiR plasmid library was provided by Professor Benjamin tenOever of Icahn School of Medicine at Mount Sinai, USA. This scrambled-amiR plasmid library is essentially a scrambled version of miR-124 pre-amiR in which miR-124 3p region (TAAGGCACGCGGTGAATGCCA) is scrambled at specific locations as indicated by an "N" (TAANNNNCGTNGTTNNTGCCA) to render it non-functional or unable to any target host. This scrambled library would have a theoretical maximum of 47 (i.e. 16,384) variants, but it was not essential for us to recover the entire library. The scrambled amiR library was inserted into the Δ15-89 nucleotide position in the 3' UTR of $WNV_{NSW2011}$ to generate full length WNV scrambled-amiR virus library by CPER, similar to the targetted library already prepared. To do this, CPER fragment 5 that encompasses NS5 and part of the 3′ UTR (before Δ15-89 amiR insertion site) was generated from d15GFP-amiR WNV cDNA, NS5_Forward and Before amiR_Reverse set of primers by PCR (Figure 3.6 A). Fragment 6, scrambled amiR library fragment, was generated by performing a 15-cycle PCR using scrambled-amiR plasmid library as template, Q5 high-fidelity DNA Polymerase PCR kit (New England Biolabs, USA), amiR_Forward and amiR_Reverse primers (Figure 3.6 A). Thereafter 0.45pmol of each fragment equivalent to 2.709 X 10^{11} DNA copies of the generated scrambled amiR library fragment, RT-PCR-amplified fragments encompassing the rest of the $WNV_{NSW2011}$ genome and CMV UTR-linker were assembled by CPER to generate infectious cDNA for transfection.

The resultant CPER product was transfected into HEK 293 cells to recover p0-293T scrambled amiR virus library. At three days post transfection, 2 mL of p0-293T virus culture supernatant was collected as p0-293T virus stock. Immunoplaque assay on Vero cell was performed on p0-293T stock and virus titre determined as 4×10^6 pfu/mL. To generate p1-Vero virus stock for subsequent experiments, Vero cells were infected at MOI =1 with p0-293T virus stock. At 3 days post infection, virus culture supernatant was harvested as p1-Vero virus stock and virus titre determined by immunoplaque assay on Vero as 4.66×10^6 pfu/mL (Figure 3.12 A). Viral RNA was purified from virus culture supernatant using Nucleospin RNA kit and protocol (Macherey Nagel, Germany). Viral cDNA was made using superscript IV reverse transcriptase kit and protocol (Thermo Scientific, USA). To generate p1-Vero virus library amplicon for deep sequencing, PCR was performed using Q5 high-fidelity DNA Polymerase PCR kit (New England Biolabs, USA), scrambled amiR library cDNA and amplicon_adaptor_F and amplicon_adaptor_R primers (Figure 3.12 B). Different amounts of cDNA for each PCR were used to obtain the best amplicon for deep sequencing. Therefore, the 10μL cDNA band, which was brightest of the three bands was chosen,

purified by DNA gel extraction and deep sequenced (Figure 3.12 B).

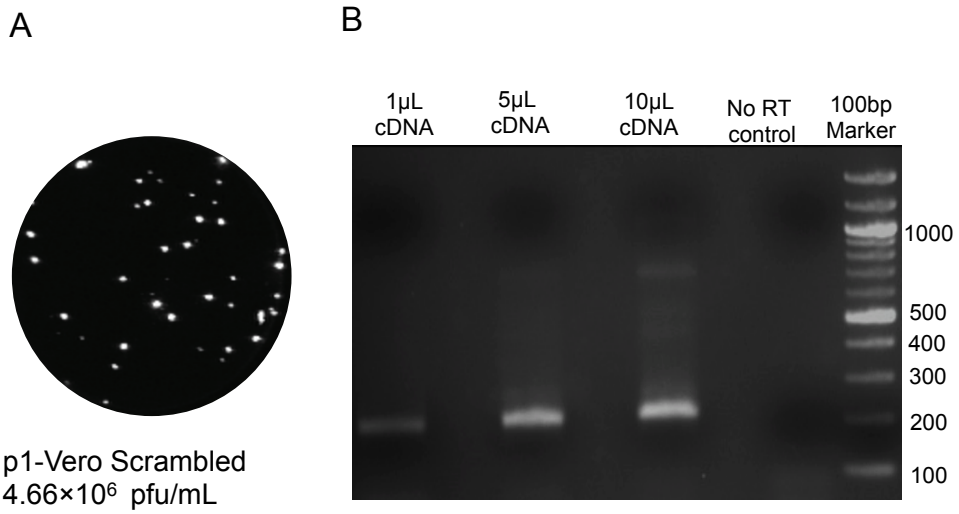

Figure 3.12 Generation of p1-Vero scrambled amiR encoding virus library. A) Virus titre was determined on Vero cells by immunoplaque assay. B) Viral RNA was purified from culture supernatant and treated with DNase I enzyme. Products of a 15-cycle PCR using cDNA generated using 1µL, 5µL, 10µL of cDNA was loaded in Lanes 1, 2 and 3 while 0.562µL of RNA was loaded in Lane 4 as no RT control. A 100bp DNA ladder was loaded in to Lane 5 as a marker. Expected DNA band size is 215bp.

Deep sequence results were uploaded onto Galaxy Australia (UQ Research Computing Center) and analysed using Salmon transcript quantification tool to ascertain enrichment of p1-Vero scrambled amiR-encoding virus library (Appendix 2). Deep sequencing revealed that the scrambled library contained 6719 scrambled amiR sequences. Fequency percentage distribution of reads corresponding to percentage enrichment of scrambled amiR-encoding viruses with in the library was determined (Figure 3.13). Analysis of deep sequence results revealed that 84.58% (5683 / 6719), 8.28% (556 / 6719), 2.13% (143 / 671) and 1.1% (143 / 6719) scrambled amiR viruses were enriched to 0.01%, 0.02%, 0.03% and 0.04% of the total scrambled amiR-encoding viruses with in the p1-Vero library respectively.

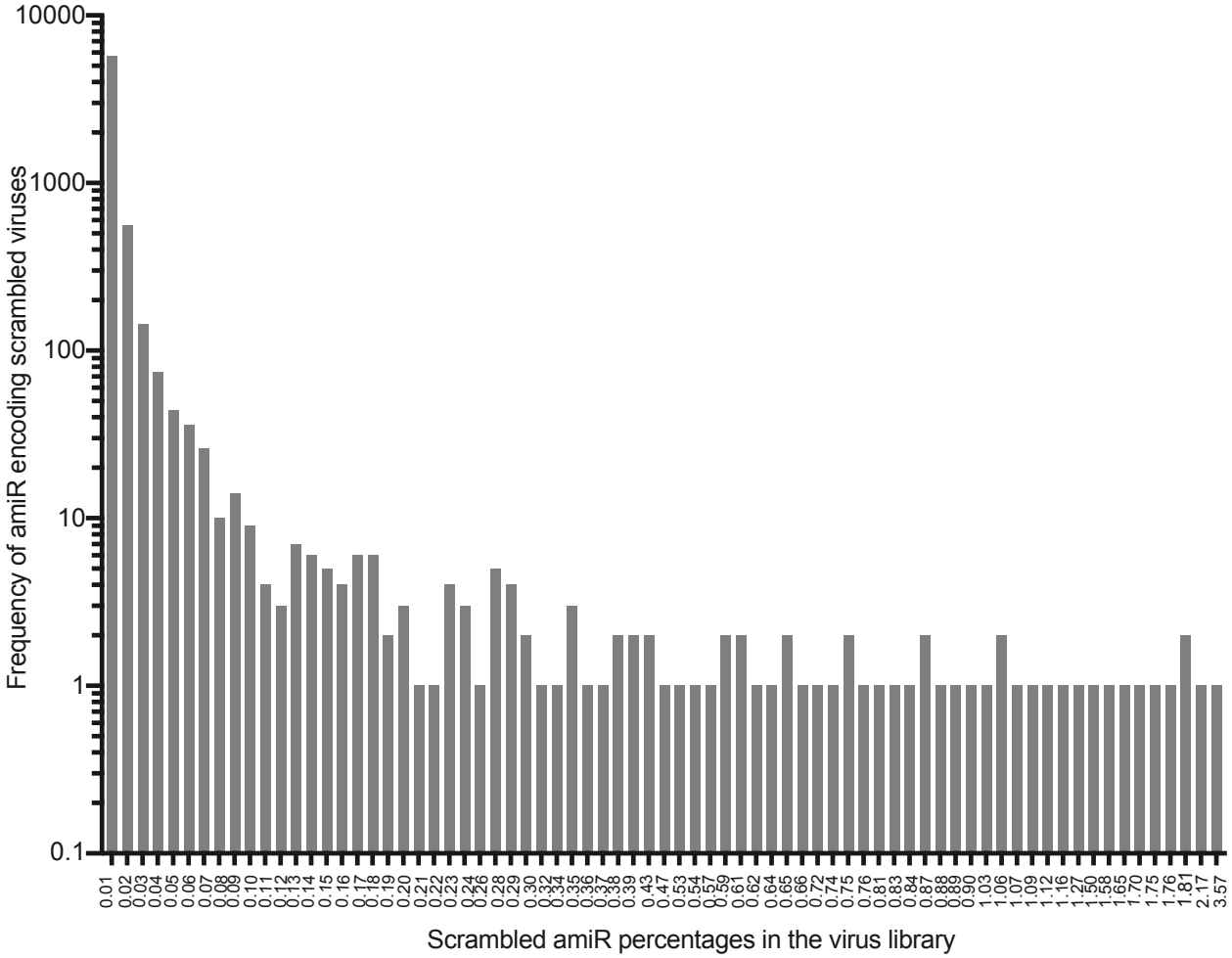

Figure 3.13 Deep sequence of p1-vero scrambled amiR virus library. A frequency distribution plot showing the percentage number of scrambled amiR-encoding virus in the entire p1-Vero scrambled amiR-encoding virus library.

3.4 Discussion

3.4.1 Generation of the amiR-encoding plasmid library

The 3' UTRs of flaviviruses have been previously shown to allow insertion of heterologous sequences [261]. Bearing this in mind the 3' UTR of $WNV_{NSW2011}$ was modified to encode a unique pre-amiR hairpin at nucleotide position Δ15-89 from the start of the 3' UTR. The pre-amiR hairpin inserted was based on miR-124, predominantly expressed in mice brains. Previous work performed using Kunjin virus replicon showed that deletion of nucleotides 29 to 102 of 3' UTR, a region, which encompasses nucleotide positions Δ15-89 does not alter replication of resultant virus [262]. When 76 nucleotides starting form nucleotide 29 in the 3' UTR of Kunjin were deleted replicon, the resultant replicon replicated efficiently. In contrast, deletion from nt 29 to 382 of 3' UTR resulted in significantly reduced replication rates [262].

Analysis of deep sequencing results of amiR-encoding plasmid library revealed that 96% (196/204)

amiR-encoding plasmids were represented at least once in the library while 3.92% (8/204) and 1.96% (4/204) plasmids were over and under represented respectively (Figure 3.11). Over-representation and under-representation could have potentially resulted from pipette mixing errors during manual combining of plasmids to generate amiR-encoding plasmid library. Some of the bias in this plasmid library was carried over to generation of virus library by CPER. To eliminate this hurdle, individual viruses would be generated by CPER, virus titre determined and individual viruses pooled together in equal amounts. However, this approach is not feasible especially when generating large-scale virus libraries, due to the intense labour involved in generating a single virus let alone generating an entire virus library individually. Nevertheless, the representation of each amiR-encoding plasmid with in plasmid library was considered adequate for subsequent generation of virus libraries. Therefore CPER approach was utilised to generate p0-293T virus library.

3.4.2 CPER approach for construction of amiR-encoding virus libraries

Traditional cloning approaches previously used for generation of large virus libraries involve extensive cloning and purification of large bacterial stocks of infectious plasmid clones before transfection or RNA electroporation in cells [263]. However cloning of full-length cDNA sequences during plasmid DNA propagation in bacteria often results in toxicity due to cryptic promoter sequences, and subsequent unsuccessful recovery of plasmid clones, or unwanted deletions and mutations (reviewed in [264]). Although this bottleneck could be countered by inserting introns into difficult regions of viral cDNA, traditional approaches would still necessitate propagation of full-length cDNA plasmid in bacteria [265]. Introns break up cryptic sequences, which are spliced when processed in vertebrate cells.

The innovation of CPER completely abolished the need for plasmid DNA propagation in bacteria and subsequent RNA transcription, reducing possible introduction of mutations from error-prone cloning and bacterial propagation steps. CPER is a next-generation reverse genetics approach streamlined to rapidly generate authentic viruses from sequence data [109, 237, 258, 260, 266, 267]. Therefore the use of CPER approach to construct ISG-targeting amiR virus libraries described in this chapter further validates the robustness and effectiveness of the CPER methodology.

3.4.3 Clone representation in virus libraries

Although both p0-293T and p1-Vero amiR-encoding virus libraries generated encoded mixed virus populations, it was noted that varaince and skewness increased down stream generation of p1-Vero virus library form p0-293T virus library. Transfection of virus library into a human cell line (HEK 293) and then infection of a monkey cell line (Vero) was expected to allow generation of an unbiased virus library as each pre-amiR sequence solely targeted mouse genes. Significant off-target genes were not found in the human genome and the monkey genome when BLAST was performed on

each amiR-encoding siRNA sequence included in the library. However, prediction of target sequences of siRNAs is often imperfect, as a number of mismatches can be tolerated [268, 269]. A total of 16/204 (7.84 %) and 21/204 (10.29%) of amiR-encoding viruses were over represented with x ≥ 1% reads after passage in HEK and Vero cells respectively. In addition comparison between plasmid and p0-293T amiR encoding libraries showed 12/ 204 (5.88%) amiR encoding clones that were not over-represented (x ≥ 1% reads) in the plasmid library were over represented after transfection in HEK 293 cells. In addition at p1-vero generation, amiR-encoding viruses with higher percentage reads were further amplified to greater enrichement suggesting that the input amount of each amiR-encoding virus was systematically amplified to higher levels (Figure 3.11). For instance, Nmi clone #2 amiR-encoding virus (NMI-amiR WNV) at p0-293T had a percentage number of 2.74% and on passage in Vero cells the percentage number of reads increased to 4.58%. The trend observed when p0-293T virus stock was amplified by passaging in Vero cells, showed that over-expressed amiR-encoding viruses at p0-293T were further amplified higher levels in p1-Vero virus stock. In addition, at least one amiR-encoding virus was represented in either p0-293T or p1-Vero thus suggesting that all intended mouse genes were targeted by at least one amiR-encoding virus.

Although there was small degree of bias in the generated amiR-encoding virus library, the library still maintained a good representation amiR population, with at least one amiR-encoding virus targeting a single host gene. Therefore given that the proportion of different amiR encoding viruses in the input virus library used for subsequent experiments was known, changes in virus populations could be easily assessed.

3.4.4 Use of *Drosha*$^{-/-}$ 293T cells to improve amplification of virus libraries

A potential way to further reduce bias in the virus library during mammalian cell amplification would be to use *Drosha*$^{-/-}$ HEK 293 cells. Drosha is an RNase III enzyme that initiates microRNA processing. Drosha cleaves primary miRNA (pri-miRNA) transcript in the nucleus to release precursor micro RNA (pre-miR), which is transported by exportin to the cytoplasm and further cleaved by Dicer to generate a 21-22 nt long mature miRNA for gene regulation [143, 270]. Therefore transfection of *Drosha*$^{-/-}$ HEK 293 cells would prevent the cleavage of pri-miRNA from the viral RNA genome since the pri-miRNA hairpin inserted in the 3' UTR would not be recognised in absence of Drosha. Therefore the amiR-encoding virus genome would not be cleaved to release the pre-miR haipin, no viral RNA would be destroyed and therefore no selection of amiR sequences would occur.

In summary, despite over- and under-represention of a small proportion amiRs in the library, an amiR-encoding plasmid DNA library was successfully generated, and a diverse virus library was recovered in p0 and propagated in p1, and represents an important tool for the study of host genes

important for control of WNV replication by *in vivo* screening.

Chapter 4: *In vitro* RNA interference screening identifies IFITM3 as a crucial antiviral gene against West Nile virus infection.

4.1 Introduction

Having generated a mouse ISG-targeting amiR-encoding virus library including a scrambled sequence amiR virus library as control, the next step was to perform RNAi screening, initially *in vitro*. Our hypothesis was that screening in wild type mouse embryonic fibroblasts (WT MEF) vs. interferon-alpha/beta receptor deficient (*Ifnar1*$^{-/-}$) MEF cells will allow us to identify new host determinants and their relative importance in controlling replication of WNV. Both mouse-derived cell lines were used because the amiR-encoding virus library targeted mouse specific ISGs. In addition, WT MEF and *Ifnar1*$^{-/-}$ MEF cells were used to assess and compare the effect of *in vitro RNAi* between an immune competent and immune compromised host respectively. To perform *in vitro* RNAi screening, three passages in WT MEFs and *Ifnar1*$^{-/-}$ MEF were performed at a low MOI of 0.1 to subject virus libraries to selective pressure and allow for natural selection to occur. West Nile virus variants that are enriched would therefore encode amiRs that down-regulate expression of antiviral host gene(s) important for restricting West Nile virus replication.

4.2 Methods and Materials

For ease of reading, I have included materials and methods specific to this chapter.

4.2.1 Generating amiR amplicons by PCR for deep sequencing

To generate amplicons for deep sequencing by PCR, virus culture fluid was first clarified to remove any cell debris by centrifugation at 1000 g for 5 minutes, and thereafter 5 mL of virus culture fluid was concentrated to 250 µL using Amicon ultra-15 mL 100 kDa centrifugal filter units, (Merck Millipore, USA) before RNA extraction. To purify viral RNA, Nucleospin RNA kit (Macherey Nagel, Germany) was used following manufacturer's instruction. Purified RNA was eluted in 30 µL of nuclease free water and treated with RQ1 RNase-free DNase enzyme (Promega, USA) to remove any traces of DNA. Thereafter a 15-cycle one-step RT-PCR was performed using purified DNase-treated RNA as template, Adaptor amplicon_Forward and Adaptor amplicon_Reverse primers (Table 4.1) and superscript III one-step RT-PCR system with platinum Taq high fidelity DNA polymerase kit (Thermo Scientific, USA). To obtain amplicons for deep sequencing, 2% (w/v) TAE agarose gel electrophoresis was performed; bands were excised from gels, purified using Monarch DNA Gel Extraction Kit, (New England Biolabs, USA). Thereafter DNA fragments concentration was determined by Nanodrop spectrophotometry before Illumina sequencing. The Expected DNA band size was 215 bp.

Table 4.1 Primers and primer sequences used to generate PCR amplicons

Primer Name	**PCR Amplicon**	**Sequence 5′- 3′**
Adaptor_amplicon _ Forward	AmiR Adaptor amplicon for deep sequencing	TCGTCGGCAGCGTCAGATGTGTATAAGAGA CAGGAAGACACGACATTTGTTGAGGATACA GTATTGTAAATAGTTTG
Adaptor_amplicon _ Reverse		GTCTCGTGGGCTCGGAGATGTGTATAAGAG ACAG CAT TCA AGT GCA GCC GTA GGC TCC GC
3′ UTR_ Forward	IFITM3-amiR or GFP-amiR WNV RNA	GAAGACACGACATTTGTTGAGGATACA
3′ UTR_Reverse		TCCTGTGTTCTCGCACCAC
NS3_Forward	NS3NS4B	GATAACTCTCCAATACACAAAGAGAGGAG
NS4_Reverse		CGTCCTTTTGCCCCACCTC
NS4A_Forward	NS4A	TTGAGTGTGATGACCATGGGAG
NS4A_Reverse		TAGCTGGTTGTCTGTCTGCG

4.2.2 Western blot analysis

Western blot analysis was performed to determine expression of proteins in cells infected with respective viruses as described in the result section. To perform western blot analysis, WT MEF and *Ifnar1*$^{-/-}$ MEF were seeded at 5 ×10^5 cells per well in 6-well plate and incubated at 37°C in 5% CO_2 humidified incubator for 12 hours until 90% confluent. The following day, MOI was determined as indicated in the figure legends and cells were infected with IFITM3-amiR WNV, GFP-amiR WNV, WT-$WNV_{NSW2011}$ or mock infected. At 48 hours post infection, infected cells were lysed in NP-40 lysis buffer, sonicated and 75 µL of each sample heated with 25 µL of 4 × NuPAGE protein loading dye at 95°C for 5 minutes. Thereafter, pre-cast NuPAGE 4-12% Bis-Tris protein gels, (Invitrogen, USA) were loaded with 25 µL of each sample per lane along with precision plus protein kaleidoscope ladder (BioRad, USA) and 1 × NuPAGE running buffer added before electrophoresis. Electrophoresis was performed at 165 V for 45 minutes. Thereafter proteins were transferred onto nitrocellulose membrane using iBlot2 dry blotting system, (Thermo Scientific, USA) following manufacturer's instruction. On completion of transfer, membranes were blocked in 1 × Pierce

blocking buffer (Thermo Scientific, USA) for 1 hour at 37°C before probing with intended primary antibody for 1 hour at 37°C. Blots were then washed five times using 1× PBS containing 0.05% Tween 20 (PBS-T) to remove unbound primary antibody, with each wash lasting for five minutes before probing with respective secondary antibody for 1 hour at 37°C in the dark. Membranes were washed five times using 1× PBS containing 0.05% Tween 20 (PBS-T) to remove unbound secondary antibody. To scan membranes LI-COR Biosciences Odyssey Infrared Imaging System with the following specifications: channel = 680/800, intensity = auto, focal length = 3 mm, resolution = 169 μM was used to visualise protein bands.

4.2.3 Northern blot analysis

To perform northern blot analysis, Vero cells were seeded at 5×10^5 cells per well in a 6-well plate and incubated at 37°C in a 5% CO_2 incubator for 12 hours until 90% confluent. The following day, cells were infected with MOI =1 with p1-Vero virus stock reconstituted in 1 mL for 1 hour, rocking every 15 minutes to prevent cells from drying. Thereafter, virus inoculum was removed and replaced with DMEM supplemented with 5% FCS, 50 units/mL of penicillin and 50 μg/mL of streptomycin and plates incubated at 37°C in a 5% CO_2 incubator for 48 hours. At 48 hpi, cells were harvested and total RNA purified using TRI Reagent kit (Sigma-Aldrich, USA) following manufacturer's instructions. RNA concentration was determined by Nanodrop spectrophotometry and 5 μg was subjected to electrophoresis in 15% TBE-urea polyacrylamide gel (Invitrogen, USA) to denature and separate RNA molecules. The gel was then stained with ethidium bromide for 1 hour at room temperature with constant rocking. Thereafter, RNA was electro-transferred to an Amersham Hybond-N+ membrane (GE Health Care Life sciences, USA) at constant 35 Voltage for 90 minutes in 0.5× tris-borate-EDTA (TBE) buffer. Transferred RNA was cross-linked to the membrane by UV cross-linking at 1,200 kDj/cm^2. The resultant was hybridised overnight with γ-P^{32}-labeled DNA oligonucleotide probe complementary to mature IFITM3-amiR sequence at 37°C in ExpressHyb hybridization solution (Clontech, USA). The following day membranes were washed four times in NorthernMax high stringency wash buffer (Thermo Scientific, USA) at 37°C and exposed overnight to phosphor imager screen (GE Healthcare). Thereafter, the nylon membrane was scanned using Typhoon 9400 variable mode imager (Amersham Pharmacia Biotech, USA).

4.2.4 Immunoprecipitation of WNV–E protein

To immunoprecipitate WNV-E protein from virus culture fluid, *Ifnar1*$^{-/-}$ MEFs were infected at MOI =1 with IFITM3-amiR WNV, GFP-amiR WNV and WT-$WNV_{NSW2011}$ viruses. At 48 hpi, virus culture fluid was harvested for each respective virus; cells washed three times with PBS and then replaced with 20mL of DMEM supplemented with 5% FCS, 50 units/mL of penicillin and 50 μg/mL of streptomycin. The cells were incubated for a further 24 hours, and then virus culture fluid

harvested as 72 hpi sample. The samples harvested at 48 hpi and 72 hpi time point samples were clarified, and concentrated using Amicon ultra- 15 mL 100 kDa centrifugal filter units, (Merck Millipore, USA). An equal amount (250 µL) of virus particles were immunoprecipitated from each sample by binding a fixed amount (5 µg) of purified anti-E monoclonal antibody (6B6C-1) as the capture antibody on Dynabead protein G (Invitrogen, USA). Immunoprecipitated WNV-E protein was then subjected to western blot analysis as described above. Membranes were transferred onto a nitrocellulose membrane using iBlot 2 dry blotting system, (Thermo Scientific, USA) following manufacturer's instruction. Thereafter, blots were blocked for 1 hour using 50 µL of 1 × Pierce Clear Milk Blocking Buffer (Thermo Scientific, USA). To determine amount of IFITM3 protein incorporated into membranes of secreted WNV virions, nitrocellulose membranes were probed with rabbit polyclonal IFITM3 antibody (ProteinTech, USA) for 1 hour at 37°C with constant rocking. Thereafter, blots were washed five times using 1× PBS containing 0.05% Tween 20 (PBS-T) to remove traces of unbound primary antibody and probed with IRDye 800 cw anti-rabbit secondary antibody (LI-COR Biosciences, USA) with constant rocking for 1 hour at 37°C in the dark. Nitrocellulose membranes were then washed five times using 1× PBS containing 0.05% Tween 20 (PBS-T) to remove any traces of unbound secondary antibody before scanning. To scan, LI-COR Biosciences Odyssey Infrared Imaging System with following specifications: channel =680/800, intensity = auto, focal length = 3 mm, resolution = 169 µM was used to visualise protein bands.

4.2.5 Determining RNA copy numbers of *Ifnar1*$^{-/-}$ MEF generated virus stocks

To ascertain RNA copy numbers of *Ifnar1*$^{-/-}$ MEF generated virus stocks, a standard curve was first generated. A CPER fragment spanning $WNV_{NSW2011}$ NS3-NS4A and NS4B regions (termed here NS3NS4B) was generated from $WNV_{NSW2011}$ cDNA using NS3_Forward and NS4_Reverse sets of primers (Table 4.1), PrimeSTAR GXL DNA Polymerase (Clontech, USA) kit and protocol. To obtain NS3NS4B CPER fragment, 1% (w/v) TAE agarose gel electrophoresis was performed; band was excised from gel and purified using Monarch DNA Gel Extraction Kit, (New England Biolabs, USA). Thereafter, DNA fragment concentration was determined by Qubit fluorometer using Qubit dsDNA BR Assay kit and protocol (Thermo Scientific, USA). RNA copy numbers were calculated basing on the concentration obtained and 10-fold serial dilutions from 10^{11} to 10^{7} RNA copies made to generate quantitative reverse transcriptase PCR (qRT-PCR) standards. Using *Ifnar1*$^{-/-}$ MEF generated virus stocks, viral RNA was extracted from 150 µL of IFITM3-amiR WNV, GFP-amiR WNV and WT-WNV using NucleoSpin RNA, (Macherey-Nagel, Germany) isolation kit and protocol. Subsequently qRT-PCR was performed using extracted RNA, serial diluted standards, NS4A_Forward and NS4A_Reverse primers upstream NS4A region of WNV (Table 4.1) and superscript III platinum SYBR Green one-step qRT-PCR (Thermo Scientific, USA) kit and protocol. A standard curve was obtained and RNA copy numbers of IFITM3-amiR WNV, GFP-

amiR WNV and WT-WNV determined.

4.2.6 Infection of mice

For every animal experiment included in this chapter, 4-week old CD-1 mice were infected via the intraperitoneal route with respective viruses as stated in the figure legends. Mice were monitored for clinical signs and each day a clinical score was recorded for a period of 21 days. To determine viraemia, mice were tail-bled from one day to seven days post infection, collected blood allowed to clot for 30 on ice and centrifuged at 500 *g* to obtain sera for immunoplaque assay on C6/36 cells as described below. To determine virus burden in the brains, mice that presented with encephalitic signs were culled and brains harvested for subsequent experiments such as confirming virus identity and viral load in the brain.

4.2.7 RNA extraction and generation of amplicons for Sanger sequencing from mouse brains

Harvested mouse brains were suspended in 1 mL of PBS and homogenised with 3 mm stainless steel beads at 30/second frequency for 3 minutes using TissueLyser II, (Qiagen, USA). Total RNA was extracted from 150 µL of brain homogenates using TRI Reagent LS (Sigma, USA) according to following manufacturer's instructions. Thereafter, RT-PCR was performed using total RNA as template, superscript III one-step RT-PCR system with platinum Taq high fidelity DNA polymerase kit (Thermo Scientific, USA) and $WNV_{NSW2011}$ 3′ UTR_Forward and 3′ UTR_Reverse primers (Table 4.1) as well as purified RNA as template. The generated 3′ UTR amplicons were visualised on 1.4%(w/v) TAE agarose gel electrophoresis, obtained bands were excised from gels and purified using Monarch DNA Gel Extraction Kit (New England, USA). Thereafter, DNA concentrations were determined by using Nanodrop spectrophotometry before Sanger sequencing.

4.2.8 Virus titration of mouse-derived samples

To determine virus titres an immunoplaque assay on C6/36 monolayer of cells was performed. C6/36 cells were seeded at 1×10^6 cells per well in a 96 well plate one day before. The next day, sera, brain or spleen homogenate samples were serially diluted with RPMI media to infect C6/36 cells for 2 hours. At two hours post-infection, 175 µL of overlay medium was added to each well. The overlay medium was made by mixing ×2 M199 medium supplemented with 5% FCS, 50 units/mL of penicillin and 50 µg/mL of streptomycin with 2% carboxymethyl cellulose in a ratio of 1:1 and plates incubated for 96 hours for C6/36 cells. At 96 hpi, the overlay was removed and 100 µL of ice-cold 80% acetone in PBS added and incubated at –20°C for 1 hour to fix the cells before completely air-drying the plates. To detect WNV-E protein, plates were first blocked by adding 50 µL of Pierce clear milk blocking buffer (Thermo Scientific, USA) to each well and incubating the plates at 37 °C for 1 hour. Thereafter, 50 µL of mAb E-16 (human anti-E) was added to each well and plates incubated at 37°C. Plates were then washed six times using 1× PBS containing 0.05%

tween 20 (PBS-T) to remove any traces of unbound primary antibody before adding 50 µL of IRDye 800 cw goat anti-human secondary antibody (LI-COR Biosciences, USA) to each well. Plates were then incubated at 37°C for 1 hour and thereafter washed six times, air-dried and then kept in the dark at room temperature until ready for imaging. Plates were scanned using the LI-COR Biosciences Odyssey Infrared Imaging System using following specifications: channel = 800, intensity = auto, focal length = 3 mm, resolution = 42 µm. Viral titres from iPA are expressed as pfu/mL. Obtained titres were log-transformed and plotted using GraphPad Prism version 8.

4.3 Results

4.3.1 *In vitro* RNAi screening with a library of West Nile viruses encoding artificial miRNAs targeting host antiviral genes identified IFITM3 as a major antiviral factor against West Nile virus.

To determine the selection and enrichment of particular ISG-targeting amiR-encoding WNV during *in vitro* culture, three independent experiments were performed in WT MEF and *Ifnar1*$^{-/-}$ MEF cells, each with three serial passages of virus stocks (Figure 4.1). Both WT MEFs and *Ifnar1*$^{-/-}$ MEFs were infected at low MOI =0.1 (10^5 pfu) with p1-Vero mouse ISG-targeting amiR-encoding virus mixed with 200 pfu of scrambled amiR virus library. At 3 days post infection, culture fluid was collected from WT MEF and *Ifnar1*$^{-/-}$ MEF as p2-WT MEF and p2- *Ifnar1*$^{-/-}$ MEF virus stocks respectively. Passage two (p2) virus titres were determined by immunoplaque assay on Vero cells, and WT MEF and *Ifnar1*$^{-/-}$ MEF infected at MOI = 0.1 to generate p3-WT MEFs and p3- *Ifnar1*$^{-/-}$ MEF virus stocks. Thereafter process was repeated to generate p4 virus stocks. These series of experiments generated three passages in WT MEF and three passages in *Ifnar1*$^{-/-}$ MEF as shown in Figure 4.1.

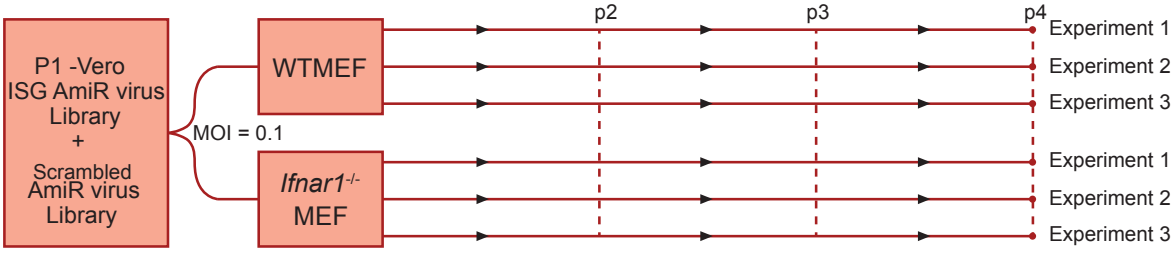

Figure 4.1 Diagram representation of experimental plan used to perform *in vitro* screening RNAi in WT MEF and *Ifnar1*$^{-/-}$ MEF cell lines. P1-Vero generated virus library (MOI = 0.1, 10^5 pfu) was mixed with 200 pfu of scrambled amiR WNV library for infection of WT MEF and *Ifnar1*$^{-/-}$ MEF. Three independent passages were performed, each time infecting at MOI =0.1.

Deep sequencing data were uploaded onto Galaxy Australia (UQ Research Computing Center) and analysed using Salmon transcript quantification data script tool to determine the population of virus variants in each passage and experiment following Salmon transcript's workflow (Appendix 2).

Results showed that IFITM3 clone #2 amiR WNV (herein referred to as IFITM3 amiR-WNV) was selected and enriched across three independent passages in WT MEF (Figure 4.2 A) and *Ifnar1*$^{-/-}$ MEF (Figure 4.2 B). By passage four (p4) in WT MEFs, 90.2%, 99.3% and 99.5% of the viruses in each independent WT MEF library preparation were IFITM-amiR-encoding viruses, whereas in *Ifnar1*$^{-/-}$ MEFs by p4, 96.5%, 89.5% and 85% of the viruses in each independent *Ifnar1*$^{-/-}$ MEF virus library consisted of IFITM3-amiR encoding virus (Appendix 3). In addition, it is noted that none of the control viruses, either scrambled amiR-encoding viruses, GFP-amiR or miR-124-amiR West Nile viruses were selected or enriched in WT MEF and *Ifnar1*$^{-/-}$ MEF cells in all three passages and independent experiments. This showed that amiRs targeting irrelevant genes are not enriched or selected across passages. However, as noted earlier, the GFP-amiR virus was absent in sequencing of the plasmid, P0, P1 libraries, suggesting that it might have been lost from the population. Furthermore, the scrambled amiR library, intended as a control, were only 200 pfu, probably representing one copy of 200 different amiR sequences. Consequently, it is not surprising that they were not selected. However, the selection and enrichment of IFITM3-amiR WNV across three independent passages in WT MEFs and *Ifnar1*$^{-/-}$ MEF highlights IFITM3's role in restricting West Nile virus replication in cells.

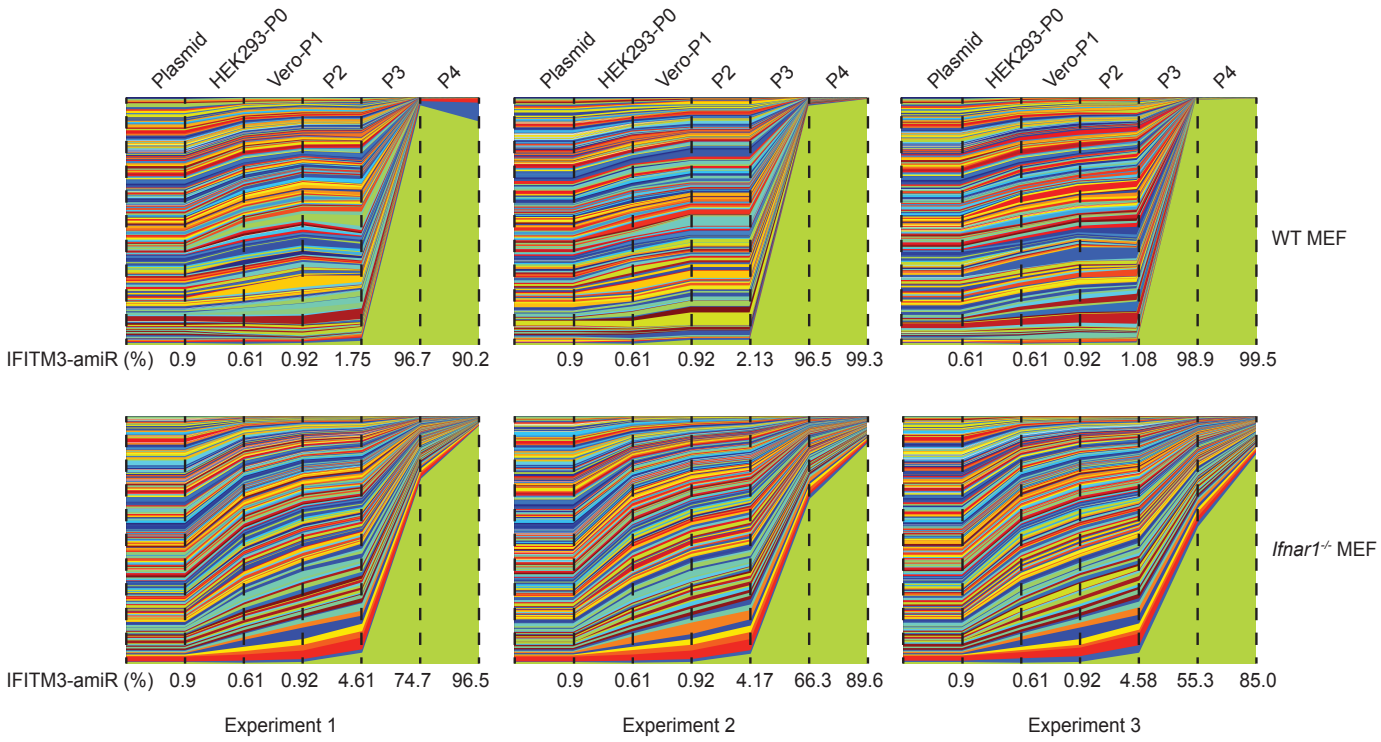

Figure 4.2 Passaging of ISG-amiR encoding West Nile virus library in WT MEF and *Ifnar1*$^{-/-}$ MEF cells selected for IFITM3-amiR encoding WNV. (A) Three passages of virus library in WT MEF and *Ifnar1*$^{-/-}$ MEF cells were performed at MOI 0.1. Deep sequencing of pre-amiR-

encoding region showed that by passage 3 (p3), more than 96% of virus library in WT-MEF consisted of IFITM3-amiR-encoding WNV. B) Deep sequencing of pre-amiR-encoding region showed that by p4, 96.5%, 89.5% and 85% of the *Ifnar1*$^{-/-}$ MEF virus library consisted of IFITM3-amiR encoding virus. IFITM3-amiR (%) denotes percentage enrichment of IFITM3-amiR WNV in corresponding library.

4.3.2 Characterisation of the role of IFITM3 in West Nile virus infection

4.3.3 Generation of IFITM3-amiR West Nile virus

Since IFITM3 amiR-encoding West Nile virus was selected and enriched during *in vitro* screening in WT MEF and *Ifnar1*$^{-/-}$ MEF, this suggested that IFITM3 plays an important role in restricting WNV replication. To investigate this, IFITM3-amiR WNV and GFP-amiR WNV (as a control virus) were generated using the CPER technique (Figure 4.3 A). To generate each individual virus, IFITM3-amiR and GFP-amiR CPER fragments were generated by PCR from respective amiR-encoding plasmids using Q5 high-fidelity DNA Polymerase PCR kit (New England Biolabs, USA) and $WNV_{NSW2011}$ 3′ UTR_Forward and amiR_Reverse set of primers (Table 4.1) and (see Chapter 3, Figure 3.6 A). Generated amiR fragments were purified by gel extraction and CPER performed (Figure 4.3 A). CPER products were transfected into HEK 293 cells to recover p0 virus stocks. At 3 days post transfection virus culture fluids were collected as p0-293T virus stocks and virus titre determined by immunoplaque assay on Vero cell monolayer (Figure 4.3 B).

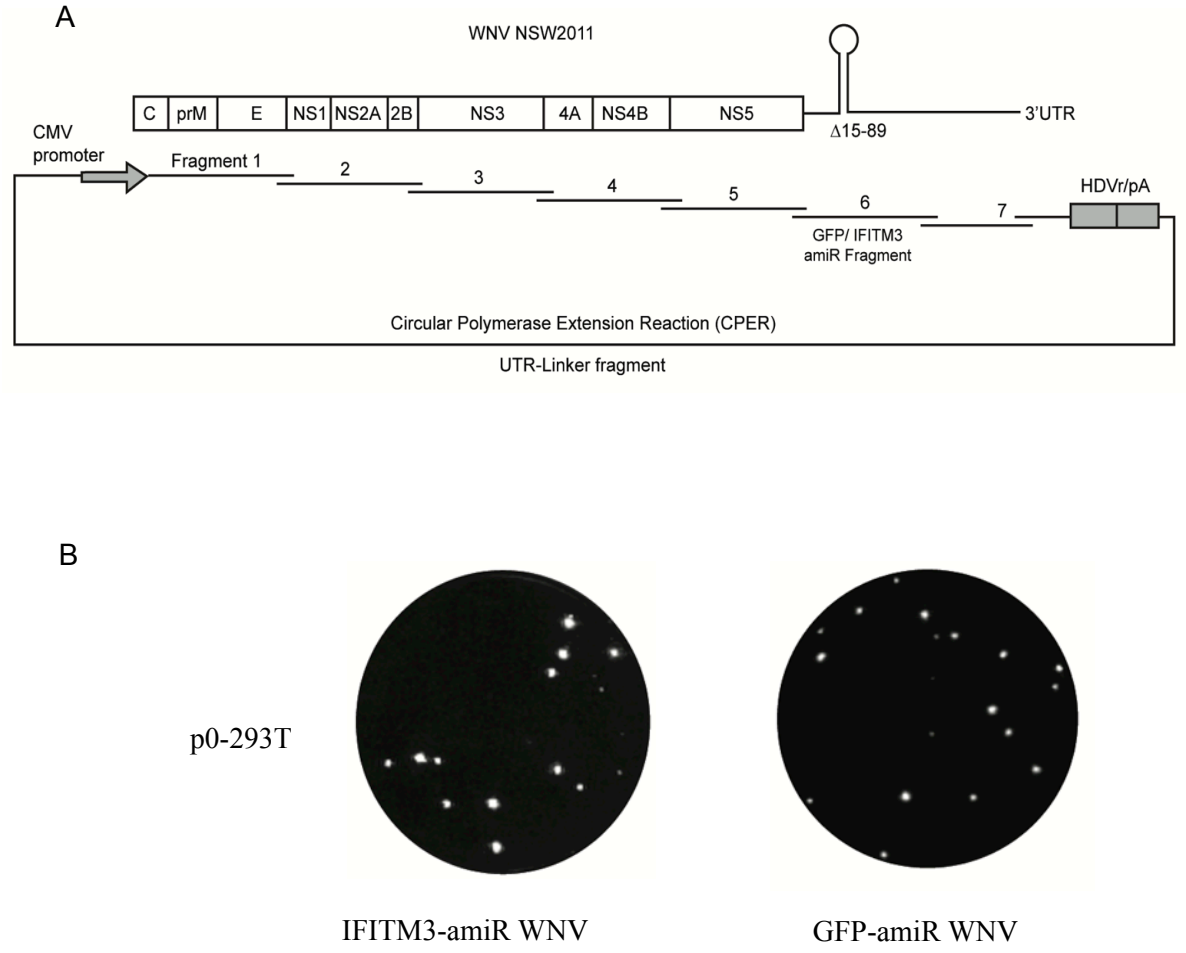

Figure 4.3 Generation of IFITM3-amiR and GFP-amiR West Nile viruses. A): Diagram representation of CPER strategy used to generate infectious IFITM3-amiR encoding cDNA and GFP-amiR encoding cDNA transfected into HEK293 cells to generate p0-293T virus library. B) Recovered p0-293T virus stocks were titred on a Vero cell monolayer by immunoplaque assay. The virus titer for p0-293T IFITM3-amiR WNV stock was 6×10^5 pfu/mL while that of GFP-amiR WNV stock was 1.72×10^5 pfu/mL.

Vero cells were then infected with p0-293T virus stocks at MOI =1 to generate larger volumes of virus stocks (named p1-Vero) for subsequent experiments. Virus titres for IFITM3-amiR and GFP-amiR encoding p1-Vero virus stocks titres were determined by immunoplaque assay on Vero cells and plaque morphology recorded (Figure 4.4 A). To confirm that the generated virus stocks contained the correct amiR hairpins, the 3′ UTRs of IFITM3-amiR WNV and GFP-amiR WNV were generated and subjected to Sanger sequencing (Figure 4.4 B). This confirmed that IFITM3-amiR and GFP-amiR encoding WNV viruses retained inserted pre-amiR hairpins. Predicted pre-amiR structures were determined by mFold and conformed to the expected structures of IFITM3 pre-amiR and GFP pre-amiR hairpin structures (Figure 4.4 C) and (Figure 4.4 D) respectively.

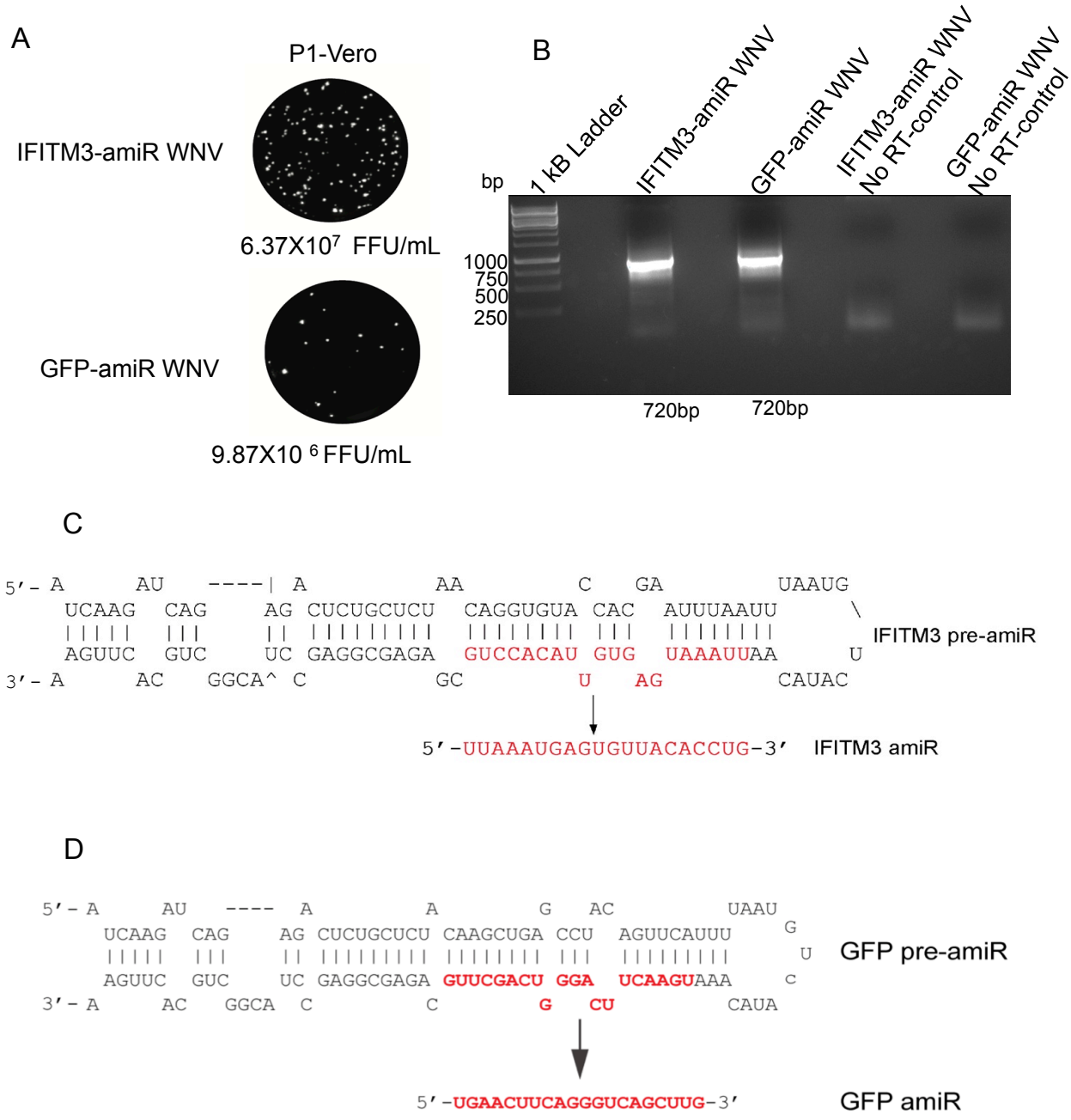

Figure 4.4 Generation of p1-Vero IFITM3-amiR and GFP-amiR West Nile virus stocks. A) Vero cells were infected with p0-293T virus stocks to generate larger volumes of p1-Vero respective virus stocks. At 72hpi, virus culture fluids were harvested, clarified by centrifugation and stored for future experiments. Generated virus stocks were titrated on Vero cells by immunoplaque assay. B) Viral RNA was extracted from culture fluid and subjected to RT-PCR using 3′ UTR_ Forward and 3′ UTR_Reverse primers. Expected DNA band size is 720bp. C) and D) predicted structures of pre-amiR hairpin in IFITM3 -amiR WNV and GFP-amiR WNV p1-Vero virus stocks respectively.

4.3.4 The IFITM3 amiR hairpin is processed by cellular machinery into functional miRNA that target specific host genes.

To determine whether inserted IFITM3 pre-amiR hairpin is processed into functional IFITM3-amiR by the host machinery, Vero cells were infected with IFITM3-amiR-encoding virus or mock infected. At 48 hpi, cellular RNA was isolated and northern blot [136] was performed to determine the expression of IFITM3 amiR. The IFITM3-amiR band (21 nt) was detected in cells infected with IFITM3-amiR encoding virus while the mock control did not produce any band as expected (Figure 4.5).

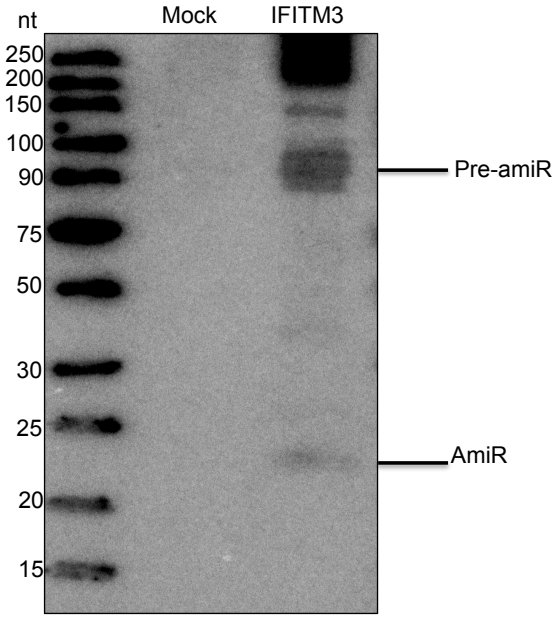

Figure 4.5 Detection of mature GFP amiR in infected Vero cells by northern blot analysis. Cells were infected with IFITM3 pre-amiR encoding WNV or mock infected. Enriched small RNA fractions were extracted at 48 hpi and 5µg of RNA was subjected to electrophoresis in 15% TBE-urea polyacrylamide gel followed by northern blot analysis with γ-^{32}P-labeled DNA probe complementary to IFITM3-amiR. The IFITM3-amiR band (21 nts) was detected in RNA samples from cells infected with IFITM3-amiR WNV. The nt denotes nucleotides.

4.3.5 The IFITM3-amiR WNV controls expression of IFITM3 expression in WT MEF cells

To ascertain whether knock down of IFITM3 in cells infected with IFITM3-amiR WNV, WT MEF were infected with IFITM3-amiR WNV, GFP-amiR WNV and WT-WNV at MOI =15 and 20 or mock infected. At 48 hpi, cell lysates were prepared and subjected to western blot analysis. Blots were probed with polyclonal rabbit anti-IFITM3, mouse anti-GAPDH and 4G2 antibody against WNV-E. Both MOI =15 and 20 produced productive virus infection of WT MEFs (positive for WNV Envelope protein) unlike lower MOI =10 (Appendix 4). IFITM3 expression was analysed using ImageJ analysis to quantify relative density of IFITM3 expression in infected cells relative to

mock-uninfected WT MEF cells (Figure 4.6 A and B).

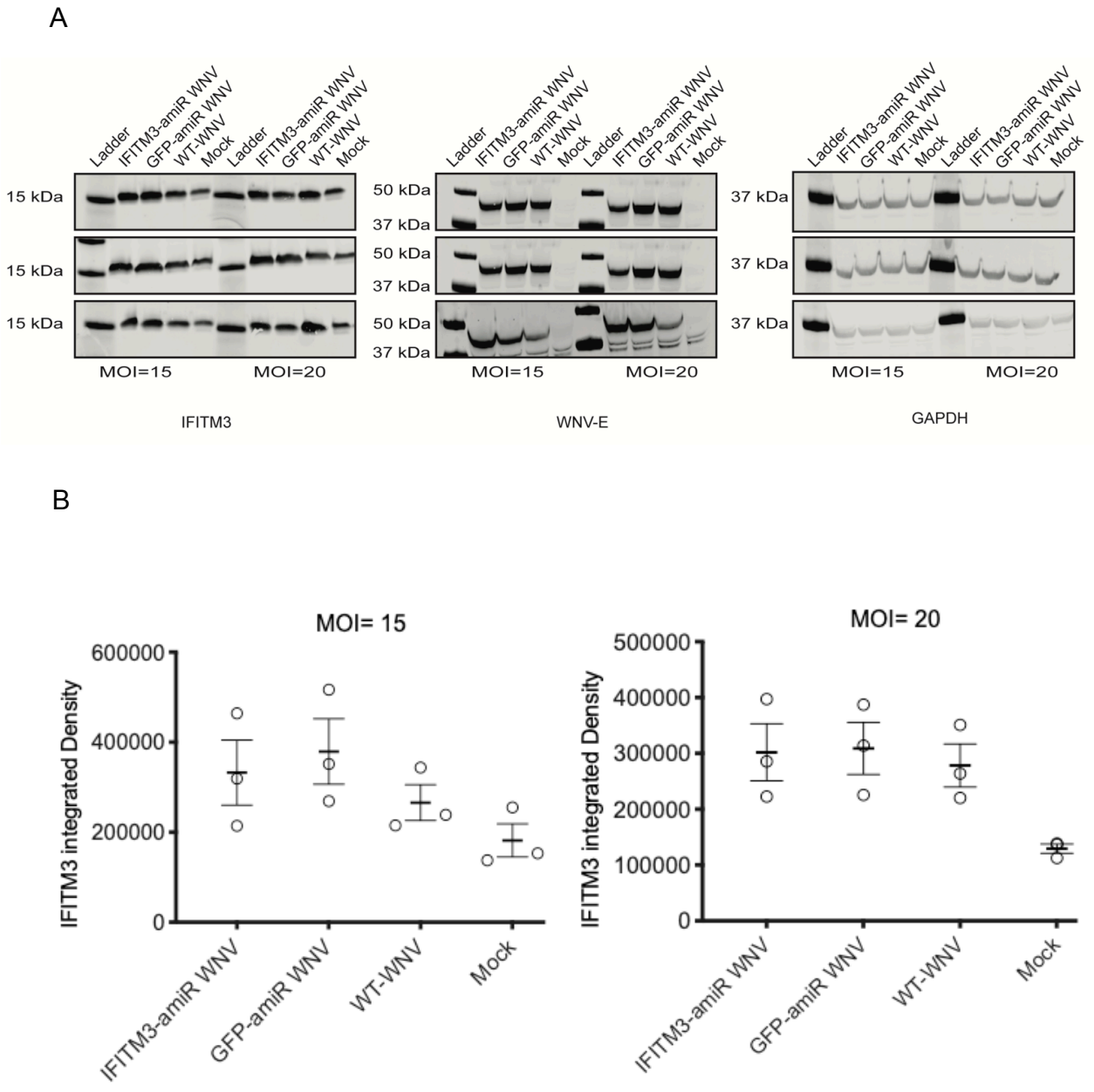

Figure 4.6 Expression of IFITM3 in WT MEF infected with respective viruses WT MEF were infected with IFITM3-amiR WNV, GFP-amiR WNV, WT-WNV at MOI =15 and MO1=20 or mock infected. At 48hpi, cell lysates were harvested in NP-40 lysis buffer and subjected to western blot analysis. Results of three independent experiments are shown. Blots were probed with rabbit polyclonal anti-IFITM3, anti-WNV-E and mouse anti-GAPDH antibodies. Expected band sizes were 14 kDa (IFITM3), 42 kDa (WNV-E) and 37 kDa (GAPDH). B) IFITM3 protein is induced by infection in WT MEF, but no decrease in protein was detected with IFITM3-amiR-WNV relative to WT-WNV. WT MEF were infected with IFITM3-amiR WNV, GFP-amiR WNV, WT-WNV or mock at MOI =15 and MO1=20. IFITM3 band integrated density ± SEM analysed by ImageJ densitometry.

4.3.6 The IFITM3-amiR WNV down-regulates expression of IFITM3 expression in *Ifnar1*$^{-/-}$ MEF cells

Similarly, *Ifnar1*$^{-/-}$ MEF cells were infected with IFITM3-amiR WNV, GFP-amiR WNV and WT-WNV at MOI =1, and at 48 hpi, cell lysates were prepared and subjected to western blot analysis. Probing for IFITM3 expression indicated knockdown of IFITM3 expression in cells infected with IFITM3-amiR WNV when compared to cells infected with GFP-amiR WNV and WT-WNV (Figure 4.7 A). Analysis of IFITM3 integrated density substantiated this observation, as knockdown of IFITM3 was significant in *Ifnar1*$^{-/-}$ MEF cells infected with IFITM3-amiR WNV compared to cells infected GFP-amiR WNV, WT-WNV and or mock uninfected (Figure 4.7 B). In contrast to WT cells (Figure 4.6), IFITM3 was not induced in the *Ifnar1*$^{-/-}$ MEF by WT-WNV infection, consistent with induction of IFITM3 by autocrine type I IFN production.

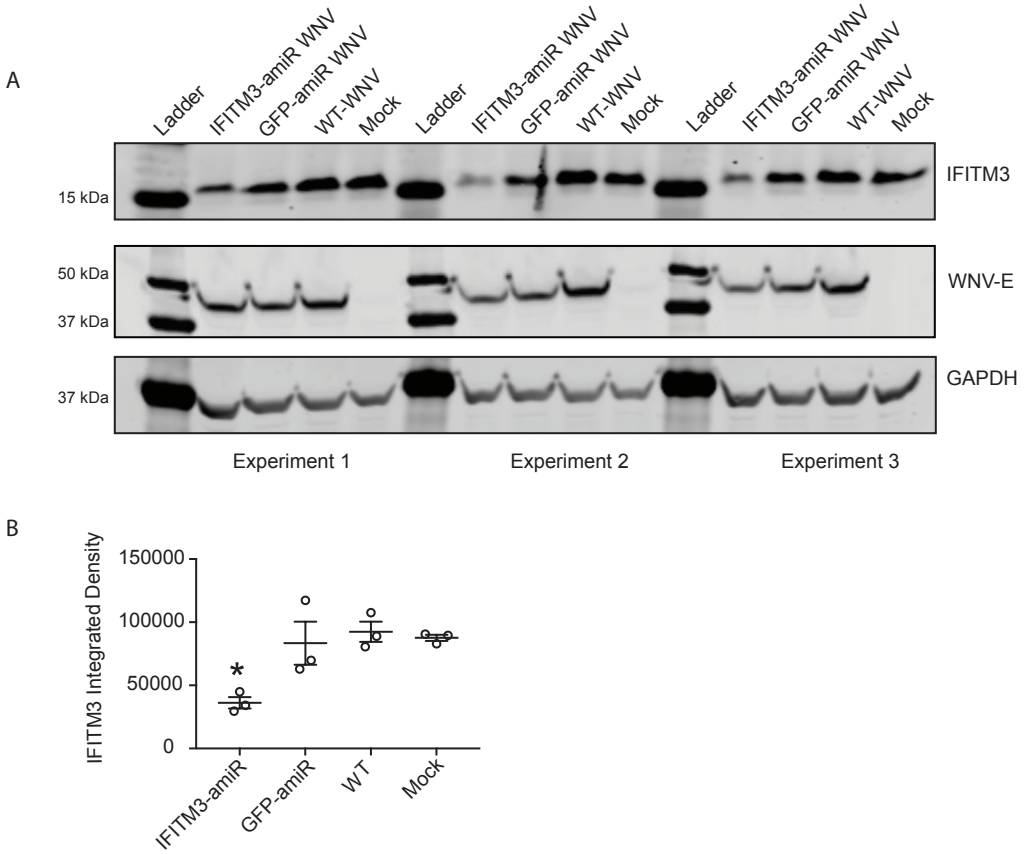

Figure 4.7 Knockdown of IFITM3 expression in Ifnar1-/- MEF infected with IFITM3-amiR WNV. A) *Ifnar1*$^{-/-}$ MEF cells were infected with IFITM3-amiR, GFP-amiR, and $WT_{NSW2011}$ viruses at MOI = 0.1, and mock uninfected. At 48 hpi cells were lysed in NP40-containing lysis buffer and subjected to western blot. Blots were probed with rabbit polyclonal anti-IFITM3, anti- WNV-E 4G2 and mouse anti-GAPDH antibodies. Predicted sizes are 14 kDa, 37 kDa and 42 kDa for IFITM3, GAPDH and E-protein respectively. B) IFITM3 integrated density ± SEM analysed by ImageJ densitometry. Results indicate that IFITM3 expression is reduced in Ifnar1-/- MEF when cells are infected with IFITM3-amiR WNV. The * denotes $p < 0.05$.

4.3.7 IFITM3-amiR WNV replicates better than GFP-amiR WNV

A growth kinetics experiment was performed on WT MEFs and *Ifnar1*$^{-/-}$ MEF cells to determine replication efficiency of IFITM3-amiR WNV compared to GFP-amiR WNV control virus. Both WT MEF and I *Ifnar1*$^{-/-}$ MEF cells were infected with IFITM3-amiR WNV and GFP-amiR WNV at MOI =1, culture medium was harvested at 0, 24, 48 and 72 hpi and virus titre determined by immunoplaque assay on Vero cell monolayer. Three independent experiments were performed. Results showed that IFITM3-amiR WNV replicated significantly better than GFP-amiR in both WT MEFs and *Ifnar1*$^{-/-}$ MEF cell lines (Figure 4.8 A and B), although in *Ifnar1*$^{-/-}$ MEF titres were only marginally higher, at 48 and 72 hours.

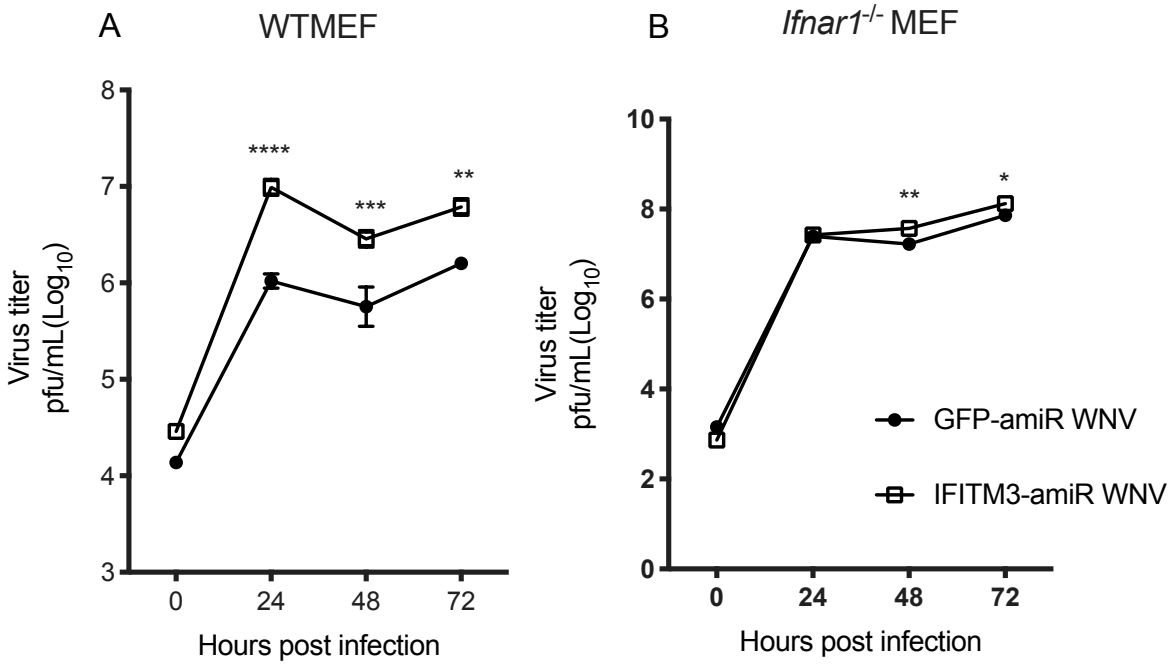

Figure 4.8 Comparison of growth kinetics between IFITM3-amiR WNV and GFP-amiR WNV on different cell lines. Cells were infected at MOI =1 for up to 72 hours using virus stocks prepared in Vero cells. Virus titres shown are $\log_{10}$ transformed mean values and represented as pfu/mL ± SEM, as determined by immunoplaque assay on Vero cells. Three independent experiments were performed for each cell line. Significant differences between the means are differentiated using two-way ANOVA with Sidak's multiple comparison tests where *p < 0.05, **p <0.005, ***p < 0.001, ****p < 0.0001.

4.3.8 Immunoprecipitation of West Nile virus particles using Flavivirus anti-E antibody shows that infection with WNV encoding IFITM3 pre-amiR reduces incorporation of IFITM3 into secreted virus particles

From the initial discovery of IFITM3 as an interferon-inducible transmembrane protein that inhibits replication of numerous unrelated viruses, various research studies have elucidated how IFITM3 antagonises virus infections. Research has shown that IFITM3 is a type II transmembrane protein

that is translocated to the plasma membrane, endocytosed and incorporated into secreted virions during biogenesis to reduce infectivity of secreted virions [271-274]. Furthermore, West Nile virus N-linked glycosylation of envelope protein controls virion assembly and infectivity [74, 275]. Based on this knowledge and observation that infection of *Ifnar1*$^{-/-}$ MEF cells with IFITM3 amiR-encoding WNV knocks down expression of IFITM3 in cells (Figure 4.7), we hypothesised that knockdown of IFITM3 in cells reduces incorporation of IFITM3 into membranes of the secreted virions. Therefore, West Nile virus particles were immunoprecipitated using anti-E monoclonal antibody (6B6C-1) and incorporation of IFITM3 in virus particles were determined by probing for IFITM3 on Western blot.

Since knockdown of IFITM3 in *Ifnar1*$^{-/-}$ MEFs infected with IFITM3-amiR encoding virus occurred as early as 48hpi in cells (Figure 4.7 A), it was assumed that newly secreted virions from this point forth would contain less IFITM3. Therefore *Ifnar1*$^{-/-}$ MEF were infected with IFITM3-amiR-encoding WNV, GFP-amiR WNV encoding and WT-WNV at MOI = 1. At 48 hpi, culture medium was removed, cells washed and new medium added to generate 72 hpi samples as described in methods. Thereafter, harvested virus samples were clarified by centrifugation, concentrated before immunoprecipitation of WNV-E performed and subsequent probing for IFITM3 expression to determine incorporation of IFITM3 into membranes of secreted virions. Results showed that less IFITM3 was incorporated into virions at 72 hpi compared to 48 hpi (Appendix 5). Therefore the 72 hpi was chosen as an optimal time point for immunoprecipitation and experiment was repeated as described in methods section. Results showed that less IFITM3 was incorporated in IFITM3-amiR WNV while amount of IFITM3 incorporated into GFP amiR-encoding WNV and WT-$_{NSW2011}$ WNV remained unchanged (Figure 4.9). Probing for WNV-E protein in culture medium showed that regardless of less incorporation of IFITM3 in secreted virions, the level of WNV-E remained unchanged. Therefore the obtained data confirmed that knockdown of IFITM3 expression in cells subsequently reduces the amount of IFITM3 incorporated into secreted virions (Figure 4.9 A, B) despite similar levels of WNV-E protein in the virus culture fluid (Figure 4.9 A, C).

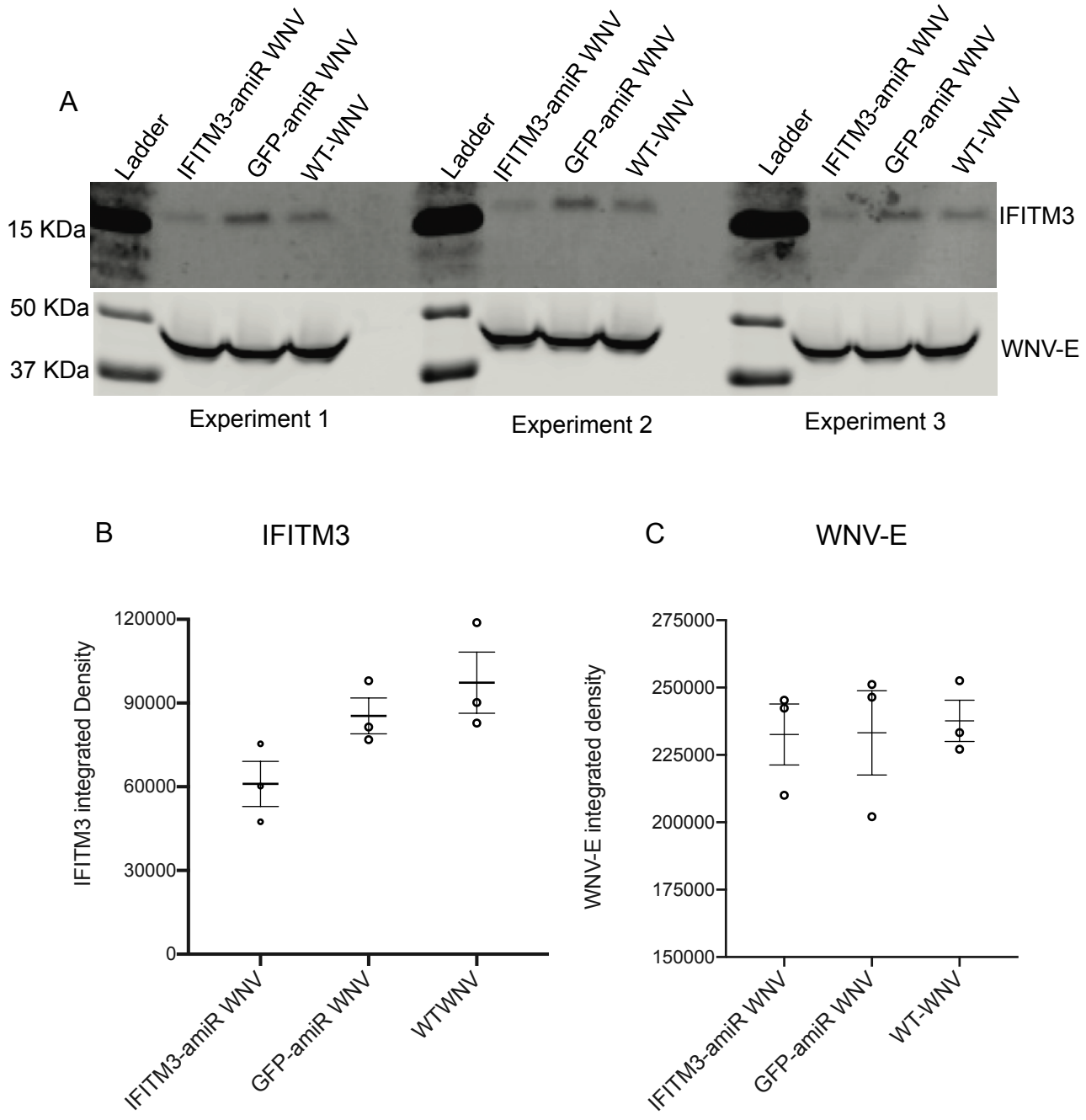

Figure 4.9 Infection with IFITM3 pre-amiR encoding WNV reduces incorporation of IFITM3 into secreted virus particles. A) *Ifnar1*$^{-/-}$ MEFs were infected at MOI =1, 48 hpi, virus culture fluid was removed, cells washed with PBS and new DMEM to generate 72 hpi sample. At 72 hpi, virions secreted into culture medium contained less IFITM3 on immunoprecipitation of WNV-E protein. The same volume of virus culture fluid was subjected to western blot analysis to determine amount WNV-E protein in secreted virions. B) Analysis of IFITM3 expression in secreted virions using ImageJ densitometry. IFITM3 Integrated density in virus culture fluid of IFITM3-amiR WNV, GFP-amiR WNV and WT-WNV *Ifnar1*$^{-/-}$ MEF stocks was determined. C) Analysis of WNV-E expression in virus culture fluid was determined by WNV-E protein western blot analysis.

4.3.9 Less incorporation of IFITM3 in virions increases infectivity of secreted virions

Given that IFITM3 is incorporated in membranes of secreted virions and negatively represses infectivity [273, 276], we sought to determine whether less incorporation of IFITM3 in secreted virions affected WNV infectivity in different cell lines. The *Ifnar1*$^{-/-}$ MEF cells were infected with p1-Vero generated IFITM3-amiR WNV, GFP-amiR WNV and WT-WNV virus stocks at MOI =1 and virus stocks harvested at 48 hpi. Thereafter, *Ifnar1*$^{-/-}$ MEF generated virus stocks were normalised by RNA copy number (Figure 4.10 A) and western performed on normalised virus stocks to determine whether similar levels of WNV-E protein were expressed in the virus stocks. Results revealed that similar number of virions in the normalised virus stocks, further validating the equivalent numbers of virions in the viral preparations (Figure 4.10 B). Using normalised virus stocks, viral infectious titres were determined by immunoplaque assay on Vero, WT MEF, *Ifnar1*$^{-/-}$ MEF, C6/36 and A549 cell monolayers. Results revealed that IFITM3-amiR WNV was more infectious than virions containing a normal level of IFITM3 on WT MEF and *Ifnar1*$^{-/-}$ MEF. This implied that knockdown of IFITM3 in murine derived cell lines, resulted into less incorporation of IFITM3 in secreted virions and subsequently improved infectivity of IFITM3-amiR WNV (Figure 4.10 C). In addition, mosquito (C6/36) and human (A549) cell lines showed a trend towards improved infectivity although there was no statistically significant difference in replication on Vero, C6/36 and A549 cells.

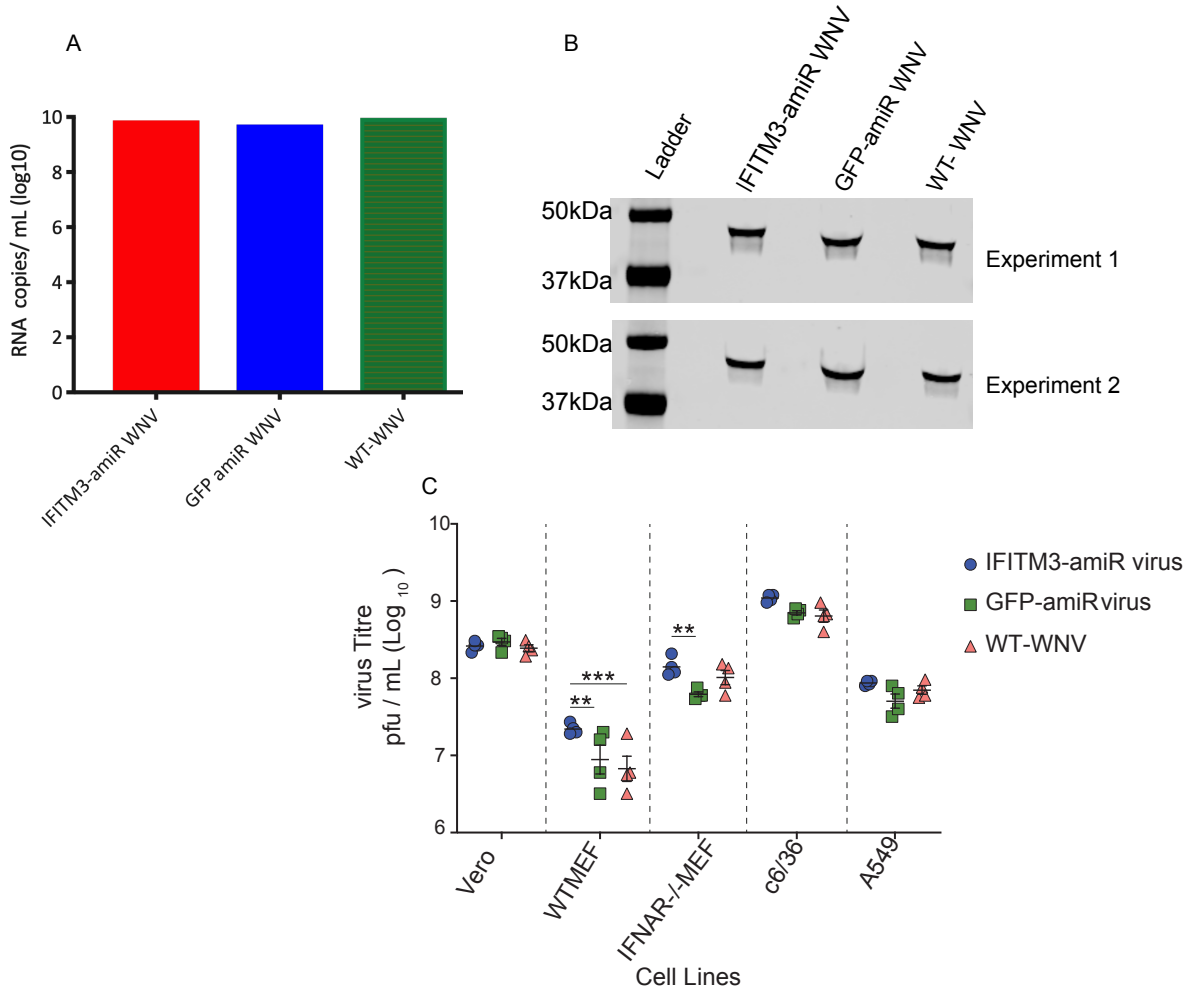

Figure 4.10 Increased infectivity of IFITM3-amiR virions prepared in *Ifnar1*$^{-/-}$ MEF. A) RNA copy numbers of *Ifnar1*$^{-/-}$ MEF-grown virus stocks were determined and found to be similar. Error bars could not be seen, because they were very short. B): Detection of WNV- E protein in normalised virus culture fluid revealed similar WNV-E expression in virus culture fluid in the three viral stocks used for infectivity assay. Two independent experiments were performed. C) A uniform volume of *Ifnar1*$^{-/-}$ MEF-grown virus stocks were used for immunoplaque assay to determine infectivity on different cell lines. For Vero, WT MEF, A549 and *Ifnar1*$^{-/-}$ MEF cells, immunoplaque assay plates were fixed 30 hpi with ice cold 80% Acetone in PBS while C6/36 were fixed at 72 hpi. Plates were probed with anti-WNV-E 4G2 to determine virus titres. Four independent experiments were performed for each of the cell line and virus. Error bars represent standard error of the mean. ** P< 0.005 and *** P<0.0005 as analysed by two-way ANOVA with Tukey's multiple comparisons test.

4.3.10 Increased mortality in mice infected with IFITM3-amiR WNV

IFITM3 knockdown in cells resulted in less incorporation of IFITM3 in membranes of secreted virions, and subsequent increased infectivity of IFITM3-amiR WNV *in vitro*. Next we determined whether virions containing less IFITM3 showed enhanced virulence *in vivo*. To determine this, 40 four-week-old CD-1 mixed sex mice were infected with IFITM3-amiR or GFP-amiR WNV generated from *Ifnar1*$^{-/-}$ MEF cells via intraperitoneal route and monitored for 21 days. Two doses were used (10^5 pfu and 10^6 pfu) to determine the optimal infection dose for subsequent animal

experiments. The 10^5 pfu cohort (Figure 4.11 A) presented with 100% (10/10) and 60% (6/10) mortality in IFITM3-amiR and GFP-amiR WNV control groups respectively; while the 10^6 pfu cohort (Figure 4.11 B) caused 100% (10/10) and 40% (4/10) mortality in IFITM3-amiR WNV and GFP-amiR WNV respectively. Therefore 10^6 pfu infection dose was chosen as the optimal dosage for viraemia, clinical score and virus burden in the brain as discussed below.

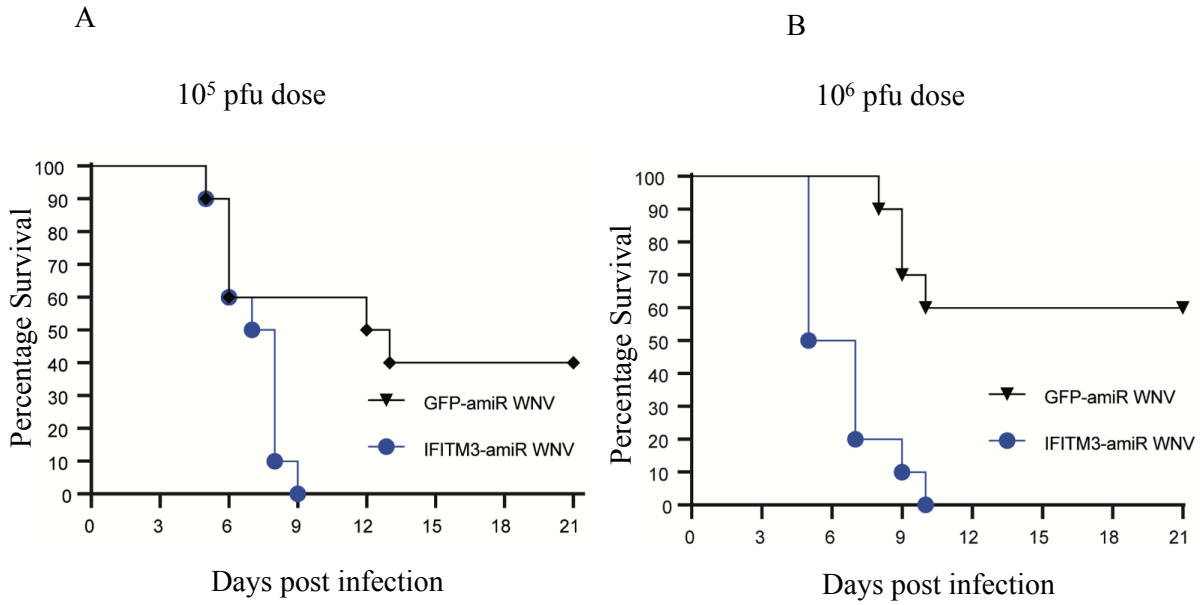

Figure 4.11 *In vivo* characterisation of IFITM3-amiR encoding $WNV_{NSW2011}$ viruses. A) 4 week old CD1 mice were challenged via the intraperitoneal route with either 10^5 pfu (A) or 10^6 pfu (B) of the IFITM3-amiR WNV or GFP-amiR WNV generated in *Ifnar1*$^{-/-}$ MEF. Each group contained 10 mice, which were monitored for 21 days and at the survival curve generated.

4.3.11 Viraemia

To determine viraemia, mice were tail bled for the first seven days to obtain sera for immunoplaque assay on C6/36 mosquito cells. The C6/36 cell line is an *Aedes albopictus* mosquito-derived cell line that is Dicer-1 deficient and lacks a functional RNAi pathway commonly used in flavivirus research and can be used for miRNA studies. After 1-2 days, mice infected with IFITM3-amiR WNV presented with apparently increased viraemia compared to mice infected with the control virus, GFP-amiR WNV, although this did not reach statistical significance (Figure 4.12). Furthermore viraemia lasted until 4dpi and by 5dpi no virus was detected in the sera.

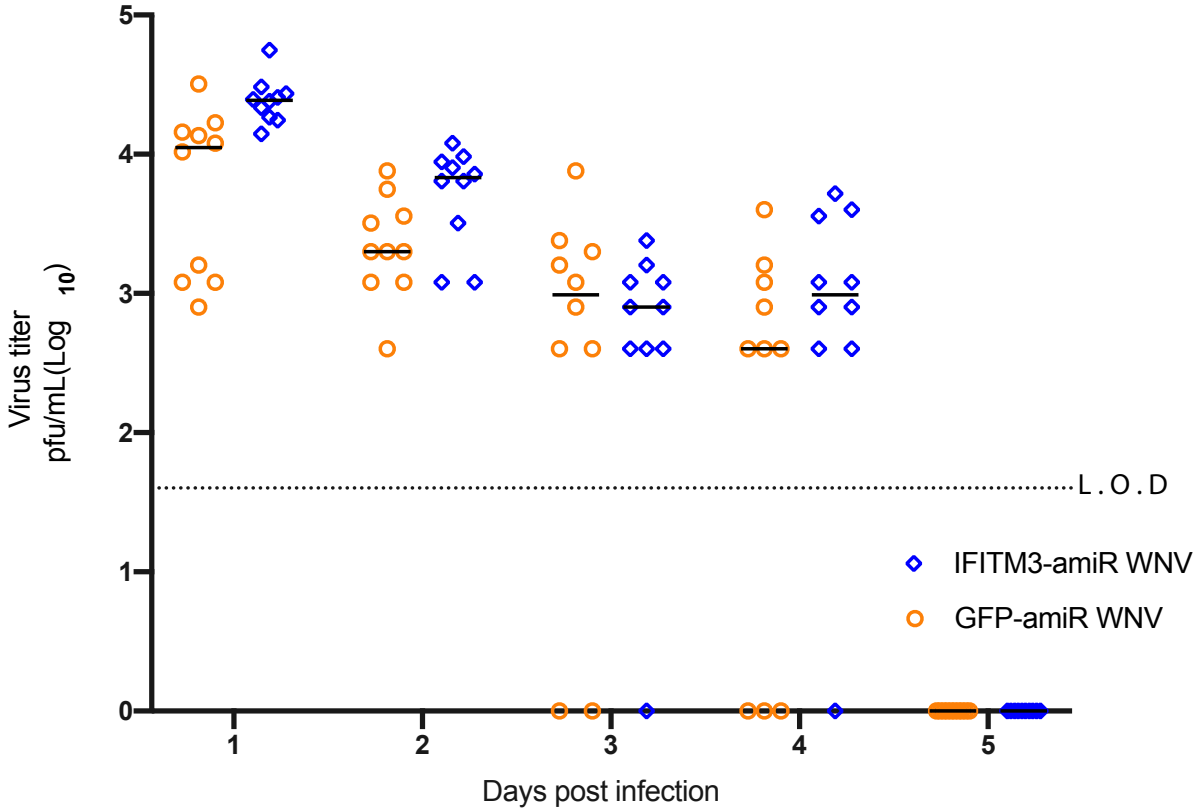

Figure 4.12 Increased early viraemia in mice infected IFTM3-amiR WNV. To determine viraemia, mice were tail bled from 1dpi to 7dpi. Sera virus titres were determined by C6/36 immunoplaque assay using WNV mAb E-16 (human anti-E). Obtained titres were log transformed and plotted using GraphPad prism version 8. Solid bars represent median of log transformed virus titre per group. L. O. D denotes Limit of Detection, which is 40 pfu/mL, equivalent to 1.602 log 10.

4.3.12 Increased progression of clinical signs in mice infected with IFITM3-amiR WNV

Mice infected with IFITM3-amiR WNV presented an increase in progression and severity of observed clinical signs, such as ruffled fur and/or general loss of condition, loss of weight, change in breathing, twitching, anti-social behaviour, severely hunched posture, paralysis among others (Figure 4.13 A, B). By 10 dpi all mice infected with IFITM3-amiR WNV had succumbed to encephalitis compared to mice infected with GFP-amiR WNV, which had 6/10 (60%) mice survive until 21dpi (Figure 4.11)

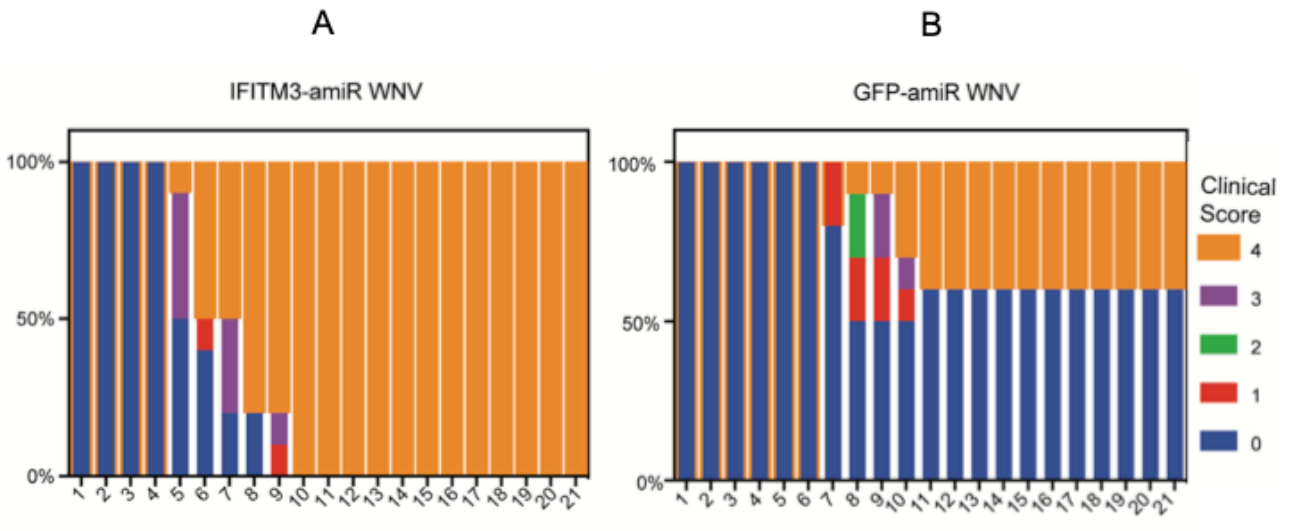

Figure 4.13 Increased progression of clinical signs in IFITM3-amiR WNV infected mice. (A) IFITM3-amiR WNV and GFP-amiR WNV (B) mouse groups were infected with 10^6 pfu of respective viruses and each group monitored daily for signs of encephalitis. Clinical scores for each group were recorded each day for 21 days. For the clinical score 0 denoted Normal feeding and appearance. Clinical score 1: denoted slightly ruffled fur and/or general loss of condition respectively. Clinical score 2: denoted increase in general loss of behaviour, appearance, breathing changes, twitching and anti-social behaviour. Clinical score 3 denoted first signs of encephalitis such as severely hunched posture, partial paralysis and or full paralysis while clinical score 4 denoted death.

4.3.13 Increased viral burden in the brains of mice infected IFITM3-amiR WNV

Mice infected with IFITM3-amiR WNV and GFP-amiR WNV that showed signs of encephalitis were culled and brains harvested to determine virus burden in the brain and whether mice retained IFITM3 pre-amiR and GFP pre-amiR insertions respectively. Total RNA was extracted and RT-PCR performed using superscript III one-step RT-PCR system with platinum Taq high fidelity DNA polymerase kit (Thermo Scientific, USA), 3′ UTR-Forward and 3′ UTR-Reverse primers (Table 4.1). Results showed that both viruses stably retained the inserted pre-amiR hairpins through virus spread to the CNS as correct sized amplicons were obtained. It should be noted that the three mouse brains from the IFITM3-amiR WNV group were harvested at 5dpi while one mouse brain for the GFP-amiR WNV group was harvested at 8dpi and the remaining two brains at 9 dpi. (Figure 4.14 A) Sanger sequencing confirmed that inserted pre-amiR hairpins were retained through virus spread to the CNS. In addition, a second portion of the mouse brain homogenate was used to determine viral burden in the brain by immunoplaque assay on C6/36 cells. This revealed that despite using the same dose of virus (10^6 pfu) for both IFITM3-amiR WNV and GFP-amiR WNV to infect mice, brain virus titres in mice infected with IFITM3-amiR WNV were higher than in mice infected with GFP-amiR WNV (Figure 4.14 B). Mouse brains for the IFITM3-amiR WNV were harvested at 5dpi (5 brains), 7dpi (3 brains), 9 dpi (1 brain) and 10 dpi (1 brain), when signs of

encephalitis were apparent (Figure 4.11). For the GFP-amiR WNV group, mouse brains were harvested at 8dpi (1 brain), 9 dpi (2 brains) and 10 dpi (1 brain) when signs of encephalitis were apparent. In addition, regardless of the time of harvest, brains from IFITM3-amiR WNV infected mice had showed higher virus burden than brains of mice infected with GFP-amiR WNV. This is because even at 10 dpi, virus burden in the brain of IFITM3-amiR WNV infected mouse was higher than that of GFP-amiR WNV infected mouse brain.

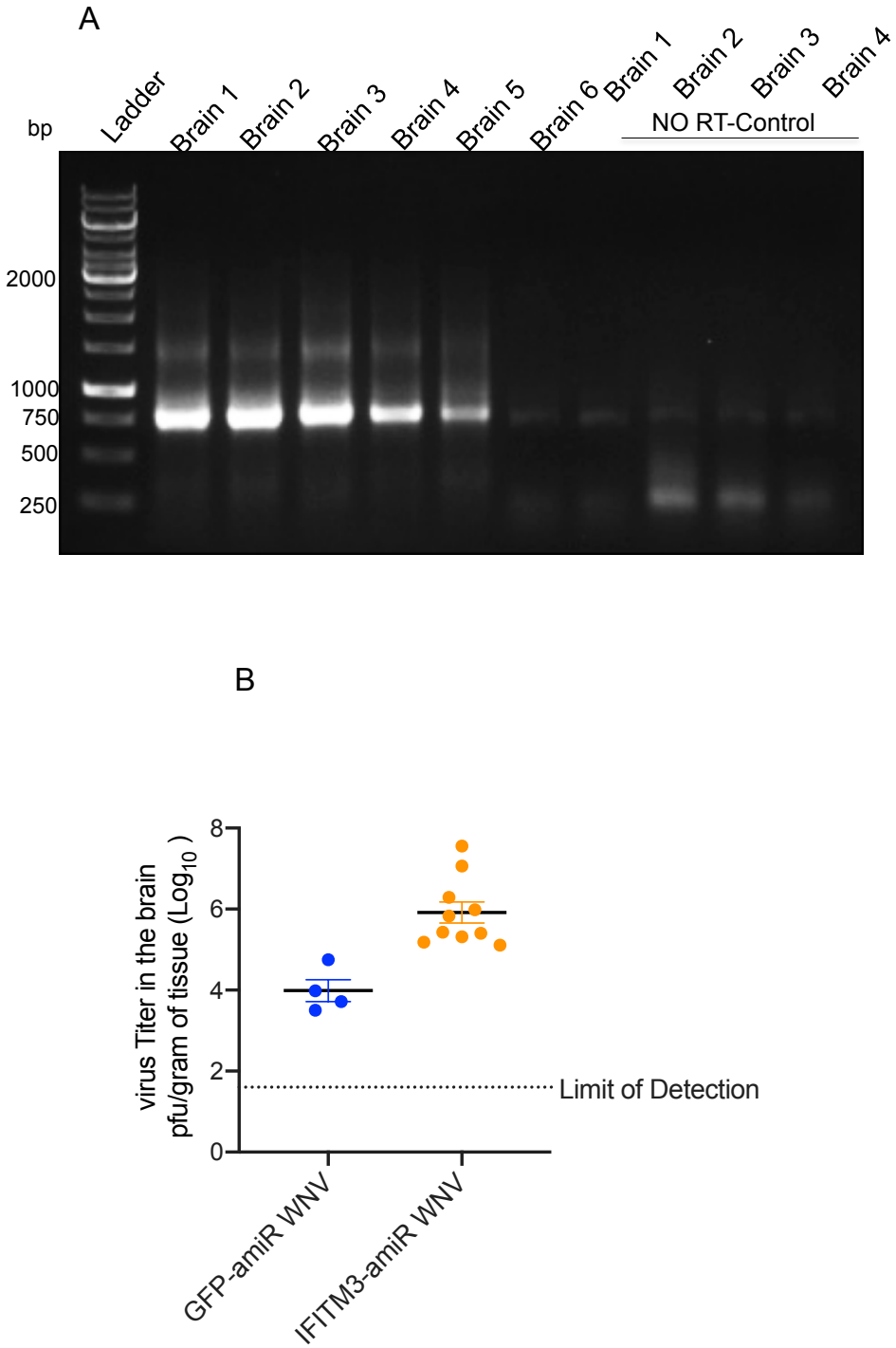

Figure 4.14 IFITM3 pre-amiR and GFP-pre-amiR inserted in 3′ UTR of WNVNSW2011 are stable throughout infection to CNS invasion. A) One step RT-PCR was performed using total

RNA and 3′ UTR_Forward and 3′ UTR_Reverse set of primers. A 1 kB DNA Gene Ruler mark (Ladder) was loaded on the left side of the gel and the expected size of amplicons was 720 base pairs. Brains 1 to 3 denote brains from mice infected with IFITM3-amiR WNV while Brain 4 to 6 are brains harvested from mice infected with GFP-amiR WNV. No RT-PCR was performed using brain homogenate derived RNA as template for Taq DNA polymerase PCR as control to determine the purity of purified RNA. B) Mouse brain homogenate titres were determined by immunoplaque assay on a C6/36 cell monolayer using WNV mAb E-16 (human anti-E). Obtained titres were log transformed and plotted using GraphPad prism version 8 software. Statistical test could not be performed since the brains were harvested on different days. Limit of Detection denotes 40 pfu/mL, equivalent to 1.602 log 10.

4.4 Discussion

4.4.1 IFITM3 restricts infection by several different viruses

Obligate intracellular parasites such as viruses access, hijack and control host cellular compartments to survive and complete life cycles. Several pieces of evidence show that following endocytosis, a drop in pH induces the enveloped virus glycoproteins to undergo a conformational rearrangement. Consequently the enveloped virus glycoproteins fuse with host cellular receptors to dispense their viral genome into host cytosol, a process known as hemifusion (reviewed in [277, 278]). Consequently a series of events occur including recruitment of cellular antiviral factors and evasion of host restriction factors as viruses establish and complete their lifecycles [276, 279]. More evidence suggests structural modification in virus glycoproteins facilitate fusion of viral and cellular membranes [278, 280]. Therefore, fusion inhibitors and neutralising antibodies against viral envelope glycoproteins have developed to block entry of virus into cells.

Recently a novel family of innate immune restriction factors, interferon inducible transmembrane proteins (IFITM) family was identified. The IFITM family of proteins hinders entry of numerous viruses into cells to block the first stages of virus life cycle such as hemifusion and pore formation to inhibit viruses from entering the cytoplasm [281]. The IFITM family consists of five genes in humans, IFITM1, IFITM2, IFITM3, IFITM5 and IFITM10 whereas murine family of IFITM consists of IFITM1, IFITM2, IFITM3 and four other IFITMs: 5, 6, 7 and 10, whose functions are currently undefined [282]. The IFITM family of proteins consists of structurally related proteins. IFITM1 contains a 13 amino acid (aa) extension at the C terminus while M2 and M3 have 20 and 21 aa extensions at the N terminus and thus differ by only one aa [283, 284]. Although the name suggests that IFITMs are interferon inducible, only IFITM1, 2 and 3 are, and are detectable in moderate to high levels in several tissues even with absence of interferon [285, 286]. IFITM5 and IFITM10 have not been shown to have any immune-related functions but IFITM5 is predominantly expressed in osteoblasts and vital in bone formation whereas functions of IFITM10 are still unknown [232, 284].

Interferon inducible IFITMs, IFITM1, IFITM2 and IFITM3, are crucial in virus-host interaction and viral pathogenesis. IFITMs prevent viral replication as well as effects of virus-associated disease such as cytopathic effects, cell death and inflammation. *In vitro* studies have shown that IFITM1, IFITM2 and IFITM3 incorporate into the membrane of various unrelated enveloped viruses to restrict virus infections of various families of viruses including cytomegalovirus (CMV), Ebola virus (EBOV), vesicular stomatitis virus (VSV), SARS coronavirus (SARS-CoV), human immunodeficiency virus (HIV), respiratory syncytial virus (RSV), hepatitis C virus (HCV), Dengue virus (DENV), Zika virus (ZIKV) and West Nile virus (WNV) [287-298]. However, infection by the non-enveloped virus reovirus is also restricted by IFITM3, with a suggested role in modifying proteolysis in endosomal compartment that is necessary for infection. Consequently, these proteins may have effects both within the host cell and as part of the virion.

Cellular localisation of IFITMs is linked to the stage of virus life cycle that they antagonise [286, 299]. Members of the IFITM family exist within cytoplasm, plasma membrane, nucleus and virus particle [232, 274, 285, 298]. For instance, *in vitro* studies have shown that IFITM1 is localised at the cell surface and early endosome to effectively restrict HIV-1 strains that utilise CCR5 co-factor to fuse envelope-cell membrane and enter into host cells [288, 300, 301]. IFITM2 and IFITM3 are localised at late endosome/ lysosome to restrict viruses that require conformation change in envelope glycoprotein prior to fusion [281, 302-305]. IFITM3 inhibits entry of virions into endosomal compartments and prevent viral infections before viruses can traverse the bilayer of target cells to access cytoplasm [282, 299].

Using small interfering RNA screening studies, IFITMs were discovered as endogenous inhibitors of Influenza A virus (IAV), WNV, and DENV infections [281]. Evidence suggested that knockdown of IFITM1, 2 and 3 increased IAV, WNV and DENV infections in mammalian cell lines whereas overexpression of IFITM1, 2 and 3 inhibited infection. However, IAV was the most susceptible to IFITM3 [281]. Subsequent studies not only confirmed the role of IFITM3 in restricting IAV, WNV and DENV, but also defined the IFITM3's role in restricting infection of other unrelated viruses (reviewed in [232, 286, 305]).

To determine the role of IFITM3 in humans, many of the studies have mostly focused on influenza virus infection [306]. One study suggested that IFITM3 inhibits IAV infection by blocking pore formation during hemifusion in a pH-dependent manner [302, 307]. While several groups have disputed this mode of action, a recent study used live imaging to corroborate that IAV is trapped in endosomal compartments enriched in fluorescent IFITM3 which apparently inhibits fusion of IAV with cellular membranes [308]. Additionally IFITM3 binds to vesicle-associated membrane protein-associated protein A (VAPA), a master regulator of endosome-ER lipid transport and alters

endosomal cholesterol levels to inhibit virus entry [300]. Further research has shown that cholesterol accumulates in the late endosome upon IFITM3 expression [274, 309].

While most of IFITM3 characterisation studies have been performed *in vitro*, IFITM3 has been shown to inhibit IAV *in vivo*. IFITM3 knockout (*Ifitm3*$^{-/-}$) mice infected with a less pathogenic IAV succumbed to IAV and failed to clear virus infection when compared to WT mice infected with the same virus [286]. Moreover, in patients hospitalised with deadly and seasonal IAV a specific IFITM3 polymorphism was shown to enhance IAV infection [310].

Lastly a recent *in vitro* study showed that IFITM3 is incorporated in HIV-1 glycoprotein (gp) particularly gp120, gp41 and gp160 to inhibit envelope processing and subsequently reducing infectivity of secreted virions [290]. Furthermore, evidence suggests that IFITM3 is incorporated into secreted virions thereby altering infectivity, impairing viral fusion and spread while another study showed that IFITM3 sequesters secreted virions in endosomal vesicles during virus assembly [273, 274, 276].

4.4.2 IFITM3 restricts West Nile virus infection

Results presented here used a virus library containing 204 variants of WNV, with each virus encoding a unique pre-amiR hairpin in the 3′ UTR of its genome targeting specific mouse ISGs. Passaging of amiR-encoding virus library at low MOI of 0.1 subjected selective pressure to the virus library and allowed selection and enrichment of IFITM3-amiR WNV in WT MEF (Figure 4.2 A) and *Ifnar1*$^{-/-}$ MEF (Figure 4.2 B). The IFITM3-amiR WNV came to completely dominate the pool of virus retrieved from culture from the second passage in the MEF cells (p3) onwards. This highlighted IFITM3 as a major antiviral host factor restricting WNV replication, consistent with the siRNA studies noted above, that showed increased WNV replication *in vitro* with *Ifitm3* knockdown [281]. Further assessment of the impact of incorporation of the IFITM3-amiR into WNV *in vitro* and *in vivo* required generation of individual IFITM3-amiR and GFP-amiR WNV using the CPER approach. Both viruses generated were viable and encoded the correct intended pre-amiR hairpins (Figure 4.4). Furthermore, when Vero cells were infected with IFITM3-amiR WNV and northern blot analysis performed, results showed that IFITM3-amiR was processed into functional mature artificial microRNA by the cellular machinery that targets specific IFITM3 mRNA transcript to block translation (Figure 4.5).

In addition, infection of *Ifnar1*$^{-/-}$ MEF cells with IFITM3-amiR WNV at MOI =0.1 down-regulated IFITM3 expression after 48 hours, as shown by western blot analysis (Figure 4.8). However, the same effect was not seen in WT MEF infected with either MOI =15 or 20. It is important to note that down-regulation of IFITM3 will only be seen in cells that are infected. Since the western blot

measures the levels of IFITM3 in the bulk population, the most likely reason for lack of apparent effect on IFITM3 expression in the WT MEF is that only a low proportion of cells were infected. This seems likely since infection at MOI =10 showed that WT MEF cells were not infected and thus at the doses presented of MOI =15 and 20, the percentage of cells infected may be minimal. This could be checked in future work by using more sensitive assay such as protein expression analysis using real time PCR. Thus, it was hypothesised that just like the *Ifnar1*$^{-/-}$ MEF, the actual infected WT MEF are likely to show IFITM3 knockdown. Consistent with this possibility infection of WT MEF at MOI =1 revealed that IFITM3-amiR WNV reached a higher titre than control virus, GFP-amiR WNV (Figure 4.9). It is possible that IFITM3 knockdown produced virions of increased infectivity limiting subsequent rounds of infection because all cells were already infected. However, IFITM3-amiR WNV had only a minor advantage in growth over the GFP-amiR WNV in *Ifnar1*$^{-/-}$ MEF when applied at MOI =1. This may be because the release of viral particles with reduced IFITM3 had minimal impact on later viral titre because at MOI =1 it was assumed that each cell was infected in the first round of infection. On balance, results in the WT MEF support the replicative advantage to the IFITM3-amiR WNV virus over GFP-amiR WNV. More convincing data in *Ifnar1* $^{-/-}$ MEF may be obtained with a lower MOI for infection, allowing multiple rounds of infection.

Lastly, the selection and enrichment of IFITM3 clone #2 amiR WNV in both WT MEF and *Ifnar1*$^{-/-}$ MEF highlighted the importance of IFITM3 in WNV replication. However only IFITM3-2-amiR WNV (IFITM3 #2) was generated and characterised. In future studies it would be wise to generate both IFITM3-1- amiR NWV and IFITM3-2- amiR WNV to check why IFITM3-1-amiR WNV was not selected. It is possible that IFITM3-1 amiR sequence was inefficient and unable to knock down IFITM3 expression as efficient as IFITM3-2 amiR. This could be confirmed by performing western blots to determine expression of IFITM3 in *Ifnar1*$^{-/-}$ MEF cells infected by both viruses. In addition, northern blot analysis would confirm whether IFITM3-1-amiR is processed inefficiently in cells.

4.4.3 Less incorporation of IFITM3 in virions improves infectivity of secreted virus particles *in vitro* and *in vivo*

Studies have revealed IFITM3 is incorporated into membranes of secreted virions to reduce their infectivity [273]. This implies that when IFITM3 expression is knocked down during infection, less IFITM3 is incorporated into secreted virions. Having shown that IFITM3 expression is knocked down as early as 48 hpi, meant that less IFITM3 in incorporated into virions from this point forth, and infectivity of IFITM3-amiR virus was expected to improve. Immunoprecipitation of virions from the medium of infected *Ifnar1*$^{-/-}$ MEF cells collected between 48 and 72 hpi showed that less IFITM3 was incorporated into secreted IFITM3-amiR virions than WT or GFP-amiR (Figure 4.10).

Based on this observation, we hypothesised that with less incorporation of IFITM3 in secreted virions, infectivity of the virus would improve. Using virus produced by *Ifnar1*$^{-/-}$ MEF between 48 and 72 hpi, an infectivity assay showed that IFITM3-amiR WNV was more infectious on WT MEF and *Ifnar1*$^{-/-}$ MEF. Therefore IFITM3-amiR WNV *Ifnar1*$^{-/-}$ MEF culture supernatants contained less IFITM3 and were more infectious both *in vitro* and *in vivo*. It was interesting that IFITM3-amiR virus was selected *in vitro*, given the lack of a cellular immune response; it can be assumed that the most critical factor for virus replication in a cell culture environment was to increase its infectivity. To further validate the role of IFITM3 in West Nile virus infection and conclusively demonstrate that IFITM3 is incorporated into virions to reduce infectivity, over expression studies using IFITM3 human homologues would be performed. It is anticipated that overexpression of IFITM3 would negatively affect infectivity of the secreted virions.

Published work has shown that mice lacking the *Ifitm3* gene readily succumbed to WNV infection that was sub-lethal in WT mice, and showed increased progression of clinical signs [311]. Consistent with that, results here showed that IFITM3-amiR WNV was more virulent than GFP-amiR WNV. IFITM3-amiR WNV infected mice showed higher and faster clinical score progression and by day 9, all mice had to be culled, whilst 60% of GFP-amiR WNV-infected mice survived. In addition, IFITM3-amiR infected mice depicted higher CNS virus infection than mice infected with GFP-amiR WNV despite similar infection doses (Figures 4.12 and 4.16 A). Thus, suggesting that IFITM3-amiR WNV was more virulent than GFP-amiR WNV. It would be important to compare viral load in the brain through intracranial infection. Intracranial infection would bypass peripheral organs and allow a better assessment of effects of infection with IFITM3-amiR WNV on different parts of the brain compared to GFP-amiR WNV.

Studies in this chapter used an *in vitro* RNAi screening technique and identified IFITM3 as a major antiviral factor during West Nile virus infection. These studies identified a proposed mechanism of action by which IFITM3 inhibits West Nile virus infection, as IFITM3 in secreted virions reduced infectivity of viruses. Therefore, with knockdown of IFITM3 in *Ifnar1*$^{-/-}$ MEF cells, less IFITM3 was incorporated into secreted virions and infectivity of IFITM3-amiR WNV in WT MEF, *Ifnar1*$^{-/-}$ MEF and in a West Nile virus mouse model improved.

Chapter 5: *In vivo* RNAi identifies ATF3 as an important antiviral factor in peripheral and CNS dissemination of West Nile virus infection

5.1 Introduction

Having identified IFITM3 as an important antiviral host gene against West Nile virus infection *in vitro*, the next step was to perform *in vivo* RNAi screening to determine which ISG-targeting amiR-encoding viruses were enriched and selected in mice. We hypothesised that *in vivo* RNAi screening using the generated amiR-encoding West Nile virus libraries would allow identification of host determinants that influence WNV infection during peripheral and CNS invasion. Therefore, two experimental groups were planned, one to look at peripheral selection (spleen) and another to look at CNS invasion (brain).

Previous work done by Varble *et al.,* 2013 developed an *in-vivo* RNAi screening approach using Sindbis amiR-encoding virus library with each virus was capable of producing a functional amiR that targets a specific host gene. Infection of mice with amiR-encoding Sindbis virus libraries led to enrichment and selection of host factors that influence Sindbis virus replication. Consequently, two host factors involved in transcription, Zfx and Mga were identified as crucial to Sindbis virus. Furthermore knockdown of Mga and Zfx resulted in change of the host transcriptome and increased Sindbis virus replication [151]. This *in vivo* RNAi screening showed that it is possible to use this approach to identify host factors that influence WNV *in vivo*. Therefore, basing on this literature, we designed our experiment with the aim of identifying host genes that influence WNV infection *in vivo.*

During WNV infection the spleen is the major site of virus replication before the virus can invade the CNS. Following peripheral infection, WNV crosses the BBB to invade and disseminate in the CNS. Therefore, it was important to determine host factors that influence early stages of WNV infection in the peripheral organs and those that facilitate CNS invasion. Furthermore, the use of *in vivo* RNAi screening approach would allow selection and enrichment of amiR-encoding viruses that silence expression of specific host gene that restrict WNV infection.

5.2 Methods and Materials

5.2.1 Animal ethics approval for use of animals in experimentation

Prior to performing animal experiments, animal ethical proposals and related statistical treatments were drafted and submitted to the University of Queensland's Molecular Biosciences Animal Ethics

Committee for approval. All animal experiments were performed according to Australian code for the care and use of animals for scientific purposes, as defined by National Health and Medical Research Council of Australia.

5.2.2 Infection of mice, blood and tissue sampling

Four-week old CD-1 mice were infected via the intraperitoneal route with respective viruses as stated in the Figure legends. Mice were monitored for clinical signs and each day a clinical score was recorded for a period of 21 days. To determine viraemia, mice were tail bled every day until seven days post infection. The collected blood processed to obtain sera for immunoplaque assay on C6/36 cells. To determine virus burden in mouse brains, mice that presented with encephalitic signs were culled and brains harvested. To determine enrichment of viruses in the spleen, mice were culled at specified time points and spleens harvested for further experimentation. Harvested spleen or brain samples were weighed and homogenised in 1 mL of PBS (TissueLyser II, QIAGEN, USA). The generated brain or spleen homogenates were aliquoted into different micro tubes and used for RNA purification, passaging or immunoplaque assay on C6/36 cells as described below.

5.2.3 Generation of amplicons by PCR for deep sequencing

Total RNA was extracted from 250 µL of spleen or brain homogenate using TRI Reagent LS (Sigma Aldrich, USA). Purified RNA was recovered in 100 µL of nuclease-free water and treated with RQ1 RNase-free DNase enzyme (Promega, USA). Thereafter 15-cycle one-step RT-PCR was performed using 5 µL of purified DNase-treated RNA as template, superscript III one-step RT-PCR system with platinum Taq high fidelity DNA polymerase kit (Thermo Scientific, USA), adaptor amplion_Forward and adaptor amplicon_Reverse set of primers as shown in chapter four, Table 4.1. This failed to provide RT-PCR product for spleen samples, and therefore 100 µL of spleen homogenate was used to infect C6/36 cells. Spleen homogenates from day 4 were used to infect C6/36 cells and at 3 dpi virus culture fluid was harvested. The 3 days time point was considered optimal to allow amplification of virus titres while minimising preferential selection of amiR-encoding viruses during passaging. This is because adequate infection of C6/36 cells with WNV often last as long as 7 days post infection. Thereafter, viral RNA was extracted and 15-cycle one-step RT-PCR performed as described in chapter four methods section. To obtain amplicons for deep sequencing, 2% (w/v) TAE agarose gel electrophoresis was performed; bands were excised from gels, purified using Monarch DNA Gel Extraction Kit, (New England Biolabs, USA). Thereafter DNA fragments concentration was determined by Nanodrop spectrophotometry before Illumina sequencing. The Expected DNA band size was 215 bp

5.2.4 RNA extraction and generation of amplicons for Sanger sequencing from mouse brains

Harvested mouse brains were suspended in 1mL of PBS and homogenised with 3 mm stainless steel

beads at 30/second frequency for 3 minutes using TissueLyser II, (Qiagen, USA). Total RNA was extracted from 150 µL of brain homogenates using TRI Reagent LS (Sigma, USA) according to following manufacturer's instructions. Thereafter, RT-PCR was performed using total RNA as template, superscript III one-step RT-PCR system with platinum Taq high fidelity DNA polymerase kit (Thermo Scientific, USA) and $WNV_{NSW2011}$ 3′ UTR_Forward and 3′ UTR_Reverse primers (as shown in chapter four, Table 4.1) as well as purified RNA as template. The generated 3′ UTR amplicons were visualised on 1.4% (w/v) TAE agarose gel electrophoresis, obtained bands were excised from gels and purified using Monarch DNA Gel Extraction Kit (New England, USA). Thereafter, DNA concentrations were determined by using Nanodrop spectrophotometry before Sanger sequencing.

5.2.5 Growth Kinetics

To perform *in vitro* growth kinetics WT MEFs and *Ifnar1*$^{-/-}$ MEF cells were seeded at 5×10^5 cells per well in six well plates and incubated at 37°C in a 5% CO_2 incubator for 12 hours until 90% confluent. Thereafter cells were infected with respective viruses at specific MOI as indicated in the Figure legends. To perform the infection 200 µL of virus inoculum was diluted to the required MOI, added to each well in six well plates and incubated at 37 °C with 5% CO_2 humidified incubator for 1 hour. For every 15 minutes plates were rocked to prevent the monolayer from drying up. Thereafter cell monolayers were washed three times with additive-free DMEM and 3 mL of DMEM supplemented with 5% FCS, 50 units/mL of penicillin and 50 µg/mL of streptomycin. At specified time point as indicated in Figure legends 150 µL of virus culture fluid was harvested and stored at –80°C. Thereafter sample titres were determined by immunoplaque assay on Vero cells as described in Chapter 2. The obtained virus titres were log transformed and analysed by GraphPad prism version 8.

5.2.6 Northern blot analysis

To perform northern blot analysis, Vero cells were seeded at 5×10^5 cells per well in a 6-well plate and incubated at 37°C in a 5% CO_2 incubator for 12 hours until 90% confluent. The following day, cells were infected with MOI =1 with p1-Vero ATF3-amiR, IRF7-amiR, and PARP11-amiR West Nile viruses as previously described in chapter four. Total RNA concentration was determined by Nanodrop spectrophotometry and 5 µg of purified RNA was subjected to electrophoresis in 15% TBE-Urea polyacrylamide gel (Invitrogen, USA) to denature and separate RNA molecules. Thereafter, separated RNA was transferred, cross-linked onto a nylon membrane and hybridised with γ-P^{32}-labeled DNA oligonucleotide probe complementary to respective amiRs. The membrane was exposed on a Storage Phosphor Screen (GE Healthcare Life Sciences) and imaged using the Typhoon FLA 7000 scanner (GE Healthcare Life Sciences).

5.2.7 Western blot analysis

Ifnar1$^{-/-}$ MEF were seeded at 5×10^5 cells per well in 6-well plate and incubated at 37°C in 5% CO_2 humidified incubator for 12 hours until 90% confluent. The following day, cells were infected with ATF3-amiR, IRF7-amiR and PARP11-amiR West Nile viruses at MOI = 1, or mock infected as indicated. At 48 hours post infection, infected cells were lysed in NP-40 lysis buffer, sonicated and 75 µL of each sample treated with 25 µL of 4 ×NuPAGE protein Loading dye at 95°C for 5 minutes. Thereafter, pre-cast NuPAGE™ 4-12% Bis-Tris Protein Gels, Invitrogen, USA were loaded with 25 µL of each sample per lane along with precision Plus Protein Kaleidoscope Ladder (BioRad, USA) and 1×NuPAGE running buffer added before electrophoresis. For electrophoresis, western blot power pack was set at 165 Volts for 45 minutes. Thereafter blots were transferred onto nitrocellulose membrane using iBlot 2 Dry Blotting System, (ThermoFisher, USA) following manufacturer's instruction. On completion of transfer, membranes were blocked in 1× Pierce blocking buffer (ThermoFisher, USA) for 1 hour at 37°C before probing with respective primary antibody for 1 hour at 37°C. Subsequently, blots were washed five times using 1× PBS containing 0.05% Tween 20 (PBS-T) to remove any traces of unbound primary antibody, with each wash lasting for five minutes before probing with respective secondary antibody as indicated in respective figure legends for 1 hour at 37°C in the dark. Membranes were then washed five times using 1× PBS containing 0.05% Tween 20 (PBS-T) to remove any traces of unbound secondary antibody. To scan membranes LI-COR Biosciences Odyssey Infrared Imaging System with the following specifications: channel =680/800, intensity = auto, focal length = 3 mm, resolution = 169 µM was used to visualise protein bands.

5.3 Results

5.3.1 *In vivo* RNAi screening shows enrichment of ATF3 amiR-encoding West Nile virus in the spleen

In order to identify host genes that influence WNV replication in peripheral organs, *in vivo* RNAi screening was performed. Four weeks old mice were infected via the intraperitoneal route with 10^6 pfu of p1-Vero ISG-targeting amiR-encoding virus library mixed with 200 pfu of scrambled amiR-encoding WNV virus library (Figure 5.1 A). For *in vivo* RNAi screening in the spleens, a higher infectious dose of 10^6 pfu was used to guarantee ample amplification of virus in peripheral since recovered virus titres for particularly $WNV_{NSW2011}$ are often very low in spleens. In addition, 10^6 pfu infection dosage was considered optimal basing on the initial weight of mice before infection. Ten mice were sacrificed at each time point (2, 3, and 4 dpi) and spleens harvested for further analysis. Splenic virus was detectable in 30-70% of mice at the various time points (Figure 5.1 B).

Several attempts to obtain an RT-PCR amplicon for deep sequencing from RNA purified from spleens failed. Hence, spleen homogenates were re-propagated on C6/36 cells, virus culture fluid harvested and RNA purified for RT-PCR. The latter method was successful with 6 out 7 spleens RT-PCR amplicons recovered at 4 dpi. This suggested that there were either inhibitory compounds in the spleen RNA that interfered with the RT-PCR, or the ratio of viral to cellular RNA was too small.

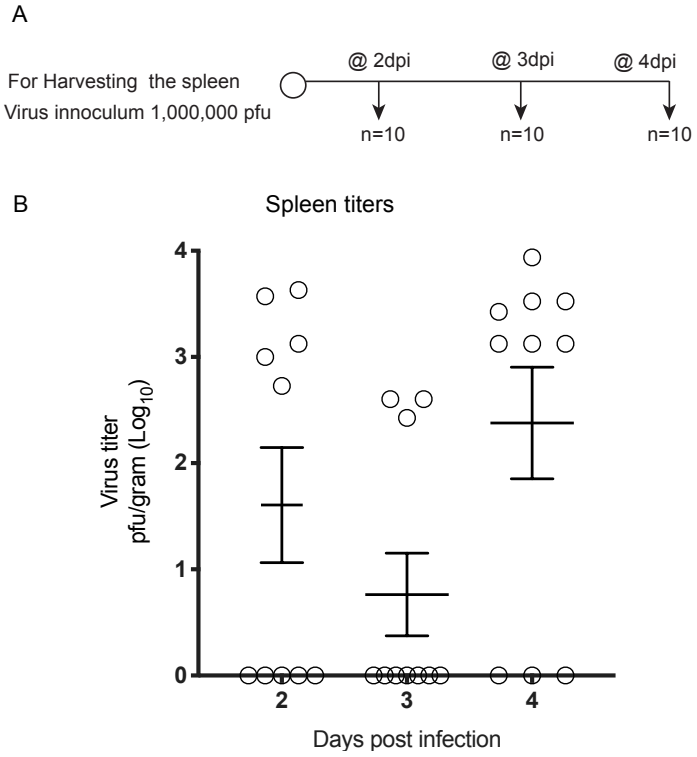

Figure 5.1 *In vivo* screening RNAi screening in periphery.A): A representation of the experimental plan used to perform *in vivo* RNAi screening in spleen. A total of 10^6 pfu of p1-Vero ISG-targeting amiR-encoding virus library was mixed with 200 pfu of Scrambled amiR-encoding WNV virus library and used to infect CD-1 mice. At 2 dpi, 3 dpi and 4 dpi 10 mice for each time point were culled and spleens harvested. B) Spleens were homogenised in 1 mL PBS and virus titres were determined on C6/36 cells. Virus titres shown were $\log_{10}$ transformed mean values and represented as pfu/gram.

Deep sequencing data were uploaded onto Galaxy Australia (UQ Research Computing Center) and analysed using Salmon transcript quantification data script tool (Appendix 2) to determine enrichment of amiR-encoding virus variants in 4 dpi mouse spleens. Deep sequencing data revealed that ATF3-amiR WNV was enriched in 4 out of 6 spleens at percentages 18.31%, 76.86%, 46.85%, 97.35% of the total amiR-encoding virus population while in the remaining two spleens ATF3-amiR WNV was present at 0.22% and 0.13% (Table 5.1 and appendix 7). Thus, ATF3 is likely to be a critical antiviral factor controlling West Nile virus splenic infection. Therefore, a more in-depth characterisation of ATF3-amiR WNV was warranted and experiments were designed to

further understand the role of ATF3 during peripheral WNV infection as discussed in subsequent sections of this thesis. Furthermore none of the scrambled amiR-encoding viurses or GFP-amiR WNV and MiR-124 amiR WNV added as internal controls were selected and enriched in the spleens. This showed that selection was not occuring at random. However to provide an adequate control for this experment p1-Vero ISG targeting amiR WNV library : p1-Vero scrambled amiR WNV library needed to be mixed in ratio of 1:1. This was not possible since the scrambled library contained more than 6000 individual amiR variants, as the control library was very large compared to the ISG- targeting virus library. Therefore it would be enlightening to repeat this experiment while using equal ratio of p1-Vero ISG targeting amiR WNV library : p1-Vero scrambled amiR WNV library. This would determine whether ATF3-amiR WNV is still selected and enriched in the spleens in presence of an equal amount of scrambled amiR-encoding viruses

Table 5.1 The most enriched amiR-encoding West Nile viruses in the spleens

Spleen 1		Spleen 2		Spleen 3		Spleen 4		Spleen 5		Spleen 6	
AmiR	%	AmiR	%	AmiR	%	AmiR	%	AmiR	%	AmiR	%
Parp10	34.45	Atf3	76.86	Atf3	46.85	Atf3	97.35	Fbxo39	80.29	Tlr3	32.77
Atf3	18.31	Usp18	6.47	Mlkl	20.58	Fbxo39	1.15	Ly6e	12.88	Irf2	19.85
Rtp4	15.77	Mapk8	5.05	Gbp2	14.64	Trex1	0.41	Adar	1.82	Mapk8	12.79
Rtp4	14.75	Ikbkb	4.69	Brd4	9.53	Ifih1	0.21	Ifitm3	0.80	Mlkl	11.30
Gbp6	6.12	Ifna1	1.38	Ddx58	4.10	Mlkl	0.07	Ifih1	0.49	Oas2	6.27
Irf7	3.62	Cpeb3	1.16	Stat1	1.52	Oas1a	0.06	Ikbke	0.41	Ikbke	4.44
Clec4d	2.03	Parp10	0.69	Wwoxv	0.87	Cytip	0.05	Mapk8	0.28	Ddx58	3.65
Fbxo39	1.77	Irf5	0.51	Fa2h	0.55	Ddx58	0.05	Eif2ak2	0.22	Fbxo39	2.34
Map4k2	1.12	Rtp4	0.37	Ifi27	0.18	Tlr9	0.04	Atf3	0.22	B2m	1.88
Gbp2	0.68	Map4k2	0.31	Map3K8	0.13	Mapk8	0.04	Dhx9	0.16	Ifna4	1.84
										Mitd1	0.53
										Ifitm3	0.25
										Parp14	0.24
										Irgm	0.24
										Atf3	0.13

To further analyse deep sequence data obtained from peripheral RNAi screening, a comparison was made between enrichment of ATF3-amiR WNV in mouse spleens and the p1-Vero virus stock that was used to infect mice (Table 5.2). Percentage enrichment of ATF3-amiR WNV at p1-Vero and mouse spleens in the whole virus libraries were determined and recorded. It was noted that ATF3 #2-amiR WNV was among the over represented amiR-encoding viruses in p1-Vero. However, other overly represented amiR-encoding viruses such as NMI clone #2 amiR-encoding virus, IFI35 clone #2-amiR WNV, which were enriched at 4.58% and 2.54% in p1-Vero respectively were not selected or enriched in any of the spleens. Furthermore, selection and enrichment of ATF3 clone #2 amiR WNV in mouse spleens highlighted the importance of ATF3 during peripheral WNV replication. However only ATF3-amiR WNV (Clone 2) but not ATF3 #1-amiR WNV was selected and enriched in mouse spleens. It is possible that the ATF3-1 amiR sequence was not as effective as ATF3-2 amiR at knocking down expression of ATF3 in cells. Future experiments should aim at addressing this research question as to why ATF3 #1 was not enriched and selected in spleens.

Table 5.2: Enrichment and selection of ATF3-amiR WNV in mouse spleen

	Percentage enrichment						
AmiR	p1-Vero	Spleen 1	Spleen 2	Spleen 3	Spleen 4	Spleen 5	Spleen 6
ATF3 #1	0.37	0	0	0	0	0	0.02
ATF3 #2	3.41	18.31	76.86	46.85	97.35	0.22	0.13

5.3.2 *In vivo* RNAi screening in the brain identifies ATF3, IRF7 and PARP11 as major antiviral factors that control West Nile virus infection

A total of 10 mice were infected intraperitoneal route with 10^5 pfu of p1-Vero ISG-targeting amiR-encoding WNV library mixed with 200 pfu of scrambled amiR-encoding WNV virus library. Mice were monitored for 21 days and clinical scores recorded each day (Figure 5.2). A relatively low infectious dose was used to allow virus competition, subsequent enrichment and selection of amiR-encoding viruses that deplete host mRNAs whose products restrict virus replication. Mice were sacrificed when they presented with encephalitic signs, and brains harvested for further analysis. A survival curve showed that 50% of the mice succumbed to 10^5 pfu of amiR WNV library (Figure 5.3A).

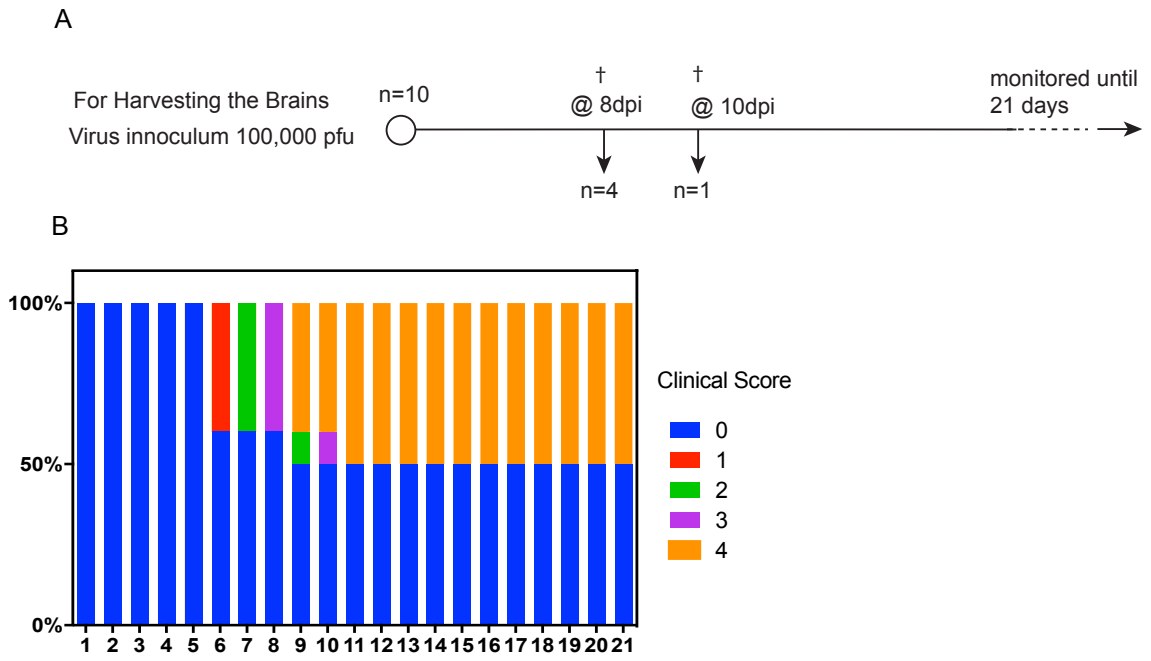

Figure 5.2 In vivo RNAi screening in the CNS. A) A representation of the experimental plan used to perform *in vivo* screening of RNAi in mouse brains. A total of 10^5 pfu of p1-Vero ISG-targeting amiR-encoding virus library was mixed with 200 pfu of scrambled amiR-encoding WNV virus library and used to infect ten 4-week old CD-1 mice, which were monitored for 21 days. Four mouse brains and one brain were harvested on signs of encephalitis at 8 and 10 dpi respectively. B) Clinical scores for each group were recorded each day for 21 days. For the clinical score 0 denoted Normal feeding and appearance. Clinical score 1: denoted slightly ruffled fur and/or general loss of condition respectively. Clinical score 2: denoted increase in general loss of behaviour, appearance, breathing changes, twitching and anti-social behaviour. Clinical score 3 denoted first signs of encephalitis such as severely hunched posture, partial paralysis and or full paralysis while clinical score 4 denoted death.

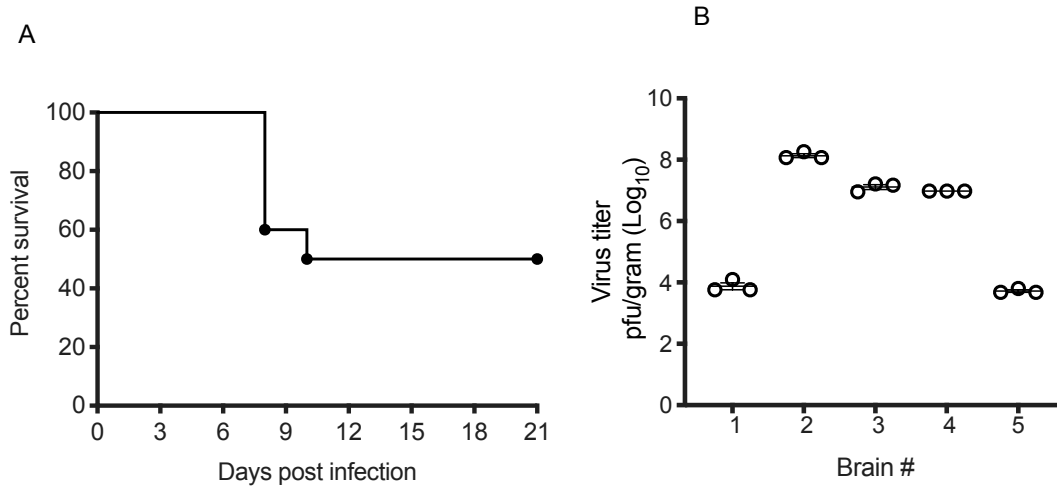

Figure 5.3 Percentage survival and virus burden in mouse brains infected with p1-Vero ISG-targeting amiR-encoding virus library. A) Percentage survival of mice infected with 10^5 pfu of p1-Vero ISG-targeting amiR-encoding virus library mixed with 200 pfu of scrambled amiR-encoding WNV virus library. Four mice and one mouse were culled on signs of encephalitis at 8 dpi and 10 dpi respectively and the remaining mice observed for signs of encephalitis until 21 dpi. B)

Virus burden in mouse brains determined by immunoplaque assay on C6/36 cells and presented as three independent experiments per mouse brain. Virus titre was determined as pfu/gram of mouse brain.

Brains of mice with encephalitic signs were homogenised in PBS and virus titre determined by immunoplaque assay (Figure 5.3B). Thereafter, using part of the brain homogenates (150 µL), total RNA was extracted and RT-PCR performed to generate an amplicon for deep sequencing. Results from RT-PCR showed that RNA extracted from three mouse brains (brains 2, 3, and 4) produced the correct sized RT-PCR amplicons, which were purified by DNA gel extraction. The two mouse brains that did not form RT-amplicons had low virus titres and it is possible that the ratio of virus RNA to cellular RNA in the brains could have been too small (Figure 5.3 B). Obtained RT-PCR amplicons were deep sequenced to determine enrichment of amiR-encoding viruses in mouse brains.

Deep sequencing data were uploaded onto Galaxy Australia (UQ Research Computing Center) and analysed using the Salmon tool for transcript quantification (Appendix 2). The analysis revealed that each of the three mouse brains contained one predominantly enriched amiR-encoding virus. Mouse brains 2, 3 and 4 (Figure 5.3 B) contained PARP11-amiR WNV, ATF3-amiR WNV and IRF7-amiR WNV respectively (Table 5.2 and appendix 8). Furthermore, each mouse had a single dominant virus with more than 97.9% representation. None of the control viruses, either scrambled amiR-encoding viruses, GFP-amiR or miR-124-amiR West Nile viruses were selected or enriched in mouse brains.

Table 5.3 Enrichment and selection of ATF3, IRF7 and PARP11 amiR encoding in mouse brains

Brain 2		Brain 3		Brain 4	
AmiR	%	AmiR	%	AmiR	%
Parp11	97.93	Atf3	99.44	Irf7	99.60
Irf7	1.38	Parp11	0.25	Atf3	0.06
Atf3	0.38	Irf7	0.06	Parp11	0.06

As a summary, the log fold change of spleen and brain samples relative to the p1-Vero virus stock (input virus stock) was determined. To determine the log $_{10}$ fold change enrichment, percentage

enrichment of individual amiR-encoding encoding viruses at p1-vero was used as baseline for comparison between enrichment in mouse spleens and brains. A ratio depicting the enrichment was obtained and log transformed to obtain the log $_{10}$ fold change and plotted by using GraphPad prism version 8. Results revealed that ATF3-amiR WNV was the most enriched virus in mouse spleens and brains (Figure 5.4).

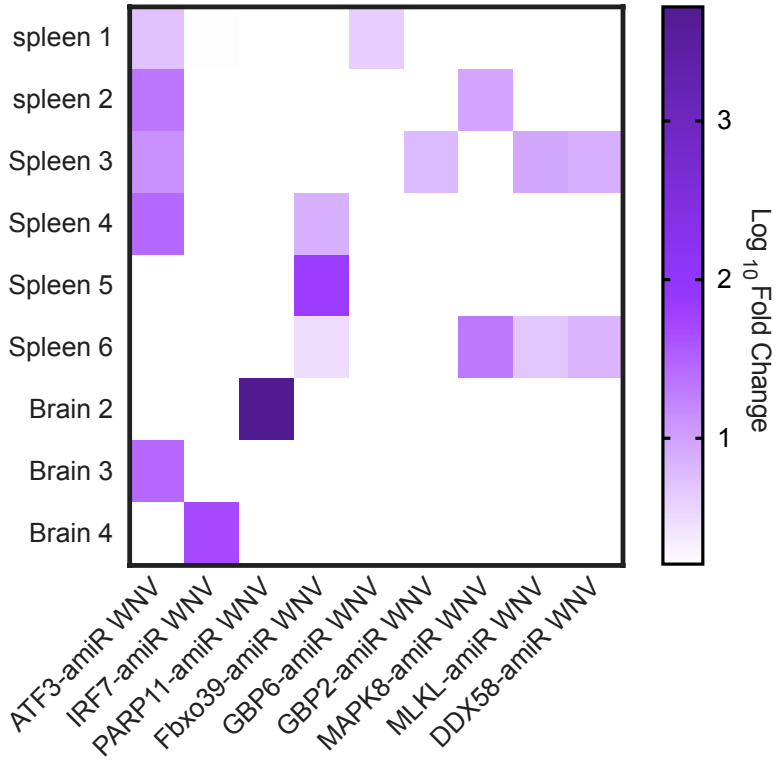

Figure 5.4 Selection and enrichment of amiR-encoding viruses in mouse spleens and brains. Diagram showing log $_{10}$ fold change in number of reads between p1-Vero virus library deep sequencing and enrichment of amiR-encoding viruses in the brain or spleen of mice infected with amiR-encoding virus libraries.

5.3.3 Generation of *in vivo* selected amiR-encoding West Nile viruses

The selection and enrichment of a different amiR-encoding virus in each of the three mouse brains suggested that the selected amiRs-encoding WNV that target ATF3, IRF7 and PARP11 host genes could function in similar biological pathways. In order to further investigate the roles of the particular genes identified, individual ATF3-amiR, IRF7-amiR and PARP11-amiR WNV were generated. Briefly, plasmid DNA for ATF3-amiR, IRF7-amiR and PARP11-amiR were retrieved and amiR fragments generated for CPER as described in Chapter 4. Thereafter CPER was performed to generate infectious cDNA for ATF3-amiR, IRF-amiR and PARP11-amiR for transfection into HEK 293 (Figure 5.5 A). Virus culture fluid was harvested at 3 days post-transfection and the p0-293T virus stocks titres determined by immunoplaque assay on Vero cells

(Figure 5.5 B).

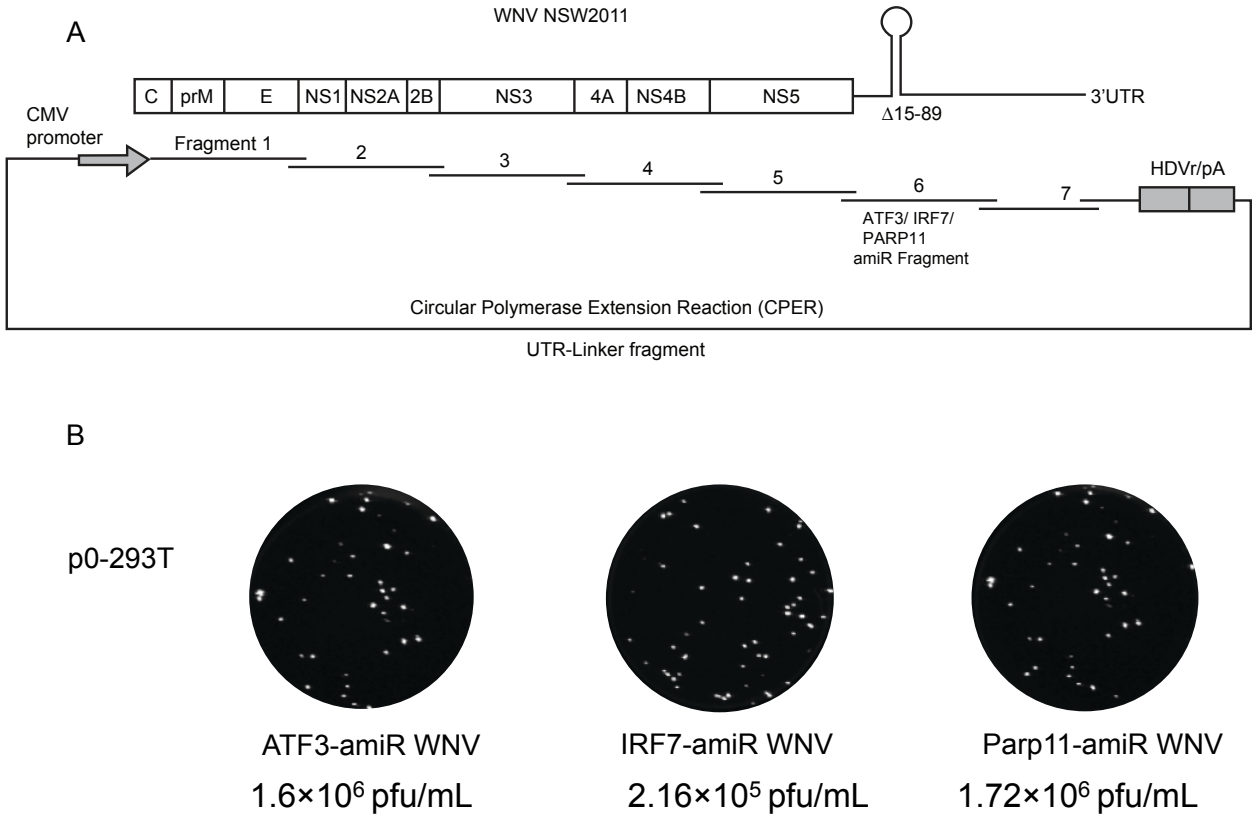

Figure 5.5 Generation of individual amiR-encoding viruses. A) Diagram representation of CPER strategy used to generate infectious ATF3-amiR, IRF7-amiR or PARP11-amiR encoding cDNA transfected into HEK293 cells to generate p0-293T virus library. B) Recovered p0-293T virus stocks were titred on a Vero cell monolayer by immunoplaque assay and plaque morphology recorded as similar between the different amiR-encoding viruses.

Vero cells were infected with p0-293T virus stocks at MOI =1 to amplify the virus titres and generate large virus stocks for subsequent experiments. At 3 days post infection, virus culture supernatants were harvested as p1-Vero and virus stock titres determined by immunoplaque assay on Vero cells (Figure 5.6 A). Thereafter, RNA was extracted and one-step RT-PCR performed to generate 3′ UTR PCR amplicons as described in chapter four. Analysis of RT-PCR gel image revealed that the generated RT-amplicons produced correct sized bands. Therefore, the generated RT-amplicons were purified by DNA gel extraction and Sanger sequenced to further confirm whether they retained the inserted pre-amiR hairpins with no mutations. Sanger sequencing revealed that all three generated amiR-encoding virus stocks retained inserted pre-amiR hairpins.

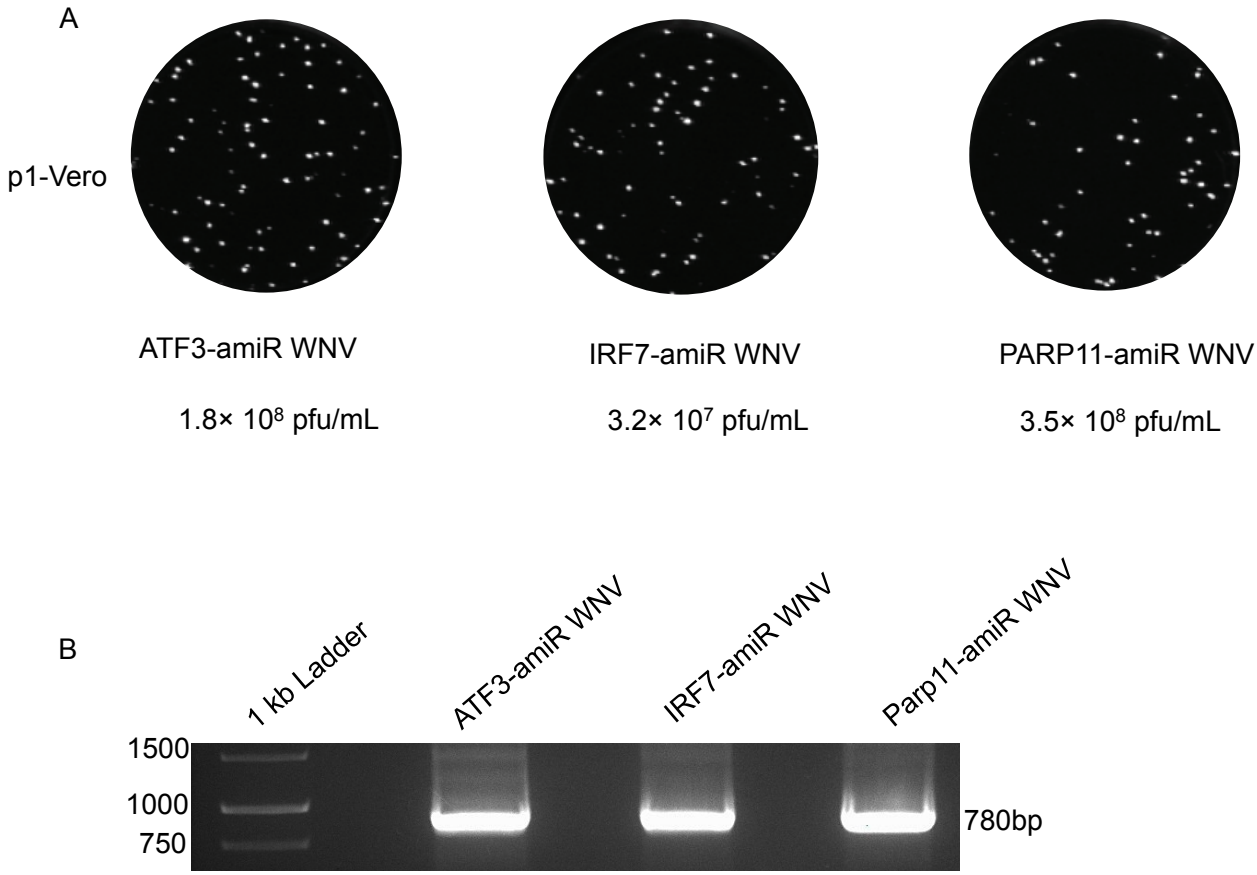

Figure 5.6 Generation of p1-Vero virus stocks. Generation West Nile virus stocks. Vero cells were infected with p0-293T virus stocks of ATF3-amiR and IRF7- amiR and PARP11-amiR at MOI =1 to generate larger volumes of p1-Vero respective virus stocks. At 72 hpi, virus culture fluids were harvested, clarified by centrifugation and stored for future experiments. Generated virus stocks were titrated on Vero cells by immunoplaque assay. B) Viral RNA was extracted from culture fluid and subjected to RT-PCR using 3′ UTR_Forward and 3′ UTR_Reverse primers. Expected DNA band size (780bp).

The obtained Sanger sequence results were validated by mfold to confirm the structure of pre-amiR hairpin. Results showed that all three amiR-encoding virus stocks conformed to pre-amiR hairpin structures (Figure 5.7).

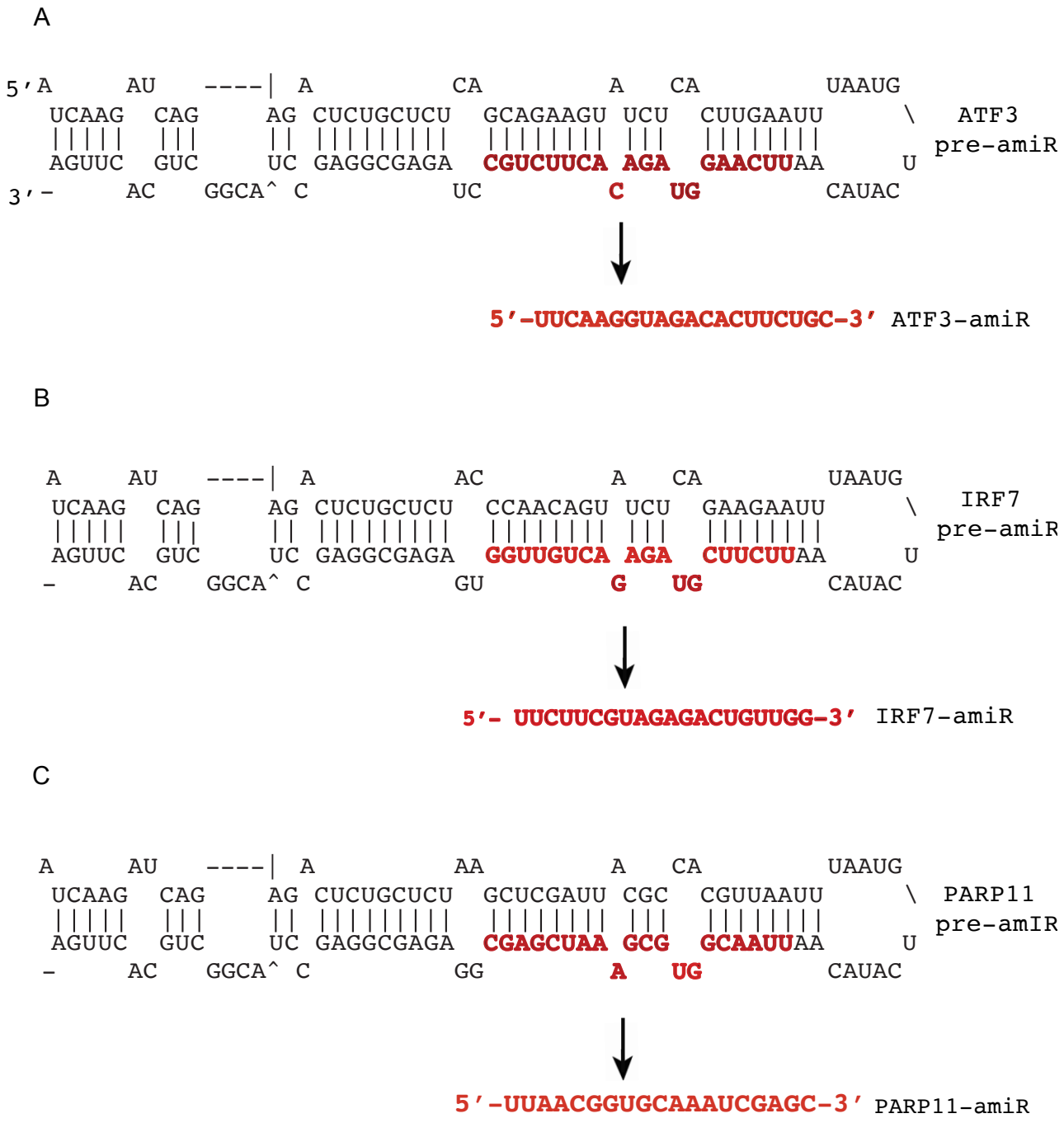

Figure 5.7 Predicted pre-amiR hairpin structures of p1-Vero virus stocks. A, B and C are predicted structures pre-amiR hairpin. All three p1-Vero virus stocks i.e., ATF3-amiR WNV, IRF7-amiR WNV and PARP11-amiR WNV retained their respective pre-amiR hairpin structures. Highlighted sequences in red represent the mature amiR sequences when pre-amiR hairpins are processed into functional amiR.

5.3.4 Generated ISG-amiR West Nile viruses produce mature amiR product in infected cells

In order to determine whether the inserted pre-amiR hairpins were processed into functional mature micro RNAs by the host cellular machinery, expression of mature miRNAs in Vero cells infected with respective amiR-encoding viruses and uninfected Vero cells was established. To do this, Vero cells were infected with ATF3-amiR WNV, IRF7-amiR WNV, PARP11-amiR WNV at MOI =1 or

mock un infected. At 48 hpi, cells were lysed and RNA extracted for northern blot analysis. Results showed that all pre-amiR hairpins inserted in the 3′ UTR of $WNV_{NSW2011}$ were processed by cellular machinery into miRNAs (Figure 5.8).

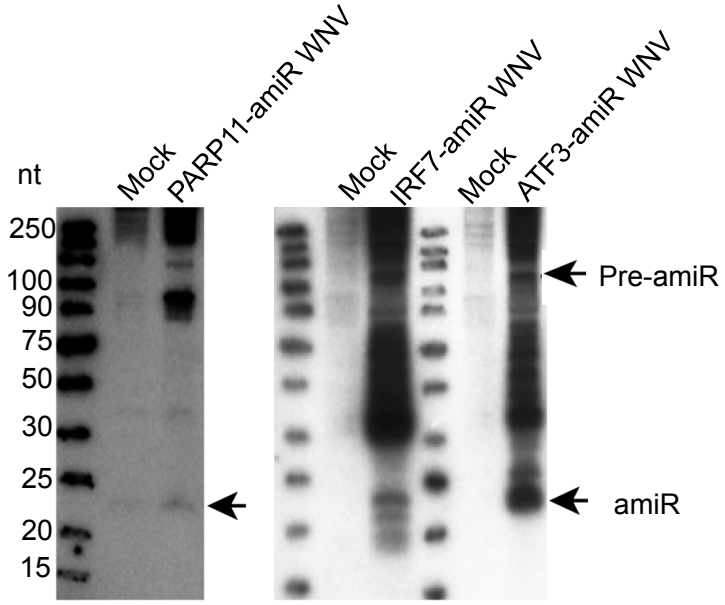

Figure 5.8 Detection of mature amiRs in infected Vero cells by northern blot analysis. Cells were infected with PARP11-amiR, IRF7-amiR and ATF3-amiR West Nile viruses or mock infected. Enriched small RNA fractions were extracted at 48 hpi using Tri reagent (Sigma Aldrich, USA) and 5 μg of RNA was subjected to electrophoresis in 15% TBE-Urea polyacrylamide gel followed by northern blot analysis with γ-P^{32}-labeled DNA probes complementary to PARP11-amiR, IRF7-amiR and ATF3-amiR respectively. The mature amiR band (21 nts) was detected in RNA samples from cells infected with respective amiR-encoding viruses. The nt denotes nucleotides.

5.3.5 Mature amiR from ISG-amiR West Nile viruses effectively knock down expression of targeted ATF3 and IRF7 protein

Ifnar1$^{-/-}$ MEF cells were infected with ATF3-amiR WNV, IRF7-amiR WNV, PARP11-amiR WNV at MOI =1. At 48 hpi, cells were lysed in NP-40 lysis buffer and western blot performed. Results showed that infection with ATF3-amiR, GFP-amiR and WT WNV generated equal amounts of WNV-E protein in infected cells. However ATF3 expression in ATF3-amiR infected cells was reduced compared to GFP-amiR and WT WNV infected *Ifnar1*$^{-/-}$ MEF cells (Figure 5.9).

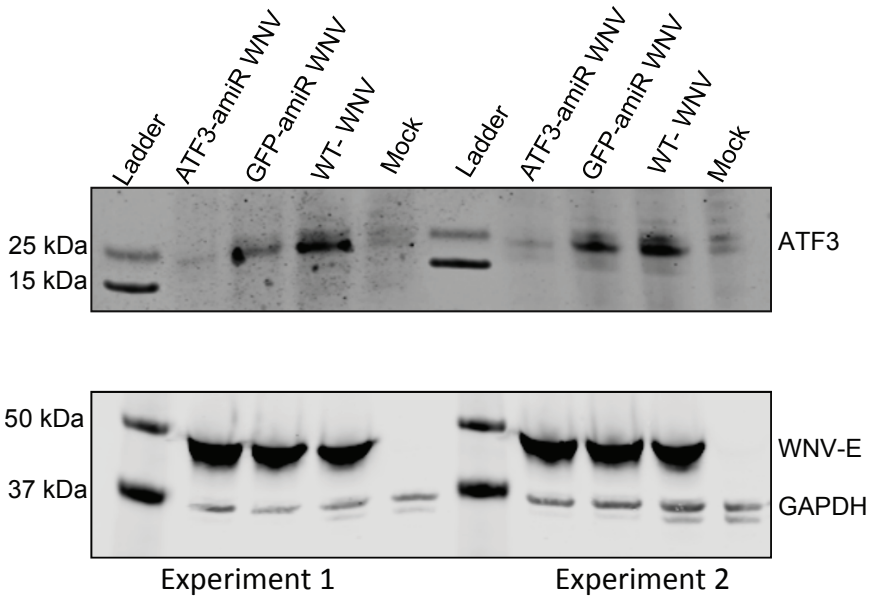

Figure 5.9 Infection with ATF3-amiR WNV knocks down expression of ATF3 gene in *Ifnar1*$^{-/-}$ MEF. *Ifnar1*$^{-/-}$ MEF cells were infected with ATF3-amiR, GFP amiR, and WT West Nile viruses at MOI =1 or mock uninfected. At 48 hpi, cells were lysed in NP40-containing lysis buffer and subjected to western blot electrophoresis. Blots were probed with anti-ATF3 mAb,, anti-WNV-E mAb (4G2) and anti-GAPDH mAbs. Predicted sizes are 24kDa, 37kDa and 42kDa for ATF3, GAPDH and E-protein respectively.

Similarly, infection of *Ifnar1*$^{-/-}$ MEF with IRF7-amiR WNV resulted in the knock down of IRF7 in *Ifnar1*$^{-/-}$ MEF, with more evident knockdown in experiment 1 and less knockdown in experiment 2 (Figure 5.10).

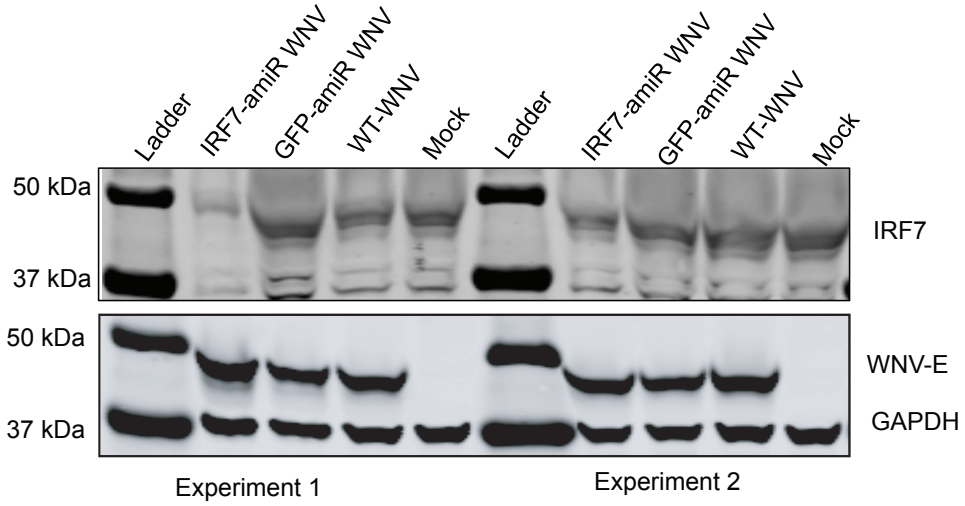

Figure 5.10 Infection with IRF7-amiR WNV knocks down expression of IRF7 in *Ifnar1*$^{-/-}$ MEF. The *Ifnar1*$^{-/-}$ MEF were infected with IRF7-amiR, GFP amiR, and $WT_{NSW2011}$ West Nile viruses at MOI =1) and mock uninfected. At 48 hpi cells were lysed in NP40-containing lysis buffer and subjected to western blot electrophoresis. Blots were probed with anti-IRF7 mAb, 4G2 WNV-E and mouse IgG GAPDH antibodies recognising IRF7, WNV-E and GAPDH respectively. Predicted sizes are 44 kDa, 37 kDa and 42 kDa for IRF7, GAPDH and E-protein respectively.

Lastly, to determine whether PARP11-amiR WNV knocks down expression of PARP11 in *Ifnar1*$^{-/-}$ MEF cells, western blot was performed using obtained cell lysates at 48 hpi. The PARP11 antibody used was not effective at detecting PARP11 expression in *Ifnar1*$^{-/-}$ MEF cells although *Ifnar1*$^{-/-}$ MEF cells were greatly infected by WNV as shown by WNV envelope protein expression (Figure 5.11). Furthermore, it is possible that PARP11-amiR did not successfully knockdown expression of PARP11 protein in cells. However, further work would have to be done to confirm that the antibody is recognising PARP11.

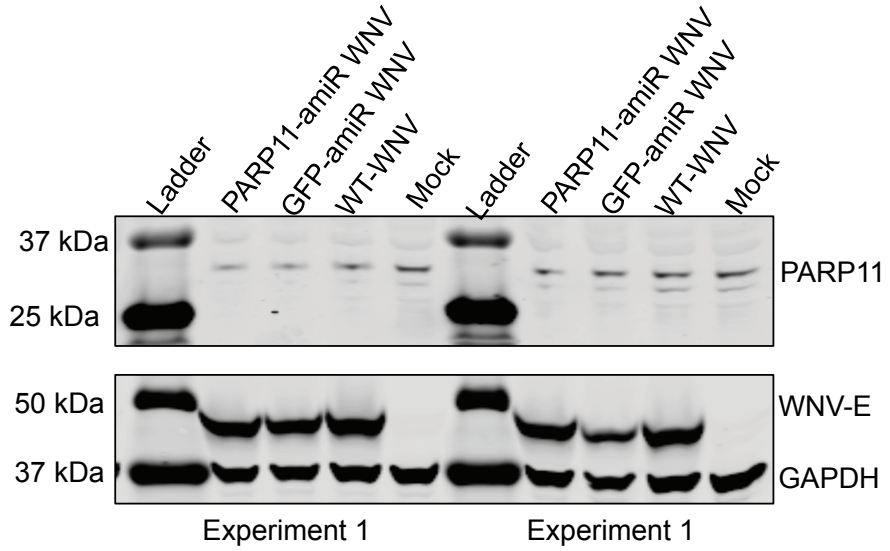

Figure 5.11 Infection of *Ifnar1*$^{-/-}$ MEF with PARP11-amiR WNV. The *Ifnar1*$^{-/-}$ MEF were infected with PARP11-amiR, GFP amiR, and WT West Nile viruses at MOI =1 or mock uninfected. At 48 hpi cells were lysed in NP40-containing lysis buffer and subjected to western blot electrophoresis. Blots were probed with anti-PARP11, mAb, anti-WNV-E mAb (4G2) and anti-GAPDH mAbs. Predicted sizes are 30 kDa, 37 kDa and 42 kDa for PARP11, GAPDH and E-protein respectively.

5.3.6 Viral Growth Kinetics

To determine the role of ATF3, IRF7 and PARP11 in WNV infection, the replication efficiency of ATF3-amiR WNV, PARP11-amiR WNV and IRF7-amiR WNV compared with GFP-amiR WNV was evaluated in WT MEFs and *Ifnar1*$^{-/-}$ MEF. Both WT MEF and *Ifnar1*$^{-/-}$ MEF were infected at MOI =1 with respective viruses. At 0, 24, 48 and 72 hpi, virus culture fluid was collected and titres determined for each time point by immunoplaque assay on Vero cells. Three independent experiments were performed for each cell lines and virus. Results revealed that ATF3-amiR WNV, PARP11-amiR WNV and IRF7-amiR WNV replicated better than GFP-amiR WNV in both WT MEF and *Ifnar1*$^{-/-}$ MEF (Figure 5.12). Despite that there was no difference in replication at 0 hpi and 24 hpi, ATF3-amiR WNV replicated significantly higher than GFP-amiR WNV in WT MEF at 48 hpi and 72 hpi (Figure 5.12 A). Infection of *Ifnar1*$^{-/-}$ MEF with ATF3-amiR WNV replicated

significantly higher than GFP-amiR WNV at 0 hpi, 24 hpi and 48hpi in, with no difference at 72 hpi. This implied that by 48 hpi, all *Ifnar1*$^{-/-}$ MEF cells are infected thus limiting further rounds of infection. Infecting WT MEF with PARP11-amiR WNV revealed that PARP11-amiR WNV replicated significantly better than GFP-amiR WNV at 48 hpi and 72 hpi. When *Ifnar1*$^{-/-}$ MEF were infected with PARP11-amiR WNV at MOI =1, PARP11-amiR WNV replicated better than GFP-amiR WNV at 0 hpi and 24 hpi and no difference in replication was observed at 48 hpi and 72 hpi. Furthermore, when WT MEF were infected with IRF7-amiR WNV, the virus replicated better at 0 hpi and 72 hpi while infection of *Ifnar1*$^{-/-}$ MEF with the same virus showed that replication improved only at 72 hpi.

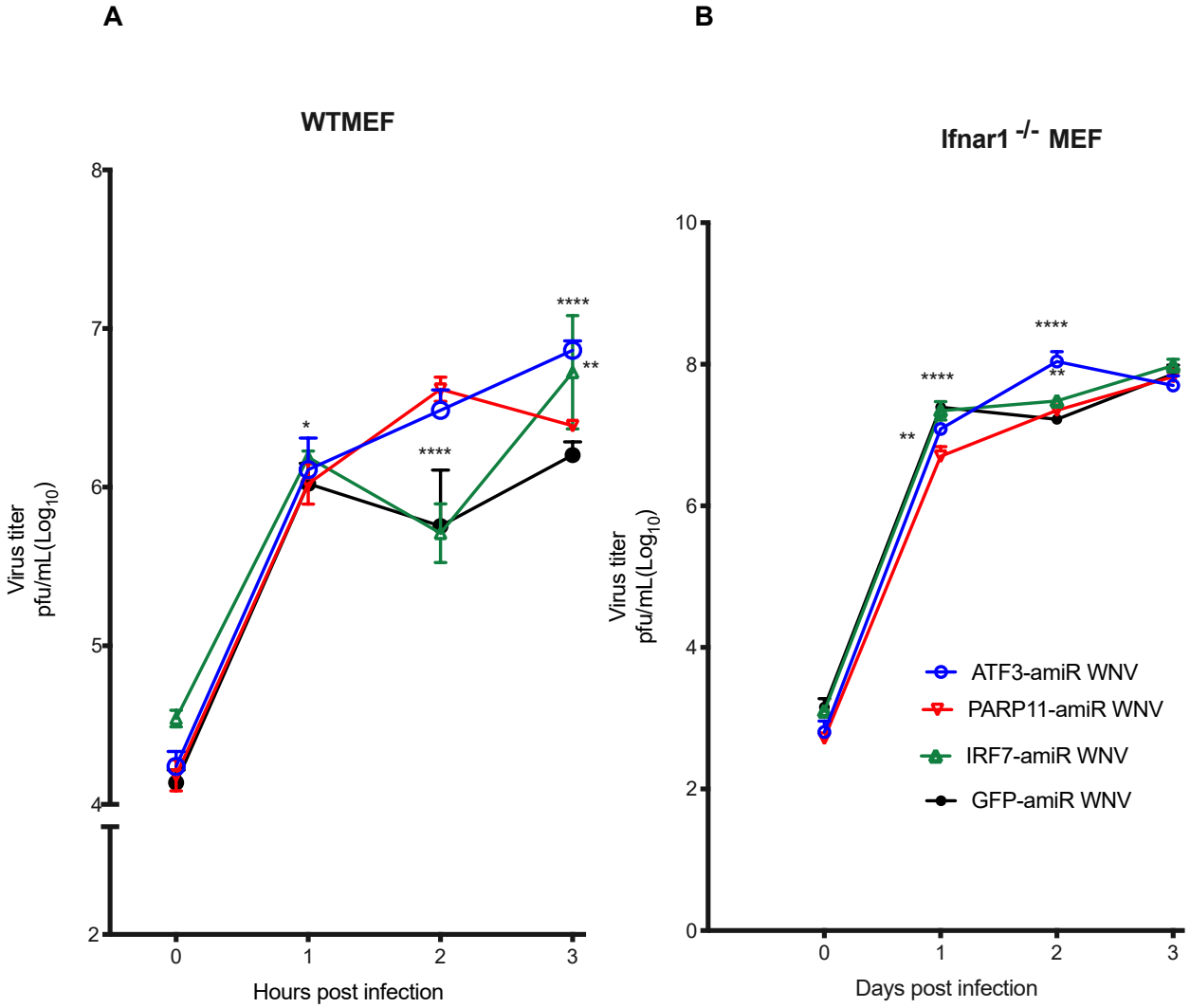

Figure 5.12 *In vivo* selected amiR-encoding viruses replicate better than GFP-amiR WNV in WT MEF and *Ifnar1*$^{-/-}$ MEF. Viral growth kinetics of ATF3-amiR WNV, IRF7-amiR WNV, PARP11-amiR WNV and GFP-amiR WNV on WT MEF and *Ifnar1*$^{-/-}$ MEF. Cells were infected at MOI =1 for up to 72 hours post infection. Virus titres shown are $\log_{10}$ transformed mean values and represented as pfu/mL ± SEM, as determined by immunoplaque assay on Vero cells. Three independent experiments were performed for each cell line. Significant differences between the means are differentiated using two-way ANOVA with Dunnett's multiple comparison test where *p

< 0.05, **p <0.005, ***p < 0.001, ****p < 0.0001. The results represent the means of three independent infection experiments and errors bars show standard error of the mean.

5.3.7 Increased virulence of ISG targeting amiR-encoding West Nile Viruses

To further investigate the role of ATF3-amiR WNV, IRF7-amiR WNV and PARP11-amiR WNV in West Nile virus infection, the generated recombinant $WNV_{NSW2011}$ viruses encoding corresponding individual amiRs were examined *in vivo*. To determine virulence of amiR-encoding viruses, 40 four-week-old CD-1 mice were infected with 10^6 pfu of respective viruses via the intraperitoneal route and monitored for 21 days post infection. Each day, each animal's clinical score was determined and recorded. Mice that succumbed to encephalitis were culled and brains harvested for further analysis. At the end of the animal experiment, a survival curve was generated to determine percentage survival of mice infected with recombinant viruses in comparison to GFP-amiR WNV control. Results revealed that infection with each of ISG-targeting amiR-encoding virus caused 100% mortality in mice and each virus was more virulent than GFP-amiR WNV (Figure 5.13). By 8 dpi and 9 dpi all mice infected with ATF3-amiR WNV and PARP11-amiR, and IRF7-amiR WNV had succumbed to WNV respectively compared to mice infected GFP-amiR WNV, which had 6/10 (60%) mice survive until 21 dpi

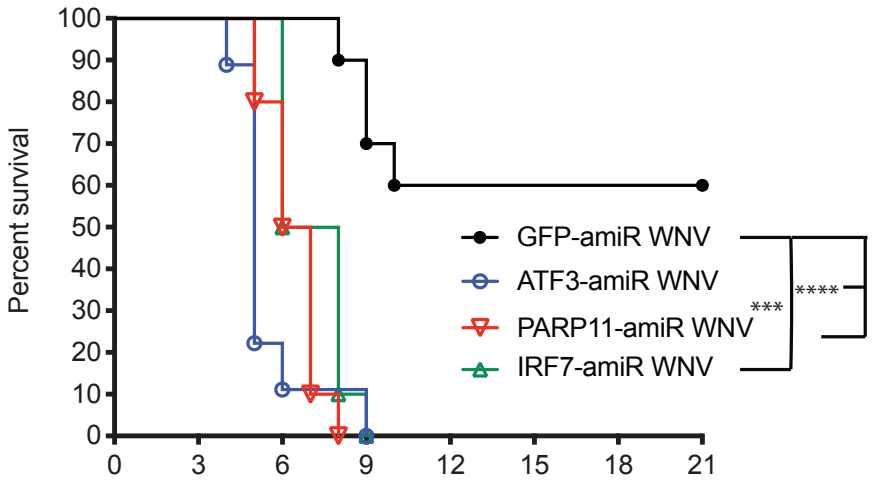

Figure 5.13 Percentage survival of *in vivo* selected ISG-targeting amiR encoding virus. Four-week-old CD-1 mice were challenged with10^6 pfu of ATF3-amiR WNV, IRF7-amiR WNV or PARP11-amiR WNV p1-Vero generated virus stocks. Each virus group contained 10 mice, which were monitored for 21 days and at the survival curve generated. Analysis was performed using Mantel-Cox log-rank test ***p < 0.001 (IRF7-amiR WNV vs GFP-amiR WNV), ****p < 0.0001 (PARP11 and ATF3-amiR WNV vs GFP-amiR WNV).

5.3.8 Increased progression of clinical signs in mice infected with ATF3-amiR, IRF7-amiR and PARP11-amiR West Nile viruses

Mice infected with ATF3-amiR WNV, IRF7-amiR WNV and PARP11-amiR WNV presented an increase in progression and severity of observed clinical signs, such as ruffled fur and/or general loss of condition, loss weight, change in breathing, twitching, anti-social behaviour, severely hunched posture, paralysis among others (Figure 5.14).

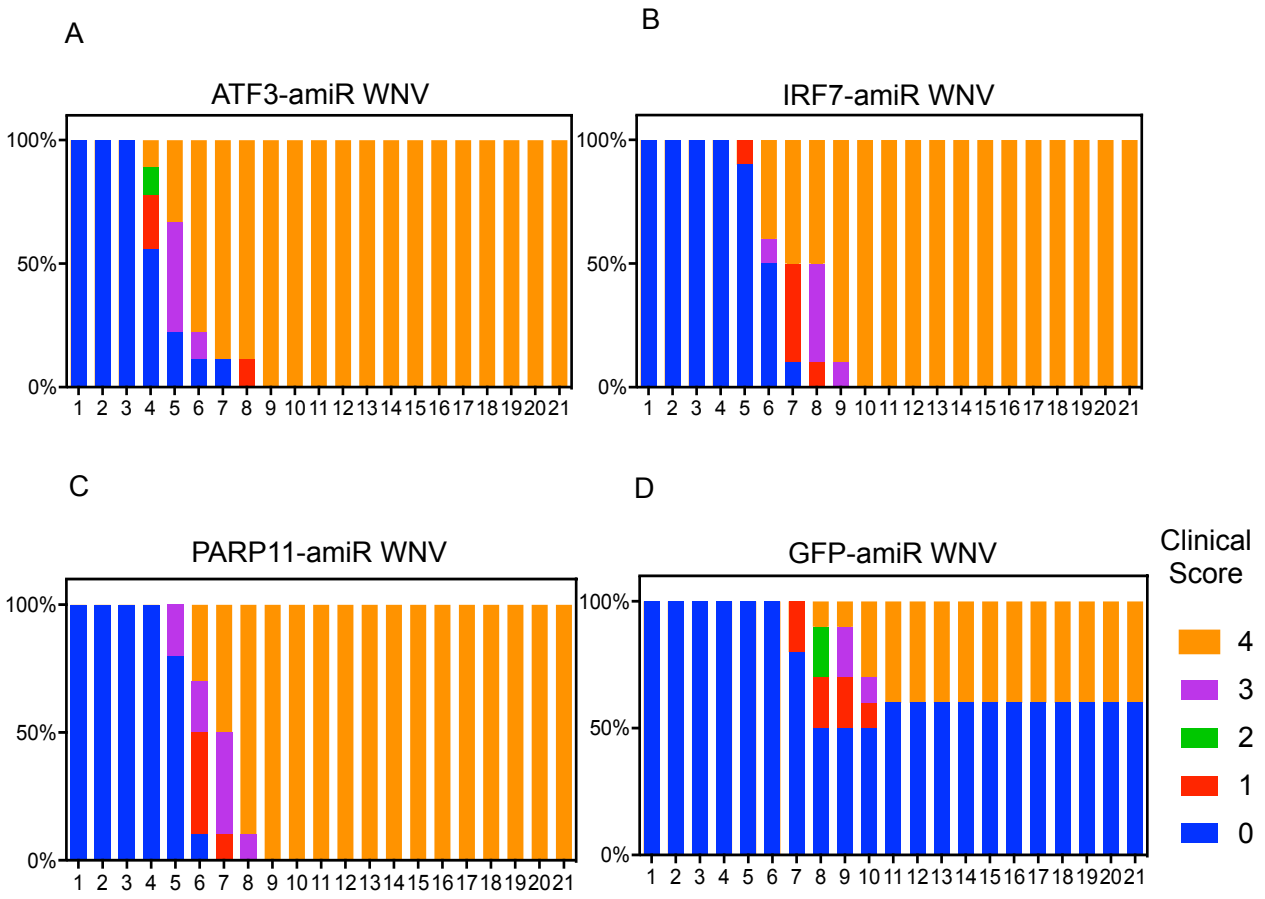

Figure 5.14 Increased progression of clinical signs in mice infected with ATF3-amiR, IRF7-amiR and PARP11-amiR West Nile viruses. Four groups of mice were infected with (A) ATF3-amiR WNV, (B) IRF7-amiR WNV, (C) PARP11-amiR WNV and (D) GFP-amiR WNV and each group monitored daily for signs of encephalitis. Clinical scores for each group were recorded each day for 21 days. For the clinical score 0 denoted Normal feeding and appearance. Clinical score 1: denoted slightly ruffled fur and/or general loss of condition respectively. Clinical score 2: denoted increase in general loss of behaviour, appearance, breathing changes, twitching and anti-social behaviour. Clinical score 3 denoted first signs of encephalitis such as severely hunched posture, partial paralysis and or full paralysis while clinical score 4 denoted death.

5.3.9 Viraemia

To determine viraemia, mice were tail bled for the first seven days to obtain sera for immunoplaque assay on C6/36 mosquito cells. Mice infected with ATF3-amiR WNV, IRF7-amiR WNV and

PARP11-amiR WNV all showed a trend for increased viraemia compared to mice infected with the control virus, GFP-amiR WNV. The differences were only significant for mice infected with ATF3-amiR WNV at 1 dpi, 3 dpi and 4 dpi (Figure 5.15). Viraemia lasted until 4 dpi and by 5 dpi, there was no viraemia detectable.

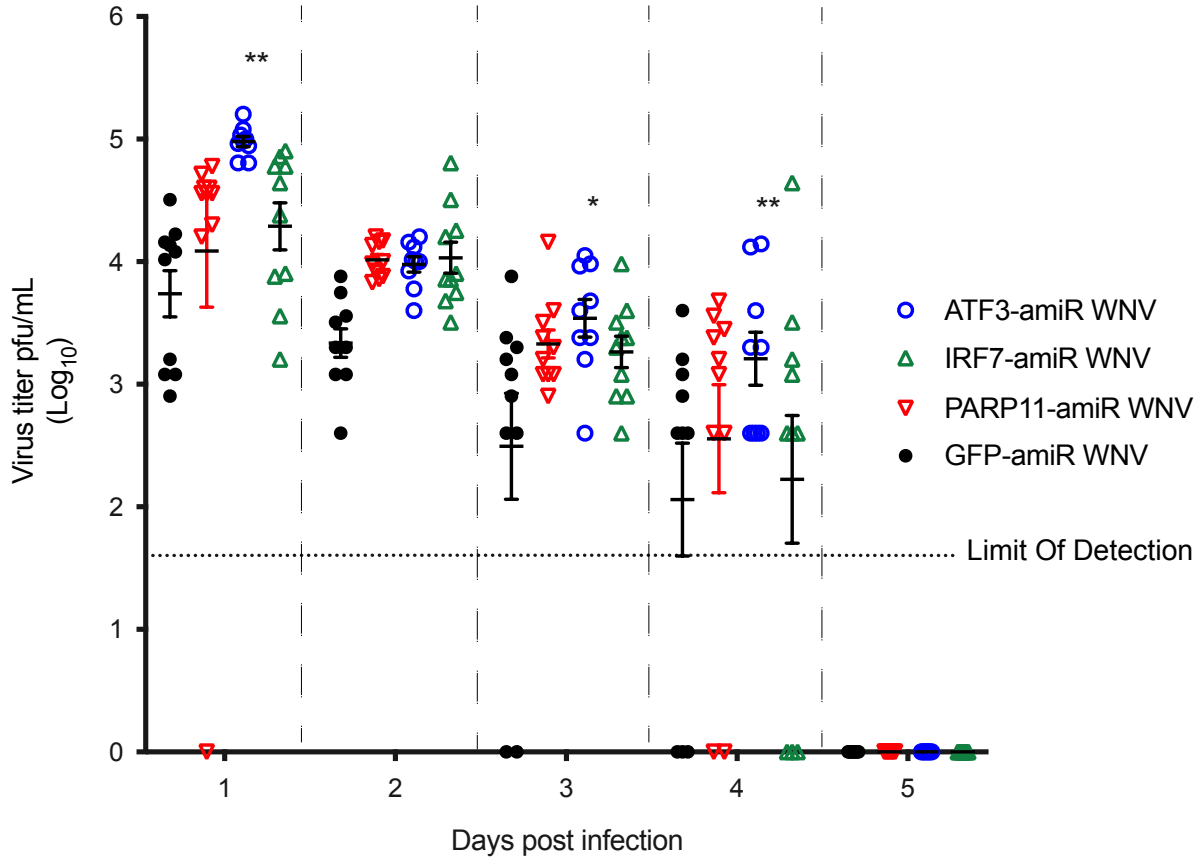

Figure 5.15 Increased viraemia in mice infected with ISG-targeting amiR encoding West Nile viruses. To determine viraemia, mice were tail bled from 1 dpi to 7 dpi. Serum virus titre was determined by C6/36 immunoplaque assay using WNV-E-16 antibody. Obtained titres were log transformed and plotted using GraphPad prism version 8. Error bars represent Standard Error of the mean log transformed virus titre per group. Analysis performed using 2-way ANOVA with Dunnett's multiple comparison against GFP-amiR WNV control *p < 0.05 and **p <0.005. The limit of detection is 40 pfu/mL, equivalent to 1.602 log 10.

5.4 Discussion

5.4.1 Selection of ATF3 as important antiviral factor in peripheral and CNS dissemination of West Nile Virus infection

ATF3 is induced by stress, such as inhibition of protein synthesis or infection, in infected cells [312, 313]. Four out of six mouse spleens that were analysed by deep sequencing showed that

ATF3-amiR WNV was selected and enriched when mice were infected with ISG-targeting amiR encoding WNV library mixed with scrambled amiR control. Furthermore, one mouse brain out of five brains showed selection and enrichment of ATF3-amiR WNV, suggesting that ATF3 is important in WNV infection. To assess the role of ATF3 as an important antiviral against WNV, *in vitro* characterisation was performed. Viral growth kinetics on WT MEF and *Ifnar1*$^{-/-}$ MEF cells revealed that ATF3-amiR WNV replicated better than GFP-amiR WNV in WT MEF and *Ifnar1*$^{-/-}$ MEF cells. Furthermore ATF3-amiR targeting murine *Atf3* expression significantly knockdown expression of *Atf3* in *Ifnar1*$^{-/-}$ MEF infected with ATF3-amiR WNV. Lastly, infection of Vero cells with ATF3-amiR WNV at MOI =1 and subsequent northern blot analysis on cellular RNA showed that ATF3-amiR is processed into a function mature ATF3 micro RNA by the host cell machinery. Therefore, it is the ATF3-amiR (siRNA) that blocks translation of Atf3 mRNA into a functional Atf3 protein. This could explain the low expression of Atf3 in *Ifnar1*$^{-/-}$ MEF cells.

Having shown this, 4-week old CD-1 mixed sex mice were infected with 10^6 pfu of ATF3-amiR WNV and monitored for a period of 21 days, recording clinical score every day. Mice infected with ATF3-amiR WNV showed increased progression of clinical signs and symptoms characterised by, increased progression of encephalitic signs and by day nine post infection, all mice had succumbed to ATF3-amiR WNV. Furthermore, mice infected with ATF3-amiR WNV exhibited significant increase in viraemia at 1 dpi and 3 dpi. Perhaps increased viraemia could have contributed to the severity of infection and disease outcome.

5.4.2 ATF3 roles in immune response

ATF3 is a member of the ATF/cyclic AMP response element binding family of transcription factors, an adaptive response element in stress regulated by stress signal. Some of the stress signals *in vivo* include: ischemia, wounding, neural damage, toxicity, and seizure while *in vitro* stress signals may include: change in serum factors, cytokines, genotoxic agents, cell death-inducing agents among others [314]. ATF3 is usually expressed at low levels in neurons but in the event of neural damage, ATF3 expression is up regulated [315]. ATF3 expression is induced during neuron injury with prolonged ATF3 expression believed to facilitate axonal renewal and recovery in the nervous system [316]. ATF3 consists of 181 amino acids with a molecular mass of 22- 24 k Da [317-319]. ATF3 expression is induced by LR ligands to negatively modulates TLR signalling early in infection or stress related events [319, 320]. Micro-array studies have shown that ATF3 enables affected cells to cope with extracellular changes while most healthy tissues/ cells express basal levels of ATF3 [315, 318, 321, 322]. Two major roles of ATF3 have been postulated such as ATF3 mediates cellular response to stress and regulates cellular proliferation with different studies suggesting that ATF3 could serve as a pro-apoptotic gene or anti apoptotic gene depending on the

promoter [323-325]. In addition, a recent study suggests that ATF3 represses cell cycle progression. Network system analysis postulated that ATF3 is an essential member of the NF-κB family of transcription factors that regulates expression of pro inflammatory cytokines such as IL-1β, IL-6, IL-12, TNFα and CCL4 [326]. Furthermore, research has shown that ATF3 expression stimulates cell death and cell cycle machinery. Although there is not much literature concerning the role of ATF3 in virus infection, ATF3 is shown to facilitate ER stress response, referred to as unfold protein response [327, 328]. Unfold protein response results from mismatched folded proteins in the lumen of the ER. ATF3 attempts to reinstate normal ER protein folding and processing through hindering translation of new protein and transportation of new protein into the ER. Therefore, ATF3 stimulates transport of unfolded protein from the ER to cytoplasm for destruction and recruits molecular markers that ensure proper protein folding. In the event that ER stresses remain, apoptosis is induced [315]. Based on this literature, there is a possibility that ATF3 is involved regulation of immune response during WNV infection. Future research should aim at understanding whether ATF3 is involved in ER response or control of apoptosis during WNV infection. This will further elucidate the role of ATF3 in WNV infection.

5.4.3 Enrichment of IRF7-amiR WNV *in vivo*

During WNV infection, specific viral motifs such as ssRNAs, dsRNAs are sensed by TLR3 and TLR7 in endosome or MDA5 and RIG-I in cytoplasm. As a result, this activates transcription of IRF-3 and IRF-7, induction of IFN response and subsequent activation of ISGs [213]. Furthermore, infection of Irf7 deficient (*Irf7*$^{-/-}$) mice with WNV results into increased viraemia, elevated virus burden in peripheral organs and CNS as well as higher mortality rate than in mice infected with WT-WNV [210]. Furthermore, when *Irf7*$^{-/-}$ primary macrophages were infected with WNV, IFN-α gene expression and protein production significantly reduced. This highlighted that IRF7 is an important antiviral host gene against WNV infection. Selection and enrichment of IRF7-amiR WNV in one mouse could be attributed to the fact that IRF7 is a known antiviral host gene against WNV. Furthermore, when mice were infected with IRF7-amiR WNV, higher mortality rate, viraemia and viral burden in the CNS was observed compared to the control group. However, it should be noted that the input virus used to infect mice contained more IRF7-amiR WNV variants at a percentage of 1.74%. This might have provided IRF7-amiR WNV greater advantage over other amiR-encoding variants in the library. It would be very informative to perform this *in vivo* RNAi screening a number of times to show whether IRF7-amiR WNV is still selected. The fact that only 10 mice were infected with the p1-Vero virus library, warranties the need for experiments. Furthermore, it was only IRF7-2-amiR WNV that was selected *in vivo* although two amiR targeting IRF7 were present in the library. Therefore, another research question would be to understand why IRF7-20amiR WNV was selected and enriched in mice brains over IRF7-1-amiR WNV. It is

important to determine the effectiveness of the other IRF7-amiR. Future work would have to examine the ability both of IRF7-amiR West Nile viruses to knockdown its targets and enhance replication. Lastly, another way to test the virulence of IRF7-amiR WNV in mice would be to infect mice via intracranial route in order to assess the effects of IRF7-amiR WNV on the brain. This would bypass the need for peripheral infection and define effects of IRF7-amiR WNV on WNV replication in the different parts of the brain.

5.4.4 Selection and enrichment of PARP11-amiR WNV *in vivo*

From the literature, PARP11 belongs to the Poly ADP-ribosyltransferase poly (ADP-ribose) polymerase family. This family consists of 17 members, each with a unique structure and cellular functions such as PARP 1, 2, 3, 4, 5a, 5b, 6, 7, 8, 9, 10, 11, 12, 13, 14, 15 and 16 [329]. Members in PARP family act as catalysts that transfer of ADP-Ribose from nicotinamide adenine dinucleotide (NAD^+) to target proteins to either form mono (ADP-ribosyl)ation (MARylation) or poly (ADP-ribosyl)ation (PARylation) of proteins. The ADP-ribosylation is a crucial stage in many biological processes such cell signalling, DNA repair, gene regulation and apoptosis [330-332]. Research has shown that PARP1 activates NF-κβ during inflammatory disorders, regulation of oxidative, genotoxic and metabolic stress responses, which are often reported during cancers, inflammatory-related diseases and metabolic disorders. Therefore, PARP1 inhibitors are beneficial in controlling these conditions [333, 334]. Moreover, PARPs are utilised in generating oncology therapeutics, with the first licenced drug being against ovarian cancers being a PARP inhibitor [335, 336].

Current research has shown that PARPs are linked to IFN-I signalling and priming of antiviral defence to protect cells from invading pathogens [337]. For instance, PARP1 and PARP10 are linked to activation of NF-κβ [334, 338]. In addition, PARP9 controls histone methylation to increase interferon signalling and expression of interferon-stimulated genes [339]. A recent study showed that PARP11 mono-ADP-ribosylates ubiquitin E3 ligase β-transducin repeat-containing protein (β-TrCP) to facilitate IFNAR1 ubiquitination and breakdown [340]. As a result knockdown of PARP11 expression blocked IFNAR-I binding, exposed ubiquitin sites and stimulated β-TrCP ubiquitination while over expression of PARP11 enhanced IFNAR-I binding [340].

Although precise mode of action of PARP11 in controlling West Nile virus infection is still unknown, infection of mice with PARP11-amiR WNV resulted into increased viraemia, mortality and progression of clinical signs, as all mice succumbed to encephalitis by day eight post infection. Selection and enrichment of PARP11-amiR WNV in one mouse implies that PARP11 is crucial in WNV replication in brain. Furthermore, basing on the input virus used to infect mice, PARP11 was represented at 0.18% *versus* the more than 97% enrichment observed in the brain. It is possible that the selection of PARP11 could have resulted from the role of PARP11 in WNV infection. It would

be very informative to perform this *in vivo* RNAi screening a number of times (for instance two more experiments) to show whether PARP11-amiR WNV is still selected. The fact that only 10 mice were infected with p1-Vero virus libraries, warranties the need for more *in vivo* RNAi screening experiments. Furthermore, it was only PARP11-2-amiR WNV that was selected *in vivo* although two amiRs targeting PARP11 were present in the library. Therefore, another research question would be to understand why PARP11-2 amiR WNV was selected and enriched in *vivo* over PARP11-1-amiR WNV. It is important to determine the effectiveness of the other PARP11-amiR. Future work would have to examine the ability both of PARP11-amiR West Nile viruses to knockdown its targets and enhance replication. Lastly, since PARP11-amiR WNV is selected in the brain, infection of mice via intracranial would provide evidence in regards to effects of PARP11-amiR WNV on the brain.

5.4.5 Interaction between *in viv*o selected amiR-encoding viruses

To determine the interaction of enriched amiR-encoding viruses and the respective biological pathways targeted, gene ontology bioinformatics analyses should be performed. This would decipher the interactions between ATF3, PARP11 and IRF7 enriched in the brains. Furthermore, gene ontology would show whether the selected and enriched amiR-encoding viruses in mouse spleens were targeting similar genes or biological pathways such as those associated with apoptosis and stress response. Gene ontology would also reveal whether most of the enriched amiR-encoding viruses in the spleens targeted genes and biological pathways that are important in the control of virus infections.

The enrichment of some genes such as PARP11, IRF7, Fbxo39 and MAPK8 in mouse spleens or brains, down-regulated enrichment of ATF3 while enrichment of ATF3 down-regulated IRF7, PARP11 among other genes. This could have been caused by (i) knockdown of either one of these expression of these proteins affects the same biological pathway (ii) knockdown of one host gene is a drawback of the system that when one virus's replication is enhanced by knockdown of any one of the antiviral pathways, this virus is enriched and outcompetes the other making the identification of additional antiviral proteins difficult.

Therefore, data presented in this chapter reveals two new antiviral host genes as Atf3 and Parp11 that influence West Nile virus infection *in vivo*. These new antiviral host genes could be utilised to generate effective antivirals although more studies are still required to understand the precise mechanism by which PARP11, IRF7 and ATF3 control West Nile virus infection.

Studies in this chapter screened and identified ATF3 as a major antiviral factor against West Nile

virus infection in peripheral and CNS infection using an *in vivo* RNAi screening technique. These studies characterised ATF3-amiR WNV, IRF7-amiR WNV and PARP11-amiR WNV both *in vitro* and *in vivo* and showed that infection all three viruses resulted into increased virulence in mice. However, further studies are desirable to understand the precise mechanism of action by which all these amiR-encoding viruses control West Nile virus infection.

Chapter 6: General Discussion and Conclusion

The strategy of this project was divided into three distinct stages: (i) generation of plasmid and virus libraries, (ii) *in vitro* and *in vivo* RNAi screening using generated virus libraries and (iii) *in vitro* and *in vivo* characterisation of selected and enriched amiR encoding viruses. Preliminary data generated by Setoh *et al*. (unpublished), revealed that deletion of nucleotides 15-89 (Δ15-89) at the start of the 3′ UTR was an optimal site for inserting pre-amiR hairpins that target specific mouse genes without attenuating the subsequent recombinant viruses. Furthermore, when WT MEF cells were infected with Δ15-89 WNV or WT-$WNV_{NSW2011}$, there was no significant difference in replication between the two viruses and Δ15-89 WNV replication and viral burden in mice was comparable with WT-$WNV_{NSW2011}$ (Setoh *et al*. unpublished). As a result, this (Δ15-89) region was used for subsequent generation of amiR-encoding plasmid and virus libraries.

6.1 Generation of plasmid and virus libraries

Having identified an optimal site for inserting pre-amiR hairpins, the next step was to generate a small amiR-encoding plasmid library by cloning. Each plasmid was designed to encode a unique amiR sequence, which targets a specific mouse gene. Consequently 204 ISG-targeting amiR-encoding plasmids were generated and combined to form an ISG-targeting amiR plasmid library. The generated plasmid libraries were subsequently used to generate p0 and p1 virus libraries through CPER. Generated virus libraries were confirmed to contain diverse amiR-encoding viruses by deep sequencing and were used as tools for both *in vitro* and *in vivo* RNAi screening.

In addition, a scrambled amiR-encoding virus library was generated as a negative control for subsequent experiments. Ultimately this scrambled library containing over 6000 individual amiR sequences did not prove to be a useful control. Initially it was envisaged as a control to ensure that selection was not occurring stochastically and none of scrambled amiR encoding viruses were selected or provided replicative advantage *in vitro* or *in vivo*. However, the library was so large compared to the ISG-targeting amiR library that it was impossible for *in vitro* or *in vivo* screening to use an inoculum of the scrambled library that included a reasonable number of virus particles containing individual sequences. Ultimately, better controls were provided by the GFP-amiR-WNV and miR-124 amiR West Nile viruses, which were present at approximately the same frequency in the p1-Vero inoculum as the tested ISG-targeting amiR-encoding viruses. In any future studies a limited number, for example ten to twenty non-targeting amiR-encoding viruses could be included at similar frequencies to the test amiRs.

6.2 *In vitro* RNAi screening revealed IFITM3 as an antiviral factor

Passaging of the ISG-amiR virus library in WT MEF and *Ifnar1*$^{-/-}$ MEF revealed selection and enrichment of IFITM3-amiR WNV. Mechanistic studies showed that amiR-mediated knockdown of *Ifitm3* improved infectivity of secreted virions and virulence in cell culture and mice respectively. The natural extension of this work would be to infect *Ifitm3*$^{-/-}$ MEF cells and mice with WT-$WNV_{NSW2011}$ and GFP-amiR WNV to determine whether a similar phenomenon would be observed in regards to infectivity. There is a substantial body of literature that suggests this will be the case. For instance, when *Ifitm3*$^{-/-}$ mice were infected with WNV were more vulnerable to virus infection characterised by increased virus accumulation in peripheral organs and CNS [311]. Similarly, when *Ifitm3*$^{-/-}$ MEF cells were infected with IAV, WNV or ZIKV, increased cytopathic effects, virus titres were observed [296, 310, 311]. Therefore, work presented here is consistent with literature that IFITM3 incorporation reduces the infectivity of virions in cells [273, 274].

IFITM3 can act to reduce viral fusion with the host cell either when it is incorporated into the virus envelope, or when it is localised in the endosomal membrane in various viral infection such as IAV and HIV [302, 341]. With the experimental strategy used here, the observed effect of the IFITM3 amiR in enhancing viral replication is presumably through lowering of virus-associated IFITM3, since when cells are first infected by virus their levels of IFITM3 will be normal. The delay in achieving knockdown of the amiR target after infection of a cell means that the difference in replication of WNV in WT *versus* *Ifitm3*$^{-/-}$ cells or mice is anticipated to be more profound than the difference in replication of control *versus* IFITM3-amiR-expressing WNV.

A second factor which may limit the effectiveness of virus-expressed amiR against ISGs is that in culture with WT cells, type I IFN will be produced early in culture and induce ISGs expression in surrounding uninfected cells. The amiR in the infecting virus then has an uphill battle overcoming the pre-induced level of the target ISG. In the *in vitro* screening done here, this problem was overcome by using *Ifnar1*$^{-/-}$ MEF. However, this also has the disadvantage that some ISGs may need type I IFN-mediated induction in order for the effect of knockdown to be seen, if their basal level in *Ifnar1*$^{-/-}$ MEF is too low for function. Consequently, a combination of screening in WT and *Ifnar1*$^{-/-}$ cells, as done here, is a good approach. This allows comparison between basal and induced level of ISG expression in terms of infection. In addition, the basal levels of ISG expression could be normalised so as to determine the exact levels of ISG expression induced.

To further validate how IFITM3 reduces virion infectivity the *Ifitm3*$^{-/-}$ cells and mice should be infectivity with GFP-amiR WNV alongside with WT-$WNV_{NSW2011}$ and determine if similar

phenomenon is observed in terms of infectivity. It is anticipated that infection with GFP-amiR WNV despite being a control virus, would result into increased cytopathic effects in cells and increased viraemia in mice.

In all three experiments IFITM3 amiR-encoding virus dominated the pool of sequenced WNV, and in all cases it was the same single amiR, although two amiRs targeting IFITM3 are present in the library. The effectiveness of the other IFITM3-amiR, and why it was not also amplified, is an important question. In future work, the second IFITM3-amiR WNV should be prepared, and examined for its ability to knockdown its target and enhance replication. Furthermore, IFITM3-amiR sequence was imported into Blastn and found to target only *mus musculus* (mouse) species. There were no other matches found for this particular IFITM3-amiR sequence. This validated that this IFITM3-amiR did not have any predicted off targets. Thus, highlighting that the shown mechanistic activities such as knockdown of ifitm3 expression in cells, generation of mature functional amiRs were indeed as a result of IFITM3-amiR WNV. However, there is need to test other IFITMs-amiR West Nile viruses to determine whether they result into similar phenomenon as IFITM3 clone 2 that was selected and enriched *in vitro*.

It would also be very insightful and enlightening to assess whether IFITM3-amiR WNV along with other *in vivo* selected and enriched amiR encoding viruses affect sfRNA production and general function of sfRNA *in vitro*. It is anticipated that all selected and enriched amiR-encoding viruses should alter sfRNA production and general function in regards to pathogenesis since the Δ15-89 site of insertion of pre-amiR hairpins is before the start of sfRNA structures as shown in Figure 1.4.

6.3 In vivo RNAi screening

In chapter 5, mice were infected with ISG-targeting amiR virus library mixed with 200 pfu of p1-Vero scrambled amiR WNV library to determine which amiR-encoding viruses were selected and enriched both in spleen and brain. This resulted in selection and enrichment of predominantly ATF3-amiR WNV in spleens, with 4/6 spleens showing ATF3-amiR WNV as the most enriched. Furthermore, *in vivo* RNAi screening in brains showed the selection and enrichment of three distinct amiR-encoding viruses, ATF3-amiR WNV, IRF7-amiR WNV and PARP11-amiR WNV in three different mouse brains. This was an unexpected observation but an assumption was made that the selected amiR-encoding viruses could be involved in similar biological pathways. In addition, the control library utilised in this screening was considered inadequate as 200 pfu of p1-Vero scrambled amiR WNV library could have been an ineffective control. Therefore to provide an adequate control for this experment p1-Vero ISG targeting amiR WNV library : p1-Vero scrambled

amiR WNV library needed to be mixed in ratio of 1:1. This was not possible since the scrambled library contained more than 6000 individual amiR variants, as the control library was very large compared to the ISG- targeting virus library. Therefore it would be enlightening to repeat this experiment while using equal ratio of p1-Vero ISG targeting amiR WNV library : p1-Vero scrambled amiR WNV library. This would determine whether the enriched amiR encoding viruses would still selected and enriched in the spleens and brains in presence of an equal amount of scrambled amiR-encoding viruses.

The gene ontology data analysis would highlight the role of first line of defence in intracellular response to West Nile virus infection. With the use of gene ontology software and databases, it would be revealed whether most of the selected and enriched amiR-encoding viruses in mouse spleens target similar biological pathways. Furthermore, gene ontology data analysis of genes targeted by amiRs that were selected and enriched in vivo and in vitro would elucidate whether IFITM3, ATF3 PARP11 and IRF7 belong to interconnected networks. Gene ontology would determine whether the enrichment of viruses encoding those amiRs that deplete host mRNAs whose products restrict virus replication enhanced amplification and dissemination of virus in mouse spleen and brains. From this analysis, further experiments geared towards determining the definite mechanisms of action of enriched genes would be designed.

Characterisation of *in vivo* selected amiR-encoding viruses revealed that all the three viruses were more infectious than control virus both *in vitro* and *in vivo*. However more mechanistic studies are still required to elucidate the role of ATF3, IRF7 and PARP11 in WNV infection. Mechanistic investigations such as using RNA sequencing (RNAseq) analysis will help identify cellular pathway(s) controlled by the selected host genes. By infecting *Atf3*$^{-/-}$, *Irf7*$^{-/-}$ and *Parp11*$^{-/-}$ cells and mice with WT-WNV cellular pathway(s) controlled by the selected host genes would be identified. As a result, more specific mechanistic studies aimed at defining precise mode of action of selected genes will be designed.

Deep sequence data were only obtained for three brains, but the fact that all three gave a different dominant amiR is of interest, and may point to some stochastic effects in viral entry into the brain. This result could be obtained if virus entry into the brain is relatively infrequent event early on in infection, and the first replicating virus in the brain has a significant "head start" and can come to dominate. If this is the case, such an effect may limit the analysis here, as there would not be a fair competition between similar numbers of starting viruses, within the brain. This would need to be assessed by infecting a larger number of mice with amiR-encoding virus libraries and analysing selection and enrichment in the brain. An approach to examining whether viral entry into the brain

is infrequent and involves minimal invading virions would be to infect mice with just 10^5 pfu of the scrambled amiR library, to see if non-targeting amiR-encoding viruses can also come to dominate.

These studies used an amiR library that was specific for ISGs, and a large proportion of the targeted genes will be antiviral. A significant fraction may be involved in limiting WNV replication. Furthermore, there may be many that have a selective advantage compared to wild type virus, but are not picked up due to the dominance of a single amiR-containing virus. The lack of IFITM3-amiR WNV enrichment after *in vivo* screening could have been influenced by tissue specificity or tropism and difference between *in vivo* and *in vitro* settings. During *in vivo* setting, each virus is faced with a robust system that ranges from host genetic factors, physical state (weight and general well being), which each virus must subdue to cause infection whereas this might not be the case during *in vitro* screening. The difference in tropism between *in vitro* and *in vivo* settings could explain the lack of enrichment of IFITM3 *in vivo*.

Indeed, when tested as individual viruses, those with amiRs targeting IFITM3, ATF3, PARP11 and IRF7 all provided some indication of improved replication *in vivo* compared to control virus. It may be that following the dynamics of virus types through the earlier stages of infection before a single virus dominates would provide a more comprehensive analysis of the antiviral target genes. For example, deep sequencing of virus from spleens from day 1 or 2 rather than day 4, would provide more insight in what happens earlier on in the spleens. Furthermore, deep sequencing viruses from blood at the time when viraemia is at its peak would expound on the trend of enrichment in the earlier stages of virus infection. However, virus titres recovered from sera are usually very low and would necessitate a number of passaging in cells such as C6/36 to be able to obtain amplicons for deep sequencing. Comparison of the early dynamics of viruses encoding ISG-targeting amiRs against a panel of control non-targeting amiRs may pick up a larger number of important anti-viral genes.

6.4 Conclusion

This project designed and generated a tool for *in vitro* and *in vivo* RNAi screening studies and subsequently identified host factors that control West Nile virus infection both *in vitro* and *in vivo.* This project was as pilot study for a bigger whole mouse genome screening using WNV termed as WNV ultramiR that is underway. For the larger project that is currently underway, the scrambled amiR-encoding virus library is an adequate control as this new amiR library referred to as ultramiR contains over 93,000 amiR sequences targeting the whole human genome. The changes that have been made is commercially purchasing a bar coded library containing all the desired amiR

sequence. This has eliminated any errors that could result from generating and preparing the library in-house. With what has been learnt from this pilot study is that with *in vivo* screening, it is not clear-cut process and therefore different individual passages and experiments need to be performed to clearly confirm that the enriched amiR-encoding viruses are indeed necessary for West Nile virus infection. Unlike in this thesis where one animal experiment was done for each *in vivo* screening. Furthermore, it would be insightful to combine a selected panel of enriched amiR encoding viruses with scrambled amiR-encoding viruses and performing an *in vivo* RNAi screen to determine whether the enriched amiR-encoding viruses are still preferentially selected to the scrambled amiR-encoding viruses. This project optimised conditions for subsequent *in vivo* screening using ultramiR WNV libraries to identify additional new host factors that control WNV virulence *in vivo*.

Reference

1. Heinz, F., et al., *Family Flaviviridae*. Virus Taxonomy, ed. E.M.e. Carstens EB. 2000, San Diego, CA, USA.: . In Regenmortel CF, Bishop DHL, . Academic Press,.
2. Maclachlan, N.J. and E.J. Dubovi, *Fenner's veterinary virology*. Fifth ed. 2017.
3. Lindenbach, B.D. and C.M. Rice, *Flaviviridae: the viruses and their replication*. 4 ed. In Fields Virology, ed. D.M. Knipe and P.M. Howley. Vol. 1. 2001, Philadelphia: Lippincott Williams & Wilkins.
4. Edgar, R.C., *MUSCLE: multiple sequence alignment with high accuracy and high throughput.* Nucleic Acids Res, 2004. **32**(5): p. 1792-7.
5. Cook, S., et al., *Molecular evolution of the insect-specific flaviviruses.* J Gen Virol, 2012. **93**(Pt 2): p. 223-34.
6. Holbrook, M.R., *Historical Perspectives on Flavivirus Research.* Viruses, 2017. **9**(5).
7. Blitvich, B.J. and A.E. Firth, *A Review of Flaviviruses that Have No Known Arthropod Vector.* Viruses, 2017. **9**(6).
8. Hartley, D.M., et al., *Effects of temperature on emergence and seasonality of West Nile virus in California.* Am J Trop Med Hyg, 2012. **86**(5): p. 884-94.
9. Lustig, Y., et al., *Surveillance and Diagnosis of West Nile Virus in the Face of Flavivirus Cross-Reactivity.* Frontiers in Microbiology, 2018. **9**.
10. Mayer, S.V., R.B. Tesh, and N. Vasilakis, *The emergence of arthropod-borne viral diseases: A global prospective on dengue, chikungunya and zika fevers.* Acta Trop, 2017. **166**: p. 155-163.
11. Musso, D. and D.J. Gubler, *Zika Virus.* Clin Microbiol Rev, 2016. **29**(3): p. 487-524.
12. Prow, N.A., et al., *The Australian Public is Still Vulnerable to Emerging Virulent Strains of West Nile Virus.* Front Public Health, 2014. **2**: p. 146.
13. Gould, E.A. and T. Solomon, *Pathogenic flaviviruses.* The Lancet, 2008. **371**(9611): p. 500-509.
14. Roby, J.A., et al., *Noncoding subgenomic flavivirus RNA: multiple functions in West Nile virus pathogenesis and modulation of host responses.* Viruses, 2014. **6**(2): p. 404-27.
15. Quicke, K.M. and M.S. Suthar, *The innate immune playbook for restricting West Nile virus infection.* Viruses, 2013. **5**(11): p. 2643-58.
16. Hanna, J.N., et al., *Two contiguous outbreaks of dengue type 2 in north Queensland.* Med J Aust, 1998. **168**(5): p. 221-5.
17. Hanna, J.N., et al., *Japanese encephalitis in north Queensland, Australia, 1998.* Med J Aust, 1999. **170**(11): p. 533-6.
18. Hanna, J.N., et al., *An outbreak of Japanese encephalitis in the Torres Strait, Australia, 1995.* Med J Aust, 1996. **165**(5): p. 256-60.
19. Johansen, C.A., et al., *Flavivirus isolations from mosquitoes collected from Saibai Island in the Torres Strait, Australia, during an incursion of Japanese encephalitis virus.* Med Vet Entomol, 2004. **18**(3): p. 281-7.
20. van den Hurk, A.F., et al., *Vector competence of Australian mosquitoes (Diptera: Culicidae) for Japanese encephalitis virus.* J Med Entomol, 2003. **40**(1): p. 82-90.
21. Pyke, A.T., et al., *The appearance of a second genotype of Japanese encephalitis virus in the Australasian region.* Am J Trop Med Hyg, 2001. **65**(6): p. 747-53.
22. Blasi, A., et al., *The phylogenetic and evolutionary history of Kokobera virus.* Asian Pac J Trop Med, 2016. **9**(10): p. 968-972.
23. Warrilow, D., et al., *Complete coding sequences of three members of the kokobera group of*

flaviviruses. Genome Announc, 2014. **2**(5).
24. Nisbet, D.J., et al., *Identification of new flaviviruses in the Kokobera virus complex.* J Gen Virol, 2005. **86**(Pt 1): p. 121-4.
25. May, F.J., et al., *Biological, antigenic and phylogenetic characterization of the flavivirus Alfuy.* J Gen Virol, 2006. **87**(Pt 2): p. 329-37.
26. Gaunt, M.W., et al., *Phylogenetic relationships of flaviviruses correlate with their epidemiology, disease association and biogeography.* J Gen Virol, 2001. **82**(Pt 8): p. 1867-76.
27. Smithburn, K.C., et al., *A Neurotropic Virus Isolated from the Blood of a Native of Uganda.* American Journal of Tropical Medicine 1940. **s1-20**(4): p. 471–472.
28. Murgue, B., et al., *West Nile in the Mediterranean basin: 1950-2000.* Ann N Y Acad Sci, 2001. **951**: p. 117-26.
29. Hayes EB, et al., *Virology, Pathology, and Clinical Manifestations of West Nile Virus Disease.* Emerg Infect Dis., 2005. **11**(8): p. 1174-9.
30. Kilpatrick, A.M., *Globalization, land use, and the invasion of West Nile virus.* Science, 2011(334): p. -323-327..
31. CDC. *CDC*. 2015; Available from: http://www.cdc.gov/westnile/statsMaps/preliminaryMapsData/.
32. Bingham, J., et al., *Experimental studies of the role of the little raven (Corvus mellori) in surveillance for West Nile virus in Australia.* Aust Vet J, 2010. **88**(6): p. 204-10.
33. Coia, G., et al., *Nucleotide and complete amino acid sequences of Kunjin virus: definitive gene order and characteristics of the virus-specified proteins.* J Gen Virol, 1988. **69 (Pt 1)**: p. 1-21.
34. Doherty, R.L., et al., *Studies of arthropod-borne virus infections in Queensland. III. Isolation and characterization of virus strains from wild-caught mosquitoes in North Queensland.* Aust J Exp Biol Med Sci, 1963. **41**: p. 17-39.
35. Hall, R.A., et al., *The ecology and epidemiology of Kunjin virus.* Curr Top Microbiol Immunol, 2002. **267**: p. 253-69.
36. Prow, N.A., *The changing epidemiology of Kunjin virus in Australia.* Int J Environ Res Public Health, 2013. **10**(12): p. 6255-72.
37. Frost, M.J., et al., *Characterization of virulent West Nile virus Kunjin strain, Australia, 2011.* Emerg Infect Dis, 2012. **18**(5): p. 792-800.
38. Mackenzie, J.S., D.J. Gubler, and L.R. Petersen, *Emerging flaviviruses: the spread and resurgence of Japanese encephalitis, West Nile and dengue viruses.* Nat Med, 2004. **10**(12 Suppl): p. S98-109.
39. Bondre, V.P., et al., *West Nile virus isolates from India: evidence for a distinct genetic lineage.* J Gen Virol, 2007. **88**(Pt 3): p. 875-84.
40. Fros, J.J., et al., *West Nile Virus: High Transmission Rate in North-Western European Mosquitoes Indicates Its Epidemic Potential and Warrants Increased Surveillance.* PLoS Negl Trop Dis, 2015. **9**(7): p. e0003956.
41. Bakonyi, T., et al., *Lineage 1 and 2 Strains of Encephalitic West Nile Virus, Central Europe.* Emerg Infect Dis, 2006. **12**(4): p. 618-23.
42. Lanciotti, R.S., et al., *Complete genome sequences and phylogenetic analysis of West Nile virus strains isolated from the United States, Europe, and the Middle East.* Virology, 2002. **298**(1): p. 96-105.
43. Hernández-Triana, L.M., et al., *Emergence of West Nile Virus Lineage 2 in Europe: A Review on the Introduction and Spread of a Mosquito-Borne Disease.* Front Public Health, 2014. **2**.
44. Berthet, F.X., et al., *Extensive nucleotide changes and deletions within the envelope glycoprotein gene of Euro-African West Nile viruses.* J Gen Virol, 1997. **78 (Pt 9)**: p. 2293-7.
45. Rappole, J.H., S.R. Derrickson, and Z. Hubalek, *Migratory birds and spread of West Nile virus in the Western Hemisphere.* Emerg Infect Dis, 2000. **6**(4): p. 319-28.

46. Tantely, M.L., et al., *Review of West Nile virus circulation and outbreak risk in Madagascar: Entomological and ornithological perspectives.* Parasite, 2016. **23**: p. 49.
47. Bakonyi, T., et al., *Novel flavivirus or new lineage of West Nile virus, central Europe.* Emerg Infect Dis, 2005. **11**(2): p. 225-31.
48. Sambri, V., et al., *West Nile virus in Europe: emergence, epidemiology, diagnosis, treatment, and prevention.* Clin Microbiol Infect, 2013. **19**(8): p. 699-704.
49. Marcantonio, M., et al., *Identifying the environmental conditions favouring West Nile Virus outbreaks in Europe.* PLoS One, 2015. **10**(3): p. e0121158.
50. Lvov, D.K., et al., *West Nile virus and other zoonotic viruses in Russia: examples of emerging-reemerging situations.* Arch Virol Suppl, 2004(18): p. 85-96.
51. Andreadis, T.G., *The contribution of Culex pipiens complex mosquitoes to transmission and persistence of West Nile virus in North America.* J Am Mosq Control Assoc, 2012. **28**(4 Suppl): p. 137-51.
52. Gomes, B., et al., *The Culex pipiens complex in continental Portugal: distribution and genetic structure.* J Am Mosq Control Assoc, 2012. **28**(4 Suppl): p. 75-80.
53. Nedry, M. and C.R. Mahon, *West Nile virus: an emerging virus in North America.* Clin Lab Sci, 2003. **16**(1): p. 43-9.
54. Colpitts, T.M., et al., *West Nile Virus: biology, transmission, and human infection.* Clin Microbiol Rev, 2012. **25**(4): p. 635-48.
55. Styer, L.M., et al., *Mosquitoes inoculate high doses of West Nile virus as they probe and feed on live hosts.* PLoS Pathog, 2007. **3**(9): p. 1262-70.
56. Sejvar, J.J., *Clinical Manifestations and Outcomes of West Nile Virus Infection.* Viruses, 2014. **6**(2): p. 606-23.
57. O'Leary, D.R., et al., *The epidemic of West Nile virus in the United States, 2002.* Vector Borne Zoonotic Dis, 2004. **4**(1): p. 61-70.
58. Petersen, L.R. and A.A. Marfin, *West Nile virus: a primer for the clinician.* Ann Intern Med, 2002. **137**(3): p. 173-9.
59. Samuel, M.A. and M.S. Diamond, *Pathogenesis of West Nile Virus infection: a balance between virulence, innate and adaptive immunity, and viral evasion.* J Virol, 2006. **80**(19): p. 9349-60.
60. Beasley, D.W., et al., *Mouse neuroinvasive phenotype of West Nile virus strains varies depending upon virus genotype.* Virology, 2002. **296**(1): p. 17-23.
61. Chan, K.W., et al., *Animal models for studying dengue pathogenesis and therapy.* Antiviral Res, 2015. **123**: p. 5-14.
62. Suen, W.W., et al., *Mechanism of West Nile virus neuroinvasion: a critical appraisal.* Viruses, 2014. **6**(7): p. 2796-825.
63. Suthar, M.S. and B. Pulendran, *Systems analysis of West Nile virus infection.* Curr Opin Virol, 2014. **6**: p. 70-5.
64. Suthar, M.S., M.S. Diamond, and M. Gale, Jr., *West Nile virus infection and immunity.* Nat Rev Microbiol, 2013. **11**(2): p. 115-28.
65. Winkelmann, E.R., H. Luo, and T. Wang, *West Nile Virus Infection in the Central Nervous System.* F1000Res, 2016. **5**.
66. Lim, S.M., et al., *West Nile virus: immunity and pathogenesis.* Viruses, 2011. **3**(6): p. 811-28.
67. Byrne, S.N., et al., *Interleukin-1beta but not tumor necrosis factor is involved in West Nile virus-induced Langerhans cell migration from the skin in C57BL/6 mice.* J Invest Dermatol, 2001. **117**(3): p. 702-9.
68. Cho, H. and M.S. Diamond, *Immune responses to West Nile virus infection in the central nervous system.* Viruses, 2012. **4**(12): p. 3812-30.
69. Arjona, A., et al., *Innate immune control of West Nile virus infection.* Cell Microbiol, 2011. **13**(11): p. 1648-58.
70. Bai, F., et al., *A paradoxical role for neutrophils in the pathogenesis of West Nile virus.* J Infect Dis, 2010. **202**(12): p. 1804-12.

71. Samuel, M.A., et al., *PKR and RNase L contribute to protection against lethal West Nile Virus infection by controlling early viral spread in the periphery and replication in neurons.* J Virol, 2006. **80**(14): p. 7009-19.
72. Beasley, D.W., et al., *Envelope protein glycosylation status influences mouse neuroinvasion phenotype of genetic lineage 1 West Nile virus strains.* J Virol, 2005. **79**(13): p. 8339-47.
73. Verma, S., et al., *West Nile virus infection modulates human brain microvascular endothelial cells tight junction proteins and cell adhesion molecules: Transmigration across the in vitro blood-brain barrier.* Virology, 2009. **385**(2): p. 425-33.
74. Hanna, S.L., et al., *N-linked glycosylation of west nile virus envelope proteins influences particle assembly and infectivity.* J Virol, 2005. **79**(21): p. 13262-74.
75. Diamond, M.S., et al., *Innate and adaptive immune responses determine protection against disseminated infection by West Nile encephalitis virus.* Viral Immunology, 2003. **16**: p. 259–278.
76. Roe, K., et al., *West Nile virus-induced disruption of the blood-brain barrier in mice is characterized by the degradation of the junctional complex proteins and increase in multiple matrix metalloproteinases.* J Gen Virol, 2012. **93**(Pt 6): p. 1193-203.
77. Verma, S., et al., *Reversal of West Nile virus-induced blood-brain barrier disruption and tight junction proteins degradation by matrix metalloproteinases inhibitor.* Virology, 2010. **397**(1): p. 130-8.
78. Diamond, M.S., et al., *B cells and antibody play critical roles in the immediate defense of disseminated infection by West Nile encephalitis virus.* J Virol, 2003. **77**(4): p. 2578-86.
79. Xiao, S.Y., et al., *West Nile virus infection in the golden hamster (Mesocricetus auratus): a model for West Nile encephalitis.* Emerg Infect Dis, 2001. **7**(4): p. 714-21.
80. Kobayashi, S., et al., *Accumulation of ubiquitinated proteins is related to West Nile virus-induced neuronal apoptosis.* Neuropathology, 2012. **32**(4): p. 398-405.
81. Samuel, M.A., J.D. Morrey, and M.S. Diamond, *Caspase 3-dependent cell death of neurons contributes to the pathogenesis of West Nile virus encephalitis.* J Virol, 2007. **81**(6): p. 2614-23.
82. Apte-Sengupta, S., D. Sirohi, and R.J. Kuhn, *Coupling of replication and assembly in flaviviruses.* Curr Opin Virol, 2014. **9**: p. 134-42.
83. Kimura, T. and A. Ohyama, *Association between the pH-dependent conformational change of West Nile flavivirus E protein and virus-mediated membrane fusion.* J Gen Virol, 1988. **69 (Pt 6)**: p. 1247-54.
84. Mazeaud, C., W. Freppel, and L. Chatel-Chaix, *The Multiples Fates of the Flavivirus RNA Genome During Pathogenesis.* Front Genet, 2018. **9**: p. 595.
85. Bollati M, Alvarez K, and e.a. Assenberg R, *Structure and functionality in flavivirus NS-proteins: Perspectives for drug design* Antiviral Research, 2010. **87**(2): p. 125-148.
86. Mackenzie, J.M., et al., *Subcellular Localization and Some Biochemical Properties of the Flavivirus Kunjin Nonstructural Proteins NS2A and NS4A.* Virology, 1998. **245**: p. 203-215.
87. Westaway, E.G., J.M. Mackenzie, and A.A. Khromykh, *Kunjin RNA replication and applications of Kunjin replicons.* Adv Virus Res, 2003. **59**: p. 99-140.
88. Westaway, E.G., A.A. Khromykh, and J.M. Mackenzie, *Nascent flavivirus RNA colocalized in situ with double-stranded RNA in stable replication complexes.* Virology, 1999. **258**(1): p. 108-17.
89. Setoh, Y.X., et al., *Identification of residues in West Nile virus pre-membrane protein that influence viral particle secretion and virulence.* J Gen Virol, 2012. **93**(Pt 9): p. 1965-75.
90. Brinton, M.A., *Replication cycle and molecular biology of the West Nile virus.* Viruses, 2014. **6**(1): p. 13-53.
91. Valiakos, G., et al., *West Nile Virus: Basic Principles, Replication Mechanism, Immune Response and Important Genetic Determinants of Virulence*. Viral Replication. 2013.
92. Colpitts, T.M., *West Nile Virus Methods and Protocols* Methods in Molecular Biology, 1435 ed. 2016 New York, NY: : Springer New York : Imprint: Humana Press. M.M.M.

93. Dokland, T., et al., *West Nile virus core protein; tetramer structure and ribbon formation.* Structure, 2004. **12**(7): p. 1157-63.
94. Jones, C.T., et al., *Flavivirus capsid is a dimeric alpha-helical protein.* J Virol, 2003. **77**(12): p. 7143-9.
95. Khromykh, A.A. and E.G. Westaway, *RNA binding properties of core protein of the flavivirus Kunjin.* Arch Virol, 1996. **141**(3-4): p. 685-99.
96. Zhang, Y., et al., *Structure of immature West Nile virus.* J Virol, 2007. **81**(11): p. 6141-5.
97. Diamond, M.S., et al., *The host immunologic response to West Nile encephalitis virus.* . Front Biosci 2009. **14**: p. 3024–3034.
98. Macdonald, J., et al., *NS1 protein secretion during the acute phase of West Nile virus infection.* J Virol, 2005. **79**(22): p. 13924-33.
99. Firth, A.E. and J.F. Atkins, *A conserved predicted pseudoknot in the NS2A-encoding sequence of West Nile and Japanese encephalitis flaviviruses suggests NS1' may derive from ribosomal frameshifting.* Virol J, 2009. **6**: p. 14.
100. Ye, Q., et al., *A single nucleotide mutation in NS2A of Japanese encephalitis-live vaccine virus (SA14-14-2) ablates NS1' formation and contributes to attenuation.* J Gen Virol, 2012. **93**(Pt 9): p. 1959-64.
101. Rastogi, M., N. Sharma, and S.K. Singh, *Flavivirus NS1: a multifaceted enigmatic viral protein.* Virol J, 2016. **13**: p. 131.
102. Liu, W.J., et al., *Inhibition of interferon signaling by the New York 99 strain and Kunjin subtype of West Nile virus involves blockage of STAT1 and STAT2 activation by nonstructural proteins.* J Virol, 2005. **79**(3): p. 1934-42.
103. Leung, J.Y., et al., *Role of nonstructural protein NS2A in flavivirus assembly.* J Virol, 2008. **82**(10): p. 4731-41.
104. Rossi, S.L., et al., *Mutations in West Nile virus nonstructural proteins that facilitate replicon persistence in vitro attenuate virus replication in vitro and in vivo.* Virology, 2007. **364**(1): p. 184-95.
105. Chappell, K.J., et al., *West Nile Virus NS2B/NS3 protease as an antiviral target.* Curr Med Chem, 2008. **15**(27): p. 2771-84.
106. Chappell, K.J., et al., *Mutagenesis of the West Nile virus NS2B cofactor domain reveals two regions essential for protease activity.* J Gen Virol, 2008. **89**(Pt 4): p. 1010-4.
107. Droll, D.A., H.M. Krishna Murthy, and T.J. Chambers, *Yellow fever virus NS2B-NS3 protease: charged-to-alanine mutagenesis and deletion analysis define regions important for protease complex formation and function.* Virology, 2000. **275**(2): p. 335-47.
108. Yusof, R., et al., *Purified NS2B/NS3 serine protease of dengue virus type 2 exhibits cofactor NS2B dependence for cleavage of substrates with dibasic amino acids in vitro.* J Biol Chem, 2000. **275**(14): p. 9963-9.
109. Setoh, Y.X., et al., *Helicase Domain of West Nile Virus NS3 Protein Plays a Role in Inhibition of Type I Interferon Signalling.* Viruses, 2017. **9**(11).
110. Evans, J.D. and C. Seeger, *Differential effects of mutations in NS4B on West Nile virus replication and inhibition of interferon signaling.* J Virol, 2007. **81**(21): p. 11809-16.
111. Shiryaev, S.A., et al., *NS4A regulates the ATPase activity of the NS3 helicase: a novel cofactor role of the non-structural protein NS4A from West Nile virus.* J Gen Virol, 2009. **90**(Pt 9): p. 2081-5.
112. Davidson, A.D., *Chapter 2. New insights into flavivirus nonstructural protein 5.* Adv Virus Res, 2009. **74**: p. 41-101.
113. Li, X.D., et al., *The interface between methyltransferase and polymerase of NS5 is essential for flavivirus replication.* PLoS Negl Trop Dis, 2014. **8**(5): p. e2891.
114. Zhou, Y., et al., *Structure and function of flavivirus NS5 methyltransferase.* J Virol, 2007. **81**(8): p. 3891-903.
115. Dong, H., B. Zhang, and P.Y. Shi, *Terminal structures of West Nile virus genomic RNA and their interactions with viral NS5 protein.* Virology, 2008. **381**(1): p. 123-35.

116. Klema, V.J., R. Padmanabhan, and K.H. Choi, *Flaviviral Replication Complex: Coordination between RNA Synthesis and 51-RNA Capping.* Viruses, 2015. **7**(8): p. 4640-56.
117. Issur, M., et al., *The flavivirus NS5 protein is a true RNA guanylyltransferase that catalyzes a two-step reaction to form the RNA cap structure.* Rna, 2009. **15**(12): p. 2340-50.
118. Egloff, M.P., et al., *An RNA cap (nucleoside-2'-O-)-methyltransferase in the flavivirus RNA polymerase NS5: crystal structure and functional characterization.* Embo j, 2002. **21**(11): p. 2757-68.
119. Laurent-Rolle, M., et al., *The NS5 protein of the virulent West Nile virus NY99 strain is a potent antagonist of type I interferon-mediated JAK-STAT signaling.* J Virol, 2010. **84**(7): p. 3503-15.
120. Best, S.M., et al., *Inhibition of interferon-stimulated JAK-STAT signaling by a tick-borne flavivirus and identification of NS5 as an interferon antagonist.* J Virol, 2005. **79**(20): p. 12828-39.
121. Wengler, G. and G. Wengler, *Terminal sequences of the genome and replicative-from RNA of the flavivirus West Nile virus: absence of poly(A) and possible role in RNA replication.* Virology, 1981. **113**(2): p. 544-55.
122. Pijlman, G.P., et al., *A highly structured, nuclease-resistant, noncoding RNA produced by flaviviruses is required for pathogenicity.* Cell Host Microbe, 2008. **4**(6): p. 579-91.
123. Roby, J.A., A. Funk, and A.A. Khromykh, *Flavivirus replication and assembly*. Molecular Virology and Control of Flaviviruses., ed. I.S.P. (ed.). 2012,

Norfolk, United Kingdom: Caister Academic Press.
124. Ng, W., et al., *The 5′ and 3′ Untranslated Regions of the Flaviviral Genome.* Viruses, 2017. **9**(6).
125. Thurner, C., et al., *Conserved RNA secondary structures in Flaviviridae genomes.* J Gen Virol, 2004. **85**(Pt 5): p. 1113-24.
126. Bidet, K. and M.A. Garcia-Blanco, *Flaviviral RNAs: weapons and targets in the war between virus and host.* Biochem J, 2014. **462**(2): p. 215-30.
127. Proutski, V., et al., *Biological consequences of deletions within the 3'-untranslated region of flaviviruses may be due to rearrangements of RNA secondary structure.* Virus Res, 1999. **64**(2): p. 107-23.
128. Akiyama, B.M., et al., *Zika virus produces noncoding RNAs using a multi-pseudoknot structure that confounds a cellular exonuclease.* Science, 2016. **354**(6316): p. 1148-1152.
129. MacFadden, A., et al., *Mechanism and structural diversity of exoribonuclease-resistant RNA structures in flaviviral RNAs.* Nat Commun, 2018. **9**(1): p. 119.
130. Chapman, E.G., et al., *The structural basis of pathogenic subgenomic flavivirus RNA (sfRNA) production.* Science, 2014. **344**(6181): p. 307-10.
131. Fernandez-Garcia, M.D., et al., *Pathogenesis of flavivirus infections: using and abusing the host cell.* Cell Host Microbe, 2009. **5**(4): p. 318-28.
132. Slonchak, A. and A.A. Khromykh, *Subgenomic flaviviral RNAs: What do we know after the first decade of research.* Antiviral Res, 2018.
133. Moon, S.L., et al., *Flavivirus sfRNA suppresses antiviral RNA interference in cultured cells and mosquitoes and directly interacts with the RNAi machinery.* Virology, 2015. **485**: p. 322-9.
134. Zambon, R.A., V.N. Vakharia, and L.P. Wu, *RNAi is an antiviral immune response against a dsRNA virus in Drosophila melanogaster.* Cell Microbiol, 2006. **8**(5): p. 880-9.
135. Pijlman, G.P., *Flavivirus RNAi suppression: decoding non-coding RNA.* Curr Opin Virol, 2014. **7**: p. 55-60.
136. Slonchak, A., et al., *Expression of mosquito microRNA Aae-miR-2940-5p is downregulated in response to West Nile virus infection to restrict viral replication.* J Virol, 2014. **88**(15): p. 8457-67.
137. Hussain, M., et al., *West Nile virus encodes a microRNA-like small RNA in the 3′ untranslated region which up-regulates GATA4 mRNA and facilitates virus replication in mosquito cells.*

Nucleic Acids Res, 2012. **40**(5): p. 2210-23.
138. Lin, B., et al., *Silencing Early Viral Replication in Macrophages and Dendritic Cells Effectively Suppresses Flavivirus Encephalitis.* PLoS ONE, 2011. **6**(3).
139. Qi, W.B., et al., *Effective inhibition of Japanese encephalitis virus replication by small interfering RNAs targeting the NS5 gene.* Virus Res, 2008. **132**(1-2): p. 145-51.
140. Bartel, D.P., *MicroRNAs: target recognition and regulatory functions.* Cell, 2009. **136**(2): p. 215-33.
141. Roberts, T.C., *The MicroRNA Biology of the Mammalian Nucleus.* Mol Ther Nucleic Acids, 2014. **3**: p. e188.
142. Gurtan, A.M. and P.A. Sharp, *The role of miRNAs in regulating gene expression networks.* J Mol Biol, 2013. **425**(19): p. 3582-600.
143. Lee, Y., et al., *The nuclear RNase III Drosha initiates microRNA processing.* Nature, 2003. **425**(6956): p. 415-9.
144. Lund, E., et al., *Nuclear export of microRNA precursors.* Science, 2004. **303**(5654): p. 95-8.
145. Bohnsack, M.T., K. Czaplinski, and D. Gorlich, *Exportin 5 is a RanGTP-dependent dsRNA-binding protein that mediates nuclear export of pre-miRNAs.* Rna, 2004. **10**(2): p. 185-91.
146. Bernstein, E., et al., *Role for a bidentate ribonuclease in the initiation step of RNA interference.* Nature, 2001. **409**(6818): p. 363-6.
147. Wang, Y., et al., *Nucleation, propagation and cleavage of target RNAs in Ago silencing complexes.* Nature, 2009. **461**(7265): p. 754-61.
148. Meijer, H.A., E.M. Smith, and M. Bushell, *Regulation of miRNA strand selection: follow the leader?* Biochem Soc Trans, 2014. **42**(4): p. 1135-40.
149. Kim, V.N., J. Han, and M.C. Siomi, *Biogenesis of small RNAs in animals.* Nat Rev Mol Cell Biol, 2009. **10**(2): p. 126-39.
150. Varble, A., et al., *Engineered RNA viral synthesis of microRNAs.* Proc Natl Acad Sci U S A, 2010. **107**(25): p. 11519-24.
151. Varble, A., et al., *An in vivo RNAi screening approach to identify host determinants of virus replication.* Cell Host Microbe, 2013. **14**(3): p. 346-56.
152. Shapiro, J.S., et al., *Evidence for a cytoplasmic microprocessor of pri-miRNAs.* RNA, 2012. **18**(7): p. 1338-46.
153. Rouha, H., C. Thurner, and C.W. Mandl, *Functional microRNA generated from a cytoplasmic RNA virus.* Nucleic Acids Res, 2010. **38**(22): p. 8328-37.
154. tenOever, B.R., *RNA viruses and the host microRNA machinery.* Nat Rev Microbiol, 2013. **11**(3): p. 169-80.
155. Barnes, D., et al., *Harnessing endogenous miRNAs to control virus tissue tropism as a strategy for developing attenuated virus vaccines.* Cell Host Microbe, 2008. **4**(3): p. 239-48.
156. Shan, C., et al., *A live-attenuated Zika virus vaccine candidate induces sterilizing immunity in mouse models.* Nat Med, 2017.
157. Heiss, B.L., et al., *MicroRNA targeting of neurotropic flavivirus: effective control of virus escape and reversion to neurovirulent phenotype.* J Virol, 2012. **86**(10): p. 5647-59.
158. Teterina, N.L., et al., *Silencing of neurotropic flavivirus replication in the central nervous system by combining multiple microRNA target insertions in two distinct viral genome regions.* Virology, 2014. **456-457**: p. 247-58.
159. Tsetsarkin, K.A., et al., *Dual miRNA targeting restricts host range and attenuates neurovirulence of flaviviruses.* PLoS Pathog, 2015. **11**(4): p. e1004852.
160. Asgari, S., *Role of microRNAs in arbovirus/vector interactions.* Viruses, 2014. **6**(9): p. 3514-34.
161. Kelly, E.J., et al., *Engineering microRNA responsiveness to decrease virus pathogenicity.* Nat Med, 2008. **14**(11): p. 1278-83.
162. Tabernero, J., et al., *First-in-humans trial of an RNA interference therapeutic targeting VEGF and KSP in cancer patients with liver involvement.* Cancer Discov, 2013. **3**(4): p. 406-17.
163. Schultheis, B., et al., *First-in-human phase I study of the liposomal RNA interference*

therapeutic Atu027 in patients with advanced solid tumors. J Clin Oncol, 2014. **32**(36): p. 4141-8.
164. Bader, A.G., et al., *Developing therapeutic microRNAs for cancer.* Gene Ther, 2011. **18**(12): p. 1121-6.
165. DeVincenzo, J., et al., *A randomized, double-blind, placebo-controlled study of an RNAi-based therapy directed against respiratory syncytial virus.* Proc Natl Acad Sci U S A, 2010. **107**(19): p. 8800-5.
166. Chandra, P.K., et al., *Inhibition of hepatitis C virus replication by intracellular delivery of multiple siRNAs by nanosomes.* Mol Ther, 2012. **20**(9): p. 1724-36.
167. Sendi, H., et al., *MiR-122 decreases HCV entry into hepatocytes through binding to the 3' UTR of OCLN mRNA.* Liver Int, 2015. **35**(4): p. 1315-23.
168. Behlke, M.A., *Progress towards in vivo use of siRNAs.* Mol Ther, 2006. **13**(4): p. 644-70.
169. Takeuchi, O. and S. Akira, *Innate immunity to virus infection.* Immunological reviews, 2009(227): p. 75-86.
170. Kawai, T. and S. Akira, *The roles of TLRs, RLRs and NLRs in pathogen recognition.* Int Immunol, 2009. **21**(4): p. 317-37.
171. Jin, M.S. and J.O. Lee, *Structures of the toll-like receptor family and its ligand complexes.* Immunity, 2008. **29**(2): p. 182-91.
172. Botos, I., D.M. Segal, and D.R. Davies, *The structural biology of Toll-like receptors.* Structure, 2011. **19**(4): p. 447-59.
173. Kawasaki, T. and T. Kawai, *Toll-like receptor signaling pathways.* Frontiers in immunology, 2014. **5**: p. 461-461.
174. Kawasaki, T. and T. Kawai, *Toll-Like Receptor Signaling Pathways.* Front Immunol, 2014. **5**.
175. Kawai, T. and S. Akira, *The role of pattern-recognition receptors in innate immunity: update on Toll-like receptors.* Nat Immunol, 2010. **11**(5): p. 373-84.
176. Celhar, T., R. Magalhaes, and A.M. Fairhurst, *TLR7 and TLR9 in SLE: when sensing self goes wrong.* Immunol Res, 2012. **53**(1-3): p. 58-77.
177. O'Neill, L.A., D. Golenbock, and A.G. Bowie, *The history of Toll-like receptors - redefining innate immunity.* Nat Rev Immunol, 2013. **13**(6): p. 453-60.
178. Alexopoulou, L., et al., *Recognition of double-stranded RNA and activation of NF-kappaB by Toll-like receptor 3.* Nature, 2001. **413**(6857): p. 732-8.
179. O'Neill, L.A. and A.G. Bowie, *The family of five: TIR-domain-containing adaptors in Toll-like receptor signalling.* Nat Rev Immunol, 2007. **7**(5): p. 353-64.
180. Akira, S. and K. Takeda, *Toll-like receptor signalling.* Nat Rev Immunol, 2004. **4**(7): p. 499-511.
181. Peteranderl, C. and S. Herold, *The Impact of the Interferon/TNF-Related Apoptosis-Inducing Ligand Signaling Axis on Disease Progression in Respiratory Viral Infection and Beyond.* Front Immunol, 2017. **8**: p. 313.
182. Verma, R. and K. Bharti, *Toll like receptor 3 and viral infections of nervous system.* J Neurol Sci, 2017. **372**: p. 40-48.
183. Liu, L., et al., *Structural basis of toll-like receptor 3 signaling with double-stranded RNA.* Science, 2008. **320**(5874): p. 379-81.
184. Daffis, S., et al., *Toll-like receptor 3 has a protective role against West Nile virus infection.* J Virol, 2008. **82**(21): p. 10349-58.
185. Wang, T., et al., *Toll-like receptor 3 mediates West Nile virus entry into the brain causing lethal encephalitis.* Nature Medicine, 2004. **10**(12): p. 1366-1373.
186. Mogensen, T.H., *Pathogen Recognition and Inflammatory Signaling in Innate Immune Defenses.* Clin Microbiol Rev, 2009. **22**(2): p. 240-73.
187. Welte, T., et al., *Toll-like receptor 7-induced immune response to cutaneous West Nile virus infection.* J Gen Virol, 2009. **90**(Pt 11): p. 2660-8.
188. Szretter, K.J., et al., *The innate immune adaptor molecule MyD88 restricts West Nile virus replication and spread in neurons of the central nervous system.* J Virol, 2010. **84**(23): p.

12125-38.
189. Sabouri, A.H., et al., *TLR signaling controls lethal encephalitis in WNV-infected brain.* Brain Res, 2014. **1574**: p. 84-95.
190. Dixit, E. and J.C. Kagan, *Intracellular pathogen detection by RIG-I-like receptors.* Adv Immunol, 2013. **117**: p. 99-125.
191. Errett, J.S., et al., *The essential, nonredundant roles of RIG-I and MDA5 in detecting and controlling West Nile virus infection.* J Virol, 2013. **87**(21): p. 11416-25.
192. Chan, Y.K. and M.U. Gack, *Viral evasion of intracellular DNA and RNA sensing.* Nat Rev Microbiol, 2016. **14**(6): p. 360-73.
193. Gack, M.U., *Mechanisms of RIG-I-Like Receptor Activation and Manipulation by Viral Pathogens.* Journal of Virology, 2014. **88**(10): p. 5213-5216.
194. Fredericksen, B.L., et al., *Establishment and maintenance of the innate antiviral response to West Nile Virus involves both RIG-I and MDA5 signaling through IPS-1.* J Virol, 2008. **82**(2): p. 609-16.
195. Loo, Y.M. and M. Gale, Jr., *Immune signaling by RIG-I-like receptors.* Immunity, 2011. **34**(5): p. 680-92.
196. Schlee, M., *Master sensors of pathogenic RNA - RIG-I like receptors.* Immunobiology, 2013. **218**(11): p. 1322-35.
197. Gack, M.U., *Mechanisms of RIG-I-like receptor activation and manipulation by viral pathogens.* J Virol, 2014. **88**(10): p. 5213-6.
198. Gack, M.U., et al., *TRIM25 RING-finger E3 ubiquitin ligase is essential for RIG-I-mediated antiviral activity.* Nature, 2007. **446**(7138): p. 916-920.
199. Wang, P., et al., *Caspase-12 controls West Nile virus infection via the viral RNA receptor RIG-I.* Nat Immunol, 2010. **11**(10): p. 912-9.
200. Liu, H.M., et al., *The mitochondrial targeting chaperone 14-3-3epsilon regulates a RIG-I translocon that mediates membrane association and innate antiviral immunity.* Cell Host Microbe, 2012. **11**(5): p. 528-37.
201. Jiang, X., et al., *Ubiquitin-induced oligomerization of the RNA sensors RIG-I and MDA5 activates antiviral innate immune response.* Immunity, 2012. **36**(6): p. 959-73.
202. Suthar, M.S., et al., *IPS-1 is essential for the control of West Nile virus infection and immunity.* PLoS Pathog, 2010. **6**(2): p. e1000757.
203. Loo, Y.M., et al., *Distinct RIG-I and MDA5 signaling by RNA viruses in innate immunity.* J Virol, 2008. **82**(1): p. 335-45.
204. Tyler, K.L., *Current developments in understanding of West Nile virus central nervous system disease.* Curr Opin Neurol, 2014. **27**(3): p. 342-8.
205. Lazear, H.M., et al., *Pattern recognition receptor MDA5 modulates CD8+ T cell-dependent clearance of West Nile virus from the central nervous system.* J Virol, 2013. **87**(21): p. 11401-15.
206. Paun, A. and P.M. Pitha, *The innate antiviral response: new insights into a continuing story.* Adv Virus Res, 2007. **69**: p. 1-66.
207. Finter, N.B., *The classification and biological functions of the interferons. A review.* J Hepatol, 1986. **3 Suppl 2**: p. S157-60.
208. Hoffmann, H.H., W.M. Schneider, and C.M. Rice, *Interferons and viruses: an evolutionary arms race of molecular interactions.* Trends Immunol, 2015. **36**(3): p. 124-38.
209. Jiang, D., et al., *Identification of five interferon-induced cellular proteins that inhibit west nile virus and dengue virus infections.* J Virol, 2010. **84**(16): p. 8332-41.
210. Daffis, S., et al., *Interferon regulatory factor IRF-7 induces the antiviral alpha interferon response and protects against lethal West Nile virus infection.* J Virol, 2008. **82**(17): p. 8465-75.
211. Samuel, M.A. and M.S. Diamond, *Alpha/beta interferon protects against lethal West Nile virus infection by restricting cellular tropism and enhancing neuronal survival.* J Virol, 2005. **79**(21): p. 13350-61.

212. Ivashkiv, L.B. and L.T. Donlin, *Regulation of type I interferon responses.* Nat Rev Immunol, 2014. **14**(1): p. 36-49.
213. Lazear, H.M., et al., *Beta interferon controls West Nile virus infection and pathogenesis in mice.* J Virol, 2011. **85**(14): p. 7186-94.
214. Shrestha, B., et al., *Gamma interferon plays a crucial early antiviral role in protection against West Nile virus infection.* J Virol, 2006. **80**(11): p. 5338-48.
215. Lazear, H.M., et al., *Interferon-λ restricts West Nile virus neuroinvasion by tightening the blood-brain barrier.* Sci Transl Med, 2015. **7**(284): p. 284ra59.
216. Schneider, W.M., M.D. Chevillotte, and C.M. Rice, *Interferon-stimulated genes: a complex web of host defenses.* Annu Rev Immunol, 2014. **32**: p. 513-45.
217. Lazear, H.M., J.W. Schoggins, and M.S. Diamond, *Shared and Distinct Functions of Type I and Type III Interferons.* Immunity, 2019. **50**(4): p. 907-923.
218. Schoggins, J.W. and C.M. Rice, *Interferon-stimulated genes and their antiviral effector functions.* Curr Opin Virol, 2011. **1**(6): p. 519-25.
219. Guo, J.T., J. Hayashi, and C. Seeger, *West Nile virus inhibits the signal transduction pathway of alpha interferon.* J Virol, 2005. **79**(3): p. 1343-50.
220. Evans, J.D., et al., *West Nile virus infection induces depletion of IFNAR1 protein levels.* Viral Immunol, 2011. **24**(4): p. 253-63.
221. Liu, W.J., et al., *A single amino acid substitution in the West Nile virus nonstructural protein NS2A disables its ability to inhibit alpha/beta interferon induction and attenuates virus virulence in mice.* J Virol, 2006. **80**(5): p. 2396-404.
222. Arjona, A., et al., *West Nile virus envelope protein inhibits dsRNA-induced innate immune responses.* J Immunol, 2007. **179**(12): p. 8403-9.
223. Zhang, H.L., et al., *West Nile Virus NS1 Antagonizes Interferon Beta Production by Targeting RIG-I and MDA5.* J Virol, 2017. **91**(18).
224. Daffis, S., et al., *2'-O methylation of the viral mRNA cap evades host restriction by IFIT family members.* Nature, 2010. **468**(7322): p. 452-6.
225. Szretter, K.J., et al., *2'-O methylation of the viral mRNA cap by West Nile virus evades ifit1-dependent and -independent mechanisms of host restriction in vivo.* PLoS Pathog, 2012. **8**(5): p. e1002698.
226. Mertens, E., et al., *Viral determinants in the NS3 helicase and 2K peptide that promote West Nile virus resistance to antiviral action of 2',5'-oligoadenylate synthetase 1b.* Virology, 2010. **399**(1): p. 176-185.
227. Hoenen, A., et al., *West Nile virus-induced cytoplasmic membrane structures provide partial protection against the interferon-induced antiviral MxA protein.* J Gen Virol, 2007. **88**(Pt 11): p. 3013-7.
228. Gack, M.U. and M.S. Diamond, *Innate immune escape by Dengue and West Nile viruses.* Curr Opin Virol, 2016. **20**: p. 119-128.
229. Krishnan, M.N., et al., *RNA interference screen for human genes associated with West Nile virus infection.* Nature, 2008. **455**(7210): p. 242-5.
230. Li, J., et al., *A short hairpin RNA screen of interferon-stimulated genes identifies a novel negative regulator of the cellular antiviral response.* MBio, 2013. **4**(3): p. e00385-13.
231. Qian, F., et al., *Identification of genes critical for resistance to infection by West Nile virus using RNA-Seq analysis.* Viruses, 2013. **5**(7): p. 1664-81.
232. Diamond, M.S. and M. Farzan, *The broad-spectrum antiviral functions of IFIT and IFITM proteins.* Nat Rev Immunol, 2013. **13**(1): p. 46-57.
233. Lazear, H.M., et al., *IRF-3, IRF-5, and IRF-7 coordinately regulate the type I IFN response in myeloid dendritic cells downstream of MAVS signaling.* PLoS Pathog, 2013. **9**(1): p. e1003118.
234. You, F., et al., *ELF4 is critical for induction of type I interferon and the host antiviral response.* Nat Immunol, 2013. **14**(12): p. 1237-46.
235. Yasunaga, A., et al., *Genome-wide RNAi screen identifies broadly-acting host factors that*

inhibit arbovirus infection. PLoS Pathog, 2014. **10**(2): p. e1003914.
236. Edmonds, J., et al., *A novel bacterium-free method for generation of flavivirus infectious DNA by circular polymerase extension reaction allows accurate recapitulation of viral heterogeneity.* J Virol, 2013. **87**(4): p. 2367-72.
237. Setoh, Y.X., et al., *Systematic analysis of viral genes responsible for differential virulence between American and Australian West Nile virus strains.* J Gen Virol, 2015. **96**(Pt 6): p. 1297-308.
238. Quicke, K.M., M.S. Diamond, and M.S. Suthar, *Negative regulators of the RIG-I-like receptor signaling pathway.* Eur J Immunol, 2017. **47**(4): p. 615-628.
239. Zhao, J., et al., *MAVS Expressed by Hematopoietic Cells Is Critical for Control of West Nile Virus Infection and Pathogenesis.* J Virol, 2016. **90**(16): p. 7098-7108.
240. Luo, H., et al., *MAVS Is Essential for Primary CD4(+) T Cell Immunity but Not for Recall T Cell Responses following an Attenuated West Nile Virus Infection.* J Virol, 2017. **91**(6).
241. Karlas, A., et al., *Genome-wide RNAi screen identifies human host factors crucial for influenza virus replication.* Nature, 2010. **463**(7282): p. 818-22.
242. Hirsch, A.J., *The use of RNAi-based screens to identify host proteins involved in viral replication.* Future Microbiol, 2010. **5**(2): p. 303-11.
243. Sessions, O.M., et al., *Discovery of insect and human dengue virus host factors.* Nature, 2009. **458**(7241): p. 1047-50.
244. Smith, J.L., et al., *A microRNA screen identifies the Wnt signaling pathway as a regulator of the interferon response during flavivirus infection.* Journal of Virology, 2017: p. JVI.02388-16.
245. Schoggins, J.W., et al., *A diverse range of gene products are effectors of the type I interferon antiviral response.* Nature, 2011. **472**(7344): p. 481-5.
246. Petrova, E., et al., *Uncovering Flavivirus Host Dependency Factors through a Genome-Wide Gain-of-Function Screen.* Viruses, 2019. **11**(1).
247. Campos, R.K., et al., *RPLP1 and RPLP2 Are Essential Flavivirus Host Factors That Promote Early Viral Protein Accumulation.* J Virol, 2017. **91**(4).
248. Chen, Z., et al., *MicroRNA-33a-5p Modulates Japanese Encephalitis Virus Replication by Targeting Eukaryotic Translation Elongation Factor 1A1.* J Virol, 2016. **90**(7): p. 3722-34.
249. Lazear, H.M. and M.S. Diamond, *New insights into innate immune restriction of West Nile virus infection.* Curr Opin Virol, 2015. **11**: p. 1-6.
250. Ha, M. and V.N. Kim, *Regulation of microRNA biogenesis.* Nat Rev Mol Cell Biol, 2014. **15**(8): p. 509-24.
251. Haasnoot, J., E.M. Westerhout, and B. Berkhout, *RNA interference against viruses: strike and counterstrike.* Nat Biotechnol, 2007. **25**(12): p. 1435-43.
252. Crotty, S. and M.E. Pipkin, *In vivo RNAi screens: concepts and applications.* Trends Immunol, 2015. **36**(5): p. 315-22.
253. Ma, H., et al., *A CRISPR-Based Screen Identifies Genes Essential for West-Nile-Virus-Induced Cell Death.* Cell Rep, 2015. **12**(4): p. 673-83.
254. Schoggins, J.W., et al., *Pan-viral specificity of IFN-induced genes reveals new roles for cGAS in innate immunity.* Nature, 2014. **505**(7485): p. 691-5.
255. Wang, X., et al., *Sindbis Virus Can Exploit a Host Antiviral Protein To Evade Immune Surveillance.* J Virol, 2016. **90**(22): p. 10247-10258.
256. Kozaki, T., et al., *Role of zinc-finger anti-viral protein in host defense against Sindbis virus.* Int Immunol, 2015. **27**(7): p. 357-64.
257. Gritsun, T.S. and E.A. Gould, *Origin and evolution of 3'UTR of flaviviruses: long direct repeats as a basis for the formation of secondary structures and their significance for virus transmission.* Adv Virus Res, 2007. **69**: p. 203-48.
258. Setoh, Y.X., et al., *De Novo Generation and Characterization of New Zika Virus Isolate Using Sequence Data from a Microcephaly Case.* mSphere, 2017. **2**(3).
259. Ritchie, W., M. Legendre, and D. Gautheret, *RNA stem-loops: to be or not to be cleaved by*

RNAse III. Rna, 2007. **13**(4): p. 457-62.
260. Setoh, Y.X., et al., *Determinants of Zika virus host tropism uncovered by deep mutational scanning.* Nature Microbiology, 2019.
261. Hoenninger, V.M., et al., *Analysis of the effects of alterations in the tick-borne encephalitis virus 3′-noncoding region on translation and RNA replication using reporter replicons.* Virology, 2008. **377**(2): p. 419-30.
262. Khromykh, A.A. and E.G. Westaway, *Subgenomic replicons of the flavivirus Kunjin: construction and applications.* J Virol, 1997. **71**(2): p. 1497-505.
263. Khromykh, A.A., et al., *Coupling between replication and packaging of flavivirus RNA: evidence derived from the use of DNA-based full-length cDNA clones of Kunjin virus.* J Virol, 2001. **75**(10): p. 4633-40.
264. Aubry, F., et al., *Flavivirus reverse genetic systems, construction techniques and applications: a historical perspective.* Antiviral Res, 2015. **114**: p. 67-85.
265. Shi, P.Y., et al., *Infectious cDNA clone of the epidemic west nile virus from New York City.* J Virol, 2002. **76**(12): p. 5847-56.
266. Amarilla, A.A., et al., *Chimeric viruses between Rocio and West Nile: the role for Rocio prM-E proteins in virulence and inhibition of interferon-α/β signaling.* Scientific Reports, 2017. **7**: p. 44642.
267. Piyasena, T.B.H., et al., *Infectious DNAs derived from insect-specific flavivirus genomes enable identification of pre- and post-entry host restrictions in vertebrate cells.* Scientific Reports, 2017. **7**(1).
268. Saxena, S., Z.O. Jonsson, and A. Dutta, *Small RNAs with imperfect match to endogenous mRNA repress translation. Implications for off-target activity of small inhibitory RNA in mammalian cells.* J Biol Chem, 2003. **278**(45): p. 44312-9.
269. Jackson, A.L. and P.S. Linsley, *Recognizing and avoiding siRNA off-target effects for target identification and therapeutic application.* Nat Rev Drug Discov, 2010. **9**(1): p. 57-67.
270. Lee, Y., et al., *MicroRNA maturation: stepwise processing and subcellular localization.* Embo j, 2002. **21**(17): p. 4663-70.
271. Compton, A.A., et al., *Natural mutations in IFITM3 modulate post-translational regulation and toggle antiviral specificity.* EMBO Rep, 2016. **17**(11): p. 1657-1671.
272. Bailey, C.C., et al., *Interferon-induced transmembrane protein 3 is a type II transmembrane protein.* J Biol Chem, 2013. **288**(45): p. 32184-93.
273. Tartour, K., et al., *Interference with the production of infectious viral particles and bimodal inhibition of replication are broadly conserved antiviral properties of IFITMs.* PLoS Pathog, 2017. **13**(9): p. e1006610.
274. Tartour, K., et al., *IFITM proteins are incorporated onto HIV-1 virion particles and negatively imprint their infectivity.* Retrovirology, 2014. **11**: p. 103.
275. Roby, J.A., R.A. Hall, and A.A. Khromykh, *West Nile virus genome with glycosylated envelope protein and deletion of alpha helices 1, 2, and 4 in the capsid protein is noninfectious and efficiently secretes subviral particles.* J Virol, 2013. **87**(23): p. 13063-9.
276. Compton, Alex A., et al., *IFITM Proteins Incorporated into HIV-1 Virions Impair Viral Fusion and Spread.* Cell Host & Microbe, 2014. **16**(6): p. 736-747.
277. White, J.M. and G.R. Whittaker, *Fusion of Enveloped Viruses in Endosomes.* Traffic, 2016. **17**(6): p. 593-614.
278. Harrison, S.C., *Viral membrane fusion.* Virology, 2015. **479-480**: p. 498-507.
279. Whelan, S.P.J., et al., *Interferon-induced transmembrane protein 3 blocks fusion of sensitive but not resistant viruses by partitioning into virus-carrying endosomes.* PLOS Pathogens, 2019. **15**(1): p. e1007532.
280. Earp LJ, et al., *The many mechanisms of viral membrane fusion proteins.* Curr Top Microbiol Immunol., 2005(285): p. 25–66.
281. Brass, A.L., et al., *The IFITM proteins mediate cellular resistance to influenza A H1N1 virus, West Nile virus, and dengue virus.* Cell, 2009. **139**(7): p. 1243-54.

282. Perreira, J.M., et al., *IFITMs restrict the replication of multiple pathogenic viruses.* J Mol Biol, 2013. **425**(24): p. 4937-55.
283. Lewin, A.R., et al., *Molecular analysis of a human interferon-inducible gene family.* Eur J Biochem, 1991. **199**(2): p. 417-23.
284. Siegrist, F., M. Ebeling, and U. Certa, *The small interferon-induced transmembrane genes and proteins.* J Interferon Cytokine Res, 2011. **31**(1): p. 183-97.
285. Shi, G., O. Schwartz, and A.A. Compton, *More than meets the I: the diverse antiviral and cellular functions of interferon-induced transmembrane proteins.* Retrovirology, 2017. **14**(1): p. 53.
286. Bailey, C.C., et al., *IFITM-Family Proteins: The Cell's First Line of Antiviral Defense.* Annu Rev Virol, 2014. **1**: p. 261-83.
287. Li, C., et al., *The Host Restriction Factor Interferon-Inducible Transmembrane Protein 3 Inhibits Vaccinia Virus Infection.* Front Immunol, 2018. **9**: p. 228.
288. Lu, J., et al., *The IFITM proteins inhibit HIV-1 infection.* J Virol, 2011. **85**(5): p. 2126-37.
289. Wrensch, F., et al., *Interferon-Induced Transmembrane Protein–Mediated Inhibition of Host Cell Entry of Ebolaviruses.* Journal of Infectious Diseases, 2015. **212**(suppl 2): p. S210-S218.
290. Yu, J., et al., *IFITM Proteins Restrict HIV-1 Infection by Antagonizing the Envelope Glycoprotein.* Cell Rep, 2015. **13**(1): p. 145-156.
291. Chan, Y.K., I.C. Huang, and M. Farzan, *IFITM proteins restrict antibody-dependent enhancement of dengue virus infection.* PLoS One, 2012. **7**(3): p. e34508.
292. Raychoudhuri, A., et al., *ISG56 and IFITM1 proteins inhibit hepatitis C virus replication.* J Virol, 2011. **85**(24): p. 12881-9.
293. Weidner, J.M., et al., *Interferon-induced cell membrane proteins, IFITM3 and tetherin, inhibit vesicular stomatitis virus infection via distinct mechanisms.* J Virol, 2010. **84**(24): p. 12646-57.
294. Smith, S.E., et al., *Interferon-Induced Transmembrane Protein 1 Restricts Replication of Viruses That Enter Cells via the Plasma Membrane.* J Virol, 2019. **93**(6).
295. Anafu, A.A., et al., *Interferon-inducible Transmembrane Protein 3 (IFITM3) Restricts Reovirus Cell Entry.* Journal of Biological Chemistry, 2013. **288**(24): p. 17261-17271.
296. Savidis, G., et al., *The IFITMs Inhibit Zika Virus Replication.* Cell Rep, 2016. **15**(11): p. 2323-30.
297. Zhao, X., et al., *Identification of Residues Controlling Restriction versus Enhancing Activities of IFITM Proteins on Entry of Human Coronaviruses.* J Virol, 2018. **92**(6).
298. Narayana, S.K., et al., *The Interferon-induced Transmembrane Proteins, IFITM1, IFITM2, and IFITM3 Inhibit Hepatitis C Virus Entry.* Journal of Biological Chemistry, 2015. **290**(43): p. 25946-25959.
299. Smith, S., et al., *IFITM proteins-cellular inhibitors of viral entry.* Curr Opin Virol, 2014. **4**: p. 71-7.
300. Amini-Bavil-Olyaee, S., et al., *The antiviral effector IFITM3 disrupts intracellular cholesterol homeostasis to block viral entry.* Cell Host Microbe, 2013. **13**(4): p. 452-64.
301. Sauter, D. and F. Kirchhoff, *IFITMs: I mportant F actors I n T rans- M ission of HIV-1.* Cell Host & Microbe, 2016. **20**(4): p. 407-408.
302. Desai, T.M., et al., *IFITM3 restricts influenza A virus entry by blocking the formation of fusion pores following virus-endosome hemifusion.* PLoS Pathog, 2014. **10**(4): p. e1004048.
303. Feeley, E.M., et al., *IFITM3 inhibits influenza A virus infection by preventing cytosolic entry.* PLoS Pathog, 2011. **7**(10): p. e1002337.
304. John, S.P., et al., *The CD225 domain of IFITM3 is required for both IFITM protein association and inhibition of influenza A virus and dengue virus replication.* J Virol, 2013. **87**(14): p. 7837-52.
305. Zani, A. and J.S. Yount, *Antiviral Protection by IFITM3 In Vivo.* Curr Clin Microbiol Rep, 2018. **5**(4): p. 229-237.

306. Allen, E.K., et al., *SNP-mediated disruption of CTCF binding at the IFITM3 promoter is associated with risk of severe influenza in humans.* Nat Med, 2017. **23**(8): p. 975-983.
307. Desai, T.M., et al., *pH regulation in early endosomes and interferon-inducible transmembrane proteins control avian retrovirus fusion.* J Biol Chem, 2017. **292**(19): p. 7817-7827.
308. Suddala, K.C., et al., *Interferon-induced transmembrane protein 3 blocks fusion of sensitive but not resistant viruses by partitioning into virus-carrying endosomes.* PLoS Pathog, 2019. **15**(1): p. e1007532.
309. Kuhnl, A., et al., *Late Endosomal/Lysosomal Cholesterol Accumulation Is a Host Cell-Protective Mechanism Inhibiting Endosomal Escape of Influenza A Virus.* MBio, 2018. **9**(4).
310. Everitt, A.R., et al., *IFITM3 restricts the morbidity and mortality associated with influenza.* Nature, 2012. **484**(7395): p. 519-23.
311. Gorman, M.J., et al., *The Interferon-Stimulated Gene Ifitm3 Restricts West Nile Virus Infection and Pathogenesis.* J Virol, 2016. **90**(18): p. 8212-25.
312. Rohini, M., A. Haritha Menon, and N. Selvamurugan, *Role of activating transcription factor 3 and its interacting proteins under physiological and pathological conditions.* Int J Biol Macromol, 2018. **120**(Pt A): p. 310-317.
313. Shu, M., et al., *Role of activating transcription factor 3 in the synthesis of latency-associated transcript and maintenance of herpes simplex virus 1 in latent state in ganglia.* Proc Natl Acad Sci U S A, 2015. **112**(39): p. E5420-6.
314. Hai, T., et al., *ATF3 and stress responses.* Gene Expr, 1999. **7**(4-6): p. 321-35.
315. Hunt, D., G. Raivich, and P.N. Anderson, *Activating transcription factor 3 and the nervous system.* Front Mol Neurosci, 2012. **5**: p. 7.
316. Campbell, G., et al., *Upregulation of activating transcription factor 3 (ATF3) by intrinsic CNS neurons regenerating axons into peripheral nerve grafts.* Exp Neurol, 2005. **192**(2): p. 340-7.
317. Hai, T.W., et al., *Transcription factor ATF cDNA clones: an extensive family of leucine zipper proteins able to selectively form DNA-binding heterodimers.* Genes Dev, 1989. **3**(12b): p. 2083-90.
318. Chen, B.P., et al., *ATF3 and ATF3 delta Zip. Transcriptional repression versus activation by alternatively spliced isoforms.* J Biol Chem, 1994. **269**(22): p. 15819-26.
319. Thompson, M.R., D. Xu, and B.R. Williams, *ATF3 transcription factor and its emerging roles in immunity and cancer.* J Mol Med (Berl), 2009. **87**(11): p. 1053-60.
320. Zmuda, E.J., et al., *Deficiency of Atf3, an adaptive-response gene, protects islets and ameliorates inflammation in a syngeneic mouse transplantation model.* Diabetologia, 2010. **53**(7): p. 1438-50.
321. Hsu, J.C., et al., *Identification of LRF-1, a leucine-zipper protein that is rapidly and highly induced in regenerating liver.* Proc Natl Acad Sci U S A, 1991. **88**(9): p. 3511-5.
322. Allen-Jennings, A.E., et al., *The roles of ATF3 in glucose homeostasis. A transgenic mouse model with liver dysfunction and defects in endocrine pancreas.* J Biol Chem, 2001. **276**(31): p. 29507-14.
323. Kawauchi, J., et al., *Transcriptional repressor activating transcription factor 3 protects human umbilical vein endothelial cells from tumor necrosis factor-alpha-induced apoptosis through down-regulation of p53 transcription.* J Biol Chem, 2002. **277**(41): p. 39025-34.
324. Nawa, T., et al., *Expression of transcriptional repressor ATF3/LRF1 in human atherosclerosis: colocalization and possible involvement in cell death of vascular endothelial cells.* Atherosclerosis, 2002. **161**(2): p. 281-91.
325. Mashima, T., S. Udagawa, and T. Tsuruo, *Involvement of transcriptional repressor ATF3 in acceleration of caspase protease activation during DNA damaging agent-induced apoptosis.* J Cell Physiol, 2001. **188**(3): p. 352-8.
326. Gilchrist, M., et al., *Systems biology approaches identify ATF3 as a negative regulator of Toll-like receptor 4.* Nature, 2006. **441**(7090): p. 173-8.

327. Karam, R., et al., *The unfolded protein response is shaped by the NMD pathway.* EMBO Rep, 2015. **16**(5): p. 599-609.
328. Jiang, H.Y., et al., *Activating transcription factor 3 is integral to the eukaryotic initiation factor 2 kinase stress response.* Mol Cell Biol, 2004. **24**(3): p. 1365-77.
329. Vyas, S., et al., *A systematic analysis of the PARP protein family identifies new functions critical for cell physiology.* Nat Commun, 2013. **4**: p. 2240.
330. Berger, F., M.H. Ramirez-Hernandez, and M. Ziegler, *The new life of a centenarian: signalling functions of NAD(P).* Trends Biochem Sci, 2004. **29**(3): p. 111-8.
331. Corda, D. and M. Di Girolamo, *Functional aspects of protein mono-ADP-ribosylation.* Embo j, 2003. **22**(9): p. 1953-8.
332. Scarpa, E.S., G. Fabrizio, and M. Di Girolamo, *A role of intracellular mono-ADP-ribosylation in cancer biology.* Febs j, 2013. **280**(15): p. 3551-62.
333. Luo, X. and W.L. Kraus, *On PAR with PARP: cellular stress signaling through poly(ADP-ribose) and PARP-1.* Genes Dev, 2012. **26**(5): p. 417-32.
334. Hassa, P.O. and M.O. Hottiger, *The functional role of poly(ADP-ribose)polymerase 1 as novel coactivator of NF-kappaB in inflammatory disorders.* Cell Mol Life Sci, 2002. **59**(9): p. 1534-53.
335. Lin, K.Y. and W.L. Kraus, *PARP Inhibitors for Cancer Therapy.* Cell, 2017. **169**(2): p. 183.
336. Kim, G., et al., *FDA Approval Summary: Olaparib Monotherapy in Patients with Deleterious Germline BRCA-Mutated Advanced Ovarian Cancer Treated with Three or More Lines of Chemotherapy.* Clin Cancer Res, 2015. **21**(19): p. 4257-61.
337. Kuny, C.V. and C.S. Sullivan, *Virus-Host Interactions and the ARTD/PARP Family of Enzymes.* PLoS Pathog, 2016. **12**(3): p. e1005453.
338. Erener, S., et al., *Inflammasome-activated caspase 7 cleaves PARP1 to enhance the expression of a subset of NF-kappaB target genes.* Mol Cell, 2012. **46**(2): p. 200-11.
339. Zhang, Y., et al., *PARP9-DTX3L ubiquitin ligase targets host histone H2BJ and viral 3C protease to enhance interferon signaling and control viral infection.* Nat Immunol, 2015. **16**(12): p. 1215-27.
340. Guo, T., et al., *ADP-ribosyltransferase PARP11 modulates the interferon antiviral response by mono-ADP-ribosylating the ubiquitin E3 ligase beta-TrCP.* Nat Microbiol, 2019.
341. !!! INVALID CITATION !!! [284, 334, 335].

Appendices

Appendix 1

Three 96 well plates were ordered from Integrated DNA technologies (IDT), with each well containing a unique primer sequence, either forward (Fw) or Reverse (Rev) in 10 **µ**M concentration.

Table showing mutagenesis primers ordered from IDT and their respective wells.

Forward and Reverse Primer Mix			
	Well	**Sequence Name**	**Sequence**
1	A1	Fw Adar-2	ATTTAATGTCATACAATTCTTGTAGGGTGAACACCGTGAGAGCGGAGCCTACGGCTGCAC
1	B1	Fw Atf2-1	ATTTAATGTCATACAATAAAGACACTTTGTAGCTGGTGAGAGCGGAGCCTACGGCTGCAC
1	C1	Fw Atf2-2	ATTTAATGTCATACAATTGACACTGTCATTACGTGCTGAGAGCGGAGCCTACGGCTGCAC
1	D1	Fw Atf3-1	ATTTAATGTCATACAATTTGAGTGGGATTAAACACTGAAGAGCGGAGCCTACGGCTGCAC
1	E1	Fw Atf3-2	ATTTAATGTCATACAATTCAAGGTAGACACTTCTGCCTAGAGCGGAGCCTACGGCTGCAC
1	F1	Fw B2m-1	ATTTAATGTCATACAATTTGGATTTCAATGTGAGGCGGAGAGCGGAGCCTACGGCTGCAC
1	G1	Fw B2m-2	ATTTAATGTCATACAATTTATTGCTCAGCTATCTAGGAAGAGCGGAGCCTACGGCTGCAC
1	H1	Fw Birc6-1	ATTTAATGTCATACAATTAACAGTCTTTCTAACTGCGGAGAGCGGAGCCTACGGCTGCAC
1	A2	Fw Birc6-2	ATTTAATGTCATACAATTCTATGATGACACTGCACCGGAGAGCGGAGCCTACGGCTGCAC
1	B2	Fw Brd4-1	ATTTAATGTCATACAATTAATCTTATAGTAATCAGGGAAGAGCGGAGCCTACGGCTGCAC
1	C2	Fw Brd4-2	ATTTAATGTCATACAATTTAAGCTATAGCTCGCTGGGAAGAGCGGAGCCTACGGCTGCAC
1	D2	Fw Cdkl4-1	ATTTAATGTCATACAATTATAGCTTTCTTAAACATCTTAGAGCGGAGCCTACGGCTGCAC
1	E2	Fw Cdkl4-2	ATTTAATGTCATACAATTTTAGAACACTTCTGCTTCTAAGAGCGGAGCCTACGGCTGCAC

1	F2	Fw Clec4d-1	ATTTAATGTCATACAATTACATCTGTCTTATTCTGGTAAGAGCGGAGCCTACGGCTGCAC
1	G2	Fw Clec4d-2	ATTTAATGTCATACAATTTAACAGTGGTCTATGACCCAAGAGCGGAGCCTACGGCTGCAC
1	H2	Fw Clec4e-1	ATTTAATGTCATACAATAATAATTTCACTTTGAACCTAAGAGCGGAGCCTACGGCTGCAC
1	A3	Fw Clec4e-2	ATTTAATGTCATACAATTTTGTTAGAGAATTGATCTGTAGAGCGGAGCCTACGGCTGCAC
1	B3	Fw Cmpk2-1	ATTTAATGTCATACAATTACAATAACAGGAAAGTTGGTAGAGCGGAGCCTACGGCTGCAC
1	C3	Fw Cmpk2-2	ATTTAATGTCATACAATAACTAGGTCAAGTACTGCCCGAGAGCGGAGCCTACGGCTGCAC
1	D3	Fw Cpeb3-1	ATTTAATGTCATACAATTATAACATTAAGAACTTGGGGAGAGCGGAGCCTACGGCTGCAC
1	E3	Fw Cpeb3-2	ATTTAATGTCATACAATTCCATCTGCATCTTGTCGGGGAGAGCGGAGCCTACGGCTGCAC
1	F3	Fw Cxcl10-1	ATTTAATGTCATACAATATAGCTTACAGTACAGAGCTAAGAGCGGAGCCTACGGCTGCAC
1	G3	Fw Cxcl10-2	ATTTAATGTCATACAATTTGATGACACAAGTTCTTCCAAGAGCGGAGCCTACGGCTGCAC
1	H3	Fw Cytip-1	ATTTAATGTCATACAATTTGTCTTCCATCGTGAGCTGGAGAGCGGAGCCTACGGCTGCAC
1	A4	Fw Cytip-2	ATTTAATGTCATACAATTCCACAGTAACAACCTTCCTTAGAGCGGAGCCTACGGCTGCAC
1	B4	Fw Daxx-1	ATTTAATGTCATACAATTTAATGTACACATAGATCTTAAGAGCGGAGCCTACGGCTGCAC
1	C4	Fw Daxx-2	ATTTAATGTCATACAATTACAATGATGCTGTCATCGGTAGAGCGGAGCCTACGGCTGCAC
1	D4	Fw Ddx58-1	ATTTAATGTCATACAATTTAGTGTCTCGGATCTGTCTGAGAGCGGAGCCTACGGCTGCAC
1	E4	Fw Ddx58-2	ATTTAATGTCATACAATTAGCTGTCAACTATAGTCTTTAGAGCGGAGCCTACGGCTGCAC
1	F4	Fw Ddx60-1	ATTTAATGTCATACAATTAAGCTGGAGTAGTCAGCCTTAGAGCGGAGCCTACGGCTGCAC

1	G4	Fw Ddx60-2	ATTTAATGTCATACAATTAATGAAATGTCGTATCGGGAAGAGCGGAGCCTACGGCTGCAC
1	H4	Fw Dhx9-1	ATTTAATGTCATACAATTTGTACTTCTTGTTCTTCCTTAGAGCGGAGCCTACGGCTGCAC
1	A5	Fw Dhx9-2	ATTTAATGTCATACAATTCACACATGAATTTCTGTCTGAGAGCGGAGCCTACGGCTGCAC
1	B5	Fw Dtx3l-1	ATTTAATGTCATACAATTACTCTATGAACTCTAGTCTAAGAGCGGAGCCTACGGCTGCAC
1	C5	Fw Dtx3l-2	ATTTAATGTCATACAATTAAACAACTAATGTATTGCTAAGAGCGGAGCCTACGGCTGCAC
1	D5	Fw Eif2ak2-1	ATTTAATGTCATACAATTTTGAGGACTTCTCTAACCTGAGAGCGGAGCCTACGGCTGCAC
1	E5	Fw Eif2ak2-2	ATTTAATGTCATACAATTTGTACTTCGTGCTCCGCCTTAGAGCGGAGCCTACGGCTGCAC
1	F5	Fw Fa2h-1	ATTTAATGTCATACAATTTGAATACTCTCTTGTGAGTGAGAGCGGAGCCTACGGCTGCAC
1	G5	Fw Fa2h-2	ATTTAATGTCATACAATTAGTACAGCTGGTATCTGGGGAGAGCGGAGCCTACGGCTGCAC
1	H5	Fw Fbxo39-1	ATTTAATGTCATACAATTTATTGTTGAACTCGAACGTTAGAGCGGAGCCTACGGCTGCAC
1	A6	Fw Fbxo39-2	ATTTAATGTCATACAATTTGTTCTCGCTCAAGGTCTCGAGAGCGGAGCCTACGGCTGCAC
1	B6	Fw Gbp2-1	ATTTAATGTCATACAATTTGTAGATGAAGGTGCTGCTGAGAGCGGAGCCTACGGCTGCAC
1	C6	Fw Gbp2-2	ATTTAATGTCATACAATTGTTTCAACAACATCTGCCTTAGAGCGGAGCCTACGGCTGCAC
1	D6	Fw Gbp3-1	ATTTAATGTCATACAATTTGGTTTGTATCTTTAACCTTAGAGCGGAGCCTACGGCTGCAC
1	E6	Fw Gbp3-2	ATTTAATGTCATACAATTTTATCTGTAGTGTACAACTGAGAGCGGAGCCTACGGCTGCAC
1	F6	Fw Gbp6-1	ATTTAATGTCATACAATTTTCTGTCTTAGTAGCTCCTGAGAGCGGAGCCTACGGCTGCAC
1	G6	Fw Gbp6-2	ATTTAATGTCATACAATTTCTGTGACATAGTGCAGCTGAGAGCGGAGCCTACGGCTGCAC

1	H6	Fw Gcc-1	ATTTAATGTCATACAATTTAAAGAACAGAATTAACCAAAGAGCGGAGCCTACGGCTGCAC
1	A7	Fw Gcc-2	ATTTAATGTCATACAATTATACTTGTCCTTCAGCTCTGAGAGCGGAGCCTACGGCTGCAC
1	B7	Fw Gvin-1	ATTTAATGTCATACAATTTCTCTTCTAGGTTTGATCTGAGAGCGGAGCCTACGGCTGCAC
1	C7	Fw Gvin-2	ATTTAATGTCATACAATTTAATTACATCACTGAAGCGGAGAGCGGAGCCTACGGCTGCAC
1	D7	Fw Ifi35-1	ATTTAATGTCATACAATTTAGAAACTACAAACTTGGGCAGAGCGGAGCCTACGGCTGCAC
1	E7	Fw Ifi35-2	ATTTAATGTCATACAATTATACAGAGAAATCTAGTCTCAGAGCGGAGCCTACGGCTGCAC
1	F7	Fw Ifi44-1	ATTTAATGTCATACAATTATTGATCCAACACAGTTCTAAGAGCGGAGCCTACGGCTGCAC
1	G7	Fw Ifi44-2	ATTTAATGTCATACAATTAATATAGCACTCTAAAGGGAAGAGCGGAGCCTACGGCTGCAC
1	H7	Fw Ifih1-1	ATTTAATGTCATACAATTTATACATCATCTTCTCTCGGAGAGCGGAGCCTACGGCTGCAC
1	A8	Fw Ifih1-2	ATTTAATGTCATACAATTAAGATTTGACAACTTCTGGAAGAGCGGAGCCTACGGCTGCAC
1	B8	Fw Ifit1-1	ATTTAATGTCATACAATTATATTAACGTCACAGAGGTGAGAGCGGAGCCTACGGCTGCAC
1	C8	Fw Ifit1-2	ATTTAATGTCATACAATTTCTCCTAAATCCTGAAGCTTAGAGCGGAGCCTACGGCTGCAC
1	D8	Fw Ifit3-1	ATTTAATGTCATACAATTTCTGCATGAACTCCATCGTTAGAGCGGAGCCTACGGCTGCAC
1	E8	Fw Ifit3-2	ATTTAATGTCATACAATTTGTCTCACCTTGTCAACGTAAGAGCGGAGCCTACGGCTGCAC
1	F8	Fw Ifitm3-1	ATTTAATGTCATACAATTTGATTCTTTCGTAGTTTGGGAGAGCGGAGCCTACGGCTGCAC
1	G8	Fw Ifitm3-2	ATTTAATGTCATACAATTAAATGAGTGTTACACCTGCGAGAGCGGAGCCTACGGCTGCAC
1	H8	Fw Ifna1-1	ATTTAATGTCATACAATTTCTCTCTCAGGTACACAGTGAGAGCGGAGCCTACGGCTGCAC

1	A9	Fw Ifna1-2	ATTTAATGTCATACAATTTTGATGTGAAGATGTTCAGGAGAGCGGAGCCTACGGCTGCAC
1	B9	Fw Ifna4-1	ATTTAATGTCATACAATTTGTGGGTCTTGTAGATGCTGAGAGCGGAGCCTACGGCTGCAC
1	C9	Fw Ifna4-2	ATTTAATGTCATACAATTTATCCACCTTCTCCAAGGGGAGAGCGGAGCCTACGGCTGCAC
1	D9	Fw Ifnb1-1	ATTTAATGTCATACAATTACAACAATAGTCTCATTCCAAGAGCGGAGCCTACGGCTGCAC
1	A1	Rev Adar-2	ATTGTATGACATTAAATTCTTGGCGGGGGAACACCGGTAGAGCAGAGTCTCTGATCTTGA
1	B1	Rev Atf2-1	ATTGTATGACATTAAATAAAGATCCTTGGTAGCTGGGTAGAGCAGAGTCTCTGATCTTGA
1	C1	Rev Atf2-2	ATTGTATGACATTAAATTGACATGGTCCTTACGTGCGTAGAGCAGAGTCTCTGATCTTGA
1	D1	Rev Atf3-1	ATTGTATGACATTAAATTTGAGGTGGAGTAAACACTTCAGAGCAGAGTCTCTGATCTTGA
1	E1	Rev Atf3-2	ATTGTATGACATTAAATTCAAGTGAGATACTTCTGCTGAGAGCAGAGTCTCTGATCTTGA
1	F1	Rev B2m-1	ATTGTATGACATTAAATTTGGAGGTCACTGTGAGGCTTAGAGCAGAGTCTCTGATCTTGA
1	G1	Rev B2m-2	ATTGTATGACATTAAATTTATTTTTCATCTATCTAGTCAGAGCAGAGTCTCTGATCTTGA
1	H1	Rev Birc6-1	ATTGTATGACATTAAATTAACATGCTTGCTAACTGCTTAGAGCAGAGTCTCTGATCTTGA
1	A2	Rev Birc6-2	ATTGTATGACATTAAATTCTATTCTGATACTGCACCTTAGAGCAGAGTCTCTGATCTTGA
1	B2	Rev Brd4-1	ATTGTATGACATTAAATTAATCGGATATTAATCAGGTCAGAGCAGAGTCTCTGATCTTGA
1	C2	Rev Brd4-2	ATTGTATGACATTAAATTTAAGTGATATCTCGCTGGTCAGAGCAGAGTCTCTGATCTTGA
1	D2	Rev Cdkl4-1	ATTGTATGACATTAAATTATAGTGTTCGTAAACATCGGAGAGCAGAGTCTCTGATCTTGA
1	E2	Rev Cdkl4-2	ATTGTATGACATTAAATTTTAGCCCACGTCTGCTTCGCAGAGCAGAGTCTCTGATCTTGA

1	F2	Rev Clec4d-1	ATTGTATGACATTAAATTACATTGGTCGTATTCTGGGCAGAGCAGAGTCTCTGATCTTGA
1	G2	Rev Clec4d-2	ATTGTATGACATTAAATTTAACCTTGGGCTATGACCTCAGAGCAGAGTCTCTGATCTTGA
1	H2	Rev Clec4e-1	ATTGTATGACATTAAATAATAAGGTCATTTTGAACCGCAGAGCAGAGTCTCTGATCTTGA
1	A3	Rev Clec4e-2	ATTGTATGACATTAAATTTTGTGCGAGCATTGATCTTGAGAGCAGAGTCTCTGATCTTGA
1	B3	Rev Cmpk2-1	ATTGTATGACATTAAATTACAAGCACATGAAAGTTGTGAGAGCAGAGTCTCTGATCTTGA
1	C3	Rev Cmpk2-2	ATTGTATGACATTAAATAACTATTTCACGTACTGCCTTAGAGCAGAGTCTCTGATCTTGA
1	D3	Rev Cpeb3-1	ATTGTATGACATTAAATTATAATCTTACGAACTTGGTTAGAGCAGAGTCTCTGATCTTGA
1	E3	Rev Cpeb3-2	ATTGTATGACATTAAATTCCATTGGCAGCTTGTCGGTTAGAGCAGAGTCTCTGATCTTGA
1	F3	Rev Cxcl10-1	ATTGTATGACATTAAATATAGCGGACATTACAGAGCGCAGAGCAGAGTCTCTGATCTTGA
1	G3	Rev Cxcl10-2	ATTGTATGACATTAAATTTGATTCCACCAGTTCTTCTCAGAGCAGAGTCTCTGATCTTGA
1	H3	Rev Cytip-1	ATTGTATGACATTAAATTTGTCGGCCAGCGTGAGCTTTAGAGCAGAGTCTCTGATCTTGA
1	A4	Rev Cytip-2	ATTGTATGACATTAAATTCCACCTTAATAACCTTCCGGAGAGCAGAGTCTCTGATCTTGA
1	B4	Rev Daxx-1	ATTGTATGACATTAAATTTAATTGACATATAGATCTGCAGAGCAGAGTCTCTGATCTTGA
1	C4	Rev Daxx-2	ATTGTATGACATTAAATTACAAGTATGTTGTCATCGTGAGAGCAGAGTCTCTGATCTTGA
1	D4	Rev Ddx58-1	ATTGTATGACATTAAATTTAGTTGCTCTGATCTGTCGTAGAGCAGAGTCTCTGATCTTGA
1	E4	Rev Ddx58-2	ATTGTATGACATTAAATTAGCTTGCAATTATAGTCTGGAGAGCAGAGTCTCTGATCTTGA
1	F4	Rev Ddx60-1	ATTGTATGACATTAAATTAAGCACGAGGAGTCAGCCGCAGAGCAGAGTCTCTGATCTTGA

1	G4	Rev Ddx60-2	ATTGTATGACATTAAATTAATGTTATGGCGTATCGGCCAGAGCAGAGTCTCTGATCTTGA
1	H4	Rev Dhx9-1	ATTGTATGACATTAAATTTGTATGTCTGGTTCTTCCGGAGAGCAGAGTCTCTGATCTTGA
1	A5	Rev Dhx9-2	ATTGTATGACATTAAATTCACATCTGACTTTCTGTCGTAGAGCAGAGTCTCTGATCTTGA
1	B5	Rev Dtx3l-1	ATTGTATGACATTAAATTACTCGCTGACCTCTAGTCGCAGAGCAGAGTCTCTGATCTTGA
1	C5	Rev Dtx3l-2	ATTGTATGACATTAAATTAAACCCCTACTGTATTGCGCAGAGCAGAGTCTCTGATCTTGA
1	D5	Rev Eif2ak2-1	ATTGTATGACATTAAATTTTGATTACTGCTCTAACCGTAGAGCAGAGTCTCTGATCTTGA
1	E5	Rev Eif2ak2-2	ATTGTATGACATTAAATTTGTATGTCGGGCTCCGCCGGAGAGCAGAGTCTCTGATCTTGA
1	F5	Rev Fa2h-1	ATTGTATGACATTAAATTTGAAGCCTCGCTTGTGAGGTAGAGCAGAGTCTCTGATCTTGA
1	G5	Rev Fa2h-2	ATTGTATGACATTAAATTAGTATCGCTTGTATCTGGTTAGAGCAGAGTCTCTGATCTTGA
1	H5	Rev Fbxo39-1	ATTGTATGACATTAAATTTATTTGTGACCTCGAACGGGAGAGCAGAGTCTCTGATCTTGA
1	A6	Rev Fbxo39-2	ATTGTATGACATTAAATTTGTTTGCGCGCAAGGTCTTTAGAGCAGAGTCTCTGATCTTGA
1	B6	Rev Gbp2-1	ATTGTATGACATTAAATTTGTATCTGACGGTGCTGCGTAGAGCAGAGTCTCTGATCTTGA
1	C6	Rev Gbp2-2	ATTGTATGACATTAAATTGTTTTCACACCATCTGCCGGAGAGCAGAGTCTCTGATCTTGA
1	D6	Rev Gbp3-1	ATTGTATGACATTAAATTTGGTGGGTAGCTTTAACCGGAGAGCAGAGTCTCTGATCTTGA
1	E6	Rev Gbp3-2	ATTGTATGACATTAAATTTTATTGGTATTGTACAACGTAGAGCAGAGTCTCTGATCTTGA
1	F6	Rev Gbp6-1	ATTGTATGACATTAAATTTTCTTGCTTCGTAGCTCCGTAGAGCAGAGTCTCTGATCTTGA
1	G6	Rev Gbp6-2	ATTGTATGACATTAAATTTCTGGTACAGAGTGCAGCGTAGAGCAGAGTCTCTGATCTTGA

1	H6	Rev Gcc-1	ATTGTATGACATTAAATTTAAATCACATAATTAACCCCAGAGCAGAGTCTCTGATCTTGA
1	A7	Rev Gcc-2	ATTGTATGACATTAAATTATACGGGTCTTTCAGCTCGTAGAGCAGAGTCTCTGATCTTGA
1	B7	Rev Gvin-1	ATTGTATGACATTAAATTTCTCGGCTATGTTTGATCGTAGAGCAGAGTCTCTGATCTTGA
1	C7	Rev Gvin-2	ATTGTATGACATTAAATTTAATGCCATTACTGAAGCTTAGAGCAGAGTCTCTGATCTTGA
1	D7	Rev Ifi35-1	ATTGTATGACATTAAATTTAGACCCTATAAACTTGGTTAGAGCAGAGTCTCTGATCTTGA
1	E7	Rev Ifi35-2	ATTGTATGACATTAAATTATACCTAGACATCTAGTCGTAGAGCAGAGTCTCTGATCTTGA
1	F7	Rev Ifi44-1	ATTGTATGACATTAAATTATTGCGCCACCACAGTTCGCAGAGCAGAGTCTCTGATCTTGA
1	G7	Rev Ifi44-2	ATTGTATGACATTAAATTAATAGCGCATTCTAAAGGTCAGAGCAGAGTCTCTGATCTTGA
1	H7	Rev Ifih1-1	ATTGTATGACATTAAATTTATATCTCAGCTTCTCTCTTAGAGCAGAGTCTCTGATCTTGA
1	A8	Rev Ifih1-2	ATTGTATGACATTAAATTAAGAGGTGATAACTTCTGTCAGAGCAGAGTCTCTGATCTTGA
1	B8	Rev Ifit1-1	ATTGTATGACATTAAATTATATGCACGGCACAGAGGGTAGAGCAGAGTCTCTGATCTTGA
1	C8	Rev Ifit1-2	ATTGTATGACATTAAATTTCTCTGAAAGCCTGAAGCGGAGAGCAGAGTCTCTGATCTTGA
1	D8	Rev Ifit3-1	ATTGTATGACATTAAATTTCTGTCTGACCTCCATCGGGAGAGCAGAGTCTCTGATCTTGA
1	E8	Rev Ifit3-2	ATTGTATGACATTAAATTTGTCGTACCGTGTCAACGGCAGAGCAGAGTCTCTGATCTTGA
1	F8	Rev Ifitm3-1	ATTGTATGACATTAAATTTGATGTTTTTGTAGTTTGTTAGAGCAGAGTCTCTGATCTTGA
1	G8	Rev Ifitm3-2	ATTGTATGACATTAAATTAAATTCGTGGTACACCTGTTAGAGCAGAGTCTCTGATCTTGA
1	H8	Rev Ifna1-1	ATTGTATGACATTAAATTTCTCGTTCATGTACACAGGTAGAGCAGAGTCTCTGATCTTGA

1	A9	Rev Ifna1-2	ATTGTATGACATTAAATTTTGAGTTGACGATGTTCATTAGAGCAGAGTCTCTGATCTTGA
1	B9	Rev Ifna4-1	ATTGTATGACATTAAATTTGTGTTTCTGGTAGATGCGTAGAGCAGAGTCTCTGATCTTGA
1	C9	Rev Ifna4-2	ATTGTATGACATTAAATTTATCTCCCTGCTCCAAGGTTAGAGCAGAGTCTCTGATCTTGA
1	D9	Rev Ifnb1-1	ATTGTATGACATTAAATTACAATCATATTCTCATTCTCAGAGCAGAGTCTCTGATCTTGA
2	A1	Fw Ifnb1-2	ATTTAATGTCATACAATTTCCTGAAGATCTCTGCTCGGAGAGCGGAGCCTACGGCTGCAC
2	B1	Fw Ikbka-1	ATTTAATGTCATACAATTAACACTCTCTCAACAGTGTTAGAGCGGAGCCTACGGCTGCAC
2	C1	Fw Ikbka-2	ATTTAATGTCATACAATTTTGTGACATCTTCTTCCCTGAGAGCGGAGCCTACGGCTGCAC
2	D1	Fw Ikbkb-1	ATTTAATGTCATACAATTATACTATGGAAATACACCTTAGAGCGGAGCCTACGGCTGCAC
2	E1	Fw Ikbkb-2	ATTTAATGTCATACAATTTGGACTAGCTGAAGTTCCTGAGAGCGGAGCCTACGGCTGCAC
2	F1	Fw Ikbke-1	ATTTAATGTCATACAATTAGATGACTGAAATTTACCTTAGAGCGGAGCCTACGGCTGCAC
2	G1	Fw Ikbke-2	ATTTAATGTCATACAATTAGACAGAAACAAACTTCTCAAGAGCGGAGCCTACGGCTGCAC
2	H1	Fw Il15-1	ATTTAATGTCATACAATTATCTTACATCTATCCAGTTGAGAGCGGAGCCTACGGCTGCAC
2	A2	Fw Il15-2	ATTTAATGTCATACAATTATCCATACAACTTTATTCCAAGAGCGGAGCCTACGGCTGCAC
2	B2	Fw Il6-1	ATTTAATGTCATACAATTAGAGTTTCTGTATCTCTCTGAGAGCGGAGCCTACGGCTGCAC
2	C2	Fw Il6-2	ATTTAATGTCATACAATTACATTCCAAGAAACCATCTGAGAGCGGAGCCTACGGCTGCAC
2	D2	Fw Irf1-1	ATTTAATGTCATACAATTTATTGATCCAGATCAGCCCTAGAGCGGAGCCTACGGCTGCAC
2	E2	Fw Irf1-2	ATTTAATGTCATACAATTTGTCTCCTAGTACAGAGCCAAGAGCGGAGCCTACGGCTGCAC

2	F2	Fw Irf2-1	ATTTAATGTCATACAATTTTCTTTATGCTTCTGTCCTTAGAGCGGAGCCTACGGC TGCAC
2	G2	Fw Irf2-2	ATTTAATGTCATACAATTACAACTATGATGTTCACCGTAGAGCGGAGCCTACGG CTGCAC
2	H2	Fw Irf3-1	ATTTAATGTCATACAATTAGTTCTGAGACTCGCAGCCAAGAGCGGAGCCTACGG CTGCAC
2	A3	Fw Irf3-2	ATTTAATGTCATACAATTTGTTCCTCAGCTAGCAGCTGAGAGCGGAGCCTACGG CTGCAC
2	B3	Fw Irf5-1	ATTTAATGTCATACAATTAGAACAGCTGGAAGTCACGGAGAGCGGAGCCTACG GCTGCAC
2	C3	Fw Irf5-2	ATTTAATGTCATACAATTTGAAGATGGTGTTGTCCCCAAGAGCGGAGCCTACGG CTGCAC
2	D3	Fw Irf7-1	ATTTAATGTCATACAATTTCCTCGTAAACACGGTCTTGAGAGCGGAGCCTACGG CTGCAC
2	E3	Fw Irf7-2	ATTTAATGTCATACAATTCTTCGTAGAGACTGTTGGTGAGAGCGGAGCCTACGG CTGCAC
2	F3	Fw Irf9-1	ATTTAATGTCATACAATTATGTAAGTATACTGTAGCTGAGAGCGGAGCCTACGG CTGCAC
2	G3	Fw Irf9-2	ATTTAATGTCATACAATTAAGTTTCAATTCTCCTCCGGAGAGCGGAGCCTACGG CTGCAC
2	H3	Fw Irgm-1	ATTTAATGTCATACAATTATGTAAGTACACTGTAGCTGAGAGCGGAGCCTACGG CTGCAC
2	A4	Fw Irgm-2	ATTTAATGTCATACAATTTCTCTTAAAGCTCTTTCGGTAGAGCGGAGCCTACGG CTGCAC
2	B4	Fw Lgals3bp-1	ATTTAATGTCATACAATTTGTCCTTGAAGAGGAAGCTGAGAGCGGAGCCTACGG CTGCAC
2	C4	Fw Lgals3bp-2	ATTTAATGTCATACAATTTAACCAAGCGCATGTCTCCAAGAGCGGAGCCTACGG CTGCAC
2	D4	Fw Lgals8-1	ATTTAATGTCATACAATTTTGCTTTGATAGTGCTTGTTAGAGCGGAGCCTACGG CTGCAC
2	E4	Fw Lgals8-2	ATTTAATGTCATACAATTTCCATACTCTGTAAATCCGAAGAGCGGAGCCTACGG CTGCAC
2	F4	Fw Lrp4-1	ATTTAATGTCATACAATTTTCAGAGCATCTTCCTCCTGAGAGCGGAGCCTACGG CTGCAC

2	G4	Fw Lrp4-2	ATTTAATGTCATACAATTTGTTGATTAGCACTTTGCGAAGAGCGGAGCCTACGG CTGCAC
2	H4	Fw Ly6e-1	ATTTAATGTCATACAATTTAGACATCCTTGTCAGTGTGAGAGCGGAGCCTACGG CTGCAC
2	A5	Fw Ly6e-2	ATTTAATGTCATACAATTAACATAGCGAGACCGTCTTAAGAGCGGAGCCTACGG CTGCAC
2	B5	Fw Map3K8-1	ATTTAATGTCATACAATTTAAACTTACACTAGAGTCGAAGAGCGGAGCCTACGG CTGCAC
2	C5	Fw Map3K8-2	ATTTAATGTCATACAATTTGACTAGTCACATTGGACTAAGAGCGGAGCCTACGG CTGCAC
2	D5	Fw Map4k2-1	ATTTAATGTCATACAATTTAACAATTCTCACACAGCGTAGAGCGGAGCCTACGG CTGCAC
2	E5	Fw Map4k2-2	ATTTAATGTCATACAATTTTGGTGTCAGGAATCTTGGTAGAGCGGAGCCTACGG CTGCAC
2	F5	Fw Mapk8-1	ATTTAATGTCATACAATTTCTTGATTGCAACATTTCTTAGAGCGGAGCCTACGG CTGCAC
2	G5	Fw Mapk8-2	ATTTAATGTCATACAATTTGTTGTCACGTTTGCTTCTGAGAGCGGAGCCTACGG CTGCAC
2	H5	Fw Mbnl1-1	ATTTAATGTCATACAATTTAGTACCAACCTCTCACGTGAGAGCGGAGCCTACGG CTGCAC
2	A6	Fw Mbnl1-2	ATTTAATGTCATACAATTCTTCTAAACTAAAGCAGCCTAGAGCGGAGCCTACGG CTGCAC
2	B6	Fw Mitd1-1	ATTTAATGTCATACAATATCACTGTGACAACTCCTGGGAGAGCGGAGCCTACGG CTGCAC
2	C6	Fw Mitd1-2	ATTTAATGTCATACAATAACTTCTGTAACTGTCTCGTGAGAGCGGAGCCTACGG CTGCAC
2	D6	Fw Mlkl-1	ATTTAATGTCATACAATTATTCCAACACTTTCGGCCTGAGAGCGGAGCCTACGG CTGCAC
2	E6	Fw Mlkl-2	ATTTAATGTCATACAATTTGAACTGGATCTCTCTGCTTAGAGCGGAGCCTACGG CTGCAC
2	F6	Fw Mov10-1	ATTTAATGTCATACAATTAGATGTGGAGTTCATAGCTTAGAGCGGAGCCTACGG CTGCAC
2	G6	Fw Mov10-2	ATTTAATGTCATACAATTCGTGGTTGTAAATCGTCCGCAGAGCGGAGCCTACGG CTGCAC

2	H6	Fw Myd88-1	ATTTAATGTCATACAATTTTGTTTGTGGGACACTGCTTAGAGCGGAGCCTACGG CTGCAC
2	A7	Fw Myd88-2	ATTTAATGTCATACAATTAAGCCGATAGTCTGTCTGTTAGAGCGGAGCCTACGG CTGCAC
2	B7	Fw Nfkbia-1	ATTTAATGTCATACAATTAAATATACATCTTAGAAGTAAGAGCGGAGCCTACGG CTGCAC
2	C7	Fw Nfkbia-2	ATTTAATGTCATACAATTTGTACAAATATACAAGTCCAAGAGCGGAGCCTACGG CTGCAC
2	D7	Fw Nmi-1	ATTTAATGTCATACAATTAGAACTGAACTCTACCTCGAAGAGCGGAGCCTACGG CTGCAC
2	E7	Fw Nmi-2	ATTTAATGTCATACAATTTATTTATGTGCATTATGCGGAGAGCGGAGCCTACGG CTGCAC
2	F7	Fw Oas1a-1	ATTTAATGTCATACAATTAAGTCTGGAGCTTCCTGGGTAGAGCGGAGCCTACGG CTGCAC
2	G7	Fw Oas1a-2	ATTTAATGTCATACAATTTTGACATCAGCACCAAAGGTAGAGCGGAGCCTACGG CTGCAC
2	H7	Fw Oas2-1	ATTTAATGTCATACAATTTCTCTGTTAGGTTTGAGGTTAGAGCGGAGCCTACGG CTGCAC
2	A8	Fw Oas2-2	ATTTAATGTCATACAATTATAATGTCAACAGCTTCCTTAGAGCGGAGCCTACGG CTGCAC
2	B8	Fw Oasl1-1	ATTTAATGTCATACAATTCTTCTTTCCACTCTCTGGTTAGAGCGGAGCCTACGGC TGCAC
2	C8	Fw Oasl1-2	ATTTAATGTCATACAATTTGTCTCTCACATACTGCTGGAGAGCGGAGCCTACGG CTGCAC
2	D8	Fw Oasl2-1	ATTTAATGTCATACAATTTGAAAGTGAAACTGCAGGGAAGAGCGGAGCCTACG GCTGCAC
2	E8	Fw Oasl2-2	ATTTAATGTCATACAATTATTTCATTCTTAATCACGCAAGAGCGGAGCCTACGG CTGCAC
2	F8	Fw p50 (RelB)-1	ATTTAATGTCATACAATAATCTCTGAGAATCTGTCCTGAGAGCGGAGCCTACGG CTGCAC
2	G8	Fw p50 (RelB)-2	ATTTAATGTCATACAATTTTCGCTTCTTGTCCACACCGAGAGCGGAGCCTACGG CTGCAC
2	H8	Fw p65 (RelA)-1	ATTTAATGTCATACAATTTGAAGGTCTCATAGGTCCTTAGAGCGGAGCCTACGG CTGCAC

2	A9	Fw p65 (RelA)-2	ATTTAATGTCATACAATTTGTTGGTCTGGATTCGCTGGAGAGCGGAGCCTACGG CTGCAC
2	B9	Fw Papr14-2	ATTTAATGTCATACAATTTGTTTCACAGCATCTTCTTTAGAGCGGAGCCTACGGC TGCAC
2	C9	Fw Parp11-1	ATTTAATGTCATACAATTTGAATGTTGGTATCCGGCTGAGAGCGGAGCCTACGG CTGCAC
2	D9	Fw Parp11-2	ATTTAATGTCATACAATTAACGGTGCGAAATCGAGCGGAGAGCGGAGCCTACG GCTGCAC
2	A1	Rev Ifnb1-2	ATTGTATGACATTAAATTTCCTTCAGAGCTCTGCTCTTAGAGCAGAGTCTCTGAT CTTGA
2	B1	Rev Ikbka-1	ATTGTATGACATTAAATTAACATGCTCGCAACAGTGGGAGAGCAGAGTCTCTGA TCTTGA
2	C1	Rev Ikbka-2	ATTGTATGACATTAAATTTTGTTCCATTTTCTTCCCGTAGAGCAGAGTCTCTGAT CTTGA
2	D1	Rev Ikbkb-1	ATTGTATGACATTAAATTATACGCTGGCAATACACCGGAGAGCAGAGTCTCTGA TCTTGA
2	E1	Rev Ikbkb-2	ATTGTATGACATTAAATTTGGATGAGCGGAAGTTCCGTAGAGCAGAGTCTCTGA TCTTGA
2	F1	Rev Ikbke-1	ATTGTATGACATTAAATTAGATTCCTGCAATTTACCGGAGAGCAGAGTCTCTGA TCTTGA
2	G1	Rev Ikbke-2	ATTGTATGACATTAAATTAGACCTAAATAAACTTCTTCAGAGCAGAGTCTCTGA TCTTGA
2	H1	Rev Il15-1	ATTGTATGACATTAAATTATCTGCCATTTATCCAGTGTAGAGCAGAGTCTCTGA TCTTGA
2	A2	Rev Il15-2	ATTGTATGACATTAAATTATCCCGACACCTTTATTCTCAGAGCAGAGTCTCTGAT CTTGA
2	B2	Rev Il6-1	ATTGTATGACATTAAATTAGAGGGTCTTTATCTCTCGTAGAGCAGAGTCTCTGA TCTTGA
2	C2	Rev Il6-2	ATTGTATGACATTAAATTACATGTCAATAAACCATCGTAGAGCAGAGTCTCTGA TCTTGA
2	D2	Rev Irf1-1	ATTGTATGACATTAAATTTATTTCTCCCGATCAGCCTGAGAGCAGAGTCTCTGA TCTTGA
2	E2	Rev Irf1-2	ATTGTATGACATTAAATTTGTCGTCTATTACAGAGCTCAGAGCAGAGTCTCTGA TCTTGA

2	F2	Rev Irf2-1	ATTGTATGACATTAAATTTTCTGGATGTTTCTGTCCGGAGAGCAGAGTCTCTGATCTTGA
2	G2	Rev Irf2-2	ATTGTATGACATTAAATTACAATGATGCTGTTCACCTGAGAGCAGAGTCTCTGATCTTGA
2	H2	Rev Irf3-1	ATTGTATGACATTAAATTAGTTTGGAGCCTCGCAGCTCAGAGCAGAGTCTCTGATCTTGA
2	A3	Rev Irf3-2	ATTGTATGACATTAAATTTGTTTTTCATCTAGCAGCGTAGAGCAGAGTCTCTGATCTTGA
2	B3	Rev Irf5-1	ATTGTATGACATTAAATTAGAATCGCTTGAAGTCACTTAGAGCAGAGTCTCTGATCTTGA
2	C3	Rev Irf5-2	ATTGTATGACATTAAATTTGAATCTGGGGTTGTCCCTCAGAGCAGAGTCTCTGATCTTGA
2	D3	Rev Irf7-1	ATTGTATGACATTAAATTTCCTTTTAACCACGGTCTGTAGAGCAGAGTCTCTGATCTTGA
2	E3	Rev Irf7-2	ATTGTATGACATTAAATTCTTCTGAGATACTGTTGGGTAGAGCAGAGTCTCTGATCTTGA
2	F3	Rev Irf9-1	ATTGTATGACATTAAATTATGTCCGTAGACTGTAGCGTAGAGCAGAGTCTCTGATCTTGA
2	G3	Rev Irf9-2	ATTGTATGACATTAAATTAAGTGGCAAGTCTCCTCCTTAGAGCAGAGTCTCTGATCTTGA
2	H3	Rev Irgm-1	ATTGTATGACATTAAATTATGTCCGTATACTGTAGCGTAGAGCAGAGTCTCTGATCTTGA
2	A4	Rev Irgm-2	ATTGTATGACATTAAATTTCTCGGAAATCTCTTTCGTGAGAGCAGAGTCTCTGATCTTGA
2	B4	Rev Lgals3bp-1	ATTGTATGACATTAAATTTGTCTGTGACGAGGAAGCGTAGAGCAGAGTCTCTGATCTTGA
2	C4	Rev Lgals3bp-2	ATTGTATGACATTAAATTTAACTCAGCTCATGTCTCTCAGAGCAGAGTCTCTGATCTTGA
2	D4	Rev Lgals8-1	ATTGTATGACATTAAATTTTGCGGTGAGAGTGCTTGGGAGAGCAGAGTCTCTGATCTTGA
2	E4	Rev Lgals8-2	ATTGTATGACATTAAATTTCCAGCCTCGGTAAATCCTCAGAGCAGAGTCTCTGATCTTGA
2	F4	Rev Lrp4-1	ATTGTATGACATTAAATTTTCATCGCAGCTTCCTCCGTAGAGCAGAGTCTCTGATCTTGA

2	G4	Rev Lrp4-2	ATTGTATGACATTAAATTTGTTTCTTATCACTTTGCTCAGAGCAGAGTCTCTGATCTTGA
2	H4	Rev Ly6e-1	ATTGTATGACATTAAATTTAGATCTCCGTGTCAGTGGTAGAGCAGAGTCTCTGATCTTGA
2	A5	Rev Ly6e-2	ATTGTATGACATTAAATTAACAGCGCGCGACCGTCTGCAGAGCAGAGTCTCTGATCTTGA
2	B5	Rev Map3K8-1	ATTGTATGACATTAAATTTAAATGTACCCTAGAGTCTCAGAGCAGAGTCTCTGATCTTGA
2	C5	Rev Map3K8-2	ATTGTATGACATTAAATTTGACGCGTCCCATTGGACGCAGAGCAGAGTCTCTGATCTTGA
2	D5	Rev Map4k2-1	ATTGTATGACATTAAATTTAACCCTTCGCACACAGCTGAGAGCAGAGTCTCTGATCTTGA
2	E5	Rev Map4k2-2	ATTGTATGACATTAAATTTTGGGTTCATGAATCTTGTGAGAGCAGAGTCTCTGATCTTGA
2	F5	Rev Mapk8-1	ATTGTATGACATTAAATTTCTTTCTTGTAACATTTCGGAGAGCAGAGTCTCTGATCTTGA
2	G5	Rev Mapk8-2	ATTGTATGACATTAAATTTGTTTGCACTTTTGCTTCGTAGAGCAGAGTCTCTGATCTTGA
2	H5	Rev Mbnl1-1	ATTGTATGACATTAAATTTAGTCTCAATCTCTCACGGTAGAGCAGAGTCTCTGATCTTGA
2	A6	Rev Mbnl1-2	ATTGTATGACATTAAATTCTTCGCAACGAAAGCAGCTGAGAGCAGAGTCTCTGATCTTGA
2	B6	Rev Mitd1-1	ATTGTATGACATTAAATATCACGTTGATAACTCCTGTTAGAGCAGAGTCTCTGATCTTGA
2	C6	Rev Mitd1-2	ATTGTATGACATTAAATAACTTTGGTACCTGTCTCGGTAGAGCAGAGTCTCTGATCTTGA
2	D6	Rev Mlkl-1	ATTGTATGACATTAAATTATTCTCACATTTTCGGCCGTAGAGCAGAGTCTCTGATCTTGA
2	E6	Rev Mlkl-2	ATTGTATGACATTAAATTTGAATGGGAGCTCTCTGCGGAGAGCAGAGTCTCTGATCTTGA
2	F6	Rev Mov10-1	ATTGTATGACATTAAATTAGATCAGGACTTCATAGCCCAGAGCAGAGTCTCTGATCTTGA
2	G6	Rev Mov10-2	ATTGTATGACATTAAATTCGTGCATGTTAATCGTCCCTAGAGCAGAGTCTCTGATCTTGA

2	H6	Rev Myd88-1	ATTGTATGACATTAAATTTTGTGGGTGTGACACTGCGGAGAGCAGAGTCTCTGA TCTTGA
2	A7	Rev Myd88-2	ATTGTATGACATTAAATTAAGCTTATATTCTGTCTGGGAGAGCAGAGTCTCTGA TCTTGA
2	B7	Rev Nfkbia-1	ATTGTATGACATTAAATTAAATCGACAGCTTAGAAGGCAGAGCAGAGTCTCTG ATCTTGA
2	C7	Rev Nfkbia-2	ATTGTATGACATTAAATTTGTATCAATCTACAAGTCTCAGAGCAGAGTCTCTGA TCTTGA
2	D7	Rev Nmi-1	ATTGTATGACATTAAATTAGAATGGAATTCTACCTCTCAGAGCAGAGTCTCTGA TCTTGA
2	E7	Rev Nmi-2	ATTGTATGACATTAAATTTATTGCTGTTCATTATGCTTAGAGCAGAGTCTCTGAT CTTGA
2	F7	Rev Oas1a-1	ATTGTATGACATTAAATTAAGTTGGGATCTTCCTGGTGAGAGCAGAGTCTCTGA TCTTGA
2	G7	Rev Oas1a-2	ATTGTATGACATTAAATTTTGATCTCATCACCAAAGTGAGAGCAGAGTCTCTGA TCTTGA
2	H7	Rev Oas2-1	ATTGTATGACATTAAATTTCTCGTTTATGTTTGAGGGGAGAGCAGAGTCTCTGA TCTTGA
2	A8	Rev Oas2-2	ATTGTATGACATTAAATTATAAGTTCACCAGCTTCCGGAGAGCAGAGTCTCTGA TCTTGA
2	B8	Rev Oasl1-1	ATTGTATGACATTAAATTCTTCGGTCCCCTCTCTGGGGAGAGCAGAGTCTCTGA TCTTGA
2	C8	Rev Oasl1-2	ATTGTATGACATTAAATTTGTCGTTCATATACTGCTTTAGAGCAGAGTCTCTGAT CTTGA
2	D8	Rev Oasl2-1	ATTGTATGACATTAAATTTGAACTTGACACTGCAGGTCAGAGCAGAGTCTCTGA TCTTGA
2	E8	Rev Oasl2-2	ATTGTATGACATTAAATTATTTTCTTCGTAATCACGTCAGAGCAGAGTCTCTGAT CTTGA
2	F8	Rev p50 (RelB)-1	ATTGTATGACATTAAATAATCTTGGAGCATCTGTCCGTAGAGCAGAGTCTCTGA TCTTGA
2	G8	Rev p50 (RelB)-2	ATTGTATGACATTAAATTTTCGTGTCTGGTCCACACTTAGAGCAGAGTCTCTGAT CTTGA
2	H8	Rev p65 (RelA)-1	ATTGTATGACATTAAATTTGAATTTCTTATAGGTCCGGAGAGCAGAGTCTCTGA TCTTGA

2	A9	Rev p65 (RelA)-2	ATTGTATGACATTAAATTTGTTTTTCTTGATTCGCTTTAGAGCAGAGTCTCTGATCTTGA
2	B9	Rev Papr14-2	ATTGTATGACATTAAATTTGTTGTACATCATCTTCTGGAGAGCAGAGTCTCTGATCTTGA
2	C9	Rev Parp11-1	ATTGTATGACATTAAATTTGAAGTTTGTTATCCGGCGTAGAGCAGAGTCTCTGATCTTGA
2	D9	Rev Parp11-2	ATTGTATGACATTAAATTAACGTGGCGCAATCGAGCTTAGAGCAGAGTCTCTGATCTTGA
3	A1	Fw Parp12-1	ATTTAATGTCATACAATTTGGAAGCTACAACTCTTCCGAGAGCGGAGCCTACGGCTGCAC
3	B1	Fw Parp12-2	ATTTAATGTCATACAATTTGTGATCAGTCTTCAAGTTGAGAGCGGAGCCTACGGCTGCAC
3	C1	Fw Parp14-1	ATTTAATGTCATACAATTTGTTGATCAAGTTCTTTGGGAGAGCGGAGCCTACGGCTGCAC
3	D1	Fw Parp9-1	ATTTAATGTCATACAATTAGCTGACTCTCATTGCTCTTAGAGCGGAGCCTACGGCTGCAC
3	E1	Fw Parp9-2	ATTTAATGTCATACAATTTGTCTTGGAAATAAAGCCGGAGAGCGGAGCCTACGGCTGCAC
3	F1	Fw Plec-1	ATTTAATGTCATACAATTACAGGTCACTGATGTGCCTCAGAGCGGAGCCTACGGCTGCAC
3	G1	Fw Plec-2	ATTTAATGTCATACAATTAGCTTGCTCACAATGCGCTGAGAGCGGAGCCTACGGCTGCAC
3	H1	Fw Ppm1k-1	ATTTAATGTCATACAATTAAACTAGACTGACTTCTCTGAGAGCGGAGCCTACGGCTGCAC
3	A2	Fw Ppm1k-2	ATTTAATGTCATACAATTAGAGCAATAATAGTATTCCGAGAGCGGAGCCTACGGCTGCAC
3	B2	Fw Ppp3cb-1	ATTTAATGTCATACAATTTCTTCAGAACATCAACCCTGAGAGCGGAGCCTACGGCTGCAC
3	C2	Fw Ppp3cb-2	ATTTAATGTCATACAATTTAAATCTATCTAATCTCCTAAGAGCGGAGCCTACGGCTGCAC
3	D2	Fw Rnasel-1	ATTTAATGTCATACAATTAATCTTGGTCCATCTGACTTAGAGCGGAGCCTACGGCTGCAC
3	E2	Fw Rnasel-2	ATTTAATGTCATACAATTTTCTGTTCGTTCTCTCCGTCAGAGCGGAGCCTACGGCTGCAC

3	F2	Fw Rsad-1	ATTTAATGTCATACAATTTAACCTGCTCATCGAAGCTGAGAGCGGAGCCTACGG CTGCAC
3	G2	Fw Rsad-2	ATTTAATGTCATACAATTATTCTAATAACAACAGTCCGAGAGCGGAGCCTACGG CTGCAC
3	H2	Fw Rtp4-1	ATTTAATGTCATACAATTTCTTGAAATGTCTGCTCCCAAGAGCGGAGCCTACGG CTGCAC
3	A3	Fw Rtp4-2	ATTTAATGTCATACAATTTTATTTAATCAACATAGCTTAGAGCGGAGCCTACGG CTGCAC
3	B3	Fw Samd9l-1	ATTTAATGTCATACAATTTGGTGGTCTTAACCAGTCTGAGAGCGGAGCCTACGG CTGCAC
3	C3	Fw Samd9l-2	ATTTAATGTCATACAATTTCTCTGGAATCTTGATTGTGAGAGCGGAGCCTACGG CTGCAC
3	D3	Fw Sfxn2-1	ATTTAATGTCATACAATTTGTTCACAAACTACAGACTGAGAGCGGAGCCTACGG CTGCAC
3	E3	Fw Sfxn2-2	ATTTAATGTCATACAATTAGAACTGGAGCATGAAGCCCAGAGCGGAGCCTACG GCTGCAC
3	F3	Fw Sh3bgrl-1	ATTTAATGTCATACAATTATACACGGATCACCATCCTGAGAGCGGAGCCTACGG CTGCAC
3	G3	Fw Sh3bgrl-2	ATTTAATGTCATACAATTAACATATGAACATAACCTGTAGAGCGGAGCCTACGG CTGCAC
3	H3	Fw Stat1-1	ATTTAATGTCATACAATTTTACTGTCCAGCTCCTTCTGAGAGCGGAGCCTACGG CTGCAC
3	A4	Fw Stat1-2	ATTTAATGTCATACAATTTTAAAGTCATATTCATCTTGAGAGCGGAGCCTACGG CTGCAC
3	B4	Fw Stat2-1	ATTTAATGTCATACAATTTCTGGTCTTCAATCCAGGTAAGAGCGGAGCCTACGG CTGCAC
3	C4	Fw Stat2-2	ATTTAATGTCATACAATTTCTGCAACATCTCCCACTGCAGAGCGGAGCCTACGG CTGCAC
3	D4	Fw Stat3-1	ATTTAATGTCATACAATTTAAGTTTCTGAACAGCTCCAAGAGCGGAGCCTACGG CTGCAC
3	E4	Fw Stat3-2	ATTTAATGTCATACAATTTGAAATCAAAGTCGTCCTGGAGAGCGGAGCCTACGG CTGCAC
3	F4	Fw Tap1-1	ATTTAATGTCATACAATTTTAGAGGAAGAAGAAACCGAAGAGCGGAGCCTACG GCTGCAC

3	G4	Fw Tap1-2	ATTTAATGTCATACAATTTCTCCATGAATCTCATTCTCAGAGCGGAGCCTACGG CTGCAC
3	H4	Fw Tapbp-1	ATTTAATGTCATACAATTAGCTTTGGGTCAAGATCTGGAGAGCGGAGCCTACGG CTGCAC
3	A5	Fw Tapbp-2	ATTTAATGTCATACAATATAGTGAACTCCATGCTGCTTAGAGCGGAGCCTACGG CTGCAC
3	B5	Fw Tbk1-1	ATTTAATGTCATACAATTCTCATTTGAACATCCACTGGAGAGCGGAGCCTACGG CTGCAC
3	C5	Fw Tbk1-2	ATTTAATGTCATACAATTTGATTTGAGGAAACAATCTTAGAGCGGAGCCTACGG CTGCAC
3	D5	Fw Ticam1-1	ATTTAATGTCATACAATTTGAGCTGGTAGATCTCCCGGAGAGCGGAGCCTACGG CTGCAC
3	E5	Fw Ticam1-2	ATTTAATGTCATACAATTTGATATCTGAACTGCACCGAAGAGCGGAGCCTACGG CTGCAC
3	F5	Fw Tlr3-1	ATTTAATGTCATACAATTTAGATAAGAGGAACACCCTTAGAGCGGAGCCTACG GCTGCAC
3	G5	Fw Tlr3-2	ATTTAATGTCATACAATTAAAGTCGAACTTAATCTCTTAGAGCGGAGCCTACGG CTGCAC
3	H5	Fw Tlr7-1	ATTTAATGTCATACAATTTTACTTTAACTTCACAAGGTAGAGCGGAGCCTACGG CTGCAC
3	A6	Fw Tlr7-2	ATTTAATGTCATACAATTAGAGTGGTTCTATAGATGGAAGAGCGGAGCCTACGG CTGCAC
3	B6	Fw Tlr9-1	ATTTAATGTCATACAATTATAGCTCAAGTTCAGCTCCTAGAGCGGAGCCTACGG CTGCAC
3	C6	Fw Tlr9-2	ATTTAATGTCATACAATTTAGCATCTAGAACCAGGATGAGAGCGGAGCCTACG GCTGCAC
3	D6	Fw Tmem140-1	ATTTAATGTCATACAATTATCTTCTGCTGTTGCAGGGAAGAGCGGAGCCTACGG CTGCAC
3	E6	Fw Tmem140-2	ATTTAATGTCATACAATTTCTAGTTTGACACTTTGCCAAGAGCGGAGCCTACGG CTGCAC
3	F6	Fw Tor3a-1	ATTTAATGTCATACAATTACGTGTCCACATACTTGGGGAGAGCGGAGCCTACGG CTGCAC
3	G6	Fw Tor3a-2	ATTTAATGTCATACAATTAAGCCTGTCAAGTTGTTGGAAGAGCGGAGCCTACGG CTGCAC

3	H6	Fw Trex1-1	ATTTAATGTCATACAATTATGTGAGTCTGTCGGTGCTTAGAGCGGAGCCTACGGCTGCAC
3	A7	Fw Trex1-2	ATTTAATGTCATACAATTAGGTTGGTTGTTCCAGTGGTAGAGCGGAGCCTACGGCTGCAC
3	B7	Fw Trim21-1	ATTTAATGTCATACAATTAGAGGGTGATATCTGCCGTGAGAGCGGAGCCTACGGCTGCAC
3	C7	Fw Trim21-2	ATTTAATGTCATACAATTTAGTTATGTGCTCCCAGCTTAGAGCGGAGCCTACGGCTGCAC
3	D7	Fw Trim25-1	ATTTAATGTCATACAATTTTAACTTGCGCAAGGAGCTGAGAGCGGAGCCTACGGCTGCAC
3	E7	Fw Trim25-2	ATTTAATGTCATACAATTTCATTTCCATATACTCCTGTAGAGCGGAGCCTACGGCTGCAC
3	F7	Fw Wwoxv-1	ATTTAATGTCATACAATATCTCTAAAGAATTGCTTGTGAGAGCGGAGCCTACGGCTGCAC
3	G7	Fw Wwoxv-2	ATTTAATGTCATACAATTATCAGGTTATTCTAAGGTTGAGAGCGGAGCCTACGGCTGCAC
3	H7	Fw Zc3hav1-1	ATTTAATGTCATACAATTTAGTGAACTTCATCTCTCCAAGAGCGGAGCCTACGGCTGCAC
3	A8	Fw Zc3hav1-2	ATTTAATGTCATACAATTATTCGTCTGAATCATCCCTTAGAGCGGAGCCTACGGCTGCAC
3	B8	Fw Zfp182-1	ATTTAATGTCATACAATTTGTTTATCTTGATGTTGCCTAGAGCGGAGCCTACGGCTGCAC
3	C8	Fw Zfp182-2	ATTTAATGTCATACAATTTGTCTACCATAGTATTTCCAAGAGCGGAGCCTACGGCTGCAC
3	D8	Fw Isg15-1	ATTTAATGTCATACAATTGCTTGATCACTGTGCACTGGAGAGCGGAGCCTACGGCTGCAC
3	E8	Fw Isg15-2	ATTTAATGTCATACAATTTAAGCGTGTCTACAGTCTGCAGAGCGGAGCCTACGGCTGCAC
3	F8	Fw Ifi27-1	ATTTAATGTCATACAATTTGAGCTGATAGAAGTGTCATAGAGCGGAGCCTACGGCTGCAC
3	G8	Fw Ifi27-2	ATTTAATGTCATACAATTTGATGTGGAGAGTCCAAGGAAGAGCGGAGCCTACGGCTGCAC
3	H8	Fw Usp18-1	ATTTAATGTCATACAATTATTTCAGACTGTTCCTTGGTAGAGCGGAGCCTACGGCTGCAC

3	A9	Fw Usp18-2	ATTTAATGTCATACAATATGTTCATCATGAACACTTGAAGAGCGGAGCCTACGGCTGCAC
3	B9	Fw Parp10-1	ATTTAATGTCATACAATTTAAGGACTTTGTAGAGCAGGAGAGCGGAGCCTACGGCTGCAC
3	C9	Fw Parp10-2	ATTTAATGTCATACAATTTGGAGACTCACTGTCTCCTCAGAGCGGAGCCTACGGCTGCAC
3	D9	Fw miR-124	ATTTAATGTCATACAATTAAGGCACGCGGTGAATGCCAAGAGCGGAGCCTACGGCTGCAC
3	A1	Rev Parp12-1	ATTGTATGACATTAAATTTGGACTCTATAACTCTTCTTAGAGCAGAGTCTCTGATCTTGA
3	B1	Rev Parp12-2	ATTGTATGACATTAAATTTGTGCGCAGGCTTCAAGTGTAGAGCAGAGTCTCTGATCTTGA
3	C1	Rev Parp14-1	ATTGTATGACATTAAATTTGTTTCTCACGTTCTTTGTTAGAGCAGAGTCTCTGATCTTGA
3	D1	Rev Parp9-1	ATTGTATGACATTAAATTAGCTTCCTCGCATTGCTCGGAGAGCAGAGTCTCTGATCTTGA
3	E1	Rev Parp9-2	ATTGTATGACATTAAATTTGTCGGGGACATAAAGCCTTAGAGCAGAGTCTCTGATCTTGA
3	F1	Rev Plec-1	ATTGTATGACATTAAATTACAGTGCACGGATGTGCCGTAGAGCAGAGTCTCTGATCTTGA
3	G1	Rev Plec-2	ATTGTATGACATTAAATTAGCTGTCTCCCAATGCGCGTAGAGCAGAGTCTCTGATCTTGA
3	H1	Rev Ppm1k-1	ATTGTATGACATTAAATTAAACGCGACGGACTTCTCGTAGAGCAGAGTCTCTGATCTTGA
3	A2	Rev Ppm1k-2	ATTGTATGACATTAAATTAGAGTCATACTAGTATTCTTAGAGCAGAGTCTCTGATCTTGA
3	B2	Rev Ppp3cb-1	ATTGTATGACATTAAATTTCTTTCGAATATCAACCCGTAGAGCAGAGTCTCTGATCTTGA
3	C2	Rev Ppp3cb-2	ATTGTATGACATTAAATTTAAAGTTATTTAATCTCCGCAGAGCAGAGTCTCTGATCTTGA
3	D2	Rev Rnasel-1	ATTGTATGACATTAAATTAATCGGGGTTCATCTGACGGAGAGCAGAGTCTCTGATCTTGA
3	E2	Rev Rnasel-2	ATTGTATGACATTAAATTTTCTTGTCGGTCTCTCCGGTAGAGCAGAGTCTCTGATCTTGA

3	F2	Rev Rsad-1	ATTGTATGACATTAAATTTAACTGGCTTATCGAAGCGTAGAGCAGAGTCTCTGATCTTGA
3	G2	Rev Rsad-2	ATTGTATGACATTAAATTATTCGCATACCAACAGTCTTAGAGCAGAGTCTCTGATCTTGA
3	H2	Rev Rtp4-1	ATTGTATGACATTAAATTTCTTTCAATTTCTGCTCCTCAGAGCAGAGTCTCTGATCTTGA
3	A3	Rev Rtp4-2	ATTGTATGACATTAAATTTTATGGAATTAACATAGCGGAGAGCAGAGTCTCTGATCTTGA
3	B3	Rev Samd9l-1	ATTGTATGACATTAAATTTGGTTTTCTGAACCAGTCGTAGAGCAGAGTCTCTGATCTTGA
3	C3	Rev Samd9l-2	ATTGTATGACATTAAATTTCTCGTGAAGCTTGATTGGTAGAGCAGAGTCTCTGATCTTGA
3	D3	Rev Sfxn2-1	ATTGTATGACATTAAATTTGTTTCCAACCTACAGACGTAGAGCAGAGTCTCTGATCTTGA
3	E3	Rev Sfxn2-2	ATTGTATGACATTAAATTAGAATGGGATCATGAAGCTTAGAGCAGAGTCTCTGATCTTGA
3	F3	Rev Sh3bgrl-1	ATTGTATGACATTAAATTATACCTGGAGCACCATCCGTAGAGCAGAGTCTCTGATCTTGA
3	G3	Rev Sh3bgrl-2	ATTGTATGACATTAAATTAACAGCTGACCATAACCTTGAGAGCAGAGTCTCTGATCTTGA
3	H3	Rev Stat1-1	ATTGTATGACATTAAATTTTACGTTCCCGCTCCTTCGTAGAGCAGAGTCTCTGATCTTGA
3	A4	Rev Stat1-2	ATTGTATGACATTAAATTTTAACTTCAGATTCATCTGTAGAGCAGAGTCTCTGATCTTGA
3	B4	Rev Stat2-1	ATTGTATGACATTAAATTTCTGTGCTTTAATCCAGGGCAGAGCAGAGTCTCTGATCTTGA
3	C4	Rev Stat2-2	ATTGTATGACATTAAATTTCTGTCACAGCTCCCACTTTAGAGCAGAGTCTCTGATCTTGA
3	D4	Rev Stat3-1	ATTGTATGACATTAAATTTAAGGGTCTTAACAGCTCTCAGAGCAGAGTCTCTGATCTTGA
3	E4	Rev Stat3-2	ATTGTATGACATTAAATTTGAACGCAACGTCGTCCTTTAGAGCAGAGTCTCTGATCTTGA
3	F4	Rev Tap1-1	ATTGTATGACATTAAATTTTAGCTGAATAAGAAACCTCAGAGCAGAGTCTCTGATCTTGA

3	G4	Rev Tap1-2	ATTGTATGACATTAAATTTCTCTCTGACTCTCATTCGTAGAGCAGAGTCTCTGATCTTGA
3	H4	Rev Tapbp-1	ATTGTATGACATTAAATTAGCTGGGGGGCAAGATCTTTAGAGCAGAGTCTCTGATCTTGA
3	A5	Rev Tapbp-2	ATTGTATGACATTAAATATAGTTCACTTCATGCTGCGGAGAGCAGAGTCTCTGATCTTGA
3	B5	Rev Tbk1-1	ATTGTATGACATTAAATTCTCAGGTGACCATCCACTTTAGAGCAGAGTCTCTGATCTTGA
3	C5	Rev Tbk1-2	ATTGTATGACATTAAATTTGATGGGAGTAAACAATCGGAGAGCAGAGTCTCTGATCTTGA
3	D5	Rev Ticam1-1	ATTGTATGACATTAAATTTGAGTGGGTCGATCTCCCTTAGAGCAGAGTCTCTGATCTTGA
3	E5	Rev Ticam1-2	ATTGTATGACATTAAATTTGATCGCTGCACTGCACCTCAGAGCAGAGTCTCTGATCTTGA
3	F5	Rev Tlr3-1	ATTGTATGACATTAAATTTAGAGCAGATGAACACCCGGAGAGCAGAGTCTCTGATCTTGA
3	G5	Rev Tlr3-2	ATTGTATGACATTAAATTAAAGGTGAATTTAATCTCGGAGAGCAGAGTCTCTGATCTTGA
3	H5	Rev Tlr7-1	ATTGTATGACATTAAATTTTACGGTAATTTCACAAGTGAGAGCAGAGTCTCTGATCTTGA
3	A6	Rev Tlr7-2	ATTGTATGACATTAAATTAGAGGTGTTTTATAGATGTCAGAGCAGAGTCTCTGATCTTGA
3	B6	Rev Tlr9-1	ATTGTATGACATTAAATTATAGTGCAATTTCAGCTCTGAGAGCAGAGTCTCTGATCTTGA
3	C6	Rev Tlr9-2	ATTGTATGACATTAAATTTAGCCGCTATAACCAGGAGTAGAGCAGAGTCTCTGATCTTGA
3	D6	Rev Tmem140-1	ATTGTATGACATTAAATTATCTGTTGCGGTTGCAGGTCAGAGCAGAGTCTCTGATCTTGA
3	E6	Rev Tmem140-2	ATTGTATGACATTAAATTTCTATGTTGCCACTTTGCTCAGAGCAGAGTCTCTGATCTTGA
3	F6	Rev Tor3a-1	ATTGTATGACATTAAATTACGTTGCCATATACTTGGTTAGAGCAGAGTCTCTGATCTTGA
3	G6	Rev Tor3a-2	ATTGTATGACATTAAATTAAGCTGGTCCAGTTGTTGTCAGAGCAGAGTCTCTGATCTTGA

3	H6	Rev Trex1-1	ATTGTATGACATTAAATTATGTTCGTCGGTCGGTGCGGAGAGCAGAGTCTCTGA TCTTGA
3	A7	Rev Trex1-2	ATTGTATGACATTAAATTAGGTGTGTTTTTCCAGTGTGAGAGCAGAGTCTCTGA TCTTGA
3	B7	Rev Trim21-1	ATTGTATGACATTAAATTAGAGTTTGAGATCTGCCGGTAGAGCAGAGTCTCTGA TCTTGA
3	C7	Rev Trim21-2	ATTGTATGACATTAAATTTAGTGCTGTTCTCCCAGCGGAGAGCAGAGTCTCTGA TCTTGA
3	D7	Rev Trim25-1	ATTGTATGACATTAAATTTTAATGTGCTCAAGGAGCGTAGAGCAGAGTCTCTGA TCTTGA
3	E7	Rev Trim25-2	ATTGTATGACATTAAATTTCATGGCCAGATACTCCTTGAGAGCAGAGTCTCTGA TCTTGA
3	F7	Rev Wwoxv-1	ATTGTATGACATTAAATATCTCGCAAGCATTGCTTGGTAGAGCAGAGTCTCTGA TCTTGA
3	G7	Rev Wwoxv-2	ATTGTATGACATTAAATTATCATTTTAGTCTAAGGTGTAGAGCAGAGTCTCTGA TCTTGA
3	H7	Rev Zc3hav1-1	ATTGTATGACATTAAATTTAGTTCACTGCATCTCTCTCAGAGCAGAGTCTCTGAT CTTGA
3	A8	Rev Zc3hav1-2	ATTGTATGACATTAAATTATTCTGCTGCATCATCCCGGAGAGCAGAGTCTCTGA TCTTGA
3	B8	Rev Zfp182-1	ATTGTATGACATTAAATTTGTTGCTCTGGATGTTGCTGAGAGCAGAGTCTCTGA TCTTGA
3	C8	Rev Zfp182-2	ATTGTATGACATTAAATTTGTCGCCCAGAGTATTTCTCAGAGCAGAGTCTCTGA TCTTGA
3	D8	Rev Isg15-1	ATTGTATGACATTAAATTGAATTCTCATTGTGCACTTTAGAGCAGAGTCTCTGAT CTTGA
3	E8	Rev Isg15-2	ATTGTATGACATTAAATTTAAGTTTGTTTACAGTCTTTAGAGCAGAGTCTCTGAT CTTGA
3	F8	Rev Ifi27-1	ATTGTATGACATTAAATTTAAGTGGATCGAAGTGTCCGAGAGCAGAGTCTCTGA TCTTGA
3	G8	Rev Ifi27-2	ATTGTATGACATTAAATTTAATTGGGATAGTCCAAGTCAGAGCAGAGTCTCTGA TCTTGA
3	H8	Rev Usp18-1	ATTGTATGACATTAAATTAAATTCGACGGTTCCTTGTGAGAGCAGAGTCTCTGA TCTTGA

3	A9	Rev Usp18-2	ATTGTATGACATTAAATATAATTCTCAGGAACACTTTCAGAGCAGAGTCTCTGATCTTGA
3	B9	Rev Parp10-1	ATTGTATGACATTAAATTTAAGTCCTTGGTAGAGCATTAGAGCAGAGTCTCTGATCTTGA
3	C9	Rev Parp10-2	ATTGTATGACATTAAATTTAAATCCTCCCTGTCTCCGTAGAGCAGAGTCTCTGATCTTGA
3	D9	Rev miR-124	ATTGTATGACATTAAATCAAGGTCCGCTGTGAACACGGAGAGCAGAGTCTCTGATCTTGA

Appendix 2

Salmon transcript workflow used to analyse deep sequencing results

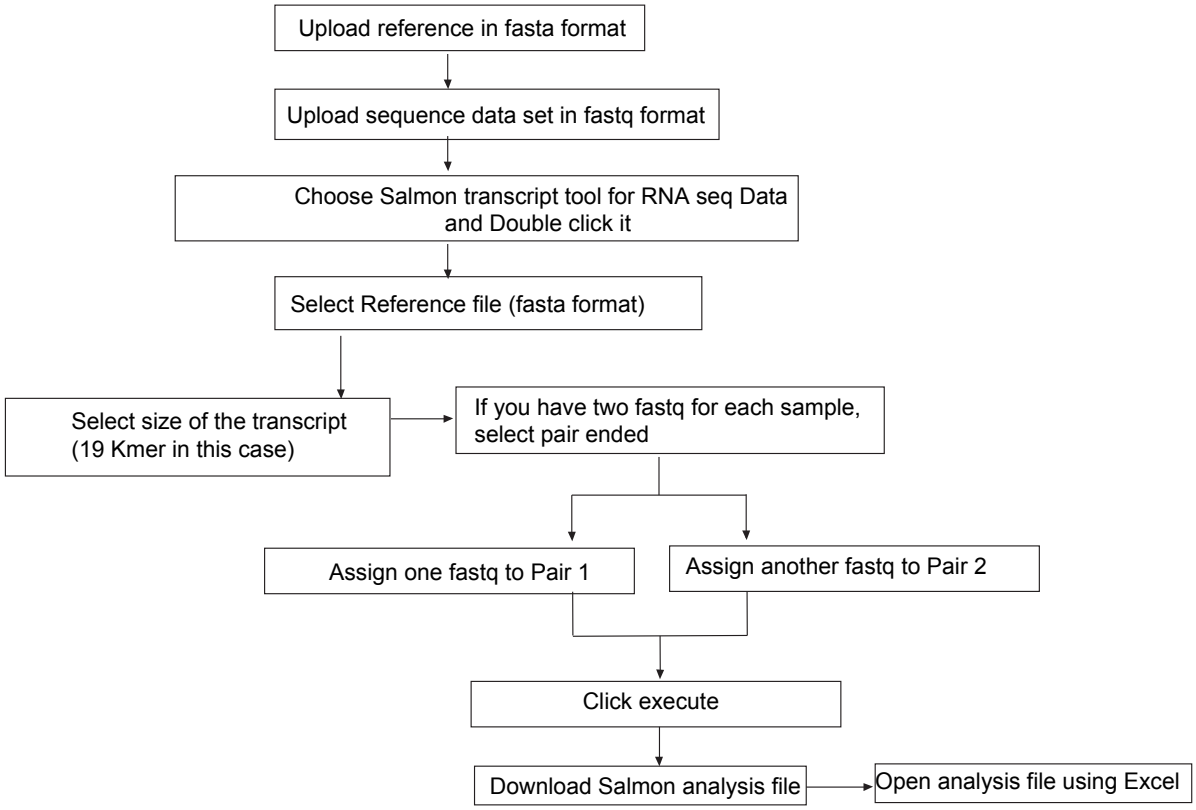

Appendix 3

I*n vitro* RNAi screening results computed into percentage enrichment of amiR-encoding viruses

WT MEF Experiment 1

	Percentage					
Name	**PLASMID LIB**	**P0-293T**	**P1-VERO**	**P2-WT**	**P3-WT**	**P4-WT**
Adar-1	0.00	0.00	0.00	0.00	0.00	0.00
Adar-2	0.66	0.16	0.09	0.09	0.00	0.00
Atf2-1	0.41	0.18	0.10	0.39	0.00	0.00
Atf2-2	1.19	0.48	0.50	0.44	0.00	0.00
Atf3-1	0.58	0.46	0.37	0.22	0.00	0.00
Atf3-2	1.95	2.44	3.41	4.22	0.02	0.00
B2m-1	0.69	0.22	0.15	0.30	0.00	0.00
B2m-2	0.37	0.41	0.42	0.25	0.00	0.00
Birc6-1	0.49	0.28	0.27	0.64	0.00	0.00
Birc6-2	0.51	0.35	0.24	0.21	0.00	0.00
Brd4-1	0.45	1.25	1.73	1.79	0.02	0.00
Brd4-2	0.62	0.54	0.54	0.55	0.00	0.00
Cdkl4-1	0.63	0.67	0.56	0.37	0.00	0.00
Cdkl4-2	0.60	0.34	0.21	0.17	0.00	0.00
Clec4d-1	0.49	0.41	0.25	0.26	0.00	0.00
Clec4d-2	0.61	0.48	0.41	0.30	0.00	0.00
Clec4e-1	0.48	0.85	0.95	0.78	0.01	0.00
Clec4e-2	0.52	0.30	0.16	0.10	0.00	0.00
Cmpk2-1	1.56	0.69	0.44	0.41	0.00	0.00
Cmpk2-2	0.72	0.13	0.08	0.08	0.00	0.00
Cpeb3-1	0.01	0.08	0.12	0.09	0.00	0.00
Cpeb3-2	0.74	0.22	0.20	0.16	0.00	0.00
Cxcl10-1	0.56	0.66	0.77	0.58	0.00	0.00
Cxcl10-2	0.57	0.46	0.33	0.16	0.00	0.01
Cytip-1	0.62	0.38	0.20	0.25	0.00	0.00
Cytip-2	0.64	0.66	0.67	0.41	0.00	0.00

Daxx-1	0.41	1.16	1.42	0.71	0.00	0.00
Daxx-2	0.85	0.22	0.10	0.56	0.00	0.00
Ddx58-1	0.55	0.50	0.53	1.49	0.00	0.00
Ddx58-2	0.53	0.60	0.57	0.39	0.00	0.00
Ddx60-1	0.66	0.20	0.10	0.11	0.00	0.00
Ddx60-2	0.88	0.26	0.15	0.12	0.00	0.00
Dhx9-1	0.73	0.77	0.59	0.54	0.00	0.00
Dhx9-2	0.46	0.28	0.27	0.72	0.00	0.00
Dtx3l-1	0.69	0.84	0.76	1.15	0.01	0.00
Dtx3l-2	0.52	0.45	0.44	0.90	0.00	0.00
EGFP	0.49	0.02	0.02	0.03	0.00	0.00
Eif2ak2-1	0.53	0.56	0.48	0.29	0.00	0.00
Eif2ak2-2	0.49	0.27	0.29	0.68	0.00	0.00
Fa2h-1	0.75	0.44	0.25	0.19	0.00	0.00
Fa2h-2	0.68	0.26	0.16	0.14	0.00	0.00
Fbxo39-1	0.59	0.97	1.10	1.42	0.00	0.00
Fbxo39-2	0.63	0.25	0.15	0.12	0.01	0.01
Gbp2-1	0.78	0.30	0.20	0.17	0.00	0.00
Gbp2-2	0.53	1.77	2.29	4.39	0.01	0.00
Gbp3-1	0.52	0.54	0.45	0.23	0.00	0.00
Gbp3-2	0.62	0.76	0.72	0.63	0.01	0.00
Gbp6-1	0.00	1.17	1.43	1.37	0.00	0.00
Gbp6-2	0.13	0.00	0.00	0.00	0.00	0.00
Gcc-1	0.63	0.21	0.16	0.09	0.00	0.00
Gcc-2	0.51	0.79	0.88	0.62	0.01	0.01
Gvin-1	0.49	0.71	0.66	0.85	0.00	0.00
Gvin-2	0.39	0.72	0.71	0.54	0.00	0.00
Ifi27-1	0.52	1.24	1.18	1.74	0.00	0.00
Ifi27-2	0.61	1.38	1.82	1.42	0.01	0.00
Ifi35-1	0.39	0.21	0.10	0.16	0.00	0.00
Ifi35-2	0.45	2.14	2.54	1.76	0.02	0.00
Ifi44-1	0.41	0.84	0.76	0.55	0.00	0.00
Ifi44-2	0.46	0.50	0.61	0.35	0.00	0.00
Ifih1-1	0.51	0.21	0.12	0.07	0.01	0.00

Ifih1-2	0.68	1.01	1.32	0.76	0.01	0.00
Ifit1-1	0.86	0.15	0.12	0.14	0.00	0.00
Ifit1-2	0.45	0.48	0.40	0.60	0.00	0.00
Ifit3-1	0.47	0.47	0.34	0.57	0.00	0.00
Ifit3-2	0.58	0.44	0.30	0.44	0.00	0.00
Ifitm3-1	0.61	0.60	0.58	0.33	0.01	0.00
Ifitm3-2	0.90	0.61	0.92	1.75	96.71	90.19
Ifna1-1	0.48	0.66	0.54	0.32	0.02	0.01
Ifna1-2	0.65	0.36	0.37	0.25	0.00	0.00
Ifna4-1	0.29	0.65	0.56	1.25	0.00	0.00
Ifna4-2	0.48	0.29	0.26	0.23	0.00	0.00
Ifnb1-1	0.90	0.49	0.34	0.20	0.00	0.00
Ifnb1-2	0.39	0.30	0.49	0.28	0.01	0.00
Ikbka-1	0.55	0.16	0.12	0.10	0.00	0.00
Ikbka-2	0.53	0.34	0.22	0.18	0.00	0.00
Ikbkb-1	0.48	0.51	0.36	0.35	0.00	0.00
Ikbkb-2	0.61	0.70	0.59	0.94	0.00	0.00
Ikbke-1	1.25	0.56	0.49	0.23	0.01	0.00
Ikbke-2	0.61	0.68	0.59	0.30	0.00	0.00
Il15-1	0.55	0.57	0.36	0.23	0.00	0.00
Il15-2	0.56	0.70	0.58	0.25	0.00	0.00
Il6-1	0.78	0.60	0.59	0.41	0.00	0.00
Il6-2	0.52	0.62	0.58	0.48	0.01	0.00
Irf1-1	0.69	0.23	0.14	0.69	0.00	0.00
Irf1-2	0.51	0.26	0.17	0.12	0.00	0.00
Irf2-1	0.56	0.49	0.50	0.36	0.00	0.00
Irf2-2	0.67	0.50	0.34	0.67	0.00	0.00
Irf3-1	0.57	0.24	0.24	0.16	0.00	0.00
Irf3-2	0.68	0.42	0.32	0.24	0.00	0.00
Irf5-1	0.62	0.30	0.22	0.13	0.00	0.00
Irf5-2	0.61	0.16	0.05	0.37	0.00	0.00
Irf7-1	0.36	0.81	0.57	1.29	1.71	7.57
Irf7-2	0.57	1.36	1.97	2.49	0.01	0.00
Irf9-1	0.44	0.28	0.27	0.28	0.00	0.00

Irf9-2	0.51	0.27	0.20	0.15	0.00	0.00
Irgm-1	0.54	0.27	0.19	0.36	0.00	0.00
Irgm-2	0.58	0.81	1.05	0.68	0.01	0.00
Isg15-1	0.54	1.02	1.40	0.94	0.01	0.00
Isg15-2	0.53	0.24	0.22	0.14	0.00	0.00
Lgals3bp-1	0.58	0.64	0.72	0.63	0.00	0.00
Lgals3bp-2	0.71	0.31	0.25	0.13	0.00	0.01
Lgals8-1	0.80	0.60	0.50	1.02	0.01	0.00
Lgals8-2	0.45	0.13	0.10	0.06	0.00	0.00
Lrp4-1	0.65	0.21	0.08	0.07	0.00	0.00
Lrp4-2	0.51	0.53	0.50	1.02	0.00	0.00
Ly6e-1	0.45	0.21	0.13	0.13	0.02	0.01
Ly6e-2	0.37	0.44	0.44	0.47	0.00	0.01
Map3K8-1	0.49	0.63	0.59	0.50	0.00	0.00
Map3K8-2	0.52	0.50	0.31	0.44	0.01	0.01
Map4k2-1	0.45	0.60	0.44	0.50	0.78	1.74
Map4k2-2	0.44	0.35	0.21	0.13	0.00	0.00
Mapk8-1	0.54	0.64	0.54	0.31	0.00	0.00
Mapk8-2	0.62	0.61	0.59	0.34	0.00	0.00
Mbnl1-1	0.44	0.34	0.30	0.31	0.00	0.00
Mbnl1-2	0.50	0.29	0.19	0.08	0.00	0.00
miR-124	0.58	0.24	0.15	0.11	0.00	0.04
Mitd1-1	0.66	0.14	0.10	0.07	0.02	0.01
Mitd1-2	0.35	0.30	0.26	0.21	0.00	0.00
Mlkl-1	0.31	0.33	0.39	0.77	0.00	0.00
Mlkl-2	0.33	1.33	2.29	1.90	0.00	0.00
Mov10-1	0.46	0.78	0.93	1.41	0.00	0.00
Mov10-2	0.32	0.53	0.38	0.25	0.00	0.00
Myd88-1	0.35	0.56	0.49	0.29	0.00	0.00
Myd88-2	0.52	0.23	0.20	0.96	0.01	0.01
Nfkbia-1	0.33	0.51	0.49	0.26	0.01	0.01
Nfkbia-2	0.45	0.27	0.18	0.10	0.00	0.00
Nmi-1	0.53	0.78	0.84	1.62	0.01	0.00
Nmi-2	0.53	2.74	4.58	2.55	0.01	0.00

Oas1a-1	0.41	0.22	0.16	0.46	0.00	0.00
Oas1a-2	0.47	0.26	0.19	0.11	0.00	0.00
Oas2-1	0.50	0.26	0.12	0.53	0.00	0.00
Oas2-2	0.94	0.28	0.17	0.09	0.00	0.00
Oasl1-1	0.41	0.71	0.84	1.35	0.00	0.00
Oasl1-2	0.22	0.57	0.43	0.27	0.00	0.00
Oasl2-1	0.59	0.51	0.40	0.34	0.00	0.00
Oasl2-2	0.23	0.52	0.34	0.18	0.00	0.00
p50	0.50	0.53	0.53	0.34	0.01	0.00
p50	0.26	0.40	0.31	0.27	0.00	0.00
p65	0.35	0.38	0.26	0.18	0.00	0.00
p65	0.30	0.18	0.11	0.15	0.00	0.00
Papr14-2	0.34	0.57	0.47	0.27	0.00	0.00
Parp10-1	0.25	0.13	0.12	0.08	0.00	0.00
Parp10-2	0.42	0.78	0.85	1.12	0.00	0.00
Parp11-1	0.34	0.04	0.02	0.03	0.00	0.00
Parp11-2	0.38	0.27	0.18	0.20	0.00	0.00
Parp12-1	0.24	0.12	0.08	0.04	0.03	0.04
Parp12-2	0.33	0.42	0.39	0.32	0.00	0.00
Parp14-1	0.13	0.48	0.43	0.22	0.01	0.00
Parp9-1	0.35	0.06	0.06	0.03	0.00	0.00
Parp9-2	0.37	0.28	0.29	0.30	0.00	0.00
Plec-1	0.37	0.12	0.05	0.06	0.00	0.00
Plec-2	0.26	0.12	0.04	0.04	0.00	0.00
Ppm1k-1	0.38	0.24	0.22	0.13	0.00	0.00
Ppm1k-2	0.22	0.38	0.29	0.14	0.02	0.01
Ppp3cb-1	0.37	0.23	0.12	0.11	0.00	0.00
Ppp3cb-2	0.47	0.48	0.43	0.25	0.00	0.00
Rnasel-1	0.33	0.74	0.90	1.05	0.00	0.00
Rnasel-2	0.30	0.24	0.20	0.19	0.00	0.00
Rsad-1	1.00	0.45	0.36	0.25	0.00	0.00
Rsad-2	0.26	0.36	0.28	0.19	0.01	0.00
Rtp4-1	0.33	0.57	0.60	0.36	0.00	0.00
Rtp4-2	1.14	1.09	1.35	0.59	0.01	0.00

Samd9l-1	0.32	0.26	0.20	0.13	0.00	0.00
Samd9l-2	0.33	0.18	0.11	0.07	0.01	0.00
Sfxn2-1	0.31	0.27	0.20	0.17	0.00	0.00
Sfxn2-2	1.22	0.20	0.11	0.06	0.00	0.00
Sh3bgrl-1	0.25	0.60	0.46	0.50	0.01	0.00
Sh3bgrl-2	0.30	0.10	0.07	0.05	0.00	0.00
Stat1-1	0.50	0.21	0.15	0.12	0.00	0.00
Stat1-2	0.32	1.87	1.45	0.87	0.01	0.00
Stat2-1	0.29	0.50	0.46	0.50	0.01	0.00
Stat2-2	0.25	0.23	0.21	0.34	0.00	0.00
Stat3-1	0.31	0.45	0.46	0.24	0.01	0.01
Stat3-2	0.35	0.89	0.64	0.52	0.00	0.00
Tap1-1	0.26	0.26	0.22	0.12	0.00	0.00
Tap1-2	0.21	0.86	0.95	0.54	0.00	0.00
Tapbp-1	0.21	0.85	1.13	1.71	0.06	0.01
Tapbp-2	0.28	0.25	0.20	0.31	0.00	0.00
Tbk1-1	0.32	0.64	0.80	0.77	0.01	0.00
Tbk1-2	0.19	0.91	0.99	0.47	0.00	0.00
Ticam1-1	0.27	0.05	0.03	0.03	0.00	0.00
Ticam1-2	0.28	0.21	0.18	0.09	0.00	0.00
Tlr3-1	0.32	0.06	0.02	0.03	0.00	0.00
Tlr3-2	0.38	1.11	1.80	2.20	0.01	0.00
Tlr7-1	0.34	0.61	0.83	0.46	0.01	0.00
Tlr7-2	0.32	0.25	0.16	0.20	0.00	0.00
Tlr9-1	0.29	0.11	0.10	0.21	0.02	0.01
Tlr9-2	0.32	0.17	0.12	0.11	0.00	0.00
Tmem140-1	0.30	0.14	0.08	0.09	0.00	0.00
Tmem140-2	0.28	0.33	0.30	0.79	0.00	0.05
Tor3a-1	0.25	0.21	0.21	0.38	0.00	0.00
Tor3a-2	0.26	0.28	0.26	0.16	0.00	0.00
Trex1-1	0.26	0.10	0.03	0.08	0.00	0.00
Trex1-2	0.28	0.16	0.09	0.06	0.00	0.00
Trim21-1	0.34	0.41	0.56	0.55	0.00	0.00
Trim21-2	0.34	0.34	0.28	0.20	0.00	0.00

Trim25-1	0.38	0.14	0.10	0.17	0.00	0.00
Trim25-2	0.30	0.35	0.32	0.24	0.00	0.00
Usp18-1	0.57	0.36	0.40	0.21	0.00	0.00
Usp18-2	0.31	0.34	0.53	0.55	0.00	0.00
Wwoxv-1	0.15	0.12	0.11	0.07	0.03	0.03
Wwoxv-2	0.29	0.22	0.22	0.16	0.00	0.00
Zc3hav1-1	0.20	0.18	0.13	0.07	0.01	0.00
Zc3hav1-2	0.17	0.38	0.39	0.30	0.00	0.00
Zfp182-1	0.00	0.13	0.04	0.05	0.00	0.00
Zfp182-2	0.36	0.75	1.12	0.82	0.01	0.01
Total	**100**	**100**	**100**	**100**	**100**	**100**

WT MEF Experiment 2

	Percentage					
Name	**PLASMID LIB**	**P0-293T**	**P1-VERO**	**P2-WT**	**P3-WT**	**P4-WT**
Adar-1	0.00	0.00	0.00	0.00	0.00	0.00
Adar-2	0.66	0.16	0.09	0.16	0.00	0.00
Atf2-1	0.41	0.18	0.10	0.30	0.00	0.00
Atf2-2	1.19	0.48	0.50	1.02	0.02	0.00
Atf3-1	0.58	0.46	0.37	0.22	0.00	0.00
Atf3-2	1.95	2.44	3.41	5.07	0.07	0.01
B2m-1	0.69	0.22	0.15	0.21	0.01	0.00
B2m-2	0.37	0.41	0.42	0.23	0.00	0.00
Birc6-1	0.49	0.28	0.27	0.18	0.01	0.00
Birc6-2	0.51	0.35	0.24	0.20	0.01	0.00
Brd4-1	0.45	1.25	1.73	0.80	0.03	0.00
Brd4-2	0.62	0.54	0.54	0.67	0.00	0.00
Cdkl4-1	0.63	0.67	0.56	0.32	0.00	0.00
Cdkl4-2	0.60	0.34	0.21	0.22	0.00	0.00
Clec4d-1	0.49	0.41	0.25	0.17	0.00	0.00
Clec4d-2	0.61	0.48	0.41	0.26	0.00	0.00
Clec4e-1	0.48	0.85	0.95	0.44	0.05	0.00
Clec4e-2	0.52	0.30	0.16	0.08	0.00	0.00
Cmpk2-1	1.56	0.69	0.44	0.25	0.01	0.00
Cmpk2-2	0.72	0.13	0.08	0.20	0.00	0.00
Cpeb3-1	0.01	0.08	0.12	0.09	0.00	0.00
Cpeb3-2	0.74	0.22	0.20	0.79	0.01	0.00
Cxcl10-1	0.56	0.66	0.77	0.57	0.01	0.00
Cxcl10-2	0.57	0.46	0.33	0.15	0.01	0.01
Cytip-1	0.62	0.38	0.20	0.22	0.00	0.00
Cytip-2	0.64	0.66	0.67	0.45	0.03	0.00
Daxx-1	0.41	1.16	1.42	0.65	0.01	0.00
Daxx-2	0.85	0.22	0.10	0.10	0.00	0.00
Ddx58-1	0.55	0.50	0.53	0.54	0.01	0.00

Ddx58-2	0.53	0.60	0.57	0.47	0.01	0.00
Ddx60-1	0.66	0.20	0.10	0.09	0.00	0.00
Ddx60-2	0.88	0.26	0.15	0.11	0.01	0.00
Dhx9-1	0.73	0.77	0.59	0.83	0.02	0.00
Dhx9-2	0.46	0.28	0.27	0.15	0.01	0.00
Dtx3l-1	0.69	0.84	0.76	0.84	0.01	0.00
Dtx3l-2	0.52	0.45	0.44	0.29	0.01	0.00
EGFP	0.49	0.02	0.02	0.02	0.00	0.00
Eif2ak2-1	0.53	0.56	0.48	0.24	0.00	0.00
Eif2ak2-2	0.49	0.27	0.29	1.21	0.00	0.00
Fa2h-1	0.75	0.44	0.25	0.40	0.00	0.00
Fa2h-2	0.68	0.26	0.16	0.71	0.01	0.00
Fbxo39-1	0.59	0.97	1.10	1.37	0.10	0.00
Fbxo39-2	0.63	0.25	0.15	0.14	0.11	0.01
Gbp2-1	0.78	0.30	0.20	0.17	0.00	0.00
Gbp2-2	0.53	1.77	2.29	2.10	0.19	0.01
Gbp3-1	0.52	0.54	0.45	0.23	0.00	0.00
Gbp3-2	0.62	0.76	0.72	0.42	0.02	0.00
Gbp6-1	0.00	1.17	1.43	1.65	0.01	0.00
Gbp6-2	0.13	0.00	0.00	0.00	0.00	0.00
Gcc-1	0.63	0.21	0.16	0.10	0.00	0.00
Gcc-2	0.51	0.79	0.88	0.92	0.03	0.01
Gvin-1	0.49	0.71	0.66	0.37	0.00	0.00
Gvin-2	0.39	0.72	0.71	0.56	0.01	0.00
Ifi27-1	0.52	1.24	1.18	0.57	0.01	0.00
Ifi27-2	0.61	1.38	1.82	1.28	0.04	0.00
Ifi35-1	0.39	0.21	0.10	0.06	0.00	0.00
Ifi35-2	0.45	2.14	2.54	1.82	0.02	0.00
Ifi44-1	0.41	0.84	0.76	0.70	0.03	0.00
Ifi44-2	0.46	0.50	0.61	0.64	0.00	0.00
Ifih1-1	0.51	0.21	0.12	0.07	0.01	0.00
Ifih1-2	0.68	1.01	1.32	1.16	0.04	0.00
Ifit1-1	0.86	0.15	0.12	0.14	0.00	0.00
Ifit1-2	0.45	0.48	0.40	0.33	0.00	0.00

Ifit3-1	0.47	0.47	0.34	0.27	0.00	0.00
Ifit3-2	0.58	0.44	0.30	0.28	0.01	0.00
Ifitm3-1	0.61	0.60	0.58	0.55	0.02	0.01
Ifitm3-2	0.90	0.61	0.92	2.13	96.54	99.26
Ifna1-1	0.48	0.66	0.54	0.39	0.01	0.01
Ifna1-2	0.65	0.36	0.37	0.26	0.03	0.00
Ifna4-1	0.29	0.65	0.56	0.97	0.01	0.00
Ifna4-2	0.48	0.29	0.26	0.21	0.00	0.00
Ifnb1-1	0.90	0.49	0.34	1.02	0.02	0.00
Ifnb1-2	0.39	0.30	0.49	0.72	0.01	0.00
Ikbka-1	0.55	0.16	0.12	1.13	0.00	0.00
Ikbka-2	0.53	0.34	0.22	0.18	0.01	0.00
Ikbkb-1	0.48	0.51	0.36	0.22	0.01	0.00
Ikbkb-2	0.61	0.70	0.59	0.72	0.01	0.00
Ikbke-1	1.25	0.56	0.49	0.22	0.00	0.00
Ikbke-2	0.61	0.68	0.59	0.30	0.02	0.00
Il15-1	0.55	0.57	0.36	0.25	0.01	0.00
Il15-2	0.56	0.70	0.58	0.26	0.01	0.00
Il6-1	0.78	0.60	0.59	0.79	0.00	0.00
Il6-2	0.52	0.62	0.58	0.31	0.04	0.00
Irf1-1	0.69	0.23	0.14	0.15	0.00	0.00
Irf1-2	0.51	0.26	0.17	0.20	0.00	0.00
Irf2-1	0.56	0.49	0.50	0.28	0.01	0.00
Irf2-2	0.67	0.50	0.34	0.21	0.02	0.00
Irf3-1	0.57	0.24	0.24	0.16	0.00	0.00
Irf3-2	0.68	0.42	0.32	0.28	0.01	0.00
Irf5-1	0.62	0.30	0.22	0.13	0.00	0.00
Irf5-2	0.61	0.16	0.05	0.13	0.00	0.00
Irf7-1	0.36	0.81	0.57	1.14	0.02	0.01
Irf7-2	0.57	1.36	1.97	1.86	0.21	0.02
Irf9-1	0.44	0.28	0.27	0.15	0.00	0.00
Irf9-2	0.51	0.27	0.20	0.13	0.00	0.00
Irgm-1	0.54	0.27	0.19	0.19	0.02	0.00
Irgm-2	0.58	0.81	1.05	1.13	0.03	0.00

Isg15-1	0.54	1.02	1.40	2.63	0.03	0.00
Isg15-2	0.53	0.24	0.22	0.18	0.00	0.00
Lgals3bp-1	0.58	0.64	0.72	0.55	0.01	0.00
Lgals3bp-2	0.71	0.31	0.25	0.11	0.03	0.01
Lgals8-1	0.80	0.60	0.50	0.41	0.02	0.00
Lgals8-2	0.45	0.13	0.10	0.06	0.00	0.00
Lrp4-1	0.65	0.21	0.08	0.07	0.00	0.00
Lrp4-2	0.51	0.53	0.50	0.74	0.01	0.00
Ly6e-1	0.45	0.21	0.13	0.09	0.03	0.01
Ly6e-2	0.37	0.44	0.44	1.18	0.01	0.00
Map3K8-1	0.49	0.63	0.59	0.36	0.01	0.00
Map3K8-2	0.52	0.50	0.31	0.53	0.02	0.02
Map4k2-1	0.45	0.60	0.44	0.39	0.02	0.00
Map4k2-2	0.44	0.35	0.21	0.27	0.00	0.00
Mapk8-1	0.54	0.64	0.54	0.56	0.01	0.00
Mapk8-2	0.62	0.61	0.59	0.40	0.01	0.00
Mbnl1-1	0.44	0.34	0.30	0.53	0.00	0.00
Mbnl1-2	0.50	0.29	0.19	0.10	0.00	0.00
miR-124	0.58	0.24	0.15	0.34	0.00	0.04
Mitd1-1	0.66	0.14	0.10	0.09	0.02	0.02
Mitd1-2	0.35	0.30	0.26	0.21	0.00	0.00
Mlkl-1	0.31	0.33	0.39	0.75	0.02	0.00
Mlkl-2	0.33	1.33	2.29	2.31	0.08	0.01
Mov10-1	0.46	0.78	0.93	1.55	0.02	0.00
Mov10-2	0.32	0.53	0.38	0.27	0.01	0.00
Myd88-1	0.35	0.56	0.49	1.02	0.03	0.00
Myd88-2	0.52	0.23	0.20	0.48	0.02	0.00
Nfkbia-1	0.33	0.51	0.49	0.27	0.01	0.01
Nfkbia-2	0.45	0.27	0.18	0.08	0.00	0.00
Nmi-1	0.53	0.78	0.84	0.69	0.04	0.00
Nmi-2	0.53	2.74	4.58	2.91	0.09	0.00
Oas1a-1	0.41	0.22	0.16	0.13	0.00	0.00
Oas1a-2	0.47	0.26	0.19	0.20	0.00	0.00
Oas2-1	0.50	0.26	0.12	0.12	0.00	0.00

Oas2-2	0.94	0.28	0.17	0.09	0.00	0.00
Oasl1-1	0.41	0.71	0.84	1.51	0.02	0.01
Oasl1-2	0.22	0.57	0.43	0.61	0.01	0.00
Oasl2-1	0.59	0.51	0.40	0.35	0.02	0.00
Oasl2-2	0.23	0.52	0.34	0.18	0.01	0.00
p50	0.50	0.53	0.53	0.39	0.01	0.00
p50	0.26	0.40	0.31	0.16	0.00	0.00
p65	0.35	0.38	0.26	0.14	0.00	0.00
p65	0.30	0.18	0.11	0.09	0.00	0.00
Papr14-2	0.34	0.57	0.47	0.27	0.01	0.00
Parp10-1	0.25	0.13	0.12	0.07	0.00	0.00
Parp10-2	0.42	0.78	0.85	0.50	0.02	0.00
Parp11-1	0.34	0.04	0.02	0.20	0.00	0.00
Parp11-2	0.38	0.27	0.18	0.24	0.00	0.00
Parp12-1	0.24	0.12	0.08	0.05	0.03	0.05
Parp12-2	0.33	0.42	0.39	0.34	0.00	0.00
Parp14-1	0.13	0.48	0.43	0.22	0.01	0.00
Parp9-1	0.35	0.06	0.06	0.13	0.00	0.00
Parp9-2	0.37	0.28	0.29	0.90	0.00	0.00
Plec-1	0.37	0.12	0.05	0.06	0.00	0.00
Plec-2	0.26	0.12	0.04	0.03	0.00	0.00
Ppm1k-1	0.38	0.24	0.22	0.14	0.03	0.01
Ppm1k-2	0.22	0.38	0.29	0.12	0.03	0.01
Ppp3cb-1	0.37	0.23	0.12	0.12	0.00	0.00
Ppp3cb-2	0.47	0.48	0.43	0.27	0.03	0.00
Rnasel-1	0.33	0.74	0.90	0.89	0.03	0.00
Rnasel-2	0.30	0.24	0.20	0.33	0.01	0.00
Rsad-1	1.00	0.45	0.36	0.24	0.00	0.00
Rsad-2	0.26	0.36	0.28	0.21	0.02	0.01
Rtp4-1	0.33	0.57	0.60	0.34	0.05	0.00
Rtp4-2	1.14	1.09	1.35	0.60	0.03	0.00
Samd9l-1	0.32	0.26	0.20	0.43	0.00	0.00
Samd9l-2	0.33	0.18	0.11	0.06	0.01	0.01
Sfxn2-1	0.31	0.27	0.20	0.16	0.00	0.00

Sfxn2-2	1.22	0.20	0.11	0.28	0.01	0.00
Sh3bgrl-1	0.25	0.60	0.46	0.63	0.03	0.00
Sh3bgrl-2	0.30	0.10	0.07	0.04	0.00	0.00
Stat1-1	0.50	0.21	0.15	0.30	0.00	0.00
Stat1-2	0.32	1.87	1.45	0.80	0.03	0.00
Stat2-1	0.29	0.50	0.46	0.35	0.01	0.00
Stat2-2	0.25	0.23	0.21	0.14	0.00	0.00
Stat3-1	0.31	0.45	0.46	0.25	0.01	0.01
Stat3-2	0.35	0.89	0.64	0.37	0.01	0.00
Tap1-1	0.26	0.26	0.22	0.12	0.00	0.00
Tap1-2	0.21	0.86	0.95	0.51	0.02	0.00
Tapbp-1	0.21	0.85	1.13	0.71	0.50	0.09
Tapbp-2	0.28	0.25	0.20	1.08	0.00	0.00
Tbk1-1	0.32	0.64	0.80	0.67	0.01	0.00
Tbk1-2	0.19	0.91	0.99	0.69	0.03	0.00
Ticam1-1	0.27	0.05	0.03	0.03	0.00	0.00
Ticam1-2	0.28	0.21	0.18	0.42	0.01	0.00
Tlr3-1	0.32	0.06	0.02	0.02	0.00	0.00
Tlr3-2	0.38	1.11	1.80	3.75	0.09	0.00
Tlr7-1	0.34	0.61	0.83	0.40	0.00	0.00
Tlr7-2	0.32	0.25	0.16	0.08	0.00	0.00
Tlr9-1	0.29	0.11	0.10	0.05	0.02	0.01
Tlr9-2	0.32	0.17	0.12	0.11	0.00	0.00
Tmem140-1	0.30	0.14	0.08	0.07	0.00	0.00
Tmem140-2	0.28	0.33	0.30	0.17	0.01	0.07
Tor3a-1	0.25	0.21	0.21	0.19	0.00	0.00
Tor3a-2	0.26	0.28	0.26	0.15	0.00	0.00
Trex1-1	0.26	0.10	0.03	0.07	0.00	0.00
Trex1-2	0.28	0.16	0.09	0.05	0.00	0.00
Trim21-1	0.34	0.41	0.56	0.53	0.03	0.00
Trim21-2	0.34	0.34	0.28	0.22	0.01	0.00
Trim25-1	0.38	0.14	0.10	0.10	0.02	0.00
Trim25-2	0.30	0.35	0.32	0.52	0.01	0.00
Usp18-1	0.57	0.36	0.40	0.50	0.02	0.00

Usp18-2	0.31	0.34	0.53	0.25	0.01	0.00
Wwoxv-1	0.15	0.12	0.11	0.05	0.04	0.02
Wwoxv-2	0.29	0.22	0.22	0.11	0.01	0.00
Zc3hav1-1	0.20	0.18	0.13	0.06	0.00	0.01
Zc3hav1-2	0.17	0.38	0.39	1.05	0.00	0.00
Zfp182-1	0.00	0.13	0.04	0.03	0.00	0.00
Zfp182-2	0.36	0.75	1.12	1.02	0.01	0.01
Total	**100**	**100**	**100**	**100**	**100**	**100**

WT MEF Experiment 3

	Percentage					
Name	**PLASMID LIB**	**P0-293T**	**P1-VERO**	**P2-WT**	**P3-WT**	**P4-WT**
Adar-1	0.00	0.00	0.00	0.00	0.00	0.00
Adar-2	0.66	0.16	0.09	0.08	0.00	0.00
Atf2-1	0.41	0.18	0.10	0.06	0.00	0.00
Atf2-2	1.19	0.48	0.50	1.24	0.00	0.00
Atf3-1	0.58	0.46	0.37	0.23	0.00	0.00
Atf3-2	1.95	2.44	3.41	4.39	0.03	0.01
B2m-1	0.69	0.22	0.15	0.21	0.00	0.00
B2m-2	0.37	0.41	0.42	0.26	0.00	0.00
Birc6-1	0.49	0.28	0.27	0.17	0.00	0.00
Birc6-2	0.51	0.35	0.24	0.22	0.00	0.00
Brd4-1	0.45	1.25	1.73	1.66	0.01	0.00
Brd4-2	0.62	0.54	0.54	1.39	0.00	0.00
Cdkl4-1	0.63	0.67	0.56	0.22	0.01	0.00
Cdkl4-2	0.60	0.34	0.21	0.45	0.00	0.00
Clec4d-1	0.49	0.41	0.25	0.17	0.00	0.00
Clec4d-2	0.61	0.48	0.41	0.26	0.00	0.00
Clec4e-1	0.48	0.85	0.95	0.51	0.00	0.00
Clec4e-2	0.52	0.30	0.16	0.09	0.00	0.00
Cmpk2-1	1.56	0.69	0.44	0.19	0.00	0.00
Cmpk2-2	0.72	0.13	0.08	0.09	0.00	0.00
Cpeb3-1	0.01	0.08	0.12	0.05	0.00	0.00
Cpeb3-2	0.74	0.22	0.20	0.63	0.00	0.00
Cxcl10-1	0.56	0.66	0.77	0.98	0.00	0.00
Cxcl10-2	0.57	0.46	0.33	0.15	0.00	0.01
Cytip-1	0.62	0.38	0.20	0.31	0.00	0.00
Cytip-2	0.64	0.66	0.67	0.39	0.00	0.00
Daxx-1	0.41	1.16	1.42	0.74	0.00	0.00
Daxx-2	0.85	0.22	0.10	0.07	0.00	0.00
Ddx58-1	0.55	0.50	0.53	0.49	0.00	0.00

Ddx58-2	0.53	0.60	0.57	0.30	0.00	0.00
Ddx60-1	0.66	0.20	0.10	0.09	0.00	0.00
Ddx60-2	0.88	0.26	0.15	0.08	0.00	0.00
Dhx9-1	0.73	0.77	0.59	0.38	0.00	0.00
Dhx9-2	0.46	0.28	0.27	0.17	0.00	0.00
Dtx3l-1	0.69	0.84	0.76	0.53	0.00	0.00
Dtx3l-2	0.52	0.45	0.44	0.69	0.00	0.00
EGFP	0.49	0.02	0.02	0.08	0.00	0.00
Eif2ak2-1	0.53	0.56	0.48	0.46	0.00	0.00
Eif2ak2-2	0.49	0.27	0.29	0.38	0.00	0.00
Fa2h-1	0.75	0.44	0.25	0.16	0.00	0.00
Fa2h-2	0.68	0.26	0.16	0.14	0.00	0.00
Fbxo39-1	0.59	0.97	1.10	1.59	0.01	0.00
Fbxo39-2	0.63	0.25	0.15	0.38	0.01	0.00
Gbp2-1	0.78	0.30	0.20	0.13	0.00	0.00
Gbp2-2	0.53	1.77	2.29	3.92	0.03	0.01
Gbp3-1	0.52	0.54	0.45	0.22	0.00	0.00
Gbp3-2	0.62	0.76	0.72	0.42	0.01	0.00
Gbp6-1	0.00	1.17	1.43	3.03	0.00	0.00
Gbp6-2	0.13	0.00	0.00	0.00	0.00	0.00
Gcc-1	0.63	0.21	0.16	0.50	0.00	0.00
Gcc-2	0.51	0.79	0.88	0.60	0.01	0.01
Gvin-1	0.49	0.71	0.66	0.37	0.00	0.00
Gvin-2	0.39	0.72	0.71	0.49	0.00	0.00
Ifi27-1	0.52	1.24	1.18	0.56	0.01	0.00
Ifi27-2	0.61	1.38	1.82	2.81	0.01	0.00
Ifi35-1	0.39	0.21	0.10	0.23	0.00	0.00
Ifi35-2	0.45	2.14	2.54	2.36	0.02	0.00
Ifi44-1	0.41	0.84	0.76	1.12	0.01	0.00
Ifi44-2	0.46	0.50	0.61	0.90	0.00	0.00
Ifih1-1	0.51	0.21	0.12	0.08	0.00	0.00
Ifih1-2	0.68	1.01	1.32	1.51	0.03	0.01
Ifit1-1	0.86	0.15	0.12	0.81	0.00	0.00
Ifit1-2	0.45	0.48	0.40	0.28	0.00	0.00

Ifit3-1	0.47	0.47	0.34	0.23	0.00	0.00
Ifit3-2	0.58	0.44	0.30	0.22	0.00	0.00
Ifitm3-1	0.61	0.60	0.58	0.32	0.00	0.00
Ifitm3-2	**0.90**	**0.61**	**0.92**	**1.08**	**98.94**	**99.48**
Ifna1-1	0.48	0.66	0.54	0.71	0.01	0.00
Ifna1-2	0.65	0.36	0.37	0.79	0.00	0.00
Ifna4-1	0.29	0.65	0.56	0.66	0.00	0.00
Ifna4-2	0.48	0.29	0.26	0.17	0.00	0.00
Ifnb1-1	0.90	0.49	0.34	0.16	0.01	0.00
Ifnb1-2	0.39	0.30	0.49	0.23	0.01	0.00
Ikbka-1	0.55	0.16	0.12	0.09	0.01	0.00
Ikbka-2	0.53	0.34	0.22	0.40	0.00	0.00
Ikbkb-1	0.48	0.51	0.36	0.21	0.00	0.00
Ikbkb-2	0.61	0.70	0.59	1.18	0.00	0.00
Ikbke-1	1.25	0.56	0.49	0.23	0.00	0.00
Ikbke-2	0.61	0.68	0.59	0.33	0.00	0.00
Il15-1	0.55	0.57	0.36	0.23	0.00	0.00
Il15-2	0.56	0.70	0.58	0.53	0.00	0.00
Il6-1	0.78	0.60	0.59	0.27	0.00	0.00
Il6-2	0.52	0.62	0.58	0.77	0.00	0.00
Irf1-1	0.69	0.23	0.14	0.35	0.00	0.00
Irf1-2	0.51	0.26	0.17	0.11	0.00	0.00
Irf2-1	0.56	0.49	0.50	0.36	0.00	0.00
Irf2-2	0.67	0.50	0.34	0.31	0.00	0.00
Irf3-1	0.57	0.24	0.24	0.13	0.00	0.00
Irf3-2	0.68	0.42	0.32	0.19	0.00	0.00
Irf5-1	0.62	0.30	0.22	0.10	0.00	0.00
Irf5-2	0.61	0.16	0.05	0.20	0.00	0.00
Irf7-1	0.36	0.81	0.57	0.97	0.00	0.01
Irf7-2	0.57	1.36	1.97	2.46	0.01	0.00
Irf9-1	0.44	0.28	0.27	0.18	0.01	0.00
Irf9-2	0.51	0.27	0.20	0.12	0.00	0.00
Irgm-1	0.54	0.27	0.19	0.13	0.00	0.00
Irgm-2	0.58	0.81	1.05	1.16	0.01	0.00

Isg15-1	0.54	1.02	1.40	1.16	0.01	0.00
Isg15-2	0.53	0.24	0.22	0.43	0.00	0.00
Lgals3bp-1	0.58	0.64	0.72	0.44	0.00	0.00
Lgals3bp-2	0.71	0.31	0.25	0.12	0.01	0.00
Lgals8-1	0.80	0.60	0.50	0.76	0.00	0.00
Lgals8-2	0.45	0.13	0.10	0.07	0.00	0.00
Lrp4-1	0.65	0.21	0.08	0.17	0.00	0.00
Lrp4-2	0.51	0.53	0.50	0.56	0.00	0.00
Ly6e-1	0.45	0.21	0.13	0.24	0.02	0.02
Ly6e-2	0.37	0.44	0.44	1.20	0.00	0.00
Map3K8-1	0.49	0.63	0.59	0.28	0.00	0.00
Map3K8-2	0.52	0.50	0.31	0.23	0.01	0.01
Map4k2-1	0.45	0.60	0.44	0.30	0.01	0.00
Map4k2-2	0.44	0.35	0.21	0.33	0.00	0.00
Mapk8-1	0.54	0.64	0.54	0.33	0.00	0.00
Mapk8-2	0.62	0.61	0.59	0.62	0.00	0.00
Mbnl1-1	0.44	0.34	0.30	0.34	0.00	0.00
Mbnl1-2	0.50	0.29	0.19	0.09	0.00	0.00
miR-124	0.58	0.24	0.15	0.25	0.00	0.03
Mitd1-1	0.66	0.14	0.10	0.08	0.02	0.01
Mitd1-2	0.35	0.30	0.26	0.34	0.00	0.00
Mlkl-1	0.31	0.33	0.39	0.99	0.00	0.00
Mlkl-2	0.33	1.33	2.29	1.74	0.05	0.02
Mov10-1	0.46	0.78	0.93	0.50	0.01	0.00
Mov10-2	0.32	0.53	0.38	0.28	0.00	0.00
Myd88-1	0.35	0.56	0.49	0.31	0.00	0.00
Myd88-2	0.52	0.23	0.20	0.12	0.01	0.00
Nfkbia-1	0.33	0.51	0.49	0.38	0.01	0.01
Nfkbia-2	0.45	0.27	0.18	0.09	0.00	0.00
Nmi-1	0.53	0.78	0.84	1.46	0.01	0.00
Nmi-2	0.53	2.74	4.58	3.86	0.03	0.00
Oas1a-1	0.41	0.22	0.16	0.10	0.00	0.00
Oas1a-2	0.47	0.26	0.19	0.10	0.00	0.00
Oas2-1	0.50	0.26	0.12	0.29	0.00	0.00

Oas2-2	0.94	0.28	0.17	0.09	0.00	0.00
Oasl1-1	0.41	0.71	0.84	1.17	0.00	0.00
Oasl1-2	0.22	0.57	0.43	0.29	0.00	0.00
Oasl2-1	0.59	0.51	0.40	0.28	0.00	0.00
Oasl2-2	0.23	0.52	0.34	0.18	0.00	0.00
p50	0.50	0.53	0.53	0.34	0.00	0.00
p50	0.26	0.40	0.31	0.31	0.00	0.00
p65	0.35	0.38	0.26	0.29	0.00	0.00
p65	0.30	0.18	0.11	0.08	0.00	0.00
Papr14-2	0.34	0.57	0.47	0.26	0.00	0.00
Parp10-1	0.25	0.13	0.12	0.10	0.00	0.00
Parp10-2	0.42	0.78	0.85	0.88	0.00	0.00
Parp11-1	0.34	0.04	0.02	0.04	0.00	0.00
Parp11-2	0.38	0.27	0.18	0.18	0.00	0.00
Parp12-1	0.24	0.12	0.08	0.03	0.03	0.03
Parp12-2	0.33	0.42	0.39	0.33	0.00	0.00
Parp14-1	0.13	0.48	0.43	0.22	0.01	0.01
Parp9-1	0.35	0.06	0.06	0.04	0.00	0.00
Parp9-2	0.37	0.28	0.29	0.20	0.00	0.00
Plec-1	0.37	0.12	0.05	0.05	0.00	0.00
Plec-2	0.26	0.12	0.04	0.04	0.00	0.00
Ppm1k-1	0.38	0.24	0.22	0.22	0.01	0.00
Ppm1k-2	0.22	0.38	0.29	0.34	0.01	0.01
Ppp3cb-1	0.37	0.23	0.12	0.11	0.00	0.00
Ppp3cb-2	0.47	0.48	0.43	0.35	0.00	0.00
Rnasel-1	0.33	0.74	0.90	0.63	0.01	0.00
Rnasel-2	0.30	0.24	0.20	0.53	0.00	0.00
Rsad-1	1.00	0.45	0.36	0.26	0.00	0.00
Rsad-2	0.26	0.36	0.28	0.21	0.01	0.01
Rtp4-1	0.33	0.57	0.60	0.87	0.00	0.00
Rtp4-2	1.14	1.09	1.35	0.86	0.00	0.00
Samd9l-1	0.32	0.26	0.20	0.13	0.00	0.00
Samd9l-2	0.33	0.18	0.11	0.06	0.01	0.00
Sfxn2-1	0.31	0.27	0.20	0.14	0.00	0.00

Sfxn2-2	1.22	0.20	0.11	0.06	0.00	0.00
Sh3bgrl-1	0.25	0.60	0.46	0.34	0.00	0.00
Sh3bgrl-2	0.30	0.10	0.07	0.04	0.00	0.00
Stat1-1	0.50	0.21	0.15	0.10	0.00	0.00
Stat1-2	0.32	1.87	1.45	1.07	0.01	0.00
Stat2-1	0.29	0.50	0.46	0.45	0.00	0.00
Stat2-2	0.25	0.23	0.21	0.53	0.00	0.00
Stat3-1	0.31	0.45	0.46	0.21	0.01	0.01
Stat3-2	0.35	0.89	0.64	0.61	0.00	0.00
Tap1-1	0.26	0.26	0.22	0.24	0.00	0.00
Tap1-2	0.21	0.86	0.95	0.74	0.00	0.00
Tapbp-1	0.21	0.85	1.13	0.95	0.21	0.03
Tapbp-2	0.28	0.25	0.20	0.16	0.00	0.00
Tbk1-1	0.32	0.64	0.80	0.80	0.01	0.00
Tbk1-2	0.19	0.91	0.99	0.49	0.01	0.00
Ticam1-1	0.27	0.05	0.03	0.02	0.00	0.00
Ticam1-2	0.28	0.21	0.18	0.10	0.00	0.00
Tlr3-1	0.32	0.06	0.02	0.03	0.00	0.00
Tlr3-2	0.38	1.11	1.80	1.38	0.02	0.00
Tlr7-1	0.34	0.61	0.83	0.37	0.00	0.00
Tlr7-2	0.32	0.25	0.16	0.11	0.00	0.00
Tlr9-1	0.29	0.11	0.10	0.06	0.01	0.01
Tlr9-2	0.32	0.17	0.12	0.11	0.00	0.00
Tmem140-1	0.30	0.14	0.08	0.06	0.00	0.00
Tmem140-2	0.28	0.33	0.30	0.47	0.00	0.04
Tor3a-1	0.25	0.21	0.21	0.17	0.00	0.00
Tor3a-2	0.26	0.28	0.26	0.14	0.00	0.00
Trex1-1	0.26	0.10	0.03	0.09	0.00	0.00
Trex1-2	0.28	0.16	0.09	0.06	0.00	0.00
Trim21-1	0.34	0.41	0.56	0.98	0.00	0.00
Trim21-2	0.34	0.34	0.28	0.33	0.00	0.00
Trim25-1	0.38	0.14	0.10	0.08	0.00	0.00
Trim25-2	0.30	0.35	0.32	0.26	0.00	0.00
Usp18-1	0.57	0.36	0.40	0.21	0.00	0.00

Usp18-2	0.31	0.34	0.53	0.22	0.00	0.00
Wwoxv-1	0.15	0.12	0.11	0.05	0.02	0.02
Wwoxv-2	0.29	0.22	0.22	0.32	0.00	0.00
Zc3hav1-1	0.20	0.18	0.13	0.05	0.00	0.00
Zc3hav1-2	0.17	0.38	0.39	0.78	0.00	0.00
Zfp182-1	0.00	0.13	0.04	0.04	0.00	0.00
Zfp182-2	0.36	0.75	1.12	0.95	0.01	0.01
Total	**100**	**100**	**100**	**100**	**100**	**100**

***Ifnar1*$^{-/-}$ MEF Experiment 1**

	Percentage					
Name	**Plasmid lib**	**P0-293T**	**P1-Vero**	**P2-** ***Ifnar1*$^{-/-}$**	**P3-** ***Ifnar1*$^{-/-}$**	**P4-** ***Ifnar1*$^{-/-}$**
Adar-1	0.00	0.00	0.00	0.00	0.00	0.00
Adar-2	0.66	0.16	0.09	0.12	0.02	0.00
Atf2-1	0.41	0.18	0.10	0.11	0.02	0.00
Atf2-2	1.19	0.48	0.50	0.93	0.12	0.01
Atf3-1	0.58	0.46	0.37	0.35	0.04	0.00
Atf3-2	1.95	2.44	3.41	4.79	1.31	0.21
B2m-1	0.69	0.22	0.15	0.40	0.04	0.01
B2m-2	0.37	0.41	0.42	0.55	0.13	0.01
Birc6-1	0.49	0.28	0.27	0.14	0.07	0.00
Birc6-2	0.51	0.35	0.24	0.35	0.04	0.00
Brd4-1	0.45	1.25	1.73	1.44	0.31	0.04
Brd4-2	0.62	0.54	0.54	0.86	0.15	0.03
Cdkl4-1	0.63	0.67	0.56	0.26	0.06	0.01
Cdkl4-2	0.60	0.34	0.21	0.18	0.05	0.01
Clec4d-1	0.49	0.41	0.25	0.23	0.04	0.00
Clec4d-2	0.61	0.48	0.41	0.38	0.12	0.02
Clec4e-1	0.48	0.85	0.95	0.65	0.12	0.01
Clec4e-2	0.52	0.30	0.16	0.08	0.01	0.00
Cmpk2-1	1.56	0.69	0.44	0.22	0.04	0.00
Cmpk2-2	0.72	0.13	0.08	0.10	0.03	0.01
Cpeb3-1	0.01	0.08	0.12	0.12	0.02	0.00
Cpeb3-2	0.74	0.22	0.20	0.27	0.04	0.01
Cxcl10-1	0.56	0.66	0.77	0.81	0.13	0.01
Cxcl10-2	0.57	0.46	0.33	0.20	0.06	0.01
Cytip-1	0.62	0.38	0.20	0.41	0.09	0.01
Cytip-2	0.64	0.66	0.67	1.07	0.27	0.04
Daxx-1	0.41	1.16	1.42	1.03	0.31	0.02
Daxx-2	0.85	0.22	0.10	0.13	0.01	0.00

Ddx58-1	0.55	0.50	0.53	0.64	0.11	0.01
Ddx58-2	0.53	0.60	0.57	0.26	0.08	0.01
Ddx60-1	0.66	0.20	0.10	0.09	0.01	0.00
Ddx60-2	0.88	0.26	0.15	0.23	0.02	0.00
Dhx9-1	0.73	0.77	0.59	0.43	0.05	0.00
Dhx9-2	0.46	0.28	0.27	0.25	0.04	0.00
Dtx3l-1	0.69	0.84	0.76	0.54	0.10	0.01
Dtx3l-2	0.52	0.45	0.44	0.40	0.19	0.02
EGFP	0.49	0.02	0.02	0.00	0.00	0.00
Eif2ak2-1	0.53	0.56	0.48	0.31	0.09	0.00
Eif2ak2-2	0.49	0.27	0.29	0.62	0.06	0.01
Fa2h-1	0.75	0.44	0.25	0.18	0.03	0.00
Fa2h-2	0.68	0.26	0.16	0.09	0.02	0.00
Fbxo39-1	0.59	0.97	1.10	1.66	0.57	0.08
Fbxo39-2	0.63	0.25	0.15	0.19	0.04	0.01
Gbp2-1	0.78	0.30	0.20	0.13	0.03	0.00
Gbp2-2	0.53	1.77	2.29	2.94	1.13	0.17
Gbp3-1	0.52	0.54	0.45	0.22	0.06	0.01
Gbp3-2	0.62	0.76	0.72	0.58	0.15	0.01
Gbp6-1	0.00	1.17	1.43	1.72	0.38	0.03
Gbp6-2	0.13	0.00	0.00	0.00	0.00	0.00
Gcc-1	0.63	0.21	0.16	0.10	0.01	0.00
Gcc-2	0.51	0.79	0.88	0.68	0.26	0.02
Gvin-1	0.49	0.71	0.66	0.48	0.10	0.01
Gvin-2	0.39	0.72	0.71	0.41	0.16	0.01
Ifi27-1	0.52	1.24	1.18	0.84	0.23	0.02
Ifi27-2	0.61	1.38	1.82	1.60	0.40	0.04
Ifi35-1	0.39	0.21	0.10	0.09	0.01	0.00
Ifi35-2	0.45	2.14	2.54	1.09	0.47	0.03
Ifi44-1	0.41	0.84	0.76	0.83	0.13	0.02
Ifi44-2	0.46	0.50	0.61	0.56	0.11	0.02
Ifih1-1	0.51	0.21	0.12	0.10	0.02	0.00
Ifih1-2	0.68	1.01	1.32	1.47	0.48	0.06
Ifit1-1	0.86	0.15	0.12	0.17	0.04	0.01

Ifit1-2	0.45	0.48	0.40	0.52	0.09	0.00
Ifit3-1	0.47	0.47	0.34	0.33	0.07	0.01
Ifit3-2	0.58	0.44	0.30	0.30	0.04	0.00
Ifitm3-1	0.61	0.60	0.58	0.27	0.11	0.02
Ifitm3-2	0.90	0.61	0.92	4.61	74.66	96.50
Ifna1-1	0.48	0.66	0.54	0.45	0.34	0.05
Ifna1-2	0.65	0.36	0.37	0.36	0.09	0.02
Ifna4-1	0.29	0.65	0.56	0.75	0.11	0.01
Ifna4-2	0.48	0.29	0.26	0.37	0.06	0.01
Ifnb1-1	0.90	0.49	0.34	0.20	0.03	0.00
Ifnb1-2	0.39	0.30	0.49	0.46	0.18	0.02
Ikbka-1	0.55	0.16	0.12	0.18	0.02	0.00
Ikbka-2	0.53	0.34	0.22	0.22	0.04	0.00
Ikbkb-1	0.48	0.51	0.36	0.33	0.04	0.00
Ikbkb-2	0.61	0.70	0.59	0.71	0.15	0.01
Ikbke-1	1.25	0.56	0.49	0.20	0.12	0.01
Ikbke-2	0.61	0.68	0.59	0.55	0.13	0.01
Il15-1	0.55	0.57	0.36	0.22	0.05	0.00
Il15-2	0.56	0.70	0.58	0.22	0.07	0.01
Il6-1	0.78	0.60	0.59	0.47	0.07	0.00
Il6-2	0.52	0.62	0.58	0.37	0.06	0.01
Irf1-1	0.69	0.23	0.14	0.15	0.02	0.01
Irf1-2	0.51	0.26	0.17	0.14	0.01	0.00
Irf2-1	0.56	0.49	0.50	0.37	0.09	0.01
Irf2-2	0.67	0.50	0.34	0.20	0.04	0.00
Irf3-1	0.57	0.24	0.24	0.32	0.07	0.01
Irf3-2	0.68	0.42	0.32	0.25	0.05	0.00
Irf5-1	0.62	0.30	0.22	0.08	0.03	0.00
Irf5-2	0.61	0.16	0.05	0.04	0.00	0.00
Irf7-1	0.36	0.81	0.57	0.95	0.22	0.05
Irf7-2	0.57	1.36	1.97	3.00	0.67	0.11
Irf9-1	0.44	0.28	0.27	0.23	0.13	0.01
Irf9-2	0.51	0.27	0.20	0.29	0.07	0.01
Irgm-1	0.54	0.27	0.19	0.22	0.04	0.00

Irgm-2	0.58	0.81	1.05	1.18	0.35	0.04
Isg15-1	0.54	1.02	1.40	1.29	0.35	0.04
Isg15-2	0.53	0.24	0.22	0.21	0.02	0.01
Lgals3bp-1	0.58	0.64	0.72	0.78	0.21	0.02
Lgals3bp-2	0.71	0.31	0.25	0.24	0.03	0.00
Lgals8-1	0.80	0.60	0.50	0.43	0.11	0.01
Lgals8-2	0.45	0.13	0.10	0.06	0.01	0.00
Lrp4-1	0.65	0.21	0.08	0.08	0.04	0.01
Lrp4-2	0.51	0.53	0.50	0.41	0.16	0.01
Ly6e-1	0.45	0.21	0.13	0.06	0.03	0.02
Ly6e-2	0.37	0.44	0.44	1.16	0.15	0.03
Map3K8-1	0.49	0.63	0.59	0.53	0.12	0.01
Map3K8-2	0.52	0.50	0.31	0.38	0.19	0.05
Map4k2-1	0.45	0.60	0.44	0.36	0.11	0.02
Map4k2-2	0.44	0.35	0.21	0.08	0.02	0.00
Mapk8-1	0.54	0.64	0.54	0.59	0.11	0.01
Mapk8-2	0.62	0.61	0.59	0.54	0.14	0.02
Mbnl1-1	0.44	0.34	0.30	0.23	0.08	0.00
Mbnl1-2	0.50	0.29	0.19	0.11	0.04	0.01
miR-124	0.58	0.24	0.15	0.07	0.05	0.03
Mitd1-1	0.66	0.14	0.10	0.11	0.03	0.02
Mitd1-2	0.35	0.30	0.26	0.30	0.02	0.01
Mlkl-1	0.31	0.33	0.39	0.77	0.16	0.03
Mlkl-2	0.33	1.33	2.29	2.50	0.92	0.19
Mov10-1	0.46	0.78	0.93	1.03	0.32	0.04
Mov10-2	0.32	0.53	0.38	0.34	0.05	0.01
Myd88-1	0.35	0.56	0.49	0.42	0.14	0.01
Myd88-2	0.52	0.23	0.20	0.24	0.02	0.01
Nfkbia-1	0.33	0.51	0.49	0.33	0.48	0.09
Nfkbia-2	0.45	0.27	0.18	0.12	0.02	0.00
Nmi-1	0.53	0.78	0.84	1.01	0.27	0.03
Nmi-2	0.53	2.74	4.58	3.24	0.89	0.12
Oas1a-1	0.41	0.22	0.16	0.15	0.03	0.01
Oas1a-2	0.47	0.26	0.19	0.09	0.00	0.00

Oas2-1	0.50	0.26	0.12	0.21	0.03	0.01
Oas2-2	0.94	0.28	0.17	0.04	0.03	0.00
Oasl1-1	0.41	0.71	0.84	1.10	0.28	0.05
Oasl1-2	0.22	0.57	0.43	0.34	0.07	0.01
Oasl2-1	0.59	0.51	0.40	0.48	0.10	0.01
Oasl2-2	0.23	0.52	0.34	0.32	0.04	0.00
p50	0.50	0.53	0.53	0.43	0.11	0.01
p50	0.26	0.40	0.31	0.30	0.06	0.01
p65	0.35	0.38	0.26	0.17	0.03	0.00
p65	0.30	0.18	0.11	0.07	0.01	0.00
Papr14-2	0.34	0.57	0.47	0.21	0.05	0.01
Parp10-1	0.25	0.13	0.12	0.09	0.03	0.00
Parp10-2	0.42	0.78	0.85	0.85	0.22	0.02
Parp11-1	0.34	0.04	0.02	0.05	0.01	0.00
Parp11-2	0.38	0.27	0.18	0.23	0.04	0.01
Parp12-1	0.24	0.12	0.08	0.06	0.02	0.02
Parp12-2	0.33	0.42	0.39	0.39	0.09	0.01
Parp14-1	0.13	0.48	0.43	0.23	0.06	0.01
Parp9-1	0.35	0.06	0.06	0.06	0.02	0.01
Parp9-2	0.37	0.28	0.29	0.32	0.08	0.02
Plec-1	0.37	0.12	0.05	0.01	0.01	0.00
Plec-2	0.26	0.12	0.04	0.02	0.01	0.00
Ppm1k-1	0.38	0.24	0.22	0.13	0.10	0.01
Ppm1k-2	0.22	0.38	0.29	0.15	0.09	0.02
Ppp3cb-1	0.37	0.23	0.12	0.21	0.01	0.00
Ppp3cb-2	0.47	0.48	0.43	0.27	0.08	0.01
Rnasel-1	0.33	0.74	0.90	0.85	0.28	0.04
Rnasel-2	0.30	0.24	0.20	0.35	0.03	0.00
Rsad-1	1.00	0.45	0.36	0.21	0.10	0.01
Rsad-2	0.26	0.36	0.28	0.16	0.03	0.01
Rtp4-1	0.33	0.57	0.60	0.53	0.15	0.01
Rtp4-2	1.14	1.09	1.35	0.91	0.32	0.05
Samd9l-1	0.32	0.26	0.20	0.20	0.02	0.00
Samd9l-2	0.33	0.18	0.11	0.06	0.04	0.01

Sfxn2-1	0.31	0.27	0.20	0.30	0.05	0.01
Sfxn2-2	1.22	0.20	0.11	0.13	0.01	0.00
Sh3bgrl-1	0.25	0.60	0.46	0.57	0.13	0.01
Sh3bgrl-2	0.30	0.10	0.07	0.05	0.00	0.00
Stat1-1	0.50	0.21	0.15	0.17	0.04	0.00
Stat1-2	0.32	1.87	1.45	0.96	0.21	0.02
Stat2-1	0.29	0.50	0.46	0.56	0.07	0.01
Stat2-2	0.25	0.23	0.21	0.19	0.03	0.00
Stat3-1	0.31	0.45	0.46	0.43	0.12	0.02
Stat3-2	0.35	0.89	0.64	0.73	0.11	0.01
Tap1-1	0.26	0.26	0.22	0.28	0.07	0.00
Tap1-2	0.21	0.86	0.95	0.75	0.12	0.01
Tapbp-1	0.21	0.85	1.13	1.33	0.76	0.25
Tapbp-2	0.28	0.25	0.20	0.25	0.04	0.00
Tbk1-1	0.32	0.64	0.80	1.08	0.18	0.02
Tbk1-2	0.19	0.91	0.99	0.74	0.13	0.01
Ticam1-1	0.27	0.05	0.03	0.02	0.01	0.00
Ticam1-2	0.28	0.21	0.18	0.07	0.06	0.00
Tlr3-1	0.32	0.06	0.02	0.01	0.01	0.00
Tlr3-2	0.38	1.11	1.80	1.97	0.73	0.11
Tlr7-1	0.34	0.61	0.83	0.59	0.13	0.01
Tlr7-2	0.32	0.25	0.16	0.12	0.00	0.00
Tlr9-1	0.29	0.11	0.10	0.05	0.04	0.01
Tlr9-2	0.32	0.17	0.12	0.14	0.05	0.00
Tmem140-1	0.30	0.14	0.08	0.12	0.01	0.00
Tmem140-2	0.28	0.33	0.30	0.25	0.09	0.04
Tor3a-1	0.25	0.21	0.21	0.27	0.06	0.01
Tor3a-2	0.26	0.28	0.26	0.12	0.06	0.01
Trex1-1	0.26	0.10	0.03	0.12	0.01	0.00
Trex1-2	0.28	0.16	0.09	0.03	0.01	0.00
Trim21-1	0.34	0.41	0.56	0.55	0.15	0.01
Trim21-2	0.34	0.34	0.28	0.15	0.08	0.00
Trim25-1	0.38	0.14	0.10	0.14	0.02	0.00
Trim25-2	0.30	0.35	0.32	0.22	0.09	0.02

Usp18-1	0.57	0.36	0.40	0.46	0.08	0.01
Usp18-2	0.31	0.34	0.53	0.32	0.15	0.02
Wwoxv-1	0.15	0.12	0.11	0.15	0.05	0.02
Wwoxv-2	0.29	0.22	0.22	0.23	0.06	0.00
Zc3hav1-1	0.20	0.18	0.13	0.04	0.02	0.01
Zc3hav1-2	0.17	0.38	0.39	0.47	0.14	0.01
Zfp182-1	0.00	0.13	0.04	0.00	0.03	0.00
Zfp182-2	0.36	0.75	1.12	1.03	0.26	0.04
Total	**100**	**100**	**100**	**100**	**100**	**100**

***Ifnar1*$^{-/-}$ MEF Experiment 2**

	Percentage					
	PLASMID LIB	**P0-293T**	**P1-VERO**	**P2-*Ifnar1*$^{-/-}$**	**P3-*Ifnar1*$^{-/-}$**	**P4-*Ifnar1*$^{-/-}$**
Adar-1	0.00	0.00	0.00	0.00	0.00	0.00
Adar-2	0.66	0.16	0.09	0.08	0.01	0.00
Atf2-1	0.41	0.18	0.10	0.10	0.03	0.01
Atf2-2	1.19	0.48	0.50	0.78	0.35	0.09
Atf3-1	0.58	0.46	0.37	0.32	0.04	0.01
Atf3-2	1.95	2.44	3.41	4.44	1.19	0.55
B2m-1	0.69	0.22	0.15	0.29	0.01	0.01
B2m-2	0.37	0.41	0.42	0.37	0.07	0.02
Birc6-1	0.49	0.28	0.27	0.24	0.08	0.02
Birc6-2	0.51	0.35	0.24	0.33	0.03	0.02
Brd4-1	0.45	1.25	1.73	1.22	0.56	0.16
Brd4-2	0.62	0.54	0.54	0.77	0.17	0.14
Cdkl4-1	0.63	0.67	0.56	0.30	0.07	0.00
Cdkl4-2	0.60	0.34	0.21	0.27	0.01	0.01
Clec4d-1	0.49	0.41	0.25	0.30	0.08	0.01
Clec4d-2	0.61	0.48	0.41	0.31	0.07	0.03
Clec4e-1	0.48	0.85	0.95	0.81	0.31	0.05
Clec4e-2	0.52	0.30	0.16	0.06	0.09	0.01
Cmpk2-1	1.56	0.69	0.44	0.21	0.03	0.00
Cmpk2-2	0.72	0.13	0.08	0.09	0.03	0.01
Cpeb3-1	0.01	0.08	0.12	0.09	0.04	0.01
Cpeb3-2	0.74	0.22	0.20	0.24	0.03	0.02
Cxcl10-1	0.56	0.66	0.77	0.67	0.28	0.07
Cxcl10-2	0.57	0.46	0.33	0.22	0.28	0.05
Cytip-1	0.62	0.38	0.20	0.27	0.02	0.01
Cytip-2	0.64	0.66	0.67	0.55	0.13	0.16
Daxx-1	0.41	1.16	1.42	0.99	0.55	0.12
Daxx-2	0.85	0.22	0.10	0.07	0.02	0.00
Ddx58-1	0.55	0.50	0.53	0.51	0.23	0.04

Ddx58-2	0.53	0.60	0.57	0.40	0.14	0.02
Ddx60-1	0.66	0.20	0.10	0.13	0.01	0.01
Ddx60-2	0.88	0.26	0.15	0.07	0.10	0.02
Dhx9-1	0.73	0.77	0.59	0.33	0.17	0.03
Dhx9-2	0.46	0.28	0.27	0.16	0.16	0.01
Dtx3l-1	0.69	0.84	0.76	0.66	0.13	0.06
Dtx3l-2	0.52	0.45	0.44	0.21	0.23	0.04
EGFP	0.49	0.02	0.02	0.02	0.02	0.01
Eif2ak2-1	0.53	0.56	0.48	0.36	0.04	0.01
Eif2ak2-2	0.49	0.27	0.29	0.50	0.02	0.05
Fa2h-1	0.75	0.44	0.25	0.11	0.03	0.01
Fa2h-2	0.68	0.26	0.16	0.19	0.02	0.01
Fbxo39-1	0.59	0.97	1.10	2.12	0.34	0.22
Fbxo39-2	0.63	0.25	0.15	0.12	0.21	0.02
Gbp2-1	0.78	0.30	0.20	0.15	0.09	0.01
Gbp2-2	0.53	1.77	2.29	2.80	1.61	0.50
Gbp3-1	0.52	0.54	0.45	0.41	0.07	0.02
Gbp3-2	0.62	0.76	0.72	0.50	0.16	0.04
Gbp6-1	0.00	1.17	1.43	1.46	0.30	0.16
Gbp6-2	0.13	0.00	0.00	0.00	0.00	0.00
Gcc-1	0.63	0.21	0.16	0.10	0.06	0.01
Gcc-2	0.51	0.79	0.88	0.71	0.24	0.06
Gvin-1	0.49	0.71	0.66	0.56	0.21	0.04
Gvin-2	0.39	0.72	0.71	0.60	0.28	0.05
Ifi27-1	0.52	1.24	1.18	0.77	0.32	0.05
Ifi27-2	0.61	1.38	1.82	1.51	0.30	0.09
Ifi35-1	0.39	0.21	0.10	0.05	0.05	0.01
Ifi35-2	0.45	2.14	2.54	1.64	0.53	0.11
Ifi44-1	0.41	0.84	0.76	0.81	0.37	0.10
Ifi44-2	0.46	0.50	0.61	0.67	0.12	0.08
Ifih1-1	0.51	0.21	0.12	0.05	0.04	0.01
Ifih1-2	0.68	1.01	1.32	1.29	0.30	0.17
Ifit1-1	0.86	0.15	0.12	0.22	0.01	0.01
Ifit1-2	0.45	0.48	0.40	0.54	0.34	0.06

Ifit3-1	0.47	0.47	0.34	0.44	0.05	0.02
Ifit3-2	0.58	0.44	0.30	0.27	0.02	0.00
Ifitm3-1	0.61	0.60	0.58	0.37	0.11	0.03
Ifitm3-2	**0.90**	**0.61**	**0.92**	**4.17**	**66.33**	**89.55**
Ifna1-1	0.48	0.66	0.54	0.41	0.22	0.07
Ifna1-2	0.65	0.36	0.37	0.36	0.12	0.06
Ifna4-1	0.29	0.65	0.56	0.51	0.10	0.05
Ifna4-2	0.48	0.29	0.26	0.26	0.10	0.02
Ifnb1-1	0.90	0.49	0.34	0.27	0.11	0.01
Ifnb1-2	0.39	0.30	0.49	0.48	0.16	0.07
Ikbka-1	0.55	0.16	0.12	0.13	0.02	0.00
Ikbka-2	0.53	0.34	0.22	0.19	0.01	0.01
Ikbkb-1	0.48	0.51	0.36	0.34	0.09	0.02
Ikbkb-2	0.61	0.70	0.59	0.78	0.14	0.05
Ikbke-1	1.25	0.56	0.49	0.30	0.08	0.01
Ikbke-2	0.61	0.68	0.59	0.56	0.08	0.02
Il15-1	0.55	0.57	0.36	0.21	0.12	0.03
Il15-2	0.56	0.70	0.58	0.40	0.14	0.03
Il6-1	0.78	0.60	0.59	0.40	0.08	0.02
Il6-2	0.52	0.62	0.58	0.41	0.25	0.04
Irf1-1	0.69	0.23	0.14	0.22	0.04	0.02
Irf1-2	0.51	0.26	0.17	0.11	0.02	0.00
Irf2-1	0.56	0.49	0.50	0.48	0.06	0.05
Irf2-2	0.67	0.50	0.34	0.24	0.05	0.01
Irf3-1	0.57	0.24	0.24	0.18	0.09	0.03
Irf3-2	0.68	0.42	0.32	0.27	0.07	0.03
Irf5-1	0.62	0.30	0.22	0.06	0.03	0.01
Irf5-2	0.61	0.16	0.05	0.05	0.01	0.00
Irf7-1	0.36	0.81	0.57	1.06	0.06	0.13
Irf7-2	0.57	1.36	1.97	2.49	0.93	0.43
Irf9-1	0.44	0.28	0.27	0.23	0.07	0.01
Irf9-2	0.51	0.27	0.20	0.19	0.05	0.01
Irgm-1	0.54	0.27	0.19	0.31	0.22	0.01
Irgm-2	0.58	0.81	1.05	1.19	0.39	0.16

Isg15-1	0.54	1.02	1.40	1.35	0.66	0.18
Isg15-2	0.53	0.24	0.22	0.18	0.04	0.01
Lgals3bp-1	0.58	0.64	0.72	0.69	0.15	0.09
Lgals3bp-2	0.71	0.31	0.25	0.13	0.06	0.01
Lgals8-1	0.80	0.60	0.50	0.59	0.11	0.04
Lgals8-2	0.45	0.13	0.10	0.07	0.03	0.01
Lrp4-1	0.65	0.21	0.08	0.05	0.15	0.02
Lrp4-2	0.51	0.53	0.50	0.44	0.08	0.02
Ly6e-1	0.45	0.21	0.13	0.07	0.04	0.02
Ly6e-2	0.37	0.44	0.44	0.81	0.53	0.07
Map3K8-1	0.49	0.63	0.59	0.73	0.07	0.03
Map3K8-2	0.52	0.50	0.31	0.29	0.62	0.12
Map4k2-1	0.45	0.60	0.44	0.37	0.14	0.03
Map4k2-2	0.44	0.35	0.21	0.11	0.05	0.01
Mapk8-1	0.54	0.64	0.54	0.32	0.10	0.03
Mapk8-2	0.62	0.61	0.59	0.43	0.15	0.04
Mbnl1-1	0.44	0.34	0.30	0.25	0.03	0.01
Mbnl1-2	0.50	0.29	0.19	0.16	0.02	0.01
miR-124	0.58	0.24	0.15	0.12	0.05	0.02
Mitd1-1	0.66	0.14	0.10	0.04	0.03	0.02
Mitd1-2	0.35	0.30	0.26	0.38	0.03	0.02
Mlkl-1	0.31	0.33	0.39	0.64	0.07	0.06
Mlkl-2	0.33	1.33	2.29	2.58	1.40	0.47
Mov10-1	0.46	0.78	0.93	1.08	0.60	0.14
Mov10-2	0.32	0.53	0.38	0.48	0.02	0.02
Myd88-1	0.35	0.56	0.49	0.35	0.08	0.03
Myd88-2	0.52	0.23	0.20	0.15	0.06	0.01
Nfkbia-1	0.33	0.51	0.49	0.22	0.33	0.14
Nfkbia-2	0.45	0.27	0.18	0.13	0.05	0.01
Nmi-1	0.53	0.78	0.84	0.98	0.17	0.08
Nmi-2	0.53	2.74	4.58	3.67	1.68	0.34
Oas1a-1	0.41	0.22	0.16	0.11	0.03	0.01
Oas1a-2	0.47	0.26	0.19	0.06	0.05	0.01
Oas2-1	0.50	0.26	0.12	0.17	0.03	0.01

Oas2-2	0.94	0.28	0.17	0.13	0.03	0.00
Oasl1-1	0.41	0.71	0.84	1.09	0.09	0.14
Oasl1-2	0.22	0.57	0.43	0.26	0.13	0.03
Oasl2-1	0.59	0.51	0.40	0.35	0.08	0.03
Oasl2-2	0.23	0.52	0.34	0.22	0.01	0.01
p50	0.50	0.53	0.53	0.59	0.14	0.03
p50	0.26	0.40	0.31	0.22	0.09	0.02
p65	0.35	0.38	0.26	0.28	0.03	0.01
p65	0.30	0.18	0.11	0.10	0.01	0.00
Papr14-2	0.34	0.57	0.47	0.38	0.15	0.02
Parp10-1	0.25	0.13	0.12	0.19	0.02	0.03
Parp10-2	0.42	0.78	0.85	0.78	0.29	0.06
Parp11-1	0.34	0.04	0.02	0.03	0.02	0.00
Parp11-2	0.38	0.27	0.18	0.42	0.01	0.03
Parp12-1	0.24	0.12	0.08	0.07	0.03	0.03
Parp12-2	0.33	0.42	0.39	0.55	0.09	0.04
Parp14-1	0.13	0.48	0.43	0.37	0.04	0.01
Parp9-1	0.35	0.06	0.06	0.10	0.13	0.01
Parp9-2	0.37	0.28	0.29	0.41	0.05	0.04
Plec-1	0.37	0.12	0.05	0.05	0.01	0.01
Plec-2	0.26	0.12	0.04	0.04	0.01	0.00
Ppm1k-1	0.38	0.24	0.22	0.22	0.15	0.03
Ppm1k-2	0.22	0.38	0.29	0.12	0.02	0.01
Ppp3cb-1	0.37	0.23	0.12	0.33	0.02	0.01
Ppp3cb-2	0.47	0.48	0.43	0.34	0.02	0.01
Rnasel-1	0.33	0.74	0.90	0.74	0.17	0.07
Rnasel-2	0.30	0.24	0.20	0.22	0.02	0.02
Rsad-1	1.00	0.45	0.36	0.39	0.11	0.02
Rsad-2	0.26	0.36	0.28	0.20	0.05	0.02
Rtp4-1	0.33	0.57	0.60	0.75	0.45	0.06
Rtp4-2	1.14	1.09	1.35	1.04	0.47	0.15
Samd9l-1	0.32	0.26	0.20	0.21	0.02	0.02
Samd9l-2	0.33	0.18	0.11	0.04	0.03	0.01
Sfxn2-1	0.31	0.27	0.20	0.32	0.06	0.02

Sfxn2-2	1.22	0.20	0.11	0.10	0.05	0.01
Sh3bgrl-1	0.25	0.60	0.46	0.76	0.10	0.05
Sh3bgrl-2	0.30	0.10	0.07	0.04	0.03	0.01
Stat1-1	0.50	0.21	0.15	0.15	0.02	0.01
Stat1-2	0.32	1.87	1.45	1.06	0.32	0.06
Stat2-1	0.29	0.50	0.46	0.51	0.06	0.03
Stat2-2	0.25	0.23	0.21	0.15	0.05	0.01
Stat3-1	0.31	0.45	0.46	0.32	0.09	0.02
Stat3-2	0.35	0.89	0.64	0.57	0.07	0.03
Tap1-1	0.26	0.26	0.22	0.23	0.03	0.02
Tap1-2	0.21	0.86	0.95	0.69	0.28	0.04
Tapbp-1	0.21	0.85	1.13	1.42	1.77	0.63
Tapbp-2	0.28	0.25	0.20	0.21	0.05	0.03
Tbk1-1	0.32	0.64	0.80	0.55	0.47	0.13
Tbk1-2	0.19	0.91	0.99	0.56	0.14	0.03
Ticam1-1	0.27	0.05	0.03	0.01	0.00	0.00
Ticam1-2	0.28	0.21	0.18	0.18	0.04	0.02
Tlr3-1	0.32	0.06	0.02	0.02	0.01	0.01
Tlr3-2	0.38	1.11	1.80	2.24	1.03	0.22
Tlr7-1	0.34	0.61	0.83	0.96	0.23	0.07
Tlr7-2	0.32	0.25	0.16	0.10	0.03	0.00
Tlr9-1	0.29	0.11	0.10	0.09	0.04	0.02
Tlr9-2	0.32	0.17	0.12	0.10	0.02	0.01
Tmem140-1	0.30	0.14	0.08	0.10	0.04	0.02
Tmem140-2	0.28	0.33	0.30	0.29	0.13	0.04
Tor3a-1	0.25	0.21	0.21	0.35	0.07	0.06
Tor3a-2	0.26	0.28	0.26	0.23	0.08	0.02
Trex1-1	0.26	0.10	0.03	0.06	0.00	0.00
Trex1-2	0.28	0.16	0.09	0.04	0.01	0.01
Trim21-1	0.34	0.41	0.56	0.68	0.25	0.11
Trim21-2	0.34	0.34	0.28	0.30	0.06	0.01
Trim25-1	0.38	0.14	0.10	0.08	0.02	0.01
Trim25-2	0.30	0.35	0.32	0.41	0.15	0.03
Usp18-1	0.57	0.36	0.40	0.49	0.09	0.05

Usp18-2	0.31	0.34	0.53	0.59	0.20	0.04
Wwoxv-1	0.15	0.12	0.11	0.07	0.08	0.04
Wwoxv-2	0.29	0.22	0.22	0.17	0.11	0.03
Zc3hav1-1	0.20	0.18	0.13	0.08	0.02	0.00
Zc3hav1-2	0.17	0.38	0.39	0.56	0.12	0.04
Zfp182-1	0.00	0.13	0.04	0.02	0.01	0.00
Zfp182-2	0.36	0.75	1.12	1.26	0.58	0.13
Total	**100**	**100**	**100**	**100**	**100**	**100**

Appendix 4

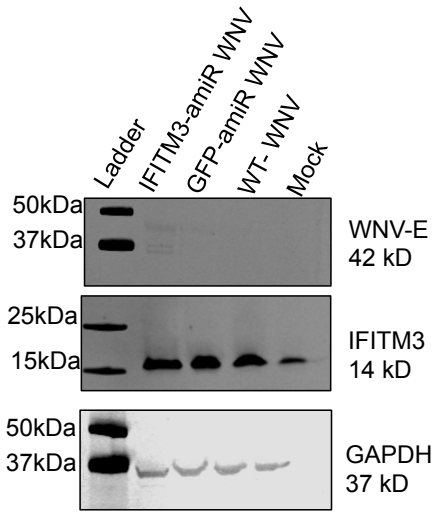

Figure 1: Infection of WTMEF cells with MOI=10 of respective viruses is not sufficient does not result into effective WNV infection. WT MEFs were infected with IFITM3-amiR WNV, GFP-amiR WNV, WT-WNV at MOI=10 or mock infected. At 48hpi, cell lysates were harvested in NP-40 lysis buffer and subjected to western blot analysis. Blots were probed with rabbit polyclonal anti-IFITM3, anti-WNV-E and mouse anti-GAPDH antibodies. Expected band sizes were 14 kDa, 42 kDa and 37 kDa for IFITM3, WNV-E and GAPDH respectively.

Appendix 5

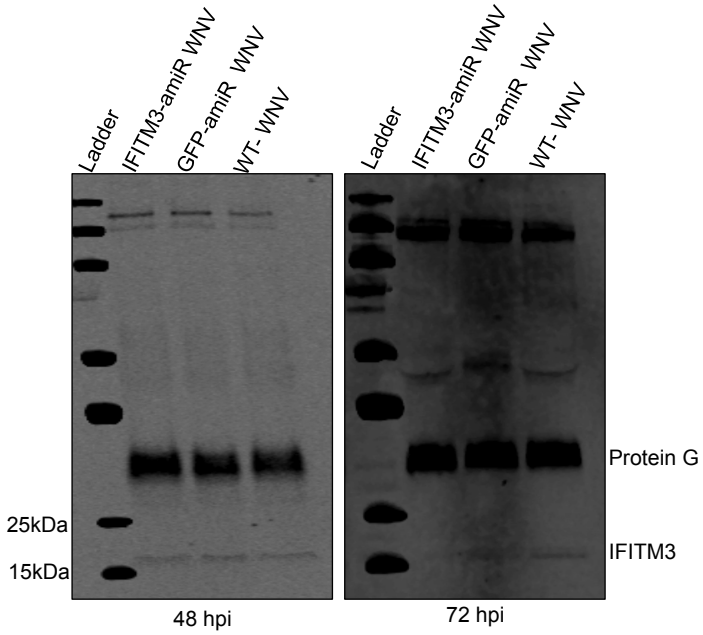

Figure 2: **Less IFITM3 was incorporated into virions secreted at 72 hpi compared to 48 hpi.** *Ifnar1*$^{-/-}$ MEFs were infected at MOI=1, 48 hpi, virus culture fluid was collected, cells washed with PBS and new DMEM to generate 72 hpi sample. At 48 hpi and 72 hpi, an equal amount (250 µL) of virus particles were immunoprecipitated from each sample by binding a fixed amount (5 µg) of purified anti-E monoclonal antibody (6B6C-1) as the capture antibody on Dynabead protein G (Invitrogen, USA). Immunoprecipitated WNV-E protein was thereafter subjected to western blot analysis. Blots were probed with rabbit polyclonal anti-IFITM3 and the expected band size was 14 kDa.

Appendix 6

Animal ethics approval certificates

THE UNIVERSITY OF QUEENSLAND
AUSTRALIA

Office of Research Ethics
Director
Nicole Shively

Animal Ethics Approval Certificate

18-Sep-2018

Please check all details below and inform the Animal Ethics Unit within 10 working days if anything is incorrect.

Activity Details

Chief Investigator: Dr Yin Xiang Setoh, Chemistry and Molecular Biosciences

Title: In vivo screening of host genes critical for controlling West Nile virus replication/pathogenesis

AEC Approval Number: SCMB/008/17

Previous AEC Number:

Approval Duration: 05-Apr-2017 to 05-Apr-2019

Funding Body:

Group: Molecular Biosciences

Other Staff/Students: Alberto Amarilla Ortiz, Faith Elizabeth Nanyonga, Kevin Wathen-Dunn

Location(s): St Lucia Bldg 75 - AIBN

Summary

Subspecies	Strain	Class	Gender	Source	Approved	Remaining
Mice - non genetically modified	CD1	Juvenile / Weaners / Pouch animal	Mix		146	130

Permits

Provisos

Approval Details

Description		Amount	Balance
Mice - non genetically modified (CD1, Mix, Juvenile / Weaners / Pouch animal,)			
5 Apr 2017	Initial approval	26	26
31 Dec 2017	Use in 2017 (from 2018 MAR; AEMAR41053)	-16	10
19 Sep 2018	Mod #1	120	130

Animal Ethics Unit
Office of Research Ethics
The University of Queensland

Cumbrae-Stewart Building
Research Road
St Lucia Qld 4072 Australia

+61 7 336 52925 (Enquiries)
+61 7 334 68710 (Enquiries)
+61 7 336 52713 (Coordinator)

animal.ethics@research.uq.edu.au
uq.edu.au/research

UQ Research and Innovation
Director, Research Management Office
Nicole Thompson

Animal Ethics Approval Certificate

10-Apr-2017

Please check all details below and inform the Animal Welfare Unit within 10 working days if anything is incorrect.

Activity Details

Chief Investigator: Dr Yin Xiang Setoh, Chemistry and Molecular Biosciences

Title: In vivo screening of host genes critical for controlling West Nile virus replication/pathogenesis

AEC Approval Number: SCMB/008/17

Previous AEC Number:

Approval Duration: 05-Apr-2017 to 05-Apr-2019

Funding Body:

Group: Molecular Biosciences

Other Staff/Students: Alberto Amarilla Ortiz, Faith Nanyonga, Kevin Wathen-Dunn

Location(s): St Lucia Bldg 75 - AIBN

Summary

Subspecies	Strain	Class	Gender	Source	Approved	Remaining
Mice - non genetically modified	CD1	Juvenile / Weaners / Pouch animal	Mix		26	26

Permits

Provisos

Approval Details

Description	Amount	Balance
Mice - non genetically modified (CD1, Mix, Juvenile / Weaners / Pouch animal,)		
5 Apr 2017 Initial approval	26	26

Please note the animal numbers supplied on this certificate are the total allocated for the approval duration

Please use this Approval Number:

1. When ordering animals from Animal Breeding Houses
2. For labelling of all animal cages or holding areas. In addition please include on the label, Chief Investigator's name and contact phone number.
3. When you need to communicate with this office about the project.

It is a condition of this approval that all project animal details be made available to Animal House OIC. (UAEC Ruling 14/12/2001)

The Chief Investigator takes responsibility for ensuring all legislative, regulatory and compliance objectives are satisfied for this project.

This certificate supercedes all preceeding certificates for this project (i.e. those certificates dated before 10-Apr-2017)

UQ Research and Innovation
Director, Research Management Office
Nicole Thompson

Animal Ethics Approval Certificate

06-Jan-2016

Please check all details below and inform the Animal Welfare Unit within 10 working days if anything is incorrect.

Activity Details

Chief Investigator: Dr Yin Xiang Setoh, Chemistry and Molecular Biosciences

Title: Investigating the role of mutant West Nile virus on viral pathogenesis and innate immune pathways

AEC Approval Number: AIBN/327/15/NHMRC

Previous AEC Number: SCMB/331/12/NHMRC

Approval Duration: 15-Sep-2015 to 15-Sep-2018

Funding Body: NHMRC

Group: Molecular Biosciences

Other Staff/Students: Gabor Pali, Judy Edmonds, Kevin Wathen-Dunn

Location(s): St Lucia Bldg 75 - AIBN

Summary

Subspecies	Strain	Class	Gender	Source	Approved	Remaining
Mice - genetically modified	IFNAR1-/-	Adults	Mix	Institutional Breeding Colony	50	50
Mice - genetically modified	IRF3/7-/-	Adults	Mix	Institutional Breeding Colony	50	50
Mice - genetically modified	IRF3-/-	Adults	Mix	Institutional Breeding Colony	50	50
Mice - genetically modified	IRF7-/-	Adults	Mix	Institutional Breeding Colony	50	50
Mice - non genetically modified	CD1	Juvenile / Weaners / Pouch animal	Mix	Commercial breeding colony	1090	1090
Mice - non genetically modified	CD1	Adults	Mix	Commercial breeding colony	810	810
Mice - non genetically modified	C57BL/6	Adults	Mix	Commercial breeding colony	50	50

Permits

Provisos

LD50 is not permitted on this project, all animals showing distress are to be humanely euthanase prior to this.

Approval Details

Description	Amount	Balance
Mice - genetically modified (IFNAR1-/-, Mix, Adults, Institutional Breeding Colony)		
2 Sep 2015 Initial approval	50	50

Mice - genetically modified (IRF3-/-, Mix, Adults, Institutional Breeding Colony)		
2 Sep 2015 Initial Approval	50	50
Mice - genetically modified (IRF3/7-/-, Mix, Adults, Institutional Breeding Colony)		
2 Sep 2015 Initial approval	50	50
Mice - genetically modified (IRF7-/-, Mix, Adults, Institutional Breeding Colony)		
2 Sep 2015 Initial Approval	50	50
Mice - non genetically modified (C57BL/6 , Mix, Adults, Commercial breeding colony)		
2 Sep 2015 Initial approval	50	50
Mice - non genetically modified (CD1, Mix, Adults, Commercial breeding colony)		
2 Sep 2015 Initial approval	810	810
Mice - non genetically modified (CD1, Mix, Juvenile / Weaners / Pouch animal, Commercial breeding colony)		
2 Sep 2015 Initial approval	1090	1090

Please note the animal numbers supplied on this certificate are the total allocated for the approval duration

Please use this Approval Number:

1. When ordering animals from Animal Breeding Houses
2. For labelling of all animal cages or holding areas. In addition please include on the label, Chief Investigator's name and contact phone number.
3. When you need to communicate with this office about the project.

It is a condition of this approval that all project animal details be made available to Animal House OIC.
(UAEC Ruling 14/12/2001)

The Chief Investigator takes responsibility for ensuring all legislative, regulatory and compliance objectives are satisfied for this project.

This certificate supercedes all preceeding certificates for this project (i.e. those certificates dated before 06-Jan-2016)

Appendix 7

Percentage enrichment in spleens

	Percentage enrichment in spleen						
NAME	**p1-vero**	**1**	**2**	**3**	**4**	**5**	**6**
Adar-1	0	0.00	0.00	0.0	0	0.0	0.01
Adar-2	0.1	0.0	0.01	0.0	0.0	1.8	0.0
Atf2-1	0.1	0.0	0.01	0.0	0.0	0.1	0.0
Atf2-2	0.5	0.0	0.01	0.0	0.0	0.0	0.0
Atf3-1	0.4	0.0	0.00	0.0	0.0	0.0	0.0
Atf3-2	3.4	18.3	76.87	46.8	97.3	0.2	0.1
B2m-1	0.2	0.0	0.00	0.0	0.0	0.0	1.9
B2m-2	0.4	0.0	0.00	0.0	0.0	0.0	0.0
Birc6-1	0.3	0.0	0.00	0.0	0.0	0.0	0.0
Birc6-2	0.2	0.0	0.00	0.0	0.0	0.0	0.0
Brd4-1	1.7	0.0	0.00	9.5	0.0	0.0	0.0
Brd4-2	0.5	0.0	0.00	0.0	0.0	0.0	0.0
Cdkl4-1	0.6	0.0	0.00	0.0	0.0	0.0	0.0
Cdkl4-2	0.2	0.1	0.01	0.0	0.0	0.0	0.0
Clec4d-1	0.3	0.0	0.00	0.0	0.0	0.0	0.0
Clec4d-2	0.4	2.0	0.05	0.0	0.0	0.0	0.0
Clec4e-1	1.0	0.0	0.00	0.0	0.0	0.0	0.0
Clec4e-2	0.2	0.0	0.00	0.0	0.0	0.0	0.0
Cmpk2-1	0.4	0.0	0.01	0.0	0.0	0.0	0.0
Cmpk2-2	0.1	0.0	0.01	0.0	0.0	0.0	0.0
Cpeb3-1	0.1	0.0	1.16	0.0	0.0	0.0	0.0
Cpeb3-2	0.2	0.0	0.00	0.0	0.0	0.0	0.0
Cxcl10-1	0.8	0	0.00	0	0	0	0
Cxcl10-2	0.3	0	0.00	0	0	0	0
Cytip-1	0.2	0.0	0.00	0.0	0.1	0.0	0.0
Cytip-2	0.7	0.0	0.01	0.0	0.0	0.0	0.0
Daxx-1	1.4	0.0	0.00	0.0	0.0	0.0	0.1
Daxx-2	0.1	0.00	0.00	0.0	5E-06	0.01	0
Ddx58-1	0.5	0.0	0.00	4.1	0.0	0.0	3.7
Ddx58-2	0.6	0.0	0.00	0.0	0.0	0.0	0.0
Ddx60-1	0.1	0.00	0.00	0.00	0.00	0.00	0.00
Ddx60-2	0.2	0.0	0.00	0.0	0.0	0.0	0.0
Dhx9-1	0.6	0.1	0.01	0.0	0.0	0.2	0.0
Dhx9-2	0.3	0.0	0.00	0.0	0.0	0.0	0.0
Dtx3l-1	0.8	0.0	0.00	0.0	0.0	0.0	0.0
Dtx3l-2	0.4	0.0	0.00	0.0	0.0	0.0	0.0
EGFP	0.0	0.0	0.00	0.0	0.0	0.0	0.0
Eif2ak2-1	0.5	0.0	0.00	0.0	0.0	0.2	0.0

Eif2ak2-2	0.3	0.0	0.01	0.6	0.0	0.0	0.0
Fa2h-1	0.2	0.0	0.01	0.0	0.0	0.0	0.0
Fa2h-2	0.2	1.8	0.06	0.0	0.0	0.0	2.3
Fbxo39-1	1.1	0.0	0.01	0.0	1.2	80.3	0.1
Fbxo39-2	0.2	0.7	0.05	0.0	0.0	0.0	0.1
Gbp2-1	0.2	0.0	0.00	14.64	0.0	0.0	0.1
Gbp2-2	2.3	0.0	0.00	0.0	0.0	0.02	0.0
Gbp3-1	0.4	0.0	0.00	0.0	0.0	0.0	0.0
Gbp3-2	0.7	6.1	0.13	0.0	0.0	0.0	0.0
Gbp6-1	1.4	0.00	0.00	0.0	0	0.0	0.0
Gbp6-2	0.0	0.0	0.00	0.0	0.0	0.00	0.0
Gcc-1	0.2	0.0	0.00	0.0	0.0	0.0	0.0
Gcc-2	0.9	0.0	0.00	0.0	0.0	0.0	0.0
Gvin-1	0.7	0.0	0.00	0.0	0.0	0.1	0.0
Gvin-2	0.7	0.0	0.01	0.0	0.0	0.0	0.0
Ifi27-1	1.2	0.0	0.03	0.2	0.0	0.0	0.0
Ifi27-2	1.8	0.0	0.00	0.0	0.0	0.0	0.0
Ifi35-1	0.1	0.0	0.03	0.0	0.0	0.0	0.0
Ifi35-2	2.5	0.0	0.01	0.0	0.2	0.0	0.0
Ifi44-1	0.8	0.0	0.00	0.0	0.0	0.0	0.0
Ifi44-2	0.6	0.0	0.01	0.0	0.0	0.0	0.0
Ifih1-1	0.1	0.0	0.00	0.0	0.0	0.0	0.0
Ifih1-2	1.3	0.0	0.00	0.0	0.0	0.5	0.0
Ifit1-1	0.1	0.0	0.00	0.0	0.0	0.0	0.0
Ifit1-2	0.4	0.0	0.01	0.0	0.0	0.0	0.0
Ifit3-1	0.3	0.0	0.00	0.1	0.0	0.1	0.0
Ifit3-2	0.3	0.0	0.01	0.0	0.0	0.1	0.0
Ifitm3-1	0.6	0.1	0.13	0.1	0.0	0.8	0.3
Ifitm3-2	0.9	0.0	1.38	0.0	0.0	0.1	0.0
Ifna1-1	0.5	0.0	0.00	0.0	0.0	0.0	0.0
Ifna1-2	0.4	0.0	0.01	0.0	0.0	0.0	0.0
Ifna4-1	0.6	0.0	0.00	0.0	0	0.0	1.84
Ifna4-2	0.3	0.0	0.00	0.0	0.0	0	0.0
Ifnb1-1	0.3	0	0.00	0	0	0.0	0.0
Ifnb1-2	0.5	0.0	0.01	0.0	0.0	0.0	0.0
Ikbka-1	0.1	0	0.00	0	0.0	0.0	0
Ikbka-2	0.2	0.0	0.00	0.0	0.0	0.0	0.0
Ikbkb-1	0.4	0.0	4.69	0.0	0.0	0.0	0.0
Ikbkb-2	0.6	0.0	0.00	0.0	0.0	0.0	0.0
Ikbke-1	0.5	0.0	0.01	0.0	0.0	0.0	4.4
Ikbke-2	0.6	0.0	0.00	0.0	0.0	0.4	0.0
Il15-1	0.4	0.0	0.00	0.0	0.0	0.0	0.0
Il15-2	0.6	0.0	0.00	0.0	0.0	0.0	0.0
Il6-1	0.6	0.0	0.00	0.0	0.0	0.0	0.0
Il6-2	0.6	0.1	0.03	0.0	0.0	0.0	0.0
Irf1-1	0.1	0.02	0.00	0.00	0.00	0.0	0.00
Irf1-2	0.2	0.0	0.01	0.0	0.0	0.00	19.8

Irf2-1	0.5	0.0	0.00	0.0	0	0.0	0.0
Irf2-2	0.3	0.0	0.00	0.0	0.0	0.0	0
Irf3-1	0.2	0.0	0.00	0.0	0.0	0	0.0
Irf3-2	0.3	0.0	0.51	0.0	0.0	0.1	0.0
Irf5-1	0.2	0.0	0.00	0.0	0.0	0.0	0.0
Irf5-2	0.1	0.0	0.00	0.0	0.0	0.0	0.0
Irf7-1	0.6	3.6	0.12	0.0	0.0	0.0	0.0
Irf7-2	2.0	0.0	0.0	0.01	0.0	0.0	0.0
Irf9-1	0.3	0.0	0.00	0.0	0.0	0.0	0.0
Irf9-2	0.2	0.0	0.00	0.0	0.0	0.0	0.0
Irgm-1	0.2	0.0	0.00	0.0	0.0	0.0	0.2
Irgm-2	1.1	0.0	0.00	0.0	0.0	0.0	0.0
Isg15-1	1.4	0	0.00	0	0	0.0	0.0
Isg15-2	0.2	0.0	0.00	0.0	0.0	0.0	0.0
Lgals3bp-1	0.7	0.0	0.00	0.0	0.0	0.0	0.0
Lgals3bp-2	0.2	0.0	0.06	0.0	0.0	0.0	0.0
Lgals8-1	0.5	0.0	0.00	0.0	0.0	0.1	0.0
Lgals8-2	0.1	0.0	0.00	0.0	0.0	0.0	0.0
Lrp4-1	0.1	0.0	0.00	0.0	0.0	0.0	0.0
Lrp4-2	0.5	0.0	0.00	0.0	0.0	0.0	0.0
Ly6e-1	0.1	0.0	0.00	0.0	0.0	0.0	0.1
Ly6e-2	0.4	0.0	0.00	0.0	0.0	12.9	0.0
Map3K8-1	0.6	0.0	0.00	0.1	0.0	0.0	0.0
Map3K8-2	0.3	0.0	0.02	0.0	0.0	0.0	0.0
Map4k2-1	0.4	1.1	0.31	0.0	0.0	0.0	0.0
Map4k2-2	0.2	0.1	5.05	0.0	0.0	0.0	0.0
Mapk8-1	0.5	0.0	0.04	0.0	0.0	0.3	12.8
Mapk8-2	0.6	0.0	0.00	0.0	0.0	0.0	0.0
Mbnl1-1	0.3	0.0	0.01	0.0	0.0	0.1	0.0
Mbnl1-2	0.2	0.0	0.00	0.0	0.0	0.0	0.0
miR-124	0.2	0.0	0.01	0.0	0.0	0.0	0.5
Mitd1-1	0.1	0.0	0.00	0.0	0.0	0.1	0.0
Mitd1-2	0.3	0.0	0.18	20.6	0.1	0.0	11.3
Mlkl-1	0.4	0.0	0.01	0.0	0.0	0.0	0.0
Mlkl-2	2.3	0.0	0.00	0.0	0.0	0.0	0.0
Mov10-1	0.9	0.0	0.05	0.0	0.0	0.0	0.0
Mov10-2	0.4	0.0	0.01	0.0	0.0	0.0	0.0
Myd88-1	0.5	0.0	0.00	0.0	0.0	0.0	0.0
Myd88-2	0.2	0.0	0.02	0.0	0.0	0.0	0.0
Nfkbia-1	0.5	0	0.00	0	0	0.0	0.0
Nfkbia-2	0.2	0.1	0.00	0.0	0.0	0	0.0
Nmi-1	0.8	0.0	0.00	0.0	0.1	0.0	0.0
Nmi-2	4.6	0.0	0.03	0.0	0.0	0.0	0.0
Oas1a-1	0.2	0	0.00	0.0	0.0	0.0	0.00
Oas1a-2	0.2	0.0	0.01	0.0	0.0	0.0	6.3
Oas2-1	0.1	0.0	0.03	0.0	0.0	0.0	0.0
Oas2-2	0.2	0.0	0.02	0.0	0.0	0.0	0.0

Oasl1-1	0.8	0.0	0.00	0.0	0.0	0.0	0.0
Oasl1-2	0.4	0.0	0.00	0.0	0.0	0.0	0.0
Oasl2-1	0.4	0.0	0.00	0.0	0.0	0.0	0.0
Oasl2-2	0.3	0.0	0.00	0.0	0.0	0.0	0.0
p50	0.5	0.0	0.00	0.0	0.0	0.0	0.0
p50	0.3	0.0	0.01	0.0	0.0	0.0	0.0
p65	0.3	0.0	0.00	0.0	0.0	0.0	0.2
p65	0.1	0.0	0.01	0.0	0.0	0.1	0.0
Papr14-2	0.5	34.5	0.00	0.0	0.0	0.0	0.0
Parp10-1	0.1	0.0	0.69	0.0	0.0	0.0	0.0
Parp10-2	0.9	0.0	0.00	0.0	0.0	0.00	0.0
Parp11-1	0.0	0.0	0.00	0.0	0.0	0.0	0.0
Parp11-2	0.2	0.0	0.00	0.1	0.0	0.0	0.0
Parp12-1	0.1	0.0	0.00	0.0	0.0	0.0	0.0
Parp12-2	0.4	0.0	0.09	0.0	0.0	0.0	0.0
Parp14-1	0.4	0.0	0.00	0.0	0.0	0.0	0.0
Parp9-1	0.1	0.0	0.00	0.0	0.0	0.0	0.0
Parp9-2	0.3	0.0	0.00	0.0	0.0	0.0	0.0
Plec-1	0.1	0.0	0.00	0.0	0.0	0.0	0.0
Plec-2	0.0	0	0.00	0	0	0.0	0
Ppm1k-1	0.2	0.0	0.00	0.0	0.0	0.01	0.0
Ppm1k-2	0.3	0.0	0.13	0.0	0.0	0.0	0.0
Ppp3cb-1	0.1	0.0	0.00	0.0	0.0	0.0	0.0
Ppp3cb-2	0.4	0.0	0.03	0.0	0.0	0.0	0.0
Rnasel-1	0.9	0.0	0.00	0.0	0.0	0.0	0.0
Rnasel-2	0.2	0.0	0.00	0.0	0.0	0.0	0.0
Rsad-1	0.4	15.8	0.00	0.0	0.0	0.0	0.0
Rsad-2	0.3	14.75	0.37	0.01	0.01	0.0	0.01
Rtp4-1	0.6	0.0	0.31	0.0	0.0	0.03	0.0
Rtp4-2	1.4	0.0	0.00	0.0	0.00	0.0	0
Samd9l-1	0.2	0.0	0.01	0.0	0.0	0.05	0.0
Samd9l-2	0.1	0.0	0.00	0.0	0.0	0.0	0.0
Sfxn2-1	0.2	0.0	0.01	0.0	0.0	0.0	0.0
Sfxn2-2	0.1	0.0	0.00	0.0	0.0	0.0	0.0
Sh3bgrl-1	0.5	0.0	0.00	0.0	0.0	0.1	0.0
Sh3bgrl-2	0.1	0.0	0.00	1.5	0.0	0.0	0.0
Stat1-1	0.2	0.0	0.00	0.0	0.0	0.1	0.0
Stat1-2	1.4	0.0	0.00	0.0	0.0	0.0	0.0
Stat2-1	0.5	0.0	0.00	0.0	0.0	0.0	0.0
Stat2-2	0.2	0.0	0.00	0.0	0.0	0.0	0.1
Stat3-1	0.5	0.0	0.00	0.0	0.0	0.0	0.0
Stat3-2	0.6	0.0	0.00	0.0	0.00	0.0	0.0
Tap1-1	0.2	0.0	0.03	0.0	0.0	0.0	0.0
Tap1-2	1.0	0.0	0.00	0.0	0.01	0.0	0.0
Tapbp-1	1.1	0.00	0.01	0.00	0.00	0.0	0.00
Tapbp-2	0.2	0.00	0.00	0.01	0.00	0.00	0.00
Tbk1-1	0.8	0.0	0.01	0.0	0.0	0.00	0.0

Tbk1-2	1.0	0.01	0.00	0.00	0.00	0.0	0.00
Ticam1-1	0.0	0.00	0.00	0.00	0.00	0.00	0.00
Ticam1-2	0.2	0.0	0.00	0.0	0.01	0.01	32.8
Tlr3-1	0.0	0.0	0.14	0.0	0.0	0.1	0.0
Tlr3-2	1.8	0.0	0.00	0.0	0.0	0.0	0.0
Tlr7-1	0.8	0.0	0.01	0.0	0.0	0.0	0.0
Tlr7-2	0.2	0.0	0.08	0.0	0.0	0.0	0.0
Tlr9-1	0.1	0	0.04	0	0	0.0	0.0
Tlr9-2	0.1	0.0	0.00	0.0	0.0	0.0	0.0
Tmem140-1	0.1	0.0	0.00	0.0	0.0	0.0	0.0
Tmem140-2	0.3	0.0	0.00	0.0	0.0	0.0	0.0
Tor3a-1	0.2	0.0	0.00	0.0	0	0.0	0.0
Tor3a-2	0.3	0.0	0.01	0.0	0.4	0.0	0.0
Trex1-1	0.0	5E-03	0.01	2E-03	0E+00	0.0	4E-03
Trex1-2	0.1	0.0	0.01	0.0	0	4E-02	0
Trim21-1	0.6	0.0	0.00	0.0	0.0	0.00	0.0
Trim21-2	0.3	0.0	0.00	0.0	0.0	0.0	0.0
Trim25-1	0.1	0.0	0.00	0.0	0.0	0.0	0.0
Trim25-2	0.3	0.0	6.47	0.0	0.0	0.0	0.0
Usp18-1	0.4	0.0	0.00	0.9	0.0	0.0	0.0
Usp18-2	0.5	0.0	0.04	0.0	0.0	0.0	0.0
Wwoxv-1	0.1	0.0	0.00	0.0	0.0	0.0	0.0
Wwoxv-2	0.2	0	0.00	0.0	0	0.0	0.0
Zc3hav1-1	0.1	0.0	0.00	0.0	0.0	0.0	0.0
Zc3hav1-2	0.4	0.0	0.05	0.0	0.0	0.0	0.0
Zfp182-1	0.0	0.0	0.00	0.00	0.0	0.0	0.0
Zfp182-2	1.1	0.0	0.0	0.0	0.0	0.0	0.0
EGFP	0.0	0.0	0.0	0.0	0.0	0.0	0.0
miR-124	0.2	0.0	0.0	0.0	0.0	0.0	0.0
TOTAL	**100**	**100**	**100**	**100**	**100**	**100**	**100**

Appendix 8

Percentage enrichment of amiR-encoding encoding viruses in the mouse brains A comparison was made between p1-Vero (inoculum used to infect mice) *vs* viruses enriched in the brains

	Percentage			
Name	**P1-vero**	**Brain 2**	**Brain 3**	**Brain 4**
Adar-1	0	0	0	0
Adar-2	0.1	0.0	0.0	0.0
Atf2-1	0.1	0.0	0.0	0.0
Atf2-2	0.5	0.0	0.0	0.0
Atf3-1	0.4	0.0	0.0	0.0
Atf3-2	3.4	0.4	99.4	0.1
B2m-1	0.2	0.0	0.0	0.0
B2m-2	0.4	0.0	0.0	0.0
Birc6-1	0.3	0.0	0.0	0.0
Birc6-2	0.2	0.0	0.0	0.0
Brd4-1	1.7	0.0	0.0	0.0
Brd4-2	0.5	0.0	0.0	0.0
Cdkl4-1	0.6	0.0	0.0	0.0
Cdkl4-2	0.2	0	0	0.0
Clec4d-1	0.3	0.0	0	0.0
Clec4d-2	0.4	0.0	0.0	0.0
Clec4e-1	1.0	0.0	0.0	0.0
Clec4e-2	0.2	0.0	0.0	0.0
Cmpk2-1	0.4	0.0	0.0	0.0
Cmpk2-2	0.1	0.0	0.0	0.0
Cpeb3-1	0.1	0.0	0.0	0.0
Cpeb3-2	0.2	0.0	0	0.0
Cxcl10-1	0.8	0	0	0
Cxcl10-2	0.3	0	0	0
Cytip-1	0.2	0	0	0.0
Cytip-2	0.7	0.0	0.0	0.0
Daxx-1	1.4	0.0	0.0	0.0
Daxx-2	0.1	0.0	0	0
Ddx58-1	0.5	0.0	0.0	0.0
Ddx58-2	0.6	0.0	0.0	0.0
Ddx60-1	0.1	0	0	0.00
Ddx60-2	0.2	0.0	0.0	0.0
Dhx9-1	0.6	0.0	0.0	0.0
Dhx9-2	0.3	0.0	0.0	0.0
Dtx3l-1	0.8	0.0	0.0	0.0
Dtx3l-2	0.4	0.0	0.0	0.0
EGFP	0.0	0.0	0	0.0
Eif2ak2-1	0.5	0.0	0.0	0.0
Eif2ak2-2	0.3	0.0	0.0	0.0

Fa2h-1	0.2	0.0	0.0	0.0
Fa2h-2	0.2	0.0	0.0	0.0
Fbxo39-1	1.1	0.0	0.0	0.0
Fbxo39-2	0.2	0.0	0.0	0.0
Gbp2-1	0.2	0.0	0.0	0
Gbp2-2	2.3	0.0	0	0.0
Gbp3-1	0.4	0.0	0.0	0.0
Gbp3-2	0.7	0.0	0.0	0.0
Gbp6-1	1.4	0	0	0
Gbp6-2	0.0	0.0	0	0.0
Gcc-1	0.2	0.0	0.0	0.0
Gcc-2	0.9	0.0	0.0	0.0
Gvin-1	0.7	0.0	0.0	0.0
Gvin-2	0.7	0.0	0.0	0.0
Ifi27-1	1.2	0.0	0.0	0.0
Ifi27-2	1.8	0.0	0	0.0
Ifi35-1	0.1	0.0	0.0	0.0
Ifi35-2	2.5	0.0	0.0	0.0
Ifi44-1	0.8	0.0	0.0	0.0
Ifi44-2	0.6	0.0	0	0.0
Ifih1-1	0.1	0.0	0.0	0.0
Ifih1-2	1.3	0.0	0.0	0.0
Ifit1-1	0.1	0.0	0.0	0.0
Ifit1-2	0.4	0.0	0.0	0.0
Ifit3-1	0.3	0.0	0.0	0.0
Ifit3-2	0.3	0.0	0.0	0.0
Ifitm3-1	0.6	0.0	0.0	0.0
Ifitm3-2	0.9	0.0	0.0	0.0
Ifna1-1	0.5	0.01	0	0.0
Ifna1-2	0.4	0.0	0.0	0.0
Ifna4-1	0.6	0.0	0.0	0
Ifna4-2	0.3	0	0	0.0
Ifnb1-1	0.3	0.0	0.0	0
Ifnb1-2	0.5	0.00	0	0.0
Ikbka-1	0.1	0.0	0.0	0
Ikbka-2	0.2	0	0	0.0
Ikbkb-1	0.4	0.0	0.0	0.0
Ikbkb-2	0.6	0.0	0.0	0.0
Ikbke-1	0.5	0.0	0.0	0.0
Ikbke-2	0.6	0.0	0.0	0.0
Il15-1	0.4	0.0	0.0	0.0
Il15-2	0.6	0.0	0.0	0.0
Il6-1	0.6	0.0	0.0	0.0
Il6-2	0.6	0.0	0.0	0.0
Irf1-1	0.1	0.0	0.0	0.00
Irf1-2	0.2	0	0	0.0
Irf2-1	0.5	0.0	0.0	0.0

Irf2-2	0.3	0.0	0.0	0
Irf3-1	0.2	0	0	0.0
Irf3-2	0.3	0.0	0.0	0.0
Irf5-1	0.2	1.4	0.1	0.0
Irf5-2	0.1	0.0	0.0	0.0
Irf7-1	0.6	0.0	0.0	0.0
Irf7-2	2.0	0.0	0.0	99.6
Irf9-1	0.3	0.0	0.0	0.0
Irf9-2	0.2	0.0	0.0	0.0
Irgm-1	0.2	0	0	0.0
Irgm-2	1.1	0.0	0.0	0.0
Isg15-1	1.4	0.0	0	0
Isg15-2	0.2	0.0	0.0	0.0
Lgals3bp-1	0.7	0.0	0.0	0.0
Lgals3bp-2	0.2	0.0	0.0	0.0
Lgals8-1	0.5	0.0	0.0	0.0
Lgals8-2	0.1	0.0	0.0	0.0
Lrp4-1	0.1	0.0	0.0	0.0
Lrp4-2	0.5	0.0	0.0	0.0
Ly6e-1	0.1	0.0	0.0	0.0
Ly6e-2	0.4	0.0	0.0	0.0
Map3K8-1	0.6	0.0	0.0	0.0
Map3K8-2	0.3	0.0	0.0	0.0
Map4k2-1	0.4	0.0	0.0	0.0
Map4k2-2	0.2	0.0	0	0.0
Mapk8-1	0.5	0.0	0.0	0.0
Mapk8-2	0.6	0.0	0.0	0.0
Mbnl1-1	0.3	0.0	0.0	0.0
Mbnl1-2	0.2	0.0	0.0	0.0
miR-124	0.2	0.0	0.0	0.0
Mitd1-1	0.1	0.0	0.0	0.0
Mitd1-2	0.3	0.0	0.0	0.0
Mlkl-1	0.4	0.0	0.0	0.0
Mlkl-2	2.3	0.0	0.0	0.0
Mov10-1	0.9	0.0	0.0	0.0
Mov10-2	0.4	0.0	0.0	0.0
Myd88-1	0.5	0.0	0.0	0.0
Myd88-2	0.2	0	0	0.0
Nfkbia-1	0.5	0.0	0.0	0
Nfkbia-2	0.2	0.0	0.0	0.0
Nmi-1	0.8	0.0	0.0	0.0
Nmi-2	4.6	0.0	0	0.0
Oas1a-1	0.2	0.0	0	0
Oas1a-2	0.2	0.0	0.0	0.0
Oas2-1	0.1	0.0	0.0	0.0
Oas2-2	0.2	0.0	0.0	0.0
Oasl1-1	0.8	0.00	0	0.0

Oasl1-2	0.4	0.0	0.0	0.0
Oasl2-1	0.4	0.0	0.0	0.0
Oasl2-2	0.3	0.0	0.0	0.0
p50	0.5	0.0	0.2	0.0
p50	0.3	0.0	0.0	0.1
p65	0.3	0.0	0.0	0.0
p65	0.1	0	0.0	0.0
Papr14-2	0.5	0	0	0.0
Parp10-1	0.1	0	0.0	0
Parp10-2	0.9	0	0.0	0.0
Parp11-1	0.0	0.0	0.0	0.0
Parp11-2	0.2	97.9	0	0.0
Parp12-1	0.1	0.0	0.0	0.0
Parp12-2	0.4	0.0	0.0	0.0
Parp14-1	0.4	0.0	0.0	0.0
Parp9-1	0.1	0	0.0	0.0
Parp9-2	0.3	0.0	0	0.0
Plec-1	0.1	0.0	0	0.0
Plec-2	0.0	0.0	0.0	0
Ppm1k-1	0.2	0	0.0	0.0
Ppm1k-2	0.3	0.0	0.0	0.0
Ppp3cb-1	0.1	0.0	0.0	0.0
Ppp3cb-2	0.4	0.0	0	0.0
Rnasel-1	0.9	0.0	0.0	0.0
Rnasel-2	0.2	0	0.0	0.0
Rsad-1	0.4	0	0	0.0
Rsad-2	0.3	0.0	0.0	0.00
Rtp4-1	0.6	0.0	0	0.0
Rtp4-2	1.4	0.0	0.0	0
Samd9l-1	0.2	0.0	0.0	0.0
Samd9l-2	0.1	0	0	0.0
Sfxn2-1	0.2	0.0	0.0	0.0
Sfxn2-2	0.1	0.0	0.0	0.0
Sh3bgrl-1	0.5	0.0	0	0.0
Sh3bgrl-2	0.1	0.0	0.0	0.0
Stat1-1	0.2	0.0	0.0	0.0
Stat1-2	1.4	0.0	0.0	0.0
Stat2-1	0.5	0.0	0.0	0.0
Stat2-2	0.2	0.00	0.0	0.0
Stat3-1	0.5	0.0	0	0.0
Stat3-2	0.6	0.0	0	0
Tap1-1	0.2	0.0	0	0.0
Tap1-2	1.0	0.0	0.00	0
Tapbp-1	1.1	0.0	0.00	0.00
Tapbp-2	0.2	0.0	0	0.00
Tbk1-1	0.8	0.0	0.02	0.0
Tbk1-2	1.0	0.0	0.00	0.00

Ticam1-1	0.0	0.0	0	0.00
Ticam1-2	0.2	0.0	0.0	0
Tlr3-1	0.0	0	0	0.0
Tlr3-2	1.8	0.00	0.0	0.0
Tlr7-1	0.8	0.00	0.0	0.0
Tlr7-2	0.2	0	0	0.0
Tlr9-1	0.1	0.00	0.0	0
Tlr9-2	0.1	0.00	0.0	0.0
Tmem140-1	0.1	0	0.0	0.0
Tmem140-2	0.3	0.0	0	0.0
Tor3a-1	0.2	2E-07	0	0
Tor3a-2	0.3	0.0	6E-09	0.0
Trex1-1	0.0	0.0	0	4E-03
Trex1-2	0.1	0	0.0	0
Trim21-1	0.6	0.0	0.0	0.0
Trim21-2	0.3	0.0	0.0	0.0
Trim25-1	0.1	0.0	0.0	0.0
Trim25-2	0.3	0.0	0.0	0.0
Usp18-1	0.4	0.0	0.0	0.0
Usp18-2	0.5	0E+00	0.0	0.0
Wwoxv-1	0.1	0.0	0	0.0
Wwoxv-2	0.2	0.0	0.0	0
Zc3hav1-1	0.1	0.0	0.0	0.0
Zc3hav1-2	0.4	0.0	0.0	0.0
Zfp182-1	0.0	0.0	0	0.0
Zfp182-2	1.1	0.0	0	0
EGFP	0.0	0.0	0	0
miR-124	0.2	0.0	0	0
TOTAL	**100**	**100**	**100**	**100**